# FUNCTIONAL ANALYSIS OF *DROSOPHILA* NEUROTROPHIN AND TOLL RECEPTOR FAMILIES IN THE DEVELOPMENT AND REPAIR OF THE LARVAL CENTRAL NERVOUS SYSTEM

by

MEI ANN LIM

A thesis submitted to

the University of Birmingham

for the degree of

DOCTOR OF PHILOSOPHY

School of Biosciences

College of Life and Environmental Sciences

University of Birmingham

January 2015

## Abstract

Drosophila neurotrophins (DNTs) - Spätzle (Spz), DNT1 and DNT2 - and 3 members of the Toll protein family – Toll, Toll-6 and Toll-7, of which Toll is Spz's receptor – have been shown to promote neuronal survival and motoneuron targeting in embryos. Yet, it remains to be understood (1) whether the DNTs influence cell number and central nervous system (CNS) development after embryonic stages to result in the behaving larva, and in turn (2) whether these events influence larval CNS repair after injury. Here, I investigated the functions of DNTs and Tolls in the formation and repair of the larval CNS, focusing mostly on Spz. I used GAL4 reporters, MiMIC-GFP protein traps and antibodies to the DNTs and Tolls to describe their larval CNS distributions. Interestingly, Spz was restricted to the mechanosensory domain in the ventral nerve cord (VNC). I generated a new loss of function allele for *spz* and showed that *spz* mutations affect glial numbers in the larval abdominal VNC. Using stabbing injury in the larval CNS, I showed that loss of *spz* antagonised wound repair. To conclude, my data show the involvement of Spz in larval CNS development, and that Spz has a prominent role in CNS repair.

*To my A-Team member Henry,*

*Sometimes life can be tough.*

*Sometimes the ride can be scary.*

*Sometimes people can be grumps.*

*But I will always love you.*

*Hetty.*

**Acknowledgements**

Over the past four years I have received support of various kinds from a good number of individuals, thus making my PhD journey a thoughtful and rewarding one. My PhD supervisor, Dr. Alicia Hidalgo, has a knack for being correct. This means that her insight and guidance have been invaluable to my growth as a scientist in the working research environment. To my steadfast supervisor who kept her encouraging ways, thank you for doing your darnedest to keep me on track, and also for providing a conducive writing environment in Room 629.

I would like to thank members of the Hidalgo lab, alumni and present. Thanks to Graham, Samaher, Martin, Jill, István, Juliet, Caitríona, Chris, Niki, Maria, Marta, Arin, Neale, Suzana and Gui Yi for discussions of a range of sorts and good company. Thanks Kentaro for straightening me out on matters of the *Drosophila* larvae and dissections. Simon, for the outreach adventures, ta! Thanks Karthik. Wiesel called Hubel his 'scientific brother'[1]. Together, they had carried out experiments every Tuesday and Thursday. Knowing this, I sometimes imagined us as scientific siblings, taking turns harvesting *Drosophila* virgins as well as acquiring microscopy data on weekends. Our collaboration period was a very fun time.

Thanks also to the Ministry of Education of the Brunei Government for my PhD scholarship.

Finally, I must acknowledge my father. Dad, you did – and still are – doing your utmost as a father of 6 to support my aspirations and dreams. With love, thank you.

[1] Source: SANDRONE, S. 2014. Q&A: Torsten Wiesel. Nature, 514, S11-S12.

**Table of Contents**

**List of Figures**

**List of Tables**

**List of Abbreviations, Symbols and Terms**

| | |
|---|---|
| 5-HT | serotonergic |
| A1-A8 | abdominal segments 1-8 |
| AEL | after egg laying |
| *alrm* | *astrocyte leucine-rich repeat molecule* |
| AMP | antimicrobial peptides |
| ANOVA | analysis of variance |
| $Antp^{Hu}$ | an allele of *Antennapedia* resulting in extra humeral bristles phenotype |
| BDNF | brain-derived neurotrophic factor |
| BL | brain lobe |
| BLAST | Basic Local Alignment Search Tool |
| bp | base pair |
| Brp | bruchpilot, an active zone protein |
| C1GalTA | Core 1 galactosyltransferases |
| *ca* | *claret* |
| CD2 | CD2 antigen |
| CD8a | CD8 antigen, alpha chain |
| cDcp1 | cleaved form of death caspase-1 |
| CDNF | cerebral dopamine neurotrophic factor |
| CI | central-intermediate |
| CK | cystine-knot, also shortened as CysKnot |
| CNS | central nervous system |
| *cu* | *curled* |
| *Cy* | *Curly* |
| *CyO* | *Curly of Oster* balancer of *Drosophila* chromosome 2 |
| CysKnot | cystine-knot, also shortened as CK |
| DA | dopaminergic |
| Dcp1 | death caspase-1 |
| *Df* | *Deficiency* |
| df | degree of freedom |
| DG | dentate gyrus |
| DGRC | *Drosophila* Genomics Resource Center |
| *Diap* | *Death-associated inhibitor of apoptosis 1* |
| Dif | dorsal-related immunity factor |
| DL | dorsal-lateral |
| DM | dorsal-medial |
| DNA | deoxyribonucleic acid |
| DNT | *Drosophila* neurotrophin |
| DNT1 | *Drosophila* Neurotrophin 1 |
| DNT2 | *Drosophila* Neurotrophin 2 |
| $Dr^{Mio}$ | an allele of *Drop* resulting in a microphthalmia (reduced eyes) phenotype |
| DSHB | Developmental Studies Hybridoma Bank |
| DsRed | *Discosoma* red fluorescent protein |
| DV | dorsal-ventral |
| *ea* | *easter* |
| Ebony | also known as N-β-ananyldopamine synthase, also shortened as NBAD synthase |

| | |
|---|---|
| ECM | extracellular matrix |
| *Ect4* | *Ectoderm-expressed 4* |
| EGFP | enhanced green fluorescent protein |
| EGFR | epidermal growth factor receptor |
| EGTA | ethylene glycol tetraacetic acid, a chelating agent and a buffer |
| Elav | embryonic lethal abnormal vision, a RNA-binding protein |
| EMS | ethyl methanesulfonate, a mutagen |
| FasII | fasciclin II, a cell adhesion molecule |
| FL | full-length |
| FLP | yeast flippase recombinase |
| FRT | flippase recombinase target |
| FUGUE | program comparing protein sequence-structure |
| fwd | forward |
| GlcAT-P | glucuronyltransferase P |
| G9 | enhanced GFP protein trap inserted into *reticulon-like 1* gene |
| GAL4 | yeast GALactose-responsive transcription factor GAL4 |
| GAL80 | yeast GALactose/lactose metabolism regulatory protein GAL80 |
| GAP43 | growth associated protein 43 |
| *GAP-GFP* | fusion of the myristoylation sequence from *GAP43* gene to GFP |
| GB | ganglionic branches |
| *gcm* | *glial cell missing* |
| GD | gastrulation-defective |
| GDNF | glial cell-derived neurotrophic factor |
| GEF | guanine nucleotide exchange factor |
| GFP | green fluorescent protein |
| *GMR* | *Glass Multimer Reporter* |
| GP | genomic primer |
| GS2 | glutamine synthetase 2 |
| *h* | *hairy* |
| *HA* | gene construct encoding a protein tag derived from amino acids 98 to 106 of haemagglutinin antigen |
| HL | homozygous lethal |
| hr | hour |
| *hsFLP* | gene construct expressing flippase recombinase upon heat shock |
| *Hu* | an allele of *Antennapedia* resulting in extra humeral bristles phenotype |
| HV | homozygous viable |
| ICD | intracellular domain |
| *If* | an allele of *Kruppel* resulting in an irregular facets phenotype |
| IG | interface glia |
| IMS | industrial methylated spirit |
| IPC | inner proliferation center |
| ISN | intersegmental nerve |
| IVS | intervening sequence |
| IκB | nuclear factor of kappa light polypeptide gene enhancer in B cells inhibitor |
| kb | kilobase |
| kDa | kilodalton |
| *kni* | *knirps* |
| $Kr^{If}$ | an allele of *Kruppel* resulting in an irregular facets phenotype |

| | |
|---|---|
| *LacZ* | gene encoding β-GALactosidase |
| LHS | left-hand side |
| L-LTP | late phase LTP |
| LN | lateral neuron |
| LTD | long term depression |
| LTP | long term potentiation |
| MANF | mesencephalic astrocyte-derived neurotrophic factor |
| MARCM | mosaic analysis with a repressible cell marker |
| *mCD8-GFP* | fusion of mouse CD8a to GFP |
| met | methionine |
| *Mi{MIC}* | *Minos*-mediated integration cassette |
| mins | minutes |
| *MKRS* | a balancer of *Drosophila* chromosome 3 which carries the alleles $M(3)76A^{1}$, $kar^{1}$, $ry^{2}$ and $Sb^{1}$ |
| mL | millilitre |
| mm | millimetre |
| mW | milliwatt |
| *myc* | gene construct encoding a 10 amino acid protein tag derived from myelocytomatosis oncogene |
| *myr-RFP* | fusion of myristoylation signal (first 90 amino acids of *Drosophila* Src oncogene at 64B) to RFP |
| *myr-tdTomato* | fusion of myristoylation signal (first 90 amino acids of *Drosophila* Src oncogene at 64B) to tdTomato |
| n | number of sample |
| n/a | not applicable |
| NA | numerical aperture |
| NaN | Not a Number |
| NBAD synthase | N-β-ananyldopamine synthase, also known as ebony |
| nc82 | antibody against Bruchpilot antigen |
| Ndl | Nudel |
| NEB | New England BioLabs |
| NFκB | nuclear factor of kappa light polypeptide gene enhancer in B cells |
| NGF | nerve growth factor |
| NHO | neurohemal organ |
| nm | nanometre |
| NMJ | neuromuscular junction |
| ns | not statistically significant |
| NT | neurotrophin |
| NT-3 | neurotrophin-3 |
| OPC | outer proliferation center |
| *p* | *pink* |
| *P{XP}* | transgenic transposon, *P-element XP* |
| p35 | baculovirus anti-apoptotic protein p35 |
| *PBac{RB}* | transgenic transposon, *piggyBac RB* |
| PBS | phosphate-buffered saline |
| PBTw | phosphate-buffered saline with dissolved Tween-20 |
| PBTx | phosphate-buffered saline with dissolved Triton X-100 |
| PCR | polymerase chain reaction |

| | |
|---|---|
| PD | Parkinson's disease |
| *Pdf* | *Pigment-dispersing factor* |
| PDGF | platelet-derived growth factor |
| PEM | buffer containing PIPES, EGTA and $MgSO_4$ |
| pH3 | phospho-histone H3 |
| Pip | Pipe |
| PIPES | piperazine-*N*,*N*'-bis(2-ethanesulfonic acid), a weak acid buffer |
| PMT | photomultiplier tube |
| PNS | peripheral nervous system |
| proSpz | Spätzle pro-protein |
| PRR | pattern recognition receptor |
| PS | posterior spiracle |
| PVR | PDGF and VEGF receptor |
| Repo | reversed polarity, a homeodomain protein |
| rev | reverse |
| RFP | red fluorescent protein |
| RHS | right-hand side |
| *rn* | *rotund* |
| RNA | ribonucleic acid |
| RNAi | RNA interference |
| ROI | region of interest |
| RT | room temperature |
| *ru* | *roughoid* |
| *Sb* | *Stubble* |
| *sc* | *scute* |
| SD | standard deviation |
| SE | standard error |
| SEG | subesophageal ganglion, also shortened as SubGgl |
| SI | survival index |
| *SM6A* | *second multiply-inverted 6A* balancer of *Drosophila* chromosome 2 |
| Snk | snake |
| SNP | single nucleotide polymorphism |
| SP | signal peptide |
| SPE | Spätzle-Processing Enzyme |
| Spz | spätzle |
| *sr* | *stripe* |
| Src64B | Src oncogene at 64B, also known as tyrosine-protein kinase Src64B |
| *st* | *scarlet* |
| SubGgl | subesophageal ganglion, also shortened as SEG |
| SVZ | subventricular zone |
| T1-T3 | thoracic segments 1-3 |
| *Tb* | *Tubby* |
| tdTomato | tandem dimer Tomato red fluorescent protein |
| TGFα | transforming growth factor alpha |
| TGFβ | transforming growth factor beta |
| TLR | Toll-like receptor |
| *TM3* | *third multiply-inverted 3* balancer of *Drosophila* chromosome 3 |
| *TM6B* | *third multiply-inverted 6B* balancer of *Drosophila* chromosome 3 |

| | |
|---|---|
| Toll | also known as Toll1 |
| Toll2 | also known as 18 wheeler |
| Toll3 | also known as MstProx |
| Toll4 | also known as Tl4 |
| Toll5 | also known as Tehao |
| Toll6 | also known as Tl6 |
| Toll7 | also known as Tl7 |
| Toll8 | also known as Tollo |
| Toll9 | also known as Tl9 |
| TRiP | Transgenic RNAi Project |
| Trk | tropomyosin-related kinase |
| TrkA | tropomyosin-related kinase A, also known as tyrosine receptor kinase A and high affinity NGF receptor |
| TrkB | tropomyosin-related kinase B, also known as BDNF/NT-3 growth factors receptor |
| *tub* | *tubulin* |
| *UAS* | *Upstream Activation Sequence*, the binding site of GAL4 |
| UTR | untranslated region |
| val | valine |
| VEGF | vascular endothelial growth factor |
| VL | ventral-lateral |
| VM | ventral-medial |
| VNC | ventral nerve cord |
| Wbl | Windbeutel |
| *wg* | *wingless* |
| *yw* | *yellow and white* |
| $\chi^2$ | Pearson's chi-square test |

# Chapter 1

## 1 Introduction

Understanding how the brain works remains an extensive research pursuit in this early 21st century (Alivisatos *et al.*, 2012). In this pursuit, one of the fundamental questions which arise is how the metazoan nervous system orchestrates its cellular parts to achieve functionality. The metazoan nervous system is central to generating behaviour (Ferreira *et al.*, 2014a), a set of adaptable and complex movements which are mediated through muscle contractions, even including the generation of communication such as gestures, speech and writing. Metazoan nervous system ranges in complexity. A simple type of nervous system is a diffuse nerve net in prebilaterians. The diffuse nerve net is exemplified in the sedentary polyps of the phylum Cnidaria, and it comprises of two fundamental neurons: sensory neurons and motoneurons (Angerer *et al.*, 2011; Arendt *et al.*, 2008; Ferreira *et al.*, 2014a). In contrast, the central nervous system (CNS) found in bilaterians are complex and delimited. The interneurons, which associated between the sensory neurons and motoneurons, are introduced in the bilaterians (Angerer *et al.*, 2011; Arendt *et al.*, 2008; Ferreira *et al.*, 2014a). When the CNS is defined anatomically as "nervous tissue that comprises distinct agglomerations of functionally specialized neurons (nuclei) interconnected by axon tracts (neuropile)" (Arendt *et al.*, 2008), and as nervous tissue which "may be subdivided into separate parts (ganglia)" (Arendt *et al.*, 2008), the CNS then takes various forms in shape and size across phyla of deuterostomes and protostomes. The deuterostomes mentioned here include the vertebrates, while the protostomes include athropods such as *Drosophila*.

The concept of the nervous system being central to creating behaviours is the basis for many histological studies on the structure of the nervous system (Ferreira *et al.*, 2014a). When the architecture of the nervous system emerges, the obvious phenomena are the accompanying growth in organ volume and an increase in cell number. Neuronal and glial cells of the nervous system have their numbers adjusted through trophic interactions to organise the development of a properly functioning nervous system (Gomes *et al.*, 2001; Hidalgo *et al.*, 2011). Neuronal cells also adjust the growth of their dendritic connections such that the circuits they form are suitably matched to the functions they perform (Tripodi *et al.*, 2008). Such coordination endows the nervous system with plasticity (i.e. the ability to undergo change). Plasticity confers structural robustness to the nervous system, that is to say that the challenges of maintaining cell identity and tissue functions in a developing, growing and changing organisation of the nervous system are met, at least partly, by counteracting structural compensations (Gomes *et al.*, 2001; Hidalgo *et al.*, 2011; Marder and Prinz, 2003; Tripodi *et al.*, 2008). Structural robustness, in turn, allows the reproducible functioning of the nervous system across individuals and throughout life such as in learning and memory. Furthermore, plasticity enables cells to undertake responses to injury by promoting repair (Hidalgo and Ffrench-Constant, 2003; Hidalgo *et al.*, 2011).

## 1.1 Neurotrophism in *Drosophila*

### 1.1.1 Definition of Neurotrophic Factors and Neurotrophins

Neurotrophic factors (NTFs) are a subset of growth factors which act in the nervous system, where they regulate survival, development and function, while neurotrophins (NTs) are one of

the major classes of NTFs (Blum and Konnerth, 2005; Boyd and Gordon, 2003; Deister and Schmidt, 2006; Huang and Reichardt, 2001; Lewin and Barde, 1996; Lu *et al.*, 2005).

### 1.1.2 Neurotrophic Factors in *Drosophila*

The effort placed into the identification and functional demonstration of neurotrophic factors in *Drosophila melanogaster* (*D. melanogaster*) has revealed that the human and fruit fly nervous systems share the same building blocks in the course of their development to organise the emergence of the nervous system circuitry (Newquist *et al.*, 2013; Palgi *et al.*, 2009; Zhu *et al.*, 2008). The corollary of this revelation is that structural robustness had extended reproducible formation and functioning of the nervous system over evolutionary time and that the *Drosophila* nervous system is also plastic like that in the mammalian (Hidalgo *et al.*, 2011). These findings place an importance on the fitting use of *Drosophila* as a choice model organism to understand the workings of the brain and to investigate regeneration of the damaged or diseased nervous system.

#### 1.1.2.1 Neurotrophins in *Drosophila*

In vertebrates, the neurotrophins (NTs) are a major class of secretory, dimeric proteins which share common structural features and which make up one of the protein families that link nervous system structure and function (Blum and Konnerth, 2005; Hidalgo *et al.*, 2011; Lewin and Barde, 1996; Lu *et al.*, 2005). Neurotrophins regulate many aspects of nervous system development and function including axon guidance, cell proliferation, cell differentiation, cell survival, axonal and dendritic elaborations, membrane trafficking, synapse

formation and synaptic plasticity (Gurthrie, 2007; Reichardt, 2006). It is therefore unsurprising that abnormal neurotrophin function is linked to brain diseases such as neurodegeneration (e.g. Alzheimer's disease), psychiatric disorders (e.g. depression) and impaired memories (Allen and Dawbarn, 2006; Martinowich *et al.*, 2007; Reichardt, 2006).

Mammalian NTs carry out their functions in conjunction with their Trk, p75 and Sortilin receptors (Bartkowska *et al.*, 2010; Devesa and Ferrer-Montiel, 2014; Jansen *et al.*, 2007; Lu *et al.*, 2005; Marchetti *et al.*, 2015; Nykjaer *et al.*, 2005; Reichardt, 2006). However, no canonical neurotrophin receptor homologues of Trk, p75 or Sortilin have been found in *Drosophila* (Manning *et al.*, 2002). Instead, the *Drosophila* neurotrophins (DNTs) found within the Spätzle protein family bind to paralogues of the Toll family. The *Drosophila* neurotrophin Spätzle (Spz) is a well-known activating ligand of the receptor Toll (Hu *et al.*, 2004; Weber *et al.*, 2003). The functional conservation between the DNTs and the mammalian NTs has been demonstrated *in vivo* in *Drosophila* by the maintenance of neuronal survival and motor-axon targeting during embryonic development (Zhu *et al.*, 2008). The DNTs are also required for synaptogenesis in the larval neuromuscular junction (NMJ) (Sutcliffe *et al.*, 2013). Toll has neurotrophic, axon-targeting and synaptogenesis functions in the embryos too (Halfon *et al.*, 1995; Inaki *et al.*, 2010; Rose *et al.*, 1997; Zhu *et al.*, 2008). The loss of Toll results in muscle defects in the larvae (Halfon *et al.*, 1995; Halfon and Keshishian, 1998). However, it remains to be understood how the DNTs influence the adjustment of cell numbers and the wiring of the nervous system after embryonic stages to result in a properly behaving larva.

It is known that the central nervous system (CNS) in humans exhibits poor regenerative ability following traumatic injury and chemotoxicity, or as a result of ongoing neurodegenerative processes (Carlson, 2007; Horner and Gage, 2000). When reiterating the fact that the neurotrophin family regulate many aspects of nervous system development and function, this characteristic naturally confers promising potential upon the neurotrophins to assist regenerative processes (Ferraro *et al.*, 2004; Horner and Gage, 2000). To date, there have been no *in vivo* functional studies of DNTs in *Drosophila* CNS regeneration.

#### 1.1.2.2 MANF and CDNF in *Drosophila*

Independent from the NTs, the second class of vertebrate neurotrophic factors consists of the Mesencephalic Astrocyte-Derived Neurotrophic Factor (MANF) and the Cerebral Dopamine Neurotrophic Factor (CDNF) (Lindholm and Saarma, 2010). In *Drosophila*, the single protein homologous to vertebrate MANF/CDNF is *Drosophila* MANF (DmMANF) (Palgi *et al.*, 2009). MANF and CDNF protect vertebrate midbrain dopaminergic (DA) neurons and DmMANF preserves the functional role of protecting DA neurons in *Drosophila* (Lindholm and Saarma, 2010). DmMANF is produced by glial cells, and this situation is comparable to mammalian astrocytes nearby DA neurons (Palgi *et al.*, 2009). Towards the end of embryogenesis, DmMANF is needed for the maturation and maintenance of DA neurites as well as the maintenance of dopamine levels (Palgi *et al.*, 2009). Without DmMANF, maturation of the nervous system is affected severely by specific and signification reduction of DA neurites (Palgi *et al.*, 2009). Hatched mutant embryos die in the first instar larval stages or immediately after the first molt (Palgi *et al.*, 2009). Given that the specific loss of dopamine in human adults is the hallmark of Parkinson's disease (PD), the study of

DmMANF in *Drosophila* models for neurodegeneration has great potential for the understanding of PD (Coulom and Birman, 2004; Palgi *et al.*, 2012; Palgi *et al.*, 2009; Whitworth *et al.*, 2006).

#### 1.1.2.3 Netrins in *Drosophila*

The DNTs found within the Spätzle protein family are expressed in the embryonic CNS midline, an intermediate target of interneurons (Zhu *et al.*, 2008). Netrins are classical axon guidance cues and they overlap their expression patterns with the DNTs in the midline target of interneurons, with Netrin-B in particular, but not Netrin-A, serving as an *en passant* neurotrophic factor (Newquist *et al.*, 2013).

#### 1.1.2.4 GDNF Family Signalling in *Drosophila*

The mammalian glial cell-line derived neurotrophic factor (GDNF) family ligands (GFLs) are growth factors related to the Transforming Growth Factor Beta (TGFβ) protein superfamily (Airaksinen and Saarma, 2002). The GFLs consist of GDNF, artemin, neurturin and persephin (Airaksinen and Saarma, 2002; Baloh *et al.*, 2000). GFLs play a crucial role in the development and maintenance of distinct neuronal populations in the vertebrate central and peripheral nervous system (PNS) (Kallijarvi *et al.*, 2012). Dimeric GFLs bind cognate GDNF family receptor alpha (GFRα) receptors to activate Ret receptor tyrosine kinase signalling (Airaksinen and Saarma, 2002; Takahashi, 2001).

While no GDNF homologue has been identified in *Drosophila* yet, a Ret homologue is conserved in *Drosophila* and is expressed in the nervous tissue where downstream Ret signalling could be conserved (Abrescia *et al.*, 2005; Aron *et al.*, 2010; Hahn and Bishop, 2001; Kallijarvi *et al.*, 2012; Sugaya *et al.*, 1994).

### 1.1.3 Gliatrophic Factors in *Drosophila*

In the adult *Drosophila* brain, glial proliferation can be induced by neuronal programmed cell death (PCD), and conversely suppressed by inhibition of neuronal PCD (Kato *et al.*, 2009). Therefore, studying the development, maintenance and survival of glia to understand the wiring of nervous system circuitry is as relevant as studying the neuronal counterpart.

Growth factors which regulate the survival of glia are called gliatrophic factors. In *Drosophila*, there is only one Epidermal Growth Factor Receptor (EGFR) which binds multiple ligands, including Spitz and Vein, homologues of Transforming Growth Factor Alpha (TGFα) and Neuregulin, respectively (Hidalgo *et al.*, 2011; Hidalgo *et al.*, 2001). A subset of midline glia expressing EGFR during embryonic development depends on Spitz to be secreted by neighbouring neurons for its survival (Bergmann *et al.*, 2002). Pioneers neurons produce Vein to maintain survival of neighbouring EGFR-expressing longitudinal glia (Hidalgo *et al.*, 2001). There is also only one homologue in *Drosophila* for both Platelet-Derived Growth Factor Receptor (PDGF) and Vascular Endothelial Growth Factor (VEGF) called PVR, and this receptor is also required by the midline glia for survival through PVF ligand secretion from midline neurons (Learte *et al.*, 2008).

Using Spitz/TGFα and Vein/Neuregulin as the growth factors to compare and contrast with NGF, Spitz/TGFα, Vein/Neuregulin and NGF are similar to each other in how they are secreted to maintain cell population survival in the nervous system. They overlap through exerting their functions through specific protein receptor families in the neighbouring cell or target field. However, the growth factors Spitz/TGFα and Vein/Neuregulin differ from NGF in the target cell type they maintain in the nervous system.

### 1.1.4 Review of the Identification of DNTs in the Spätzle Protein Family

The mammalian NT family consists of the Nerve Growth Factor (NGF), Brain-Derived Neurotrophic Factor (BDNF), Neurotrophin-3 (NT3) and Neurotrophin-4/5 (NT4/5) (Lewin and Barde, 1996). From teleost bony fish, Neurotrophin-6 (NT6) and Neurotrophin-7 (NT7) have been isolated (Gotz *et al.*, 1994; Nilsson *et al.*, 1998). Mature NTs are derived after the synthesis and modification of precursors called proneurotrophins (proNTs) (Edwards *et al*., 1998; Lewin & Barde, 1996). Both mature NTs and proNTs carry out functions through their Trk, p75 and Sortilin receptors in an assortment of receptor complexes, including as simple homodimeric structures or as multimeric co-receptor partners (Jansen *et al.*, 2007; Lu *et al.*, 2005; Nykjaer *et al.*, 2005; Reichardt, 2006) (Bartkowska *et al.*, 2010; Devesa and Ferrer-Montiel, 2014; Marchetti *et al.*, 2015).

Structurally, members of the NT family adopt a three-dimensional (3D) fold so-called the cystine-knot (CysKnot), an elongated anti-parallel β-strand with 3 disulphide bridges among intra-cysteine residues (DeLotto and DeLotto, 1998; Hoffmann *et al.*, 2008; Mizuguchi *et al.*, 1998; Weber *et al.*, 2007). The NTs share common structural features including the formation

of homo- and hetero- dimers (Lewin and Barde, 1996; McDonald and Hendrickson, 1993). Spz, having a CysKnot and capable of dimerising, belongs with NTs in the CysKnot superfamily of proteins (DeLotto and DeLotto, 1998; Gangloff *et al.*, 2008; Hoffmann *et al.*, 2008; Hu *et al.*, 2004; Mizuguchi *et al.*, 1998; Parthier *et al.*, 2014; Stelter *et al.*, 2013; Weber *et al.*, 2007; Weber *et al.*, 2005; Weber *et al.*, 2003). Of the 4 classical NTs, Spz is most similar to NGF according to these criteria: amino acid sequence alignment of the CysKnot, consistency between predicted comparative structural modelling and experimented biochemical treatment of dimeric Spz, and matching crystallographic structure of the CysKnot (DeLotto and DeLotto, 1998; Gangloff *et al.*, 2008; Hoffmann *et al.*, 2008; Mizuguchi *et al.*, 1998; Weber *et al.*, 2007; Weber *et al.*, 2003). NGF is most well-understood for its trophic effect in the development of early PNS (Cohen and Levi-Montalcini, 1956; Davies, 1996; Levi-Montalcini and Cohen, 1960; Lewin and Barde, 1996). For clarity, a neurotrophic effect is defined as the mediation of axon outgrowth as well as long-term dependence between neurons and the target cells they innervate such that the neurons can survive (Gurthrie, 2007). Biologically, Spz promotes motor axon targeting (Zhu *et al.*, 2008). Put together, Spz is a structural and functional homologue of mammalian NTs.

DNT1 and DNT2 are Spz paralogues Spz2 and Spz5, respectively (Parker *et al.*, 2001; Zhu *et al.*, 2008). DNT1 was identified as related to BDNF using amino acid sequence alignment and comparative protein structure tools (Zhu *et al.*, 2008). In particular, DNT1 retains all the residues relevant to forming the human CysKnot (Zhu *et al.*, 2008). Akin to Spz, DNT1 also has the dimerising features of canonical NTs (Zhu *et al.*, 2008). Another protein structurally close to DNT1, Spz and the human NTs is DNT2, but the other Spz paralogues – Spz3, Spz4 and particularly Spz6 – are divergent (Parker *et al.*, 2001; Zhu *et al.*, 2008). DNT2 also

dimerises (McIlroy *et al.*, 2013). According to structure-based alignment, among the Spz paralogues, DNT1 and DNT2 are the closest to the NT superfamily, followed by Spz (Zhu *et al.*, 2008). DNT1 and DNT2, like Spz, are required for axon targeting, as disrupting their functions causes motor axon terminals to sprout and misroute (Zhu *et al.*, 2008). DNT1 and DNT2 maintain neuronal survival too, as exemplified by loss of function mutants having an increase in neurons undergoing programmed cell death (PCD) in the embryonic CNS, while neurons can be rescued from naturally occurring cell death (NOCD) upon overexpression of DNT1 and DNT2 *in vivo* (Zhu *et al.*, 2008). In short, at least DNT1, DNT2 and Spz form a *Drosophila* NT family on the basis of structural and functional criteria to the mammalian NTs (Zhu *et al.*, 2008).

So far, the similarities of DNTs to mammalian NTs described above have been based on structural and functionally homology. In particular, the functional comparison was based on NGF's first discovered role, that is, the growth and survival effect of NTs. Beginning with M. Shorey's work to observe embryonic chick nerve development in the absence of the organs to which nerves normally innervate (Shorey, 1909), and up to the experiments establishing purified NGF's role as a trophic factor (Cohen and Levi-Montalcini, 1956; Levi-Montalcini and Cohen, 1960), a succession of key ideas: (i) that the size of the target field, to which nerves innervate, influences the size of the surviving neuronal population (Hamburger, 1939); (ii) that the target provides the necessary conditions for neurite outgrowth and maintenance of the nerves (Hamburger and Levi-Montalcini, 1949); and (iii) that the survival is mediated through a target-derived soluble protein which exerts a trophic effect (Cohen *et al.*, 1954). Such ideas paved the way to develop the concept of the "neurotrophic hypothesis" whereby "the survival of developing neurons depends on the supply of a neurotrophic factor that is

synthesized in limiting amount in their target fields" (Davies, 1996; Gilbert, 2000; Guthrie, 2007). Again, there are parallels to be drawn between the *in vivo* functions of DNTs with the neurotrophic hypothesis. Firstly, transcripts of *spz*, *dnt1* and *dnt2* are produced in relevant areas: the embryonic CNS midline, an *en-passant* target of interneurons, and the muscles, the target field of motor neurons (Zhu *et al.*, 2008). At least DNT1 has been shown to operate in a target-dependent manner (Zhu *et al.*, 2008). The use of RNAi knockdown restricted to the midline induces neuronal death in the CNS while conversely, the overexpression of active DNT1 at the midline rescues neuronal survival. Secondly, the appropriate support by DNTs is dependent on concentration. Having too little of DNTs by way of loss of function mutants or RNAi knockdowns, as well as having too much by gain of function, will both cause misrouting in motor axon terminals (Zhu *et al.*, 2008). Therefore, beyond structural and functional homology, the physiology of DNTs is also consistent with the neurotrophic hypothesis which focuses on the non-autonomous growth and survival effects of NTs.

The regulation of appropriate cell number comes through the balance of cell proliferation, cell survival and cell death (Hidalgo and Ffrench-Constant, 2003). The mammalian NTs, through their receptors, also adjust cell numbers through cell proliferation and cell death (Gupta et al., 2013; Huang and Reichardt, 2003; Lu et al., 2005; Nykjaer et al., 2005). For example, high affinity binding of proNTs to p75 induces apoptosis (Lee et al., 2001; Lu et al., 2005; Nykjaer et al., 2005). The importance of regulating appropriate cell number is highlighted in cases when upregulation of BDNF/TrkB signaling leads to abnormal cellular proliferative changes and pathological conditions such as cancer (Gupta et al., 2013). In *Drosophila*, developing tissues eliminate compromised cells which present health risks to the animal through a proposed Spz-dependent apoptotic pathway (Meyer et al., 2014).

On top of adjusting cell number, NTs also regulate functions such as synaptogenesis and synaptic plasticity, with the latter encompassing long-term potentiation (LTP), long-term depression (LTD) and structural changes to synapses (Lu et al., 2005; Martinowich et al., 2007; Poo, 2001). Since the discovery of the DNT family, the study of Spz and their paralogues (including Spz3, Spz4 and Spz6) within the context of development and nervous system have been centred around synaptogenesis and synaptic transmission in the larval NMJ (Ballard et al., 2014; Sutcliffe et al., 2013) and the removal of unfit cells by apoptosis in the larval wing disc (Meyer et al., 2014).

### 1.1.5 DNT Signalling

#### 1.1.5.1 Molecular Mechanism of Spz Activation

After protein translation, an inactive Spz pre-pro-protein consists of an N-terminus signal peptide, a regulatory prodomain and a C-terminus CysKnot domain (DeLotto and DeLotto, 1998; Schneider *et al.*, 1994; Weber *et al.*, 2003). The N-terminus signal peptide has a signal sequence (Morisato and Anderson, 1994), which is needed to instruct the delivery of proteins through correct cytoplasmic routes to be secreted outside the cytosol. The regulatory prodomain has sequences essential for efficient folding and secretion of dimeric Spz (Weber *et al.*, 2007). Spz's dimerising feature is due to a disulphide bond between inter-CysKnot subunits (DeLotto and DeLotto, 1998; Gangloff *et al.*, 2008; Hoffmann *et al.*, 2008; Hu *et al.*, 2004; Mizuguchi *et al.*, 1998; Parthier *et al.*, 2014; Stelter *et al.*, 2013; Weber *et al.*, 2007; Weber *et al.*, 2005; Weber *et al.*, 2003).

Spz is a secreted protein (Morisato and Anderson, 1994). Before being secreted, Spz pre-pro-protein is processed internally to remove the signal peptide and the resulting Spz pro-protein (proSpz), consisting of the regulatory prodomain and C-terminus CysKnot, is secreted into the extracellular space as a native and unstructured 80kDa homodimer (DeLotto and DeLotto, 1998; Schneider *et al.*, 1994; Weber *et al.*, 2003). The 12kDa CysKnot domain consists of 106 amino acids and is hence also known as C106 (DeLotto and DeLotto, 1998; Morisato and Anderson, 1994). C106 itself is the activing and mature fragment of Spz (DeLotto and DeLotto, 1998; Schneider *et al.*, 1994). It binds Toll ectodomain with high specificity and high affinity in a 2:2 stoichiometry to activate Toll-receptor signalling pathway (Weber *et al.*, 2003). In contrast, the prodomain is natively largely unstructured but has an amphipathic helix which masks a hydrophobic region of Spz (Arnot *et al.*, 2010; Weber *et al.*, 2003). In pro-protein form, Spz acts to prevent itself interacting with Toll's binding region (Arnot *et al.*, 2010; Weber *et al.*, 2003). Upon proteolytic cleavage of dimeric proSpz, the prodomain and C106 remain associated non-covalently to stabilise C106 (Hoffmann *et al.*, 2008; Weber *et al.*, 2007). However, upon the cleaved-complex binding allosterically to Toll, the prodomain gets released, leaving the binding between active C106 and Toll to initiate signalling (Gangloff *et al.*, 2008; Weber *et al.*, 2007). The released prodomain has been proposed to act as a negative regulator for both the protease cleaving proSpz and the Spz-processing reaction.

#### 1.1.5.2 Spz in Dorsal-Ventral Patterning and Immunity

Spz has two well-known functions. Together with its receptor Toll, they are first discovered for their roles in generating dorsal-ventral (DV) polarity in the development of the *Drosophila* embryo (Anderson and Nusslein-Volhard, 1984; Morisato and Anderson, 1994; Schneider *et*

*al.*, 1994; Stein and Nusslein-Volhard, 1992). When third instar larvae and adult are immune-challenged by fungal and Gram-positive bacteria, both *spz* and *Toll* expression are up-regulated for immune responses (Buchon *et al.*, 2009; Jang *et al.*, 2006; Kambris *et al.*, 2006; Lemaitre *et al.*, 1996; Tauszig *et al.*, 2000).

To carry out DV patterning and immunity functions, the Spz pro-protein (proSpz) has to be within the extracellular space for proteolytic cleavage by clip-domain serine proteases (Hecht and Anderson, 1992; Jang *et al.*, 2006; Misra *et al.*, 1998). For DV patterning, Easter (Ea) is the responsible protease which cleaves proSpz to release C106 (Anderson and Nusslein-Volhard, 1984; DeLotto and DeLotto, 1998; Morisato and Anderson, 1994). As for Toll-dependent antimicrobial responses, Spätzle Processing Enzyme (SPE) instead is the required terminal enzyme (Jang *et al.*, 2006; Kambris *et al.*, 2006). SPE processes proSpz identically to Ea and their functional homology is demonstrated by activated SPE rescuing DV polarity in embryos lacking *easter* (Jang *et al.*, 2006). However, just as DV patterning and immune responses are different functions from each other, the origins and activation cascades of the zymogens Ea and SPE are also different (Figure 1.1).

In specifying DV polarity, Spz and its upstream processing enzymes, including Ea, are maternally-derived and deposited into the perivitelline space during the syncytial blastoderm stage (Anderson and Nusslein-Volhard, 1984; Chasan *et al.*, 1992). The zymogens of the activating cascade of Spz, in sequence, are: (i) Gastrulation Defective (GD), (ii) Snake (Snk), and (iv) Ea (Anderson and Nusslein-Volhard, 1984; Morisato and Anderson, 1995). Active GD cleaves zymogen Snk. In turn, active Snk cleaves Ea. The activation of Ea by Snk is the key ventrally-restricted event in the embryonic patterning of DV polarity (Cho *et al.*, 2012).

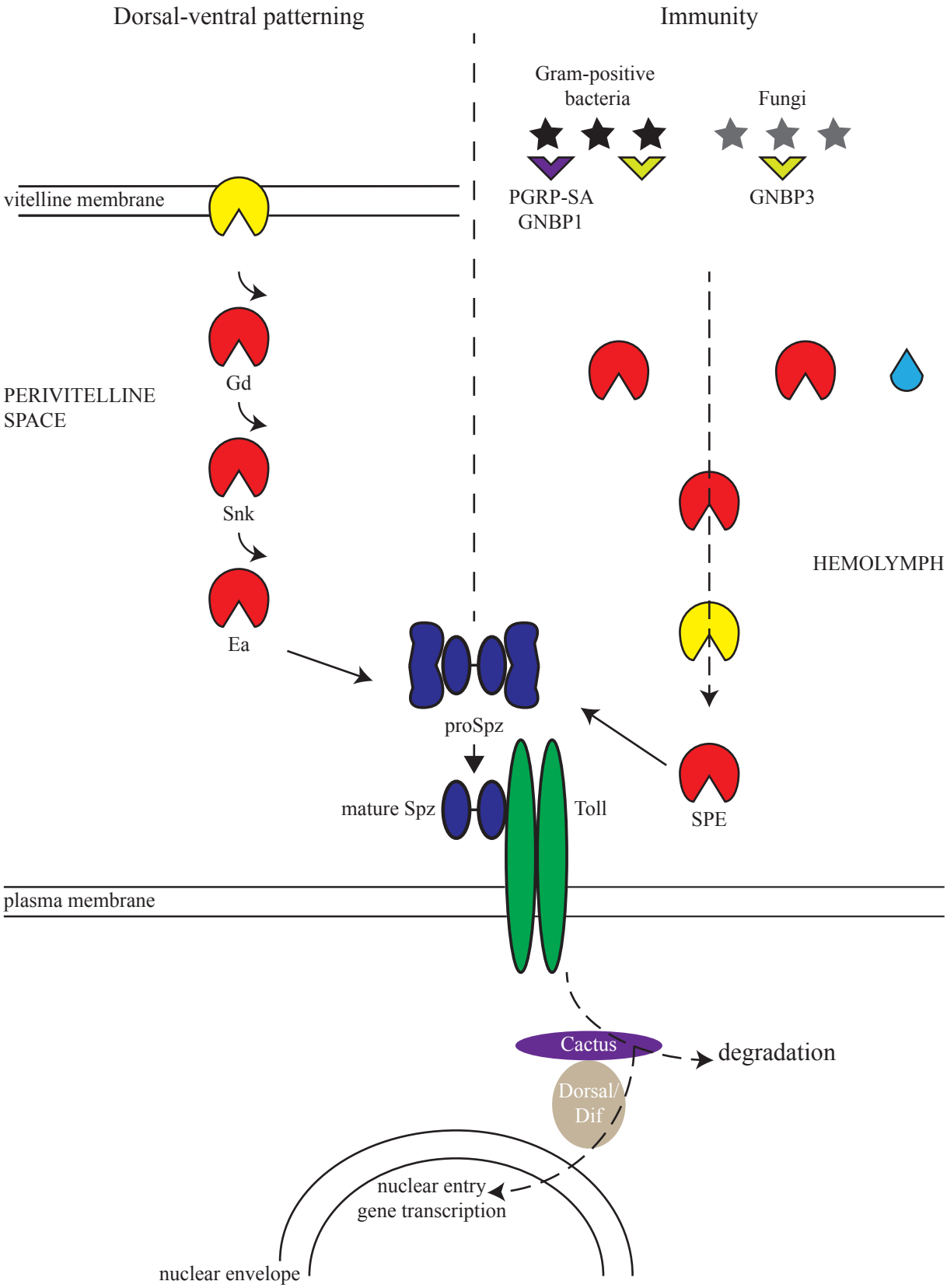


**Figure 1.1** The spätzle-Toll pathway in embryonic dorsal-ventral patterning and immunity. For references, see main text (Section 1.1.5.2).

Active Ea then cleaves proSpz and the binding of mature Spz to Toll initiates ventralising signal (Morisato and Anderson, 1995).

SPE is a zygotic product of immune tissues such as the lymph gland, fat body (functional analogy of human liver) and mature hemocytes (analogous to phagocytes) (Mulinari *et al.*, 2006). Zygotic proSpz is present in hemocytes which circulates the hemolymph (Irving *et al.*, 2005; Lemaitre *et al.*, 1996; Weber *et al.*, 2003). Circulating pattern recognition receptors (PRRs), such as peptidoglycan recognition protein SA (PGRP-SA) and Gram-negative binding protein 1 (GNBP1), initiate a protease cascade which eventually cleaves and activates SPE, in turn cleaving proSpz to activate Toll-signalling in the fat body for immune responses (Jang *et al.*, 2006; Kambris *et al.*, 2006; Michel *et al.*, 2001). The activation of SPE-Spz-Toll signalling also leads to transcriptional positive feedback of SPE to ensure adequate response to microbial infection (Jang *et al.*, 2006; Kambris *et al.*, 2006). Surprisingly, the *spz* gene, encoding for the substrate of SPE, is not the target of Toll signalling in the fat body (Irving *et al.*, 2005).

Within the cytoplasm, activation of Toll ultimately leads to the phosphorylation of Cactus (IκB), which causes the disruption of the complex between Cactus and transcription factor Dorsal, a NFκB homolog, followed by the release and nuclear translocation of Dorsal required for DV patterning (Morisato and Anderson, 1995). In immune response, the NFκB homolog is Dorsal-related immunity factor (Dif), and Toll activation degrades Cactus of the Dif/Cactus complex, leading to Dif nuclear translocation and transcription of immunity-related genes (Ip *et al.*, 1993; Lemaitre *et al.*, 1996; Nicolas *et al.*, 1998).

Put together, the activation of Spz for competent Toll signalling can be achieved by different spatiotemporal expression of two distinct serine proteases, and that the same ligand-receptor pair can be utilised for different physiological processes (Jang *et al.*, 2006; Jang *et al.*, 2008; Mulinari *et al.*, 2006).

#### 1.1.5.3 Similarities between Spz, Coagulogen and BDNF

The mechanism of Spz cleavage by active Ea and SPE in the perivitelline fluid and hemolypmh, respectively, bears resemblances to two systems: the clotting cascade in the hemolymph of horseshoe crab (*Limulus*), and the expression of protein-synthesis-dependent, late-phase, long-term LTP (L-LTP) in the mouse hippocampal synaptic cleft.

Of the clotting cascade, coagulogen belongs to the CysKnot superfamily and its CysKnot resembles those of Spz and NGF (Bergner *et al.*, 1996). Coagulogen is actually closest in structural identity to Spz4 than it is to Spz, but current phylogenetic tools do not resolve coagulogen as sufficiently different from Spz and NTs (Zhu *et al.*, 2008). Although a Toll homology in horseshoe crab (tToll) does exist to mediate immunity, it is yet unknown if coagulogen may serve as a ligand for tToll and if coagulogen have neurotrophic functions in horseshoe crab (Inamori *et al.*, 2004; Zhu *et al.*, 2008). Unlike Spz and NGF, coagulogen does not dimerise (Bergner *et al.*, 1996; DeLotto and DeLotto, 1998; Mizuguchi *et al.*, 1998). Instead, coagulogen is proteolytic processed by a proclotting enzyme into insoluble coagulin which aggregates with each other into a gel (Bergner *et al.*, 1996; Iwanaga, 1993). The proclotting enzyme bears similarity to Ea and SPE in that they all need to be activated through a protease cascade (Bergner *et al.*, 1996; Iwanaga, 1993).

Spz and BDNF belong to the NT superfamily. BDNF in the adult brain regulates synaptic plasticity with important implications for depression and memory (Lu *et al.*, 2005; Martinowich *et al.*, 2007; Poo, 2001). BDNF is secreted constitutively in its pro-form (proBDNF) from post-synaptic hippocampal neurons (Lu *et al.*, 2005; Mowla *et al.*, 1999). Without cleavage to release the prodomain, proBDNF facilitate LTD through receptor p75 signalling (Lu *et al.*, 2005; Rosch *et al.*, 2005; Woo *et al.*, 2005). Upon high stimulus stimulation, tissue plasminogen activator (tPA) is released from the pre-synaptic neuron (Lu *et al.*, 2005; Pang *et al.*, 2004). In the synaptic cleft, tPA meets and cleaves inactive zymogen plasminogen into active serine protease plasmin (Lu *et al.*, 2005; Pang *et al.*, 2004). Plasmin, in turn, cleaves extracellular proBDNF into mature BDNF (mBDNF), a key protein product for the expression of L-LTP through receptor TrkB signalling as well as the increase in spine density which is analogous to synaptic structure formation (Lu *et al.*, 2005; Pang *et al.*, 2004).

In short, Spz, NGF and coagulogen share similarities in CysKnot structure, with Spz and coagulogen serving roles in immunity. Spz and coagulogen are both processed by extracellular proteases. Recently, NGF has been demonstrated to have a Spz-like immunity role against *Staphylococcus aureus* infection in vertebrates through receptor TrkA (Hepburn *et al.*, 2014). Given the active roles Spz/Toll and NGF/TrkA signalling play in the immune and nervous systems, it is therefore intriguing to speculate if coagulogen and tToll exert neurotrophic effects in the horseshoe crab too. Between Spz and BDNF, they share similar traits in the manner of their secretion as pro-forms and in the cleavage of their pro-forms by active serine proteases, albeit for the separate physiological functions of development, immunity and L-LTP.

Comparing secretion of Spz in the *Drosophila* and mammalian systems adds further parallels between the two and alongside structural and functional homology. However, secretion of NTs is influenced by the cell type, the environment and whether or not the function will be carried out in an autocrine or paracrine manner. NGF is well-understood for its role as a target-derived trophic factor during development of early peripheral nervous system (Cohen and Levi-Montalcini, 1956; Davies, 1996; Levi-Montalcini and Cohen, 1960; Lewin and Barde, 1996). In this case, NGF is well-known to be cleaved by furin through the constitutive secretory pathway within the target tissue to be secreted for the survival of sufficient numbers of connecting neurons (Lu *et al.*, 2005; Mowla *et al.*, 1999). In spite of NGF's discovery as a neurotrophic factor, NGF mediates apoptosis too (Lu *et al.*, 2005; Nykjaer *et al.*, 2005). As an example, when the tissue environment is perturbed, as in the case of adult brain injury, proNGF is secreted and binds p75 *in vivo* to trigger lesion-induced death of adult corticospinal neurons (Harrington *et al.*, 2004). For the expression of hippocampal L-LTP, proBDNF is secreted by the post-synaptic neuron and is processed extracellularly by plasmin into mBDNF, which acts in an autocrine manner on TrkB on the post-synaptic side (Lu *et al.*, 2005; Pang *et al.*, 2004). For LTD, proBDNF binds p75 (Rosch *et al.*, 2005). These do not rule out proBDNF being processed intracellularly. Indeed, mBDNF is found intracellularly and differs from mNGF in that mBDNF is better retained by the regulated secretory pathway within hippocampal neurons (Mowla *et al.*, 1999). The release of both mBDNF and isolated BDNF pro-domain from hippocampal neurons requires high frequency activity (Anastasia *et al.*, 2013; Nagappan *et al.*, 2009). However, for Schwann cells, the principal glia of the PNS, both proBDNF and mBDNF are released into the extracellular space without stimulation, suggesting that differential intracellular sorting of pro- and mature NTs occurs in different cell

types (Lu *et al.*, 2005; Mowla *et al.*, 1999). At present time, our knowledge of sorting the DNTs pertains to the extracellular secretion of proSpz.

#### 1.1.5.4 Mutations in *dnt* Genes

At the time of identifying DNTs within the Spz protein family, the mutants used to study Spz, DNT1 and DNT2 were $spz^{2}$, $dnt1^{41}$, $dnt1^{55}$ and $dnt2^{e03444}$ (Zhu *et al.*, 2008).

##### 1.1.5.4.1 Point Mutations in *spz*

$Spz^{2}$ is a point mutant allele which arose from the carcinogenic mutagen ethyl methanesulfonate (EMS) (Tearle and Nusslein-Volhard, 1987). The use of EMS brings about mutagenesis in a stochastic manner throughout the genome such that it is very likely *spz* would not be the only gene affected by the mutagenic treatment. Within the *spz* locus anyhow, the point mutation is a nucleotide substitution of a thymine base at position 400 into an adenine which results in an amino acid replacement of tyrosine-134 into asparagine (Y134N) (Weber *et al.*, 2007). The amino acid residue 134 is located in the pro-domain 31 amino acids preceding Ea's proteolytic processing site (Weber *et al.*, 2007). The effect of the $spz^{2}$ mutation is twofold: secretion of proSpz is ineffective and any secreted proSpz exists either as monomers (with an absent disulphide bond) or as multimers (with multiple disulphide-linked aggregates) (Weber *et al.*, 2007). The importance of the prodomain is highlighted also in NGF as critical for the secretion and proper folding of mNGF (Rattenholl *et al.*, 2001; Suter *et al.*, 1991). However, the prodomain does not interfere with Toll signalling so any phenotype which arise from $spz^{2}$ would be restrictive to defective processing of dimeric Spz pro-protein

and would not in principle encompass Toll and associated downstream signalling (Weber *et al.*, 2007). Nonetheless, the $spz^2$ allele remains interesting for the reason that there is a common single nucleotide polymorphism (SNP) which converts valine to methionine at codon 66 within the prodomain of the human *bdnf* gene ($bdnf^{Val66Met}$) (Egan *et al.*, 2003).

Human subjects heterozygous for the variant BDNF ($bdnf^{Val66}/bdnf^{Met}$), the most predominant expression profile, were associated with poorer episodic memory and abnormal hippocampal activation (Egan *et al.*, 2003; Hariri *et al.*, 2003). In the Golgi apparatus, Sortilin interacts with the prodomain of BDNF in the specific region containing codon 66 and mediates the efficient intracellular targeting of proBDNF to the regulatory secretory pathways (Chen *et al.*, 2005). The Met66 substitution alters the binding interaction between proBDNF and Sortilin in the Golgi apparatus such that the intracellular trafficking of proBDNF is inefficiently sorted into secretory granules in cortical neurons (Chen *et al.*, 2005; Chen *et al.*, 2004). $ProBDNF^{Val66}$ is distributed more uniformly in the hippocampal cell bodies and dendrites while $proBDNF^{Met66}$ aggregates in the perinuclear region (Egan *et al.*, 2003). The inefficient trafficking and sorting of proBDNF ultimately results in less proBDNF secreted from cortical and hippocampal neurons upon stimulating activity (Chen *et al.*, 2004; Egan *et al.*, 2003). So there are parallels between $spz^2$ and $bdnf^{Val66Met}$ in the way the prodomain mutation affect its secretion. Proteolytic processing of proBDNF is unaffected (Chen *et al.*, 2004), but in the mice subventricular zone (SVZ) and dentate gyrus (DG), the two brain areas important for adult neurogenesis (Ming and Song, 2011), TrkB activation is decreased (presumably due to less proBDNF secretion), LTP is affected and there are less survival of newborn neural progenitor cells (Bath *et al.*, 2012; Bath *et al.*, 2008). Single- and double-copy $bdnf^{Met66}$ knock-in mice have smaller hippocampal volume (Chen *et al.*, 2006). Because BDNF

regulates neuronal differentiation and synaptic plasticity, the impact on hippocampal volume is attributed to altered neuronal morphology, and indeed, *bdnf*$^{Met66}$ knock-in mice display decreased dendritic arbor complexity (according to Sholl analysis) and smaller dendritic field occupancy by DG neurons (Chen *et al.*, 2006).

The prodomain itself is an interesting entity because its biological function, if any, is unknown, even though the isolated prodomain is a natural cleavage by-product of the proNTs into mature NTs. So far, the prodomain in proSpz form is known molecularly to prevent proSpz from interacting with Toll to limit bioavailability and to stabilise C106 (Arnot *et al.*, 2010; Hoffmann *et al.*, 2008; Weber *et al.*, 2007; Weber *et al.*, 2003). Weber *et al.* (2007) hypothesised that the prodomain of Spz remains associated to CysKnot and would not be released until after Toll binding to limit the diffusion of the CysKnot and thereby ensure a maximal impactful ventralising signal. Following receptor engagement, the prodomain would be released for subsequent lateral inhibition by acting as a negative regulator at the level of Easter processing, active Easter or the Spz processing reaction (Weber *et al.*, 2007). It is easy to wonder if the isolated prodomain of Spz also acts as a negative regulator of SPE in immunity after Toll-dependent upregulation of SPE. When the prodomain of BDNF is released, it is monomeric (Anastasia *et al.*, 2013). The function of the isolated Val66 prodomain remains to be elucidated, but the Met66 prodomain in the extracellular space is an active ligand which promotes growth cone retraction in hippocampal neurons via p75 and SorCS2, a sortilin-related sorting receptor (Anastasia *et al.*, 2013).

There are two other EMS-derived point mutants of *spz* available: *spz*$^{3}$ and *spz*$^{4}$ (Tearle and Nusslein-Volhard, 1987). Both alleles are point mutants in the CysKnot domain (Weber *et al.*,

2007). In *spz*$^{3}$, glutamine-207 is replaced by arginine (Q207R), while in *spz*$^{4}$, a conserved cysteine residue of Spz, NGF, BDNF and NT-3 is replaced by serine (C232S) (Weber *et al.*, 2007). The Q207R mutation of *spz*$^{3}$ is thought to cause conformational changes in C106 such that Spz's interaction with Toll is abolished. With *spz*$^{4}$, the CysKnot structure could be compromised by changes in protein packing or by an absence of a canonical intra-disulphide bond (Mizuguchi *et al.*, 1998; Weber *et al.*, 2007).

#### 1.1.5.4.2 Mutations in *dnt1* and *dnt2* Genes

*Dnt1*$^{41}$ and *dnt1*$^{55}$ were generated by homologous recombination for the studies in Zhu *et al.* (2008), and were verified to be genetic null alleles by PCR, Southern blot and reverse transcriptase PCR. The nulls *dnt1*$^{41}$ and *dnt1*$^{55}$ are ideal standard loss of function mutants.

*Dnt2*$^{e03444}$ was the only available mutant allele at the time of study by Zhu *et al.* (2008), and it is the *dnt2* allele with a large 5.9 kb transposon insert in its intronic region, after the exon encoding the signal peptide (Dos Santos *et al.*, 2015). The downside of using *dnt2*$^{e03444}$ is the possibility of the insert being spliced out and excluded from the mature RNA for protein translation. This could effectively create functional DNT2 protein.

### 1.1.5.5 Toll Receptors of DNTs

The Toll receptor superfamily, comprising the *Drosophila* Tolls and the vertebrate Toll-like receptors (TLRs), is collectively known for innate immunity functions (Leulier and Lemaitre, 2008; Ooi *et al.*, 2002; Tauszig *et al.*, 2000). There are 9 Toll receptor paralogues in

*Drosophila*: Toll, Toll2/18wheeler, Toll3/MstProx, Toll4, Toll5/Tehao, Toll6, Toll7, Toll8/Tollo and Toll9 (Leulier and Lemaitre, 2008). Spz is the ligand for Toll (Weber *et al.*, 2003), and is proposed to bind more than one Toll receptor to activate NFκB-dependent apoptosis, prominently Toll2, Toll3, Toll8 and Toll9, to remove unfit cells such that they do not become part of future tissue materials (Meyer *et al.*, 2014b). Spz3 paralogue is reported to be a likely ligand for Tollo genetically (Ballard *et al.*, 2014). All the mentioned receptors proposed for Spz requires biochemical confirmation.

## 1.2 *Drosophila* as a Model Organism and Technical Approach

### 1.2.1 Larval CNS Anatomy

The larval CNS is comprised of: (1) the brain in two hemispheres, each with an optic lobe, and connected by the central brain commissures; and (2) the VNC, with thoracic and abdominal parts (Hartenstein, 1993). The VNC is homologous to the human spinal cord. The thoracic VNC is made up of 3 segments, T1 to T3, while the abdominal VNC is made up of 8 or 9 segments, A1 to A8/9 (Ito *et al.*, 1995). An open-access figure on the schematics of neurons in the *Drosophila* CNS is provided in Figure 1.2 (Sanchez-Soriano *et al.*, 2005).

Synaptic contacts are restricted to the neuropile, a cell-body free area. The neuropile also contains the ascending, descending and commissural axon fiber tracts (Ito *et al.*, 1995). Neuronal and glia cell bodies, and neuroblasts, are restricted to the cortex, a synapse-free area (Hartenstein, 1993; Ito *et al.*, 1995). The VNC circuitry consists of interneurons and efferent neurons which send out monopolar projections into the neuropile, where they form

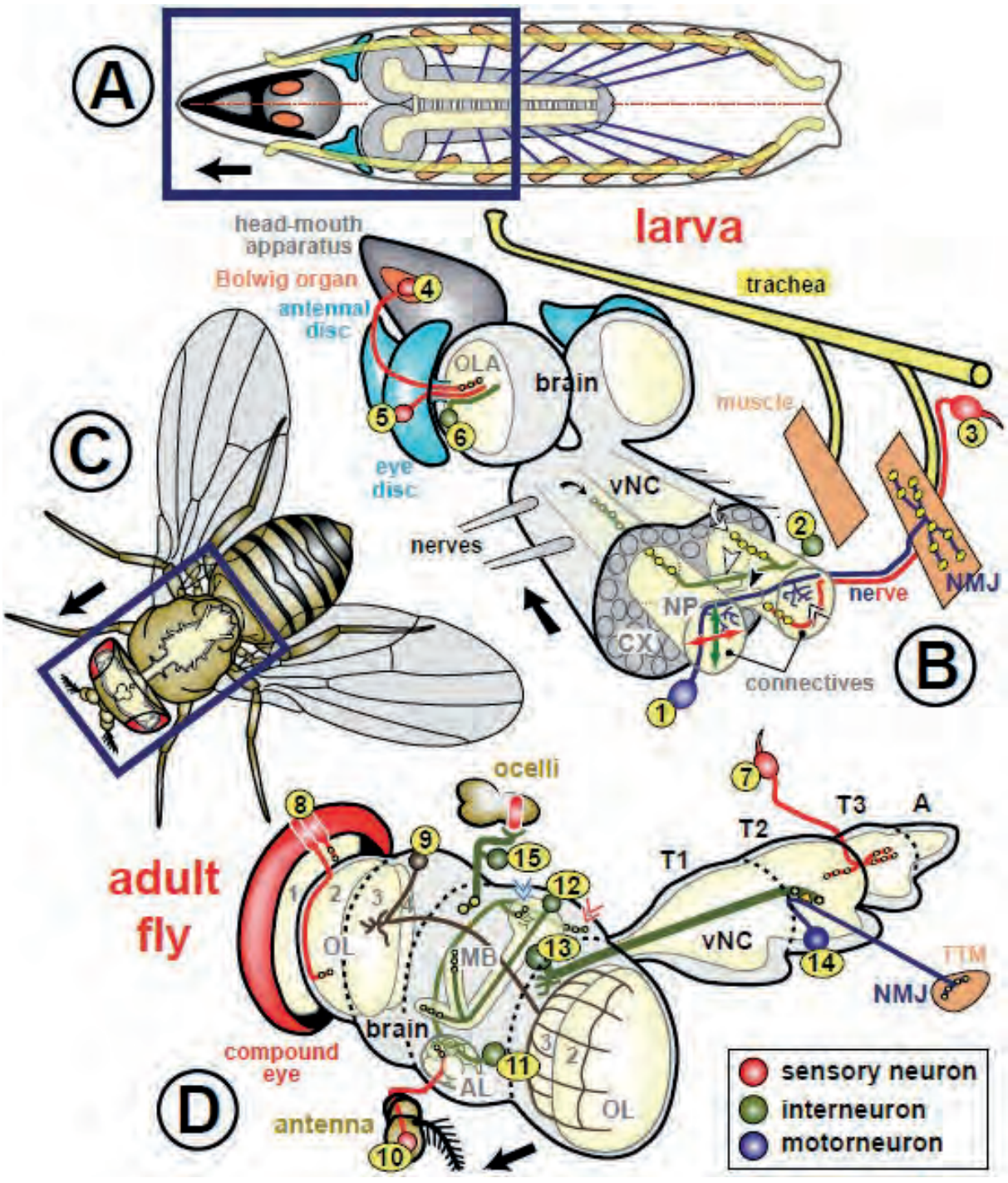


**Figure 1.2** Schematics of neurons in the Drosophila CNS reproduced from Sanchez-Soriano *et al*. (2005).

arborisations and synapses (Sanchez-Soriano *et al.*, 2005). The neurites of the CNS interneurons and efferent neurons are joined by projections from the peripheral afferent, sensory neurons (Landgraf *et al.*, 2003). Efferent neurons also project from theneuropile through segmentally repeated nerves into the periphery, where motoneurons meet muscle and form neuromuscular junctions (NMJs) (Landgraf *et al.*, 2003). Sensory neurons (such as mechanosensory chordotonal neurons) project through ventral nerve roots to innervate the sensory output region in the ventral VNC while motoneurons project through dorsal nerve roots from the motor input area in the dorsal VNC (Landgraf *et al.*, 2003; Zlatic *et al.*, 2009). All the motoneurons form dendrites in the dorsal neuropile, including aCC and RP2 motoneurons (Landgraf *et al.*, 2003).

Glial cells in the VNC are classified into surface, cortex and neuropile-associated glia (Ito *et al.*, 1995). Interface glia (IG) are a subset of neuropile-associated glia at the cortex-neuropile boundary (Ito *et al.*, 1995). The surface of the CNS is covered by the perineurium, which consists of the acellular extracellular matrix (ECM), called the neural lamella, and the surface-associated glial cells underneath (Ito *et al.*, 1995). Anti-Ebony, anti-GS2 and anti-Repo antibodies are all glial differentiation markers, and all three can detect IG. IG can also be visualised using *alrm-GAL4*. All glia nuclei, except those of midline glia, can be marked by anti-Repo.

#### 1.2.1.1 Mutations Affecting VNC Length

Towards the end of embryogenesis, the VNC condenses, while in the larval stages, there is growth in the VNC. During larval development, the neural lamella adjust to the growing

nervous system and perineural glial cells secrete proteases to remodel the neural lamella (Meyer *et al.*, 2014a).

Earlier, PVR was mentioned to be a gliatrophic factor (Learte *et al.*, 2008). Disrupting *pvr* inhibits hemocyte migration, which in turn means deposition of extracellular matrix (ECM) around embryonic tissues is lost and VNC fails to condense (Olofsson and Page, 2005).

RK2 is a glial specific homeodomain protein which is expressed in all embryonic glial cells, with the exception of midline glia and glia cells sibling to external sensory neurons (Campbell *et al.*, 1994). Embryos mutant for *rk2* are embryonic lethal and their nerve cord fails to condense properly (Campbell *et al.*, 1994).

Core 1 galactosyltransferases (C1GalTA) elongate their substrates by adding galactose, and it is expressed in the embryonic amnioserosa and CNS (Lin *et al.*, 2008). Mutant *C1GalTA* animals exhibited elongated larval VNC and misshaped brain hemispheres (Lin *et al.*, 2008). C1GalTA is required to glycosylate laminin, a component of the ECM (Lin *et al.*, 2008).

Impaired enzyme activity of glucuronyltransferase P (GlcAT-P) also results in elongated larval VNC (Pandey *et al.*, 2011). With *repo-GAL4* in the background of mutant *GlcAT-P*, VNC elongation enhanced (Pandey *et al.*, 2011). Overexpressing GlcAT-P in hemocytes in the background of mutant *GlcAT-P* rescues VNC length (Pandey *et al.*, 2011).

In short, mutations which intricately affect the extracellular matrix, glia and hemocytes generally result in an elongated VNC phenotype.

#### 1.2.1.2 Mutations Affecting Cell Numbers in the Larval VNC

Neuroblasts are *Drosophila* neural progenitor cells which are capable of self-renewing, differentiating or entering quiescence (Lai and Doe, 2014; Maurange and Gould, 2005; Maurange and Lanet, 2014). With the neuroblasts, *Drosophila* undergo two distinct phases of neurogenesis, embryonic and postembryonic, which are separated by quiescence (Saini and Reichert, 2012). The embryonic neurogenesis is responsible for building the larval CNS, whereas embryonic and postembryonic neurogenesis are both responsible together for building the adult fly CNS. During the third larval instar, thoracic and abdominal VNC neuroblasts acquire competence to undergo apoptosis, but the only brain and thoracic neuroblasts re-enter the cell cycle while abdominal neuroblast undergo cell death (Maurange and Gould, 2005; Maurange and Lanet, 2014). Unregulated neuroblast division has been shown to result in tumorous overproliferation (Saini and Reichert, 2012; Southall *et al.*, 2008). Postmitotic neurons are also capable of dedifferentiating to neural progenitor cell-like state, as in *lola* mutants, in which the number of neurons decrease but the number of progenitors increase to form tumors (Southall *et al.*, 2014). Mutations in cell fate determinants such as Brat, Numb and Prospero will affect neuronal number due to disruption in the neurogenic differentiation pathway (Saini and Reichert, 2012; Southall *et al.*, 2014; Southall *et al.*, 2008).

With the exception of midline glia, all embryonic gliogenesis is promoted by *glial cell missing* (*gcm*) which suppressed neuronal fate and induced *reverse polarity* (*repo*) to confer stable glial identity through (Awasaki *et al.*, 2008; Flici *et al.*, 2014; Jones *et al.*, 1995). In

general, glial number is tightly coordinated with signals from neurons (Hidalgo and Griffiths, 2004; Hidalgo *et al.*, 2011; Hidalgo *et al.*, 2001; Kinrade *et al.*, 2001).

### 1.2.2 Injury in the Larval CNS

Regeneration is a biological phenomenon which confers a metazoan the ability to physically and functionally restore its damaged or lost body parts. This regenerative ability occurs at many levels throughout the animal kingdom including humans (Carlson, 2007). While regeneration in humans is prominent in certain tissues and organs such as the skin and the liver, the central nervous system (CNS) exhibits poor regenerative ability following traumatic injury and chemotoxicity, or as a result of ongoing degenerative processes (Carlson, 2007; Horner and Gage, 2000). As such, injured and degenerating CNS is devastating and debilitating (Horner and Gage, 2000). It is acknowledged that the poor regenerative ability of the CNS comes down to the fact that CNS regeneration itself is a multistep process at the cellular level, and yet this process is challenged by diminishing intrinsic growth ability and a series of antagonistic events at the lesion site (Ferraro *et al.*, 2004; Fitch and Silver, 2008; Horner and Gage, 2000; Liu *et al.*, 2011). (a) An injured neuron must first survive, but secondary damage by the immune system exacerbates neuronal damage. (b) Then, surviving damaged axons must circumvent the inhibitory factors in the CNS environment to extend and to re-establish connections with their target cells; otherwise, misrouting can occur, leading to axonal degeneration or faulty connections. (c) Upon contact, axons need to be remyelinated in order to mediate reliable electrical conduction. (d) Finally, functional synapses must form for connectivity. In pursuing and developing strategies for promoting CNS regeneration, promising leads include drug-induced release of neurotrophic factors by glia or neurons, and

the possibility of therapeutic delivery of neurotrophic factors (Ahmed *et al.*, 2009; Douglas *et al.*, 2009; Jacques *et al.*, 2012).

*Drosophila* is an incredibly powerful model organism to investigate gene function *in vivo* and discover gene networks as well as neuronal circuits (Bier, 2005; Olsen and Wilson, 2008). Many gene functions and gene networks have a high degree of evolutionary conservation. *Drosophila* offers a wide variety of experimental tools and has repeatedly propelled mammalian research and the understanding of human diseases, including developmental and neurological disorders (Bellen *et al.*, 2010; Bier, 2005; Jeibmann and Paulus, 2009).

As the nervous system develops in volume and cell number, wiring connections are established. Injury models can help our understanding of how growth happens as the nervous system develops and wires. Injury paradigms link to understanding development by addressing how the nervous system deal with injury to restore a working organ with wiring re-established. Also, attempts at recapitulating development itself in adulthood can maximise the effectiveness of biological processes in regeneration (Harel and Strittmatter, 2006). An example of applying this form of scientific thinking into action uncovered the gene network consisting of cell cycle inhibitor Prospero (Pros) and cell cycle activators, Notch and Dorsal/NFκB, which together maintain an arrested, proliferative ability of glial cells in the *Drosophila* larvae (Kato *et al.*, 2011). Glial cells proliferate in response to VNC injury in the larvae using the Pros-Notch-NFκB gene network (Kato *et al.*, 2011). Glial cells which lose proliferative potential, such as those in adult flies 8 days after eclosion, do not respond to brain injury (Kato *et al.*, 2009).

When a stabbing injury is applied dorsally to a normal larva's abdominal VNC using a fine tungsten needle, a wound is generated which initially expands in area and subsequently shrinks, indicating gross anatomical repair to an extent (Kato and Hidalgo, 2013). When the intracellular domain of Notch ($Notch^{ICD}$) is overexpressed from glia, the larval VNC length extended due to an increase in glial numbers (Kato *et al.*, 2011). Remarkably, upon injury of VNC in the background of $Notch^{ICD}$ being overexpressed from glia, wound enlargement is prevented, injury-induced apoptosis is rescued, and the wound effectively closed as observed by time-lapse imaging of the area of lesion shrinking completely (Kato *et al.*, 2011). This suggests either $Notch^{ICD}$ in glia has a pro-survival function, or that the increase in glia numbers, in the background of $Notch^{ICD}$ being overexpressed, led to an overproduction of a trophic factor. Spz could be expressed in larval glia (Sutcliffe, 2011), and so Spz could be overproduced to provide more trophic support.

Spz binds Toll, which act upstream of NFκB. Upon injury of the CNS, NFκB is important for promoting glial cell division (Kato *et al.*, 2011). Such links makes the DNTs, as secreted ligands with trophic activity, interesting candidates to study for potential roles in CNS repair. In particular, Spz would be most promising because its receptor, Toll, has an additional function of cellular adhesion, important for cell-cell interactions (Halfon *et al.*, 1995; Keith and Gay, 1990). Also, Spz is thought to bind to other Toll receptors, including Toll-2, Toll6 and Toll-8 (McIlroy, 2012; Meyer *et al.*, 2014b), receptors which mediate heterophilic interactions between cells to promote oriented cell arrangements (Pare *et al.*, 2014). Recently, a Spz-independent Toll/NFκB pathway has been characterised for epidermal wound repair in *Drosophila* (Carvalho *et al.*, 2014). This suggest that Spz is not the only activating ligand of

Toll (Carvalho *et al.*, 2014). Nonetheless, this does not rule out the role Spz could possibly play for CNS repair.

## 1.3 Rationale of the Project

*Spz*, *dnt1* and *dnt2* are expressed in the embryonic CNS and muscle, where they are required for neuronal survival and targeting by motoneurons (Zhu *et al.*, 2008). In the larvae, *spz, dnt1* and *dnt2* are expressed in the body wall muscles, where they regulate NMJ synaptogenesis (Sutcliffe *et al.*, 2013). Yet, two issues remain to be understood: (1) to what extent do the DNTs influence cell number in the formation of the nervous system circuitry after embryonic stages to result in a behaving larva; and (2) to what extent do the developmental functions of DNTs influence the capacity of the larval CNS to repair after injury.

To contribute to an understanding towards the functional role of DNTs in the regulation of cell numbers within the larval CNS, this project needs to first address whether or not the DNTs remain biologically relevant after embryonic stages in the larval CNS (see Chapter 3).

To study loss of function effects, there must be appropriate loss of function mutants. There are suitable null mutants for *dnt1* for studying loss of function effects, but more appropriate loss of function mutants for *spz* and *dnt2* could be generated (Section 1.1.5.4). For this purpose, this project aims to generate null mutants of *dnt2* and *spz* via targeted deletions (see Chapter 4). Since there is a naturally occurring SNP in the prodomain of BDNF, the $spz^2$ allele is still interesting to study (Section 1.1.5.4.1). Therefore, the effects of $spz^2$ in the larval CNS will be characterised (see Chapter 5).

Toll6 and Toll7 genetically rescue the viability of homozygous *spz*$^{2}$ mutants (Dr A. Hidalgo, personal communication). Homozygous *spz*$^{2}$ adult mutants have been reported to have very small optic lobes (N. Ruiz & Dr J. Wentzell, personal communication). By extending the viability experiment and looking into the effect Toll6 and Toll7 genetically exert on homozygous *spz*$^{2}$ CNS size, Toll6 and Toll7 will be tested as potential receptors for Spz (see Chapter 5).

The overexpression of Notch$^{ICD}$ in glia prevents injury-induced apoptosis. The pro-survival effect could be exerted directly by Notch$^{ICD}$ or indirectly through increasing glia numbers upon the overexpression of Notch$^{ICD}$. This project will test for an interaction between the DNTs and Notch in the background of pan-glial overexpression of Notch$^{ICD}$ (see Chapter 5). The project will also use the stabbing injury method developed by Kato *et al.* (2011) to investigate the function of DNTs in gross CNS repair (see Chapter 6).

## 1.4 Aims of the Project

- To characterise the larval expression patterns of *spz*, *dnt1* and *dnt2* using the GAL4 reporter system.
- To determine the larval distribution patterns of Spz, DNT1, DNT2, Toll, Toll6 and Toll7 using purposely developed antibodies.
- To generate *spz* and *dnt2* null alleles as tools for functional analysis.
- To characterise the *spz*$^{2}$ allele by examining its effect on glial and neuronal structures.
- To test whether Toll6 and Toll7 are potential receptors of Spz using genetics.

- To investigate the functions of *spz*, *dnt1* and *dnt2* in the larval CNS by examining their effects on glial, mitotic and apoptotic cell numbers.
- To test whether there is an interaction between the DNTs and the Notch member of the gene network underlying glial cell proliferation upon VNC injury.
- To investigate whether loss or gain of function in components of the DNT system affects larval gross CNS repair.

# Chapter 2

# 2 Materials and Methods

## 2.1 Genetics

### 2.1.1 Housing and Handling *Drosophila*

Flies were bred on cornmeal agar medium made by the Central Services Team of the School of Biosciences in the University of Birmingham. Cornmeal agar medium was dispensed as 12mL food aliquots into glass vials. Vials contained food at the bottom and were plugged with cotton wool. Female flies lay their eggs on the food surface where the larvae hatch. Larvae go through three instar stages, living and feeding in the food until wandering stage, that is, when third instar larvae undergo a behavioural change (Ashburner *et al.*, 2005). Wandering larvae are larvae which leave the moist food medium to preferably climb up the dry walls of the vial where they will pupariate and subsequently eclose as flies (Ashburner *et al.*, 2005; Godoy-Herrera *et al.*, 1984; Roote and Prokop, 2013). Stock-keeping involved mass transferring flies to fresh food vials every 28 days. The fly stocks used in this project are listed in Table 2.1. Unless otherwise indicated, stocks were maintained in temperature-controlled incubators at 18°C while experiments and crosses to make stocks were conducted at 25°C. Stocks and experiments were both kept under a 24-hour cycle of 12hrs dark and 12hrs light in the temperature-controlled incubators to ensure a constant lighting condition surrounding circadian-regulated proteins.

| No. | Genotype | Source (and Publication) | Use |
|---|---|---|---|
| 1 | *yw;;* | Hidalgo Lab | Chapters 3 to 6 |
| 2 | *Oregon-R* | Hidalgo Lab < J. Wentzell | Chapter 3 |
| 3 | *w;;MKRS/TM6B,LacZ* | Hidalgo Lab | as intermediate to make fly stocks |
| 4 | *w;If/CyO;MKRS/TM6B* | Hidalgo Lab | as intermediate to make fly stocks |
| 5 | *hsFLP*, $y^1$ $w^{1118}$;;$Dr^{Mio}$/*TM3*, $ry^*$ $Sb^1$ | BDSC #7 | as intermediate to make fly stocks |
| 6 | $w^{118}$;*PBac{RB}dnt2*$^{e03444}$ | BDSC #18155 < Exelixis at HMS #e03444 (Thibault *et al.*, 2004) | as intermediate to make fly stocks |
| 7 | ;;*P{XP}d05170* | Exelixis at HMS #d05170 (Thibault *et al.*, 2004) | as intermediate to make fly stocks |
| 8 | ;;*P{XP}spz*$^{d00069}$ | Exelixis at HMS #d00069 (Thibault *et al.*, 2004) | as intermediate to make fly stocks |
| 9 | ;;*PBac{RB}e00046* | Exelixis at HMS #e00046 (Thibault *et al.*, 2004) | as intermediate to make fly stocks |
| 10 | *w;alrm-GAL4#3/CyO;Dr/TM3,Sb* | Hidalgo Lab < M. Freeman (Doherty *et al.*, 2009) | Chapter 3 (as larval interface glia driver) |
| 11 | ;;*elav-GAL4* | Hidalgo Lab < Goodman Lab | Chapters 3, 5 and 6 (as neuronal driver) |
| 12 | *yw;pdf-GAL4;* | Hidalgo Lab | Chapters 3 (as larval lateral neuron driver) |
| 13 | ;;*repo-GAL4/TM6B* | Hidalgo Lab < K. Kato (Kato *et al.*, 2011) | Chapters 3, 5 and 6 (as glial driver) |
| 14 | $w^*$;*UAS-GAP-GFP;* | Hidalgo Lab < BDSC #4522 < A. Chiba | Chapter 3 (as fluorescent protein reporter) |
| 15 | ;*UAS-mCD8-GFP;* | Hidalgo Lab | Chapter 3 (as fluorescent protein reporter) |
| 16 | $w^*$;;*10xUAS-myr-tdTomato* | Hidalgo Lab < B. Pfeiffer (Pfeiffer *et al.*, 2010) | Chapter 3 (as fluorescent protein reporter) |
| 17 | *yw;;spz*$^{MI08633}$ | BDSC #51092 | Chapter 3 |

Table 2.1 Fly stocks used in this project (part 1/4).
The use of parenthesis surrounding balancers or markers in genotype labels indicates that a proportion of the stock can homozygosed and exists without having the stated balancers or markers. BDSC: Bloomington *Drosophila* Stock Centre. HMS: Harvard Medical School.

Table 2.1 Fly stocks used in this project (part 2/4).

| No. | Genotype | Source (and Publication) | Use |
|---|---|---|---|
| 18 | *;;Toll6$^{Mi02127}$/(TM6B,LacZ)* | M. A. Lim, protocol A (Figure 2.3) < BDSC #34467 | Chapter 3 (after balancer change) |
| 19 | *w$^{+}$;;spz$^{2}$ca$^{1}$/TM6B,LacZ* | Hidalgo Lab < B. Sutcliffe (Sutcliffe, 2011) < BDSC #3115 | Chapters 4 and 5 |
| 20 | *w$^{+}$;;spz$^{2}$ca$^{+}$.33/TM6B,LacZ* | M. A. Lim (Figure 2.8) | Chapter 5 |
| 21 | *w$^{+}$;;spz$^{2}$ca$^{+}$.56/TM6B,LacZ* | M. A. Lim (Figure 2.8) | Chapter 5 |
| 22 | *;;ru$^{1}$ st$^{1}$ ea$^{14}$ spz$^{3}$ ca$^{1}$/TM6B,LacZ* | Hidalgo Lab < B. Sutcliffe < BDSC #3287 | Chapters 4 and 5 |
| 23 | *;;ru$^{1}$ Diap$^{1}$ st$^{1}$ kni$^{ri-1}$ rn$^{roe-1}$ p$^{p}$ e$^{1}$ spz$^{4}$/TM6B,LacZ* | Hidalgo Lab < B. Sutcliffe (Sutcliffe, 2011)< BDSC #30915 | Chapters 4 and 5 |
| 24 | *w$^{-}$;;spz$^{MA05}$/TM6B* | M. A. Lim (Figure 2.11) | Chapters 3 to 6 |
| 25 | *w$^{-}$;;spz$^{MA10}$/TM6B* | M. A. Lim (Figure 2.11) | Chapter 4 |
| 26 | *w$^{-}$;;spz$^{MA12}$/TM6B* | M. A. Lim (Figure 2.11) | Chapter 4 |
| 27 | *spz-GAL4/(FM7);;+/(Sb$^{-}$)* | Hidalgo Lab < J. Wentzell | Chapter 5 |
| 28 | *spz-GAL4;;10xUAS-myr-tdTomato* | M. A. Lim, protocol C (Figure 2.5) | |
| 29 | *y$^{1}$ sc$^{*}$ v$^{1}$;P{TRiP.HMS01178}attP2* | BDSC #34699 (Ni *et al.*, 2011) | Chapter 3 (to knockdown *spz*) |
| 30 | *;;dnt1$^{41}$* | Hidalgo Lab < B. Zhu (Zhu *et al.*, 2008) | Chapters 3 to 5 |
| 31 | *;;dnt1$^{55}$* | Hidalgo Lab < B. Zhu (Zhu *et al.*, 2008) | Chapter 5 |
| 32 | *w;;dnt1-I-GAL4* | Hidalgo Lab < A. Hidalgo | Chapter 3 |
| 33 | *w;dntI-II-GAL4;* | Hidalgo Lab < A. Hidalgo | Chapter 3 |
| 34 | *w;+/(CyO);dnt1-III-GAL4/(MKRS)* | Hidalgo Lab < A. Hidalgo | Chapter 3 |
| 35 | *w;+/(CyO);dnt1-IV-GAL4/(MKRS)* | Hidalgo Lab < A. Hidalgo | Chapter 3 |
| 36 | *;;dnt2$^{18}$* | Hidalgo Lab < J. Wentzell | Chapter 4 |
| 37 | *;;dnt2$^{37}$/(TM6B)* | Hidalgo Lab < J. Wentzell | Chapters 3 to 4 |
| 38 | *w;+/(CyO);dnt2-GAL4/(MKRS)* | Hidalgo Lab < S. Alahmed | Chapter 3 |
| 39 | *;;Df(3R)Exel6205/TM6B* | Hidalgo Lab < B. Sutcliffe < BDSC #7684 (Parks *et al.*, 2004) | Chapters 3 to 6 |
| 40 | *;;Df(3L)Exel6101/TM6B* | Hidalgo Lab < J. Wentzell < BDSC #7580 (Parks *et al.*, 2004) | Chapter 3 |
| 41 | *;;Df(3L)Exel6092/TM6B* | Hidalgo Lab < J. Wentzell < BDSC #7571 (Parks *et al.*, 2004) | Chapter 3 |
| 42 | *ru$^{1}$ h$^{1}$ Diap$^{1}$ st$^{1}$ cu$^{1}$ sr$^{1}$ e$^{s}$ ca$^{1}$* | BDSC #576 | Chapter 5 |
| 43 | *;;spz$^{2}$,elav-GAL4/TM6B,LacZ* | Hidalgo Lab < B. Sutcliffe | Chapter 5 |
| 44 | *;;spz$^{2}$,repo-GAL4/TM6B,LacZ* | M. A. Lim, protocol B (Figure 2.4) | Chapter 5 |
| 45 | *;UAS-Toll$^{10bB}$;* | Hidalgo Lab (Zhu *et al.*, 2008) < T. Ip | Chapter 5 |

Table 2.1 Fly stocks used in this project (part 3/4).

| No. | Genotype | Source (and Publication) | Use |
|---|---|---|---|
| 46 | *UAS-Toll$^{10bB}$;spz$^{2}$ca$^{1}$/TM6B,LacZ* | Hidalgo Lab < Ben Sutcliffe (Sutcliffe, 2011) | Chapter 5 |
| 47 | *;UAS-Toll6$^{CY}$/SM6a;spz$^{2}$ca$^{1}$/TM6B* | Hidalgo Lab < A. Hidalgo (McIlroy *et al.*, 2013) | Chapter 5 |
| 48 | *;UAS-Toll7$^{CY}$;spz$^{2}$ca$^{1}$/TM6B* | Hidalgo Lab < A. Hidalgo (McIlroy *et al.*, 2013) | Chapter 5 |
| 49 | *w$^{*}$;;UAS-p35(2)* | BDSC #5073 | Chapter 5 |
| 50 | *;;UAS-p35,spz$^{2}$/TM6B,LacZ* | Hidalgo Lab < B. Sutcliffe (Sutcliffe, 2011) | Chapter 5 |
| 51 | *;+/(CyO);UAS-Notch$^{ICD}$-myc* | Hidalgo Lab < K. Kato (Kato *et al.*, 2011) < A. Martinez-Arias | Chapter 5 |
| 52 | *;UAS-histone-YFP/CyO,GAL80; repo-GAL4,UAS-Notch$^{ICD}$-myc#5.0/TM6B* | Hidalgo Lab < A. Hidalgo | Chapter 5 |
| 53 | *w;;UAS-actSpz(2);* | Hidalgo Lab (Zhu *et al.*, 2008) < J. M. Reichhardt | Chapters 3 and 5 |
| 54 | *w;;UAS-spz-FL-HA* | Hidalgo Lab | Chapter 5 |
| 55 | *w;;UAS-spz$^{2}$-E1* | Hidalgo Lab | Chapter 5 |
| 56 | *w;;UAS-DNT1-CK3'+* | Hidalgo Lab < B. Zhu (Zhu *et al.*, 2008) | Chapters 5 and 6 |
| 57 | *w;;UAS-DNT1-FL* | Hidalgo Lab < B. Zhu (Zhu *et al.*, 2008) | Chapter 5 |
| 58 | *w;;UAS-DNT2-CK-6A* | Hidalgo Lab < B. Zhu (Zhu *et al.*, 2008) | Chapters 5 and 6 |
| 59 | *;;UAS-DNT2-FL-47C* | Hidalgo Lab < B. Zhu | Chapter 5 |
| 60 | *;;Toll$^{r3}$ca$^{1}$/TM6B,LacZ* | Hidalgo Lab < B. Sutcliffe (Sutcliffe, 2011) < BDSC #3238 | Chapter 5 |
| 61 | *;;Df(3R)ro80b,st$^{1}$ e$^{1}$/TM6B* | Hidalgo Lab < B. Sutcliffe (Sutcliffe, 2011) < BDSC #2198 | Chapter 5 |
| 62 | *w;Toll7$^{P8}$;Toll6$^{26}$* | Hidalgo Lab < G. McIlroy (McIlroy *et al.*, 2013) | Chapters 5 and 6 |
| 63 | *w;Toll7$^{P114}$;Toll6$^{31}$* | Hidalgo Lab < G. McIlroy (McIlroy *et al.*, 2013) | Chapters 5 and 6 |
| 64 | *w;;RN2-FLP* | Hidalgo Lab < M. Landgraf (Ou *et al.*, 2008) | Chapter 5 |
| 65 | *;;spz$^{2}$,RN2-FLP/TM6B,LacZ* | Hidalgo Lab < Ben Sutcliffe | Chapter 5 |
| 66 | *w;UAS-myr-RFP, tub-FRT-CD2-FRT-GAL4, UAS-FLP/CyO,wg-LacZ;* | Hidalgo Lab < M. Landgraf | Chapter 5 |
| 67 | *;UAS-myr-RFP, tub-FRT-CD2-FRT-GAL4, UAS-FLP/CyO;spz$^{2}$ca$^{1}$/TM6B* | M. A. Lim & M. P. Nallasivan, protocol D (Figure 2.6) | Chapter 5 |

| No. | Genotype | Source (and Publication) | Use |
|---|---|---|---|
| 68 | *w*;*UAS-myr-RFP, tub-FRT-CD2-FRT-GAL4, UAS-FLP*/CyO; *Df(3R)Exel6205/TM6B* | M. A. Lim & M. P. Nallasivan, protocol D (Figure 2.6) | Chapter 5 |
| 69 | ;*G9*; | Hidalgo Lab < K. Kato (Kato *et al.*, 2011) < W. Chia (Morin *et al.*, 2001) | Chapter 6 |
| 70 | ;*G9*;*spz*$^{MA05}$/*TM6B* | M. A. Lim, protocol D (Figure 2.6) | Chapter 6 |

Table 2.1 Fly stocks used in this project (part 4/4).

For the purposes of selecting sex, collecting virgin females and scoring genetic markers, flies were first immobilised on porous pads through which carbon dioxide dispensed. Immobilised flies on porous pads were then visualised under a dissecting scope.

Unwanted flies were discarded into a morgue, which is a basic set-up of a jar containing industrial methylated spirit (IMS). Flies of desired phenotypes were transferred to fresh vials using a paint brush. Crosses to make stocks were established on Friday as day 0 to begin virgin female collection on day 10, Monday. These crosses were discarded after day 16 to prevent any recovery of second generation offspring.

Figure 2.1 shows how sex was routinely identified among *Drosophila*. Male flies were distinguished by the presence of sex combs in the first tarsal segment on the first pair of legs, while the female flies do not have sex combs (Ahuja and Singh, 2008; Ng and Kopp, 2008). Also, the males tend to have fully pigmented tergites in abdominal segments A5 and A6 while the females do not have full pigmentation in the corresponding tergites (Kopp *et al.*, 2000), so the males displayed uniformly dark dorsal cuticle plates at the posterior tip of the abdomen while the females displayed dark stripes dorsally. Males and females have dark and fair external genitalia, respectively (Bridges, 1936). After sex identification, females were securely recognised as virgins by meconium visible through the pleural cuticle of the abdominal sternum (Roote and Prokop, 2013). In other words, the first faecal waste product of the female was seen through the non-bristled areas on the ventral side of the abdomen as a dark spot (Weigmann *et al.*, 2003), as shown in Figure 2.1.

Mass transfer of flies to fresh food vials every 28 days was effective for stock-keeping

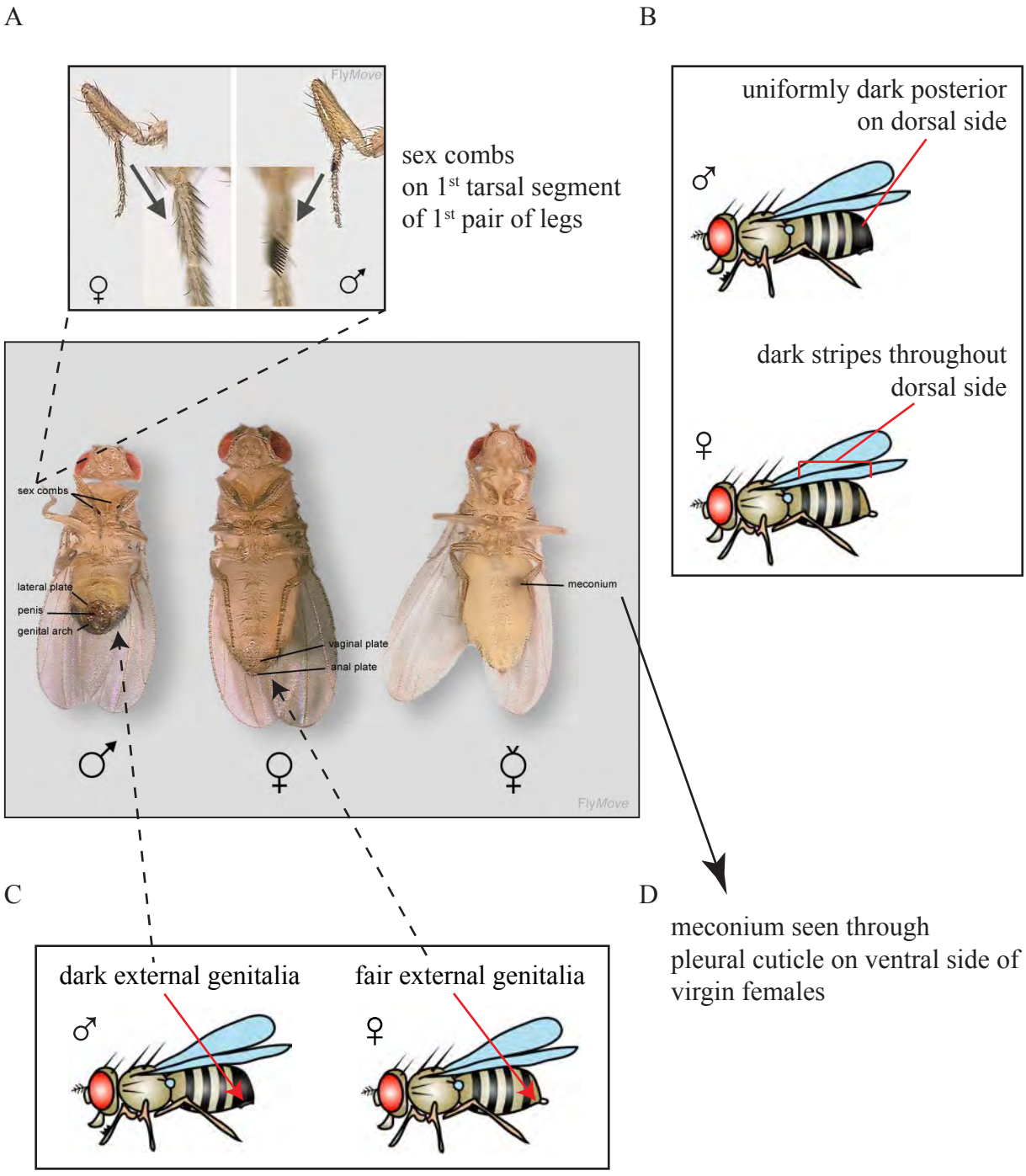


**Figure 2.1** Identification of sex and determination of sexual maturity among *Drosophila melanogaster*. **(A)** Sex combs, **(B)** pigmentation pattern of abdominal tergites, and **(C)** pigmentation levels of external genitalia were features used to identify sex. **(D)** Meconium of females were used to distinguished that the females were virgins. Fly photographs were reproduced from FlyMove website with permission (Weigmann *et al*., 2003). Fly images were constructed from the Genotype Builder Photoshop file published by Roote and Prokop (2013).

purposes, but it could result in overcrowded cultures. To prevent overcrowding when making fly stocks, 10 virgin females were inseminated by 6 males in an en masse cross, and the cross was transferred to a new vial every two or three days. To prevent overcrowding when conducting experiments, between 10-30 virgin females were crossed to 6-20 male flies in one vial, and the cross was transferred to a new vial every three hours, such that the egg laying time (ELT) was 3 hours. Only larvae from crosses with 3hrs ELT were used for experiments while larvae from crosses maintained overnight were discarded.

### 2.1.2 Standard Genetic Mating Protocols

A balancer is a chromosome with inversion breakpoints and deleterious (homozygous lethal) mutations, such that the same balancer chromosome cannot exist in homozygosis, but is instead useful to maintain other deleterious mutations in stable stocks from being lost from the population. Balancers also prevent recombination on the same chromosome and they allow chromosomes to be followed in genetic mating schemes using genetic markers. Some balancers carry transgenes such as *P{LacZ},* which is plasmid encoding the β-GALactosidase enzyme. The *LacZ* could be used for specific experiments, but no β-GALactosidase staining was performed in this project and so the mention of *LacZ* is limited to the fly stocks listed in Table 2.1.

Figure 2.2 illustrates the common genetic markers and balancers used in this project. A 'minus' symbol in superscript ($^{-}$), when used in labelling genotype, generally stands for any allele variants which is not wild-type while a 'plus' script, or superscript, symbolises the wild-type chromosome (+) and allele ($^{+}$). *Mini-white* ($w^{+m}$) is a gene construct derived from full-

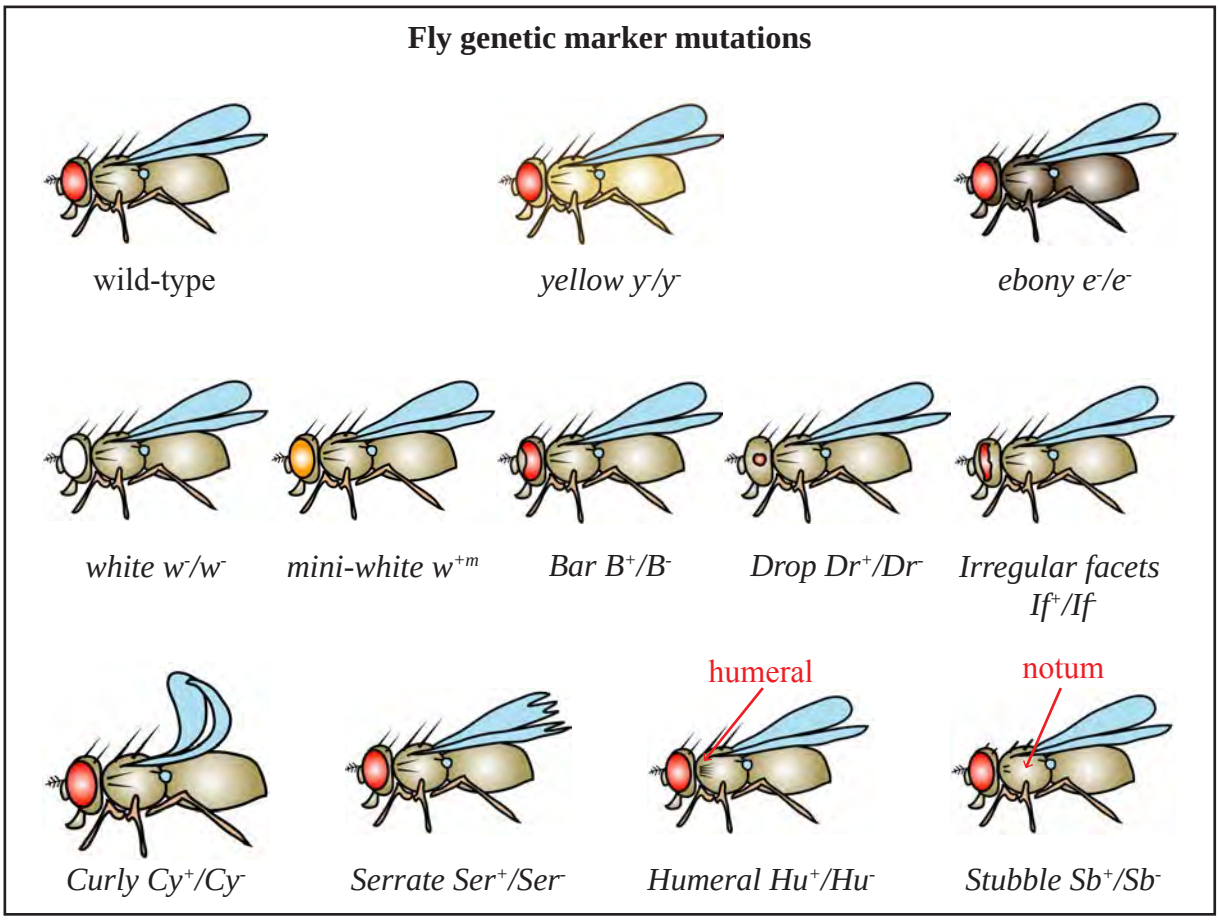


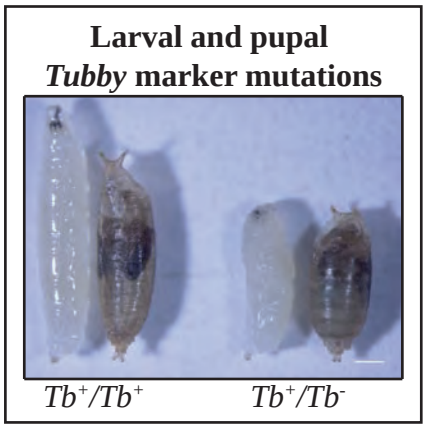


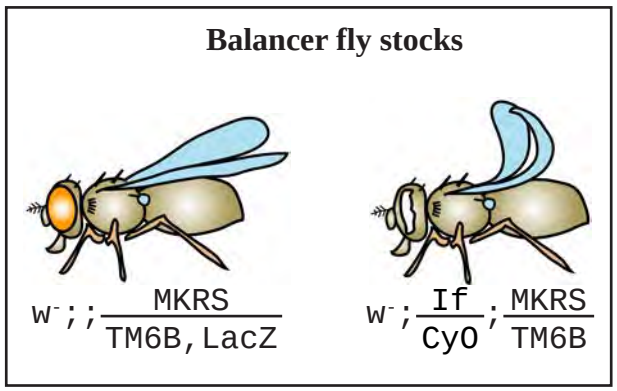


**Figure 2.2** Common *Drosophila* genetic markers and balancers used in this project. The recessive visible alleles are $y^-$, $e^-$ and $w^-$. The dominant visible alleles are $B^-$, $Dr^-$, $If^-$, $Cy^-$, $Ser^-$, $Hu^-$, $Sb^-$ and $Tb^-$. *Mini-white* ($w^{+m}$) is a transgene which results in orange eyes when inserted into flies with $w^-$ background. Flies of genotype *w-;;MKRS/TM6B,LacZ* (stock no. 3, Table 2.1) have orange eyes because the plasmid encoding *LacZ* also carried the sequence construct for $w^{+m}$. In addition, *w-;;MKRS/TM6B,LacZ* flies display stubble bristles on the notum and excess humeral bristles. Flies of genotype *w-;If/CyO;MKRS/TM6B* (stock no. 4, Table 2.1) are marked by white eyes having irregular facets, curly wings, stubble bristles on the notum and excess humeral bristles. Scale bar represents 0.5mm. Fly images were constructed from the Genotype Builder Photoshop file published by Roote and Prokop (2013).

length wild-type *white* gene ($w^+$), and when inserted into flies with $w^-$ background, the flies have orange eyes. $Dr^{Mio}$ is the dominant visible allele for the *Drop* gene which results in microphthalmia (reduced eyes) phenotype (Figure 2.2). The *Kruppel* allele, which arises in irregular facets in the eyes is $Kr^{If}$, but it is more commonly known as $If^-$ (Figure 2.2). Chromosome 1 in this project was balanced by *FM7*, which carries the dominant visible and non-lethal allele for the *Bar* gene, $B^1$ (Dos Santos *et al.*, 2015; Lindsley and Zimm, 1992). Heterozygous $B^+/B^1$ alleles manifest in the *Drosophila* fly as bar-shaped eyes (Figure 2.2), while flies which are homozygous $B^1/B^1$ display narrowly bar-shaped eyes. Chromosome 2 was balanced either by *CyO* or *SM6A*, which both carry the dominant visible allele for the *Curly* gene ($Cy^1$) that manifest in the *Drosophila* fly as curly wings (Dos Santos *et al.*, 2015; Lindsley and Zimm, 1992). *MKRS* and *TM3* are chromosome 3 balancers, and they carry the dominant visible allele for *Stubble* ($Sb^1$) which results in stubble bristles on the notum of the *Drosophila* fly (Dos Santos *et al.*, 2015; Lindsley and Zimm, 1992). *TM3* can also carry the dominant visible allele for the *Serrate* gene, $Ser^1$ (Dos Santos *et al.*, 2015; Lindsley and Zimm, 1992). Serrated wings appear to be clipped (Holtzman and Kaufman, 2013). *TM6B* is also a chromosome 3 balancer. In this project, the *TM6B* balancer used carries the dominant visible alleles for the *Antennapedia* ($Antp^{Hu}$ or *Hu*) and *Tubby* ($Tb^1$) genes, as well as the recessive visible alleles for *claret* ($ca^-$) and *ebony* ($e^-$) (Dos Santos *et al.*, 2015; Lindsley and Zimm, 1992). Given that $Tb^1$ manifest in the *Drosophila* larvae and pupae in the form of tubby bodies (Figure 2.2), *TM6B* was preferentially used over *MKRS* and *TM3* for balancing chromosome 3. $Antp^{Hu}$ results in excess humeral bristles in the *Drosophila* fly (Figure 2.2). The $ca^-$ and $e^-$ alleles give rise to phenotypes in the fly too. Flies have reduced red eye pigment and a black body as a result of homozygous $ca^-$ and $e^-$, respectively.

The exchange of balancers on chromosome 3 for the *TM6B* balancer was carried out according to protocol A (Figure 2.3). Alleles and transgenes on chromosome 3 were combined by recombination following protocol B (Figure 2.4). With alleles and transgenes on chromosomes 1 and 3 separately, they were combined according to protocol C (Figure 2.5). Genetic elements on chromosomes 2 and 3 separately were combined according to protocol D (Figure 2.6).

Gene expression was driven using the standard GAL4/UAS system as illustrated in Figure 2.7 (Brand and Perrimon, 1993). GAL4 is a yeast transcription factor and its expression in *Drosophila* is under the control of genomic enhancers. Targeted gene expression is dependent on activation of GAL4 binding sites called *Upstream Activation Sequence* (*UAS*). In the offspring of GAL4-expressing flies crossed to flies carrying the target gene behind the *UAS*, the target gene is activated in a cell- or tissue-specific pattern.

Exelixis fly deficiency lines are stocks with chromosomal deletion. *Df(3R)Exel6205/TM6B* (stock no. 39, Table 2.1), *Df(3L)Exel6101/TM6B* (stock no. 40, Table 2.1) and *Df(3L)Exel6092/TM6B* (stock no. 41, Table 2.1) were the deficiency lines used for the *spz*, *dnt1* and *dnt2* genes, respectively.

### 2.1.3 Genetic Protocol for Cleaning the $spz^2$ Allele of $ca^1$ Mutation

The fly stock $w^+;;spz^2ca^1/TM6B$ (stock no. 19, Table 2.1) had its $spz^2$ allele cleaned of the *claret* mutation ($ca^1$) by recombination according to the genetic scheme in Figure 2.8. All genotypes were in $w^+$ background to follow the *claret* allele which affects the red eye pigment

Protocol A: swapping balancers on chromosome 3

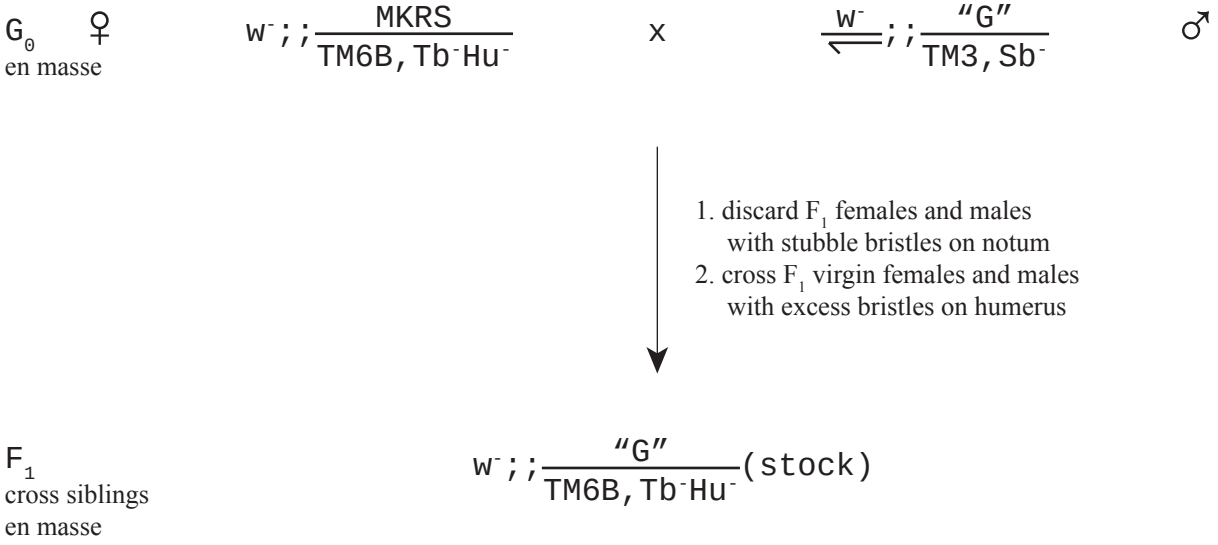


**Figure 2.3** Genetic protocol for swapping balancers on chromosome 3. This protocol allowed alleles or transgenes (illustrated as "G") in the larval and pupal stage to be identified in experiments by following the *Tb*$^{-}$ marker.

Protocol B: recombination of two genetic elements on chromosome 3

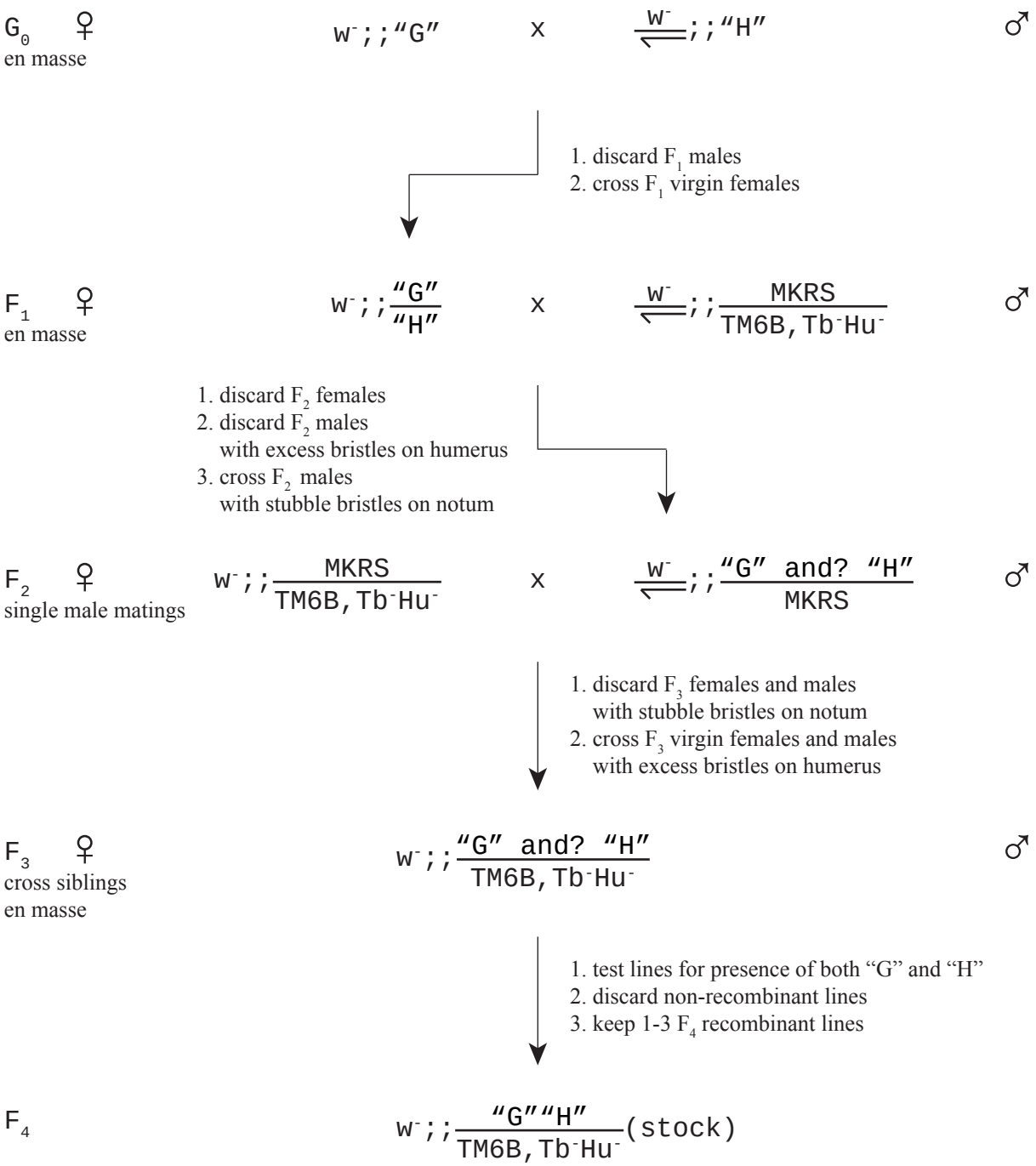


**Figure 2.4** Genetic protocol for combining two genetic elements on chromosome 3 by recombination. The two genetic elements in different fly stocks are illustrated by "G" and "H". Multiple crosses of a single $F_2$ male to 3 virgin females were established to set up multiple unique $F_3$ lines because each $F_2$ putative recombinant could arise from different chiasmata during recombination within the germline of $F_1$ mothers. Each $F_3$ lines were tested for the presence of recombined genetic elements. For example, alleles were tested by lethality, PCR or phenotype. *GAL4*-transgenes were tested by crossing to *UAS*-transgenes encoding fluorescent protein and examining the next filial generation with epifluorescence.

Protocol C: combination of two genetic elements separated on 1st and 3rd chromosomes

CONSIDER CHROMOSOME 1:

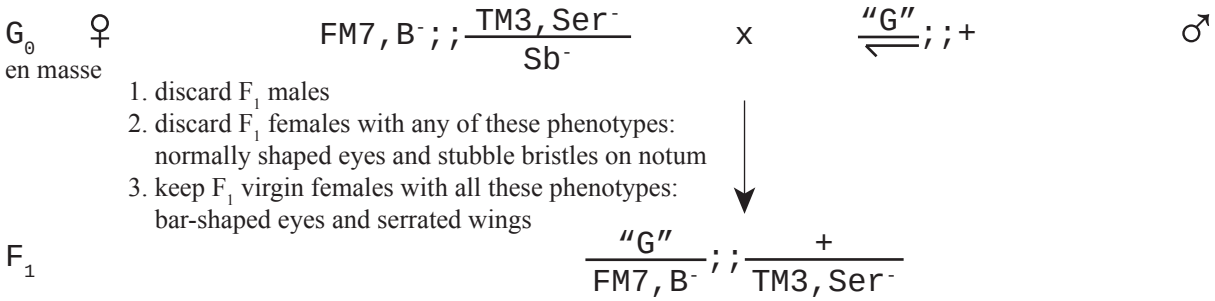


CONSIDER CHROMOSOME 3:

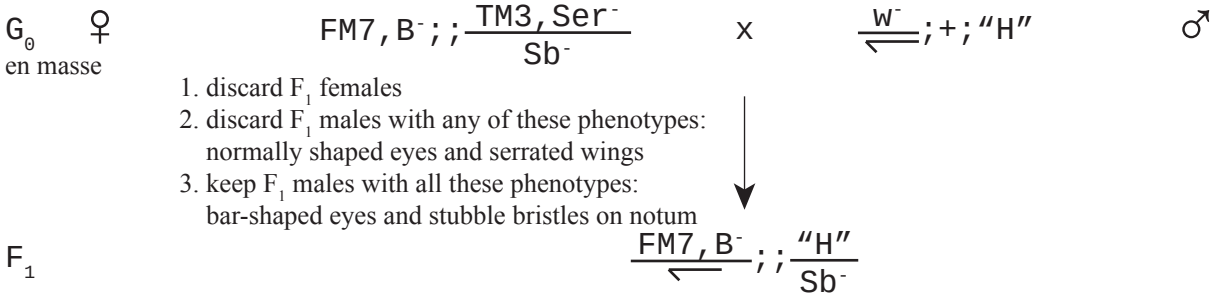


CONSIDER CHROMOSOMES 1 AND 3:

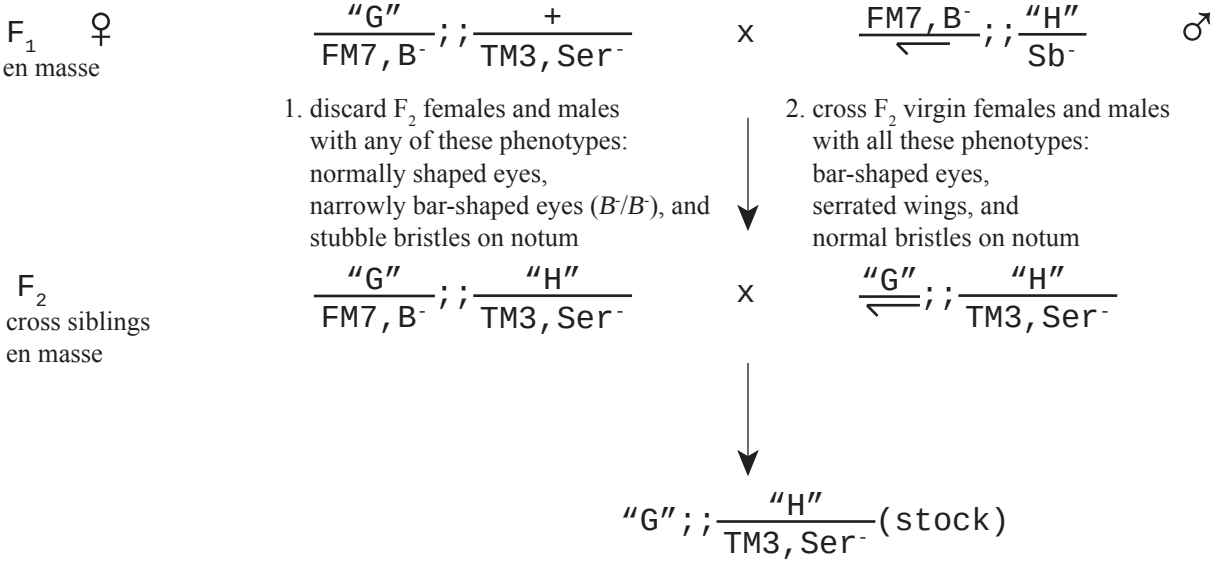


**Figure 2.5** Genetic protocol for combining two genetic elements on chromosomes 1 and 3. The two genetic elements in different fly stocks are illustrated by "G" and "H" on chromosomes 1 and 3, respectively. Combining two genetic elements on separate chromosomes requires two simultaneous and separate parental crosses ($G_0$).

Protocol D: combination of two genetic elements separated on 2nd and 3rd chromosomes

CONSIDER CHROMOSOME 2:

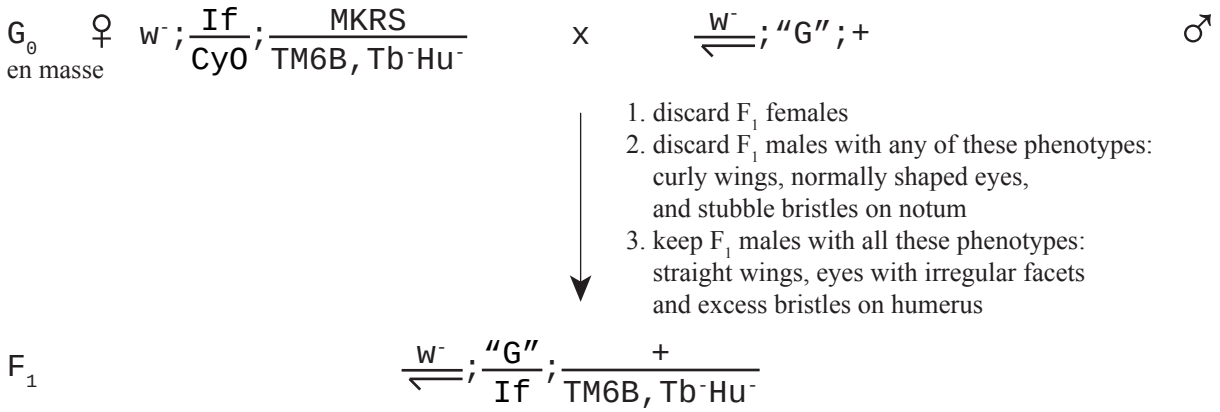


CONSIDER CHROMOSOME 3:

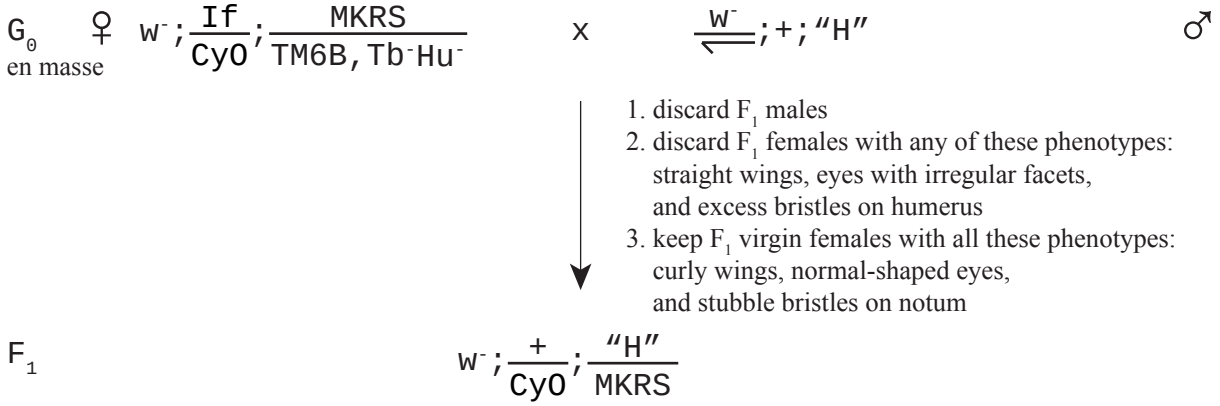


CONSIDER CHROMOSOMES 2 AND 3:

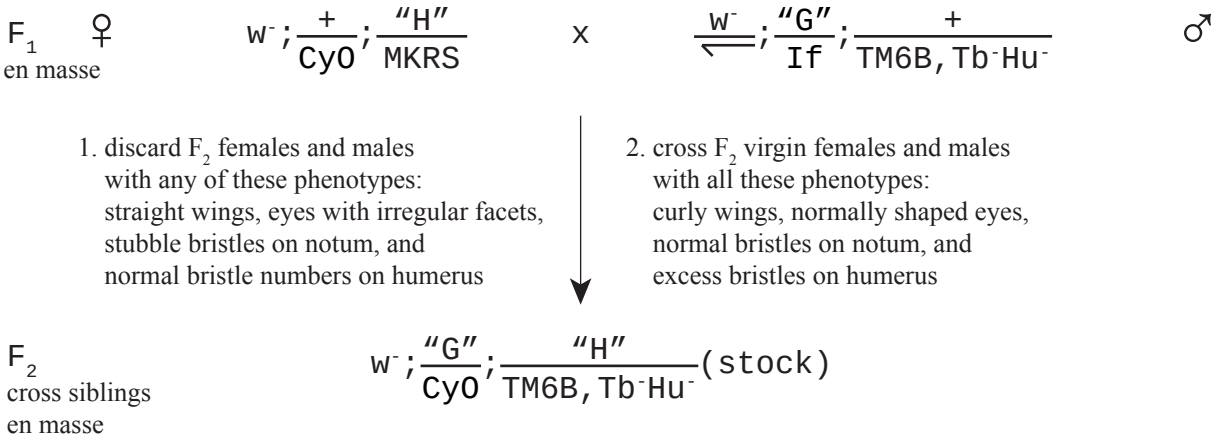


**Figure 2.6** Genetic protocol for combining two genetic elements on chromosomes 2 and 3. The two genetic elements in different fly stocks are illustrated by "G" and "H" on chromosomes 2 and 3, respectively. Combining two genetic elements on separate chromosomes requires two simultaneous and separate parental crosses ($G_0$).

The GAL4/UAS system

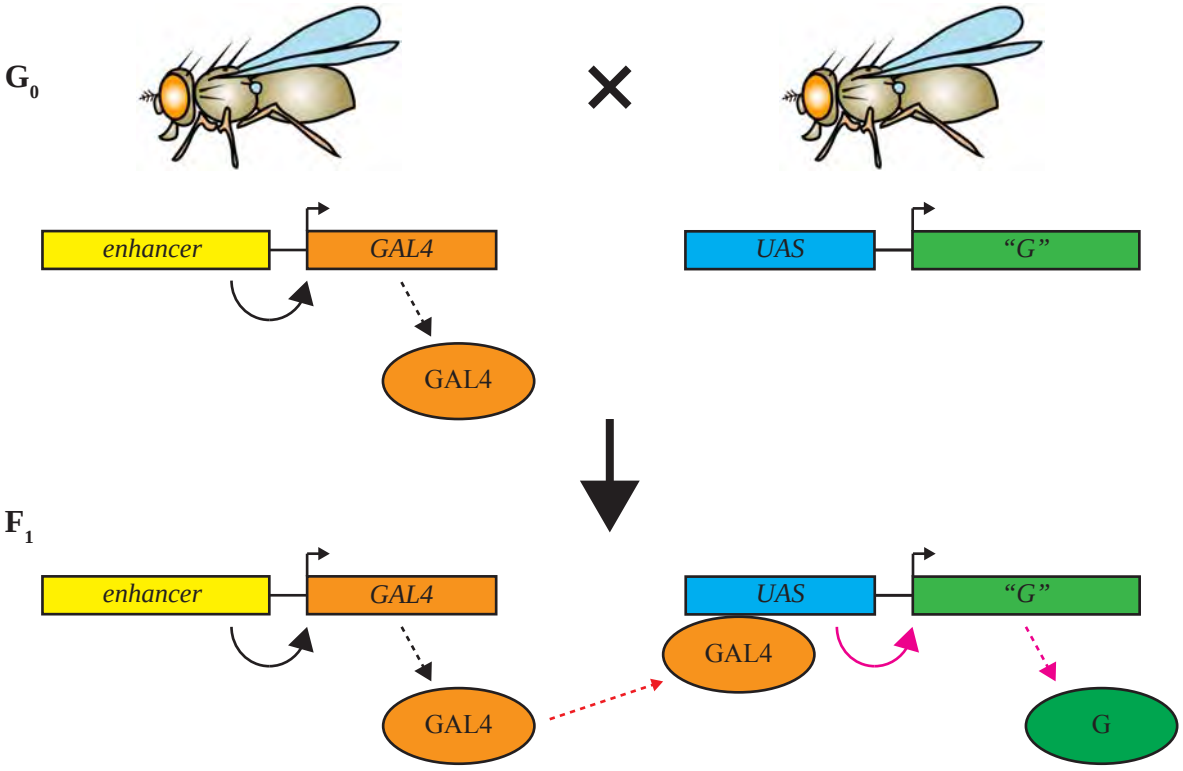


**Figure 2.7** Illustration of the GAL4/UAS system adopted from Brand & Perrimon (1993). **Left hand side of $G_0$ cross:** The expression of yeast transcription factor GAL4 is driven from genomic enhancers. **Right hand side of $G_0$ cross:** The target gene "*G*" is behind the *Upstream Activation Sequence* (*UAS*) and "*G*" is silent in the absence of GAL4. **$F_1$ cross:** The expression of "*G*" is active whenever and wherever GAL4 is driven. Fly images were constructed from the Genotype Builder Photoshop file published by Roote and Prokop (2013).

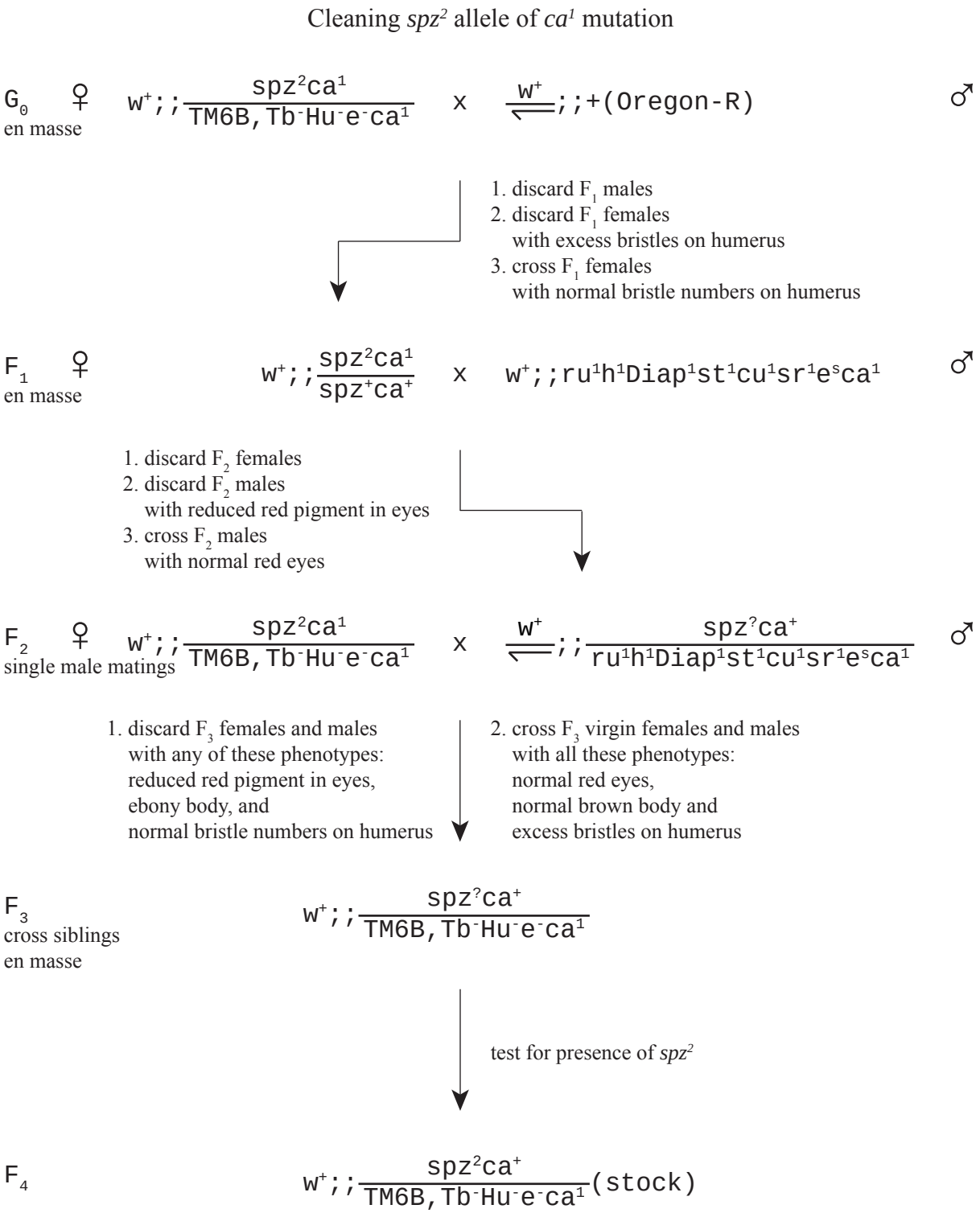


**Figure 2.8** Genetic scheme for cleaning *spz*$^{2}$ allele of *ca*$^{1}$ mutation. All crosses used *w*$^{+}$ background on chromosome 1 to follow alleles affecting eye pigment phenotype. Individual $F_2$ males carrying wild-type *ca*$^{+}$ allele were crossed to 3 virgin females to establish multiple unique $F_3$ lines because each $F_2$ putative recombinant could arise from different chiasmata during recombination within the germline of $F_1$ mothers. Each $F_3$ lines were tested for the presence of recombined *spz*$^{2}$ to *ca*$^{+}$ by lethality.

level (Cheli *et al.*, 2010; Harris *et al.*, 2011; Holtzman and Kaufman, 2013). The $G_0$ cross used $w^+$*;;*$spz^2ca^1$*/TM6B* and *Oregon-R* to obtain wild-type $ca^+$ for recombination to $spz^2$ in the germline of $F_1$ females. Recombination could arise from different chiasmata so the $F_2$ cross used single males carrying $ca^+$. 78 single male matings were established. Out of the 78 matings, 15 of them had $F_3$ offspring with $ca^+$ balanced over *TM6B.* The 15 $F_3$ lines were tested to determine whether or not the *spätzle* locus carried the $spz^2$ or $spz^+$ allele. The test by lethality was carried out according to the genetic scheme in Figure 2.9. If $w^+$*;;*$spz^?ca^1$*/TM6B* was crossed to *Df(3R)Exel6205/TM6B* in the $G_0$ generation, and the resulting $F_1$ $spz^?ca^1$*/Df(3R)Exel6205* mothers laid $F_2$ eggs which hatch, then the *spätzle* locus carried the $spz^+$ allele. If the $F_2$ eggs were not viable, then the *spätzle* locus carried the $spz^2$ allele and the fly line had its $spz^2$ allele cleaned of $ca^1$ (genotype: $w^+$*;;*$spz^2ca^+$*/TM6B*, stock no. 20 and 21, Table 2.1).

### 2.1.4 Genetic Protocol for Generating *dnt2* and *spz* Loss of Function Alleles

The genetic protocols for generating *dnt2* and *spz* loss of function alleles in this project followed the deletion strategy of using heat-shock driven flippase recombinase (hsFLP) with Exelixis transposons, which are *P-element XP* (*P{XP}*) and *piggyBac* (*PBac*) insertion lines containing flippase recombinase target (FRT) sites (Parks *et al.*, 2004; Thibault *et al.*, 2004). Insertions lines *PBac{RB}*$dnt2^{e03444}$ (stock no. 6, Table 2.1) and *P{XP}d05170* (stock no. 7, Table 2.1) were paired for *dnt2* locus deletion, while *P{XP}*$spz^{d00069}$ (stock no. 8, Table 2.1) was paired with *PBac{RB}e00046* (stock no. 9, Table 2.1) for *spz* locus deletion. Figure 2.10 and Figure 2.11 provide the schematic of the genetic crosses used for generating new *dnt2* and *spz* alleles, respectively. At $G_0$, males carrying the lower coordinate transposons

Testing for the presence of *spätzle* loss of function allele

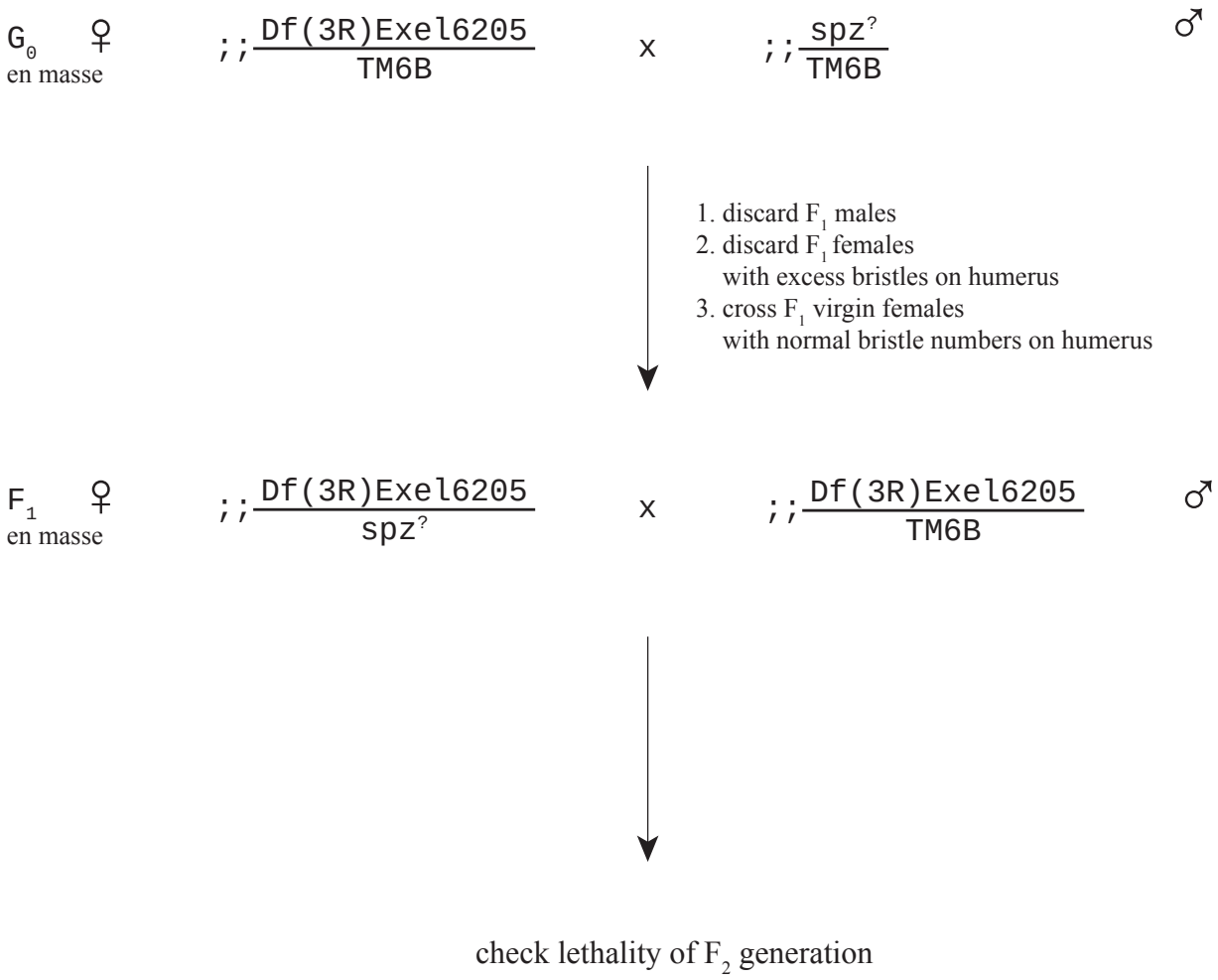


**Figure 2.9** Testing for the presence of *spätzle* loss of function allele by lethality at $F_2$ generation. If the $F_2$ generation is viable, the *spätzle* locus carries the wild-type allele ($spz^+$). If the $F_2$ generation is instead not viable, the *spätzle* locus carries the loss of function allele ($spz^-$).

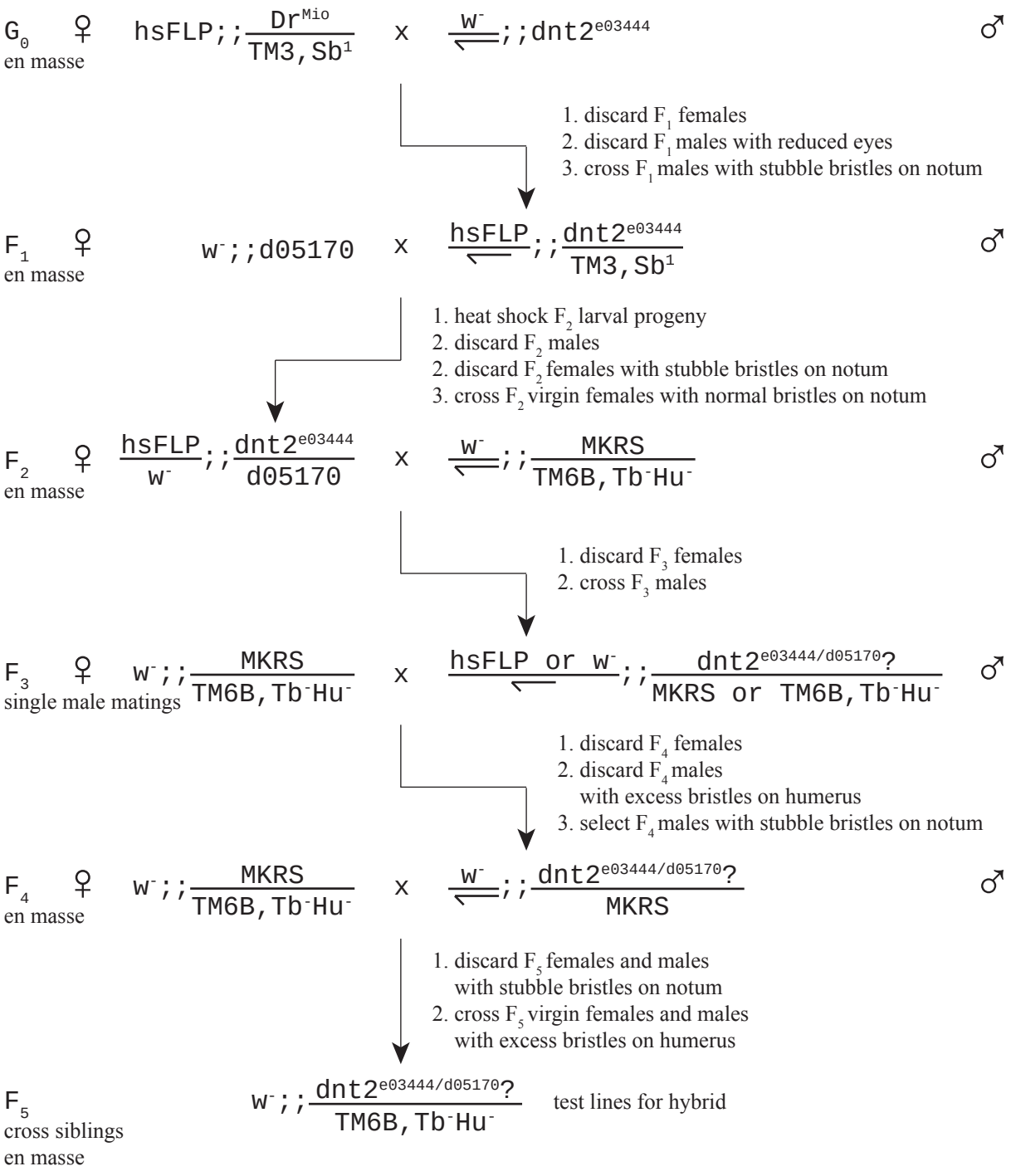


**Figure 2.10** Genetic scheme used for generating a *dnt2* loss of function allele. By the $F_2$ generation, crosses would place two FRT-bearing transposon insertions in *trans* (*e03444* and *d05170*) and in the presence of a heat-shock driven flippase recombinase (*hsFLP*). Activation of flippase recombinase in $F_2$ would result in the $F_3$ generation of a hybrid element (*e03444/d05170*) with a genomic deletion between insertions *e03444* and *d05170*. Multiple crosses of a single $F_3$ male to 3 virgin females were established to isogenise chromosome 1 and to test for hybrid *dnt2*$^{e03444/d05170}$ by PCR.

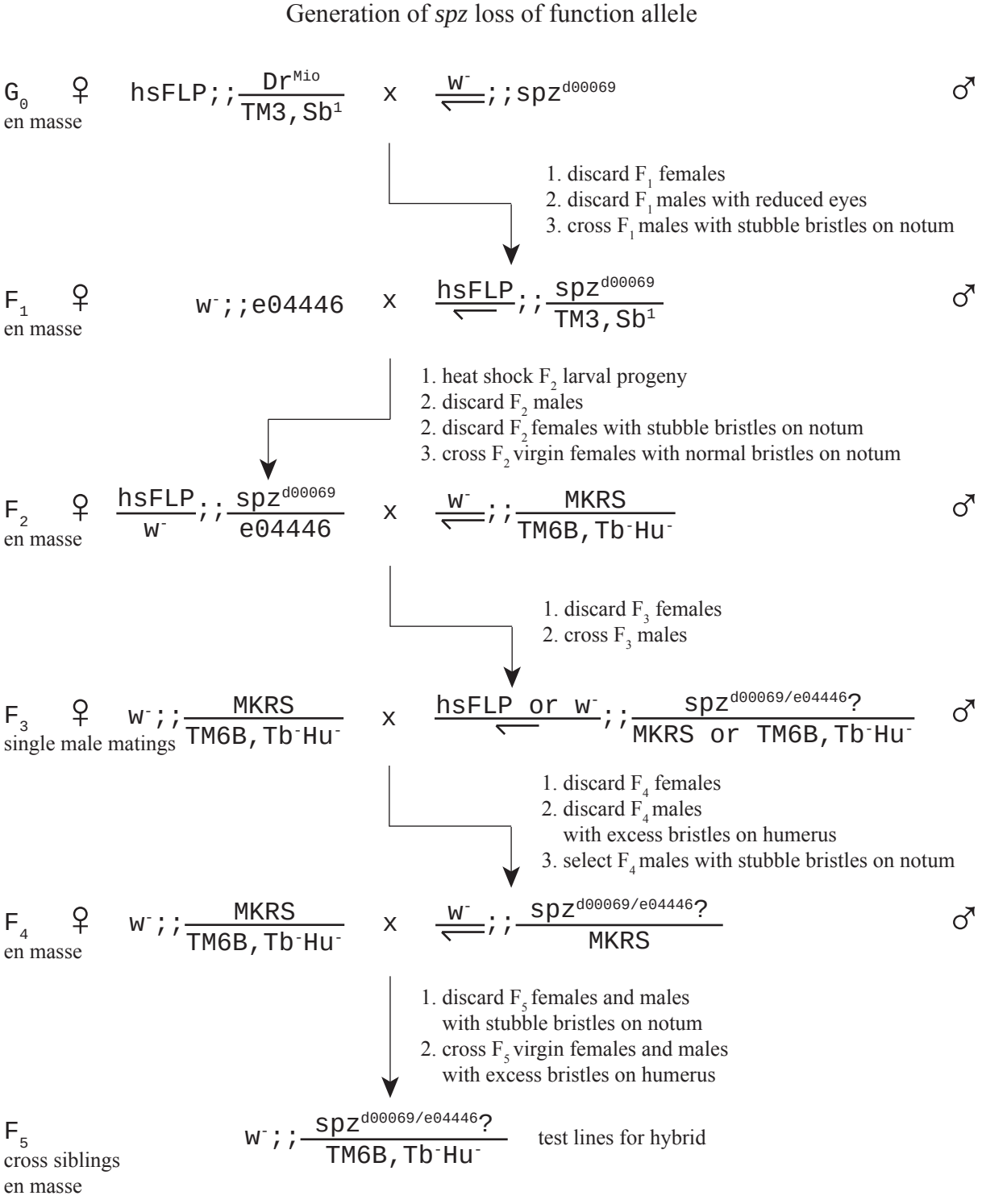


**Figure 2.11** Genetic scheme used for generating a *spz* loss of function allele. By the $F_2$ generation, crosses would place two FRT-bearing transposon insertions in *trans* (*d00069* and *e04446*) and in the presence of a heat-shock driven flippase recombinase (*hsFLP*). Activation of flippase recombinase in $F_2$ would result in the $F_3$ generation of a hybrid element (*d00069/e04446*) with a genomic deletion between insertions *d00069* and *e04446*. Multiple crosses of a single $F_3$ male to 3 virgin females were established to isogenise chromosome 1 and to test for hybrid $spz^{d00069/e04446}$ by PCR.

(*PBac{RB}dnt2*$^{e03444}$ and *P{XP}spz*$^{d00069}$) were mated with virgin females carrying hsFLP transgene. $F_1$ male progenies, which carrying both the lower coordinate transposon and hsFLP, were then mated to virgin females carrying the higher coordinate insertions (*P{XP}d05170* and *PBac{RB}e00046*). After 2 days, $F_1$ parents and $F_2$ germ-line progenies were subjected to a 1 hour, 37°C heat shock. The next day, the parents were removed while the progenies were subjected to daily 1 hour, 37°C heat shocks for 4 consecutive days. $F_2$ progenies were raised to adulthood to collect virgin female flies. These $F_2$ females were crossed to male flies containing marked balancer chromosomes (*w*$^-$*;;MKRS/TM6B*, stock no. 3, Table 2.1). Resulting $F_3$ white-eyed (*w*$^-$) progeny males were collected and individually crossed to virgin female flies of genotype *w*$^-$*;;MKRS/TM6B*. Due to the $F_4$ female population inheriting *hsFLP*, $F_4$ males were crossed to virgin female balancers (*w*$^-$*;;MKRS/TM6B*) to isogenise chromosome 1 and to retrieve a suitable stock in the next $F_5$ generation. A total of 21 and 17 *w*$^-$ isolate fly lines were established for generating new *dnt2* (*dnt2*$^{e03444/d05170}$) and *spz* (*spz*$^{d00069/e04446}$) alleles, respectively, including *w*$^-$*;;spz*$^{MA05}$*/TM6B* (stock no. 24, Table 2.1), *w*$^-$*;;spz*$^{MA10}$*/TM6B* (stock no. 25, Table 2.1) and *w*$^-$*;;spz*$^{MA12}$*/TM6B* (stock no. 26, Table 2.1).

### 2.1.5 Survival Index Assay

In order to test the viability of alleles over *TM6B*, crosses were set up in vials between virgin females and males of relevant genotypes. Vials were incubated at 25°C unless otherwise stated. The crosses were transferred to new vials with fresh food daily. As soon as flies began to eclose, normally 10 days after setting up the cross and incubating at 25°C, the vials were emptied of flies every day at 9am and 5pm until there was no further eclosion. The numbers of *Tb*$^+$ and *Tb*$^-$ pupal cases (Figure 2.2) were counted from the first cross and subsequent

transfers to calculate survival index (SI), a measure of allele viability over *TM6B*:

$$SI = 2 \times \frac{number\ of\ Tb^{+}}{number\ of\ Tb^{-}}$$

For wild-type alleles over *TM6B* segregating in Mendelian fashion, the expected value of SI is 1 (Figure 2.12):

$$SI = 2 \times \frac{1/3}{2/3} = 1$$

When SI is significantly less than 1, there are fewer non-tubby homozygotes than would be expected for wild-type, indicating that the allele reduced viability of larvae reaching pupal stages and is therefore semi-lethal. If SI is more than 1, there are more homozygotes than would be expected for wild-type segregration. SI is 0 when there are no homozygotes, indicating that an allele is fully lethal.

### 2.1.6 Visualising RP2 Neurons

To visualise wild-type RP2 neurons in third instar larval CNS, *w;;RN2-FLP* (stock no. 64, Table 2.1) flies were first crossed to *w;UAS-myr-RFP, tub-FRT-CD2-FRT-GAL4, UAS-FLP/CyO,wg-LacZ;* (stock no. 66, Table 2.1). Yeast flippase recombinase (FLP) was under the *RN2* regulatory element control. In $F_1$ generation, when FLP induced recombination between *FRT* sites (which were separated by the *CD2* linker), myr-RFP was expressed under the control of *tub-GAL4*. The inclusion of *UAS-FLP* allowed irregular GAL4 expression to be stabilised such that GAL4 was always expressed. $F_1$ third instar larvae were selected for myr-RFP expression under the Leica MZ FLIII stereo-fluorescence microscope to be dissected. To visualise RP2 neurons in loss of function background, *spz*$^{2}$*,RN2-FLP/TM6B,LacZ* (stock no. 65, Table 2.1) flies were crossed to *UAS-myr-RFP, tub-FRT-CD2-FRT-GAL4, UAS-FLP/*

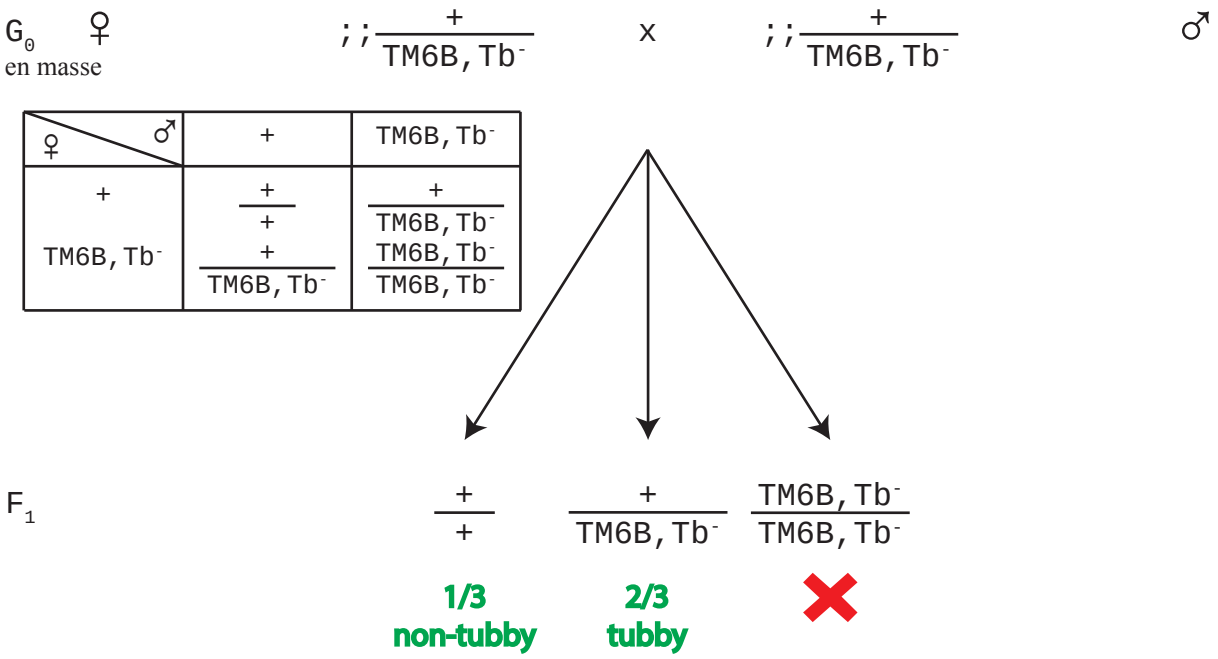


**Figure 2.12** Segregation of balanced wild-type chromosomes according to Mendelian inheritance. When heterozygous alleles over *TM6B* are crossed in $G_0$ and the $F_1$ progeny counted, a third of $F_1$ are expected to be homozygous and two-thirds heterozygous according to Mendelian segregation. *TM6B/TM6B* homozygotes are embryonic lethal, and thus, not viable and never pupate.

*CyO;spz*$^{2}$*ca*$^{1}$*/TM6B* (stock no. 67, Table 2.1) and *UAS-myr-RFP, tub-FRT-CD2-FRT-GAL4, UAS-FLP/CyO;Df(3R)Exel6205/TM6B* (stock no. 68, Table 2.1). This part of the project was contributed equally by M. P. Nallasivan up until the point of analysis (Section 2.5.3).

## 2.2 Molecular Biology

### 2.2.1 Genomic DNA Extraction

Whenever possible, genomic DNA from homozygous males of each isolate fly line was purified. Otherwise, heterozygous males were used. Of the 21 $w^-$ isolate fly lines for the FLP-FRT deletion of *dnt2*, 14 were homozygous viable while the remaining 7 were homozygous lethal. All 17 isolates for FLP-FRT deletion of *spz* were homozygous lethal. Genomic DNA was prepared from 15 male flies using Gentra® Puregene® DNA Purification System Kit (Qiagen®). The procedures of cell lysis, RNase A treatment, protein precipitation, nucleic acid precipitation and DNA hydration followed the manufacturer's protocol for *D. melanogaster* (Qiagen, 2010).

### 2.2.2 Conventional PCR

Different polymerase chain reaction (PCR) strategies were used for confirming deletion by hsFLP-FRT strategy (Section 2.1.4), including the deletions resulting in fly lines $w^-$ *;;spz*$^{MA05}$*/TM6B* (stock no. 24, Table 2.1), $w^-$*;;spz*$^{MA10}$*/TM6B* (stock no. 25, Table 2.1) and $w^-$ *;;spz*$^{MA12}$*/TM6B* (stock no. 26, Table 2.1). Figure 2.13B provides a schematic and description for the different PCR strategies, while Table 2.2 and Table 2.3 list the expected PCR fragment

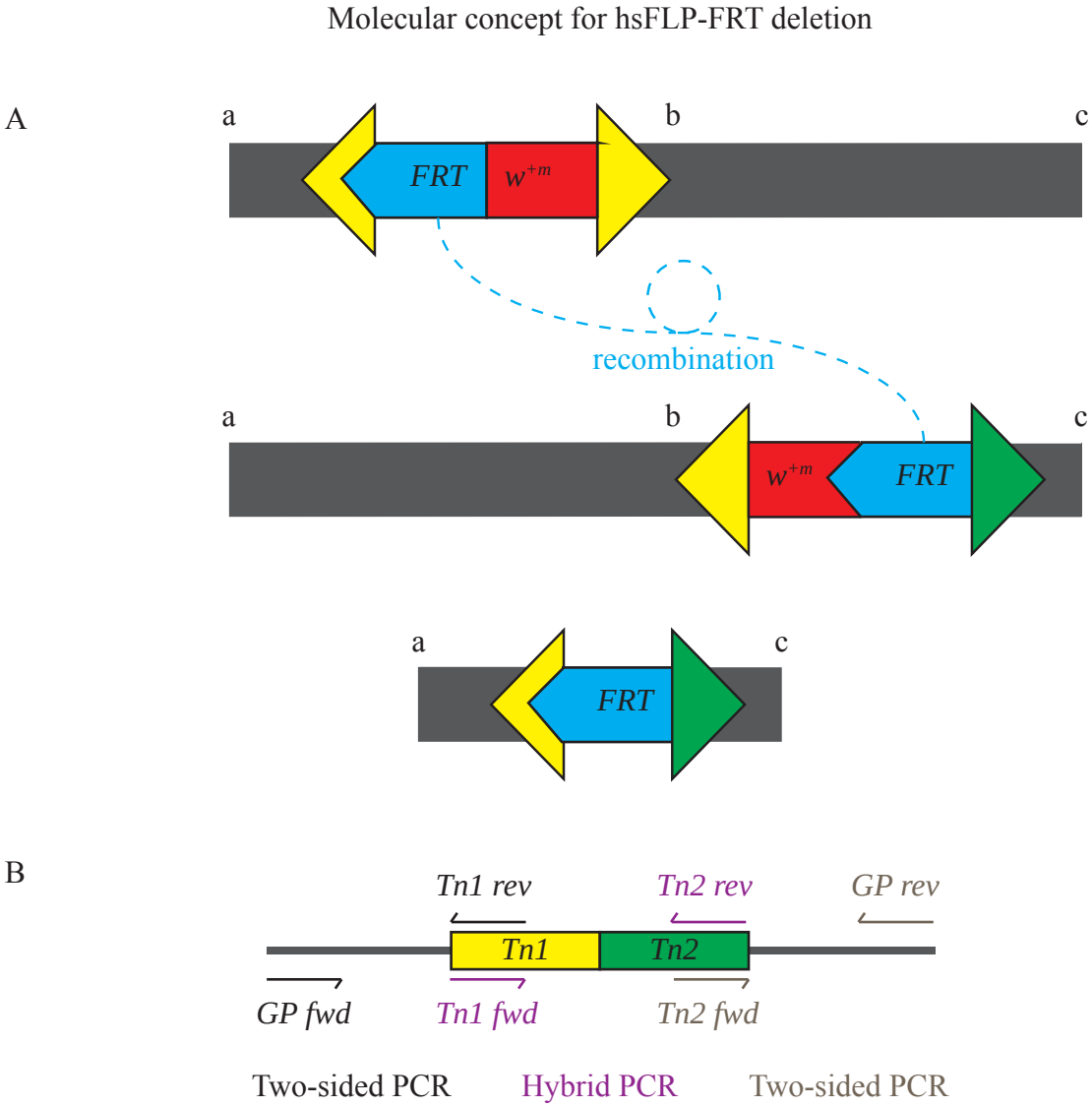


**Figure 2.13** Precise-end point hsFLP-FRT deletion adapted from Parks *et al.* (2004). **(A)** Using hsFLP-FRT recombination to generate $w^-$ deficiencies by deletions to lose the $w^{+m}$ marker. **(B)** Successful hsFLP-FRT recombination will result in a genomic deletion which leaves behind a resulting hybrid element at the recombination site. The residual transposon element (*Tn1/Tn2*) can be detected by PCR in three ways: (i) hybrid PCR, (ii) two-sided PCR, and (iii) genomic PCR. Element-specific forward (*Tn1 fwd*) and reverse (*Tn2 rev*) primers can detect the hybrid element of two transposons in hybrid PCR, while the hybrid element's residual ends can be detected using paired element-specific and genomic-specific primers in two-sided PCR (*GP fwd* with *Tn1 rev*, and *Tn2 fwd* with *GP rev*). Further confirmation can be supported by genomic PCR using genome-specific primers on their own (*GP fwd* and *GP rev*).

sizes using various primer pair combinations. Transposon primers for both 'hybrid' and 'two-sided' PCR were already previously published (Parks *et al.*, 2004), whereas genomic primers were custom made in-house using NetPrimer (PREMIER Biosoft) and Primer-BLAST (National Centre for Biotechnology Information). All primers were manufactured by Eurofins MWG Operon. For products longer than 2kb, PCR was carried out using Phusion® High-Fidelity DNA Polymerase (New England Biolabs). For products less than 2kb, PCR was carried out using Taq DNA Polymerase (Invitrogen).

### 2.2.3 Inverse PCR

Inverse PCR permit the recovery of sequences flanking transposon elements. Briefly, the protocol entailed genomic DNA extraction (Section 2.2.1) from *P{XP}d05170* flies, digestion, ligation, PCR and sequencing. Digestion was carried out using restriction enzyme Sau3AI (Promega) at 37°C for 1 hour (hr), then at 65°C for 20 minutes (mins). Ligation was carried out using T4 DNA Ligase (New England BioLabs) at 18°C overnight. To confirm transposon insertion in *P{XP}d05170*, two rounds of PCR was set up using primers designed by Exelixis (Table 2.4). The PCR product was purified by preparative gel electrophoresis and column-spin purification to be sent for sequencing (Genomics Lab at University of Birmingham). Sequencing primers were designed by Exelixis (Table 2.4). The resulting nucleotide sequence output was retrieved using Chromas Lite (Technelysium) and the transposon insertion determined using the BLAST feature in FlyBase. Sequencing was repeated twice.

| PCR confirmation of hsFLP-FRT based deletion for *dnt2* | | | | |
|---|---|---|---|---|
| **PCR Type** | **Left Primer** | **Right Primer** | **Expected Fragment Size When Hybrid Element Present** | **Expected Fragment Size When Hybrid Element Absent** |
| Internal | *deleteGP fwd* | *deleteGP rev* | No band | 195bp |
| Hybrid | *Tn1 fwd* | *Tn2 rev* | 1.7kb | No band |
| LHS two-sided | *GP fwd* | *Tn1 rev* | 408bp | * see legend |
| RHS two-sided | *Tn2 fwd* | *GP rev* | 619bp | |
| Genomic | *GP fwd* | *GP rev* | 5.2kb (balancer) 3.1kb ('mutant') | 5.2kb only |
| **Verification of *PBac{RB}dnt2$^{e03444}$* insertion** | | | | |
| **PCR Type** | **Left Primer** | **Right Primer** | **Expected Fragment Size When Transposon Present** | **Expected Fragment Size When Transposon Absent** |
| LHS two-sided | *GP fwd* | *Tn1 rev* | 408bp | No band |
| **Verification of *P{XP}d05170* insertion** | | | | |
| **PCR Type** | **Left Primer** | **Right Primer** | **Expected Fragment Size When Transposon Present** | **Expected Fragment Size When Transposon Absent** |
| RHS two-sided | *Tn2 fwd* | *GP rev* | 619bp | No band |
| Genomic | *GP fwd* | *GP rev* | 12.5kb | 5.2kb |
| **Primer Sequences** | | | | |
| **Name** | **Sequence (5' to 3')** | | | |
| *deleteGP fwd* | GAA GAT CTC GAG CTG TGG GCG GCT ACT GT | | | |
| *deleteGP rev* | CGG AAT TCA TGC AAA TCG ACG GCG AAT GA | | | |
| *Tn1 fwd* | TGC ATT TGC CTT TCG CCT TAT | | | |
| *Tn1 rev* | AAT GAT TCG CAG TGG AAG GCT | | | |
| *Tn2 fwd* | CCT CGA TAT ACA GAC CGA TAA AAC | | | |
| *Tn2 rev* | TTT ACT CCA GTC ACA GCT TTG | | | |
| *GP fwd* | CAT TAC CAA CTA ACG CAC ATT | | | |
| *GP rev* | AAT TCC CAA TAT ACC TGT GCT | | | |

Table 2.2 Primers for screening putative *dnt2* loss of function allelic stocks.
The left- and right-hand sides of the two-sided PCR must both give bands of expected sizes (408bp and 619bp) from an isolate fly line to determine that the hybrid element is present. **LHS:** left-hand side. **RHS:** right-hand side.

| PCR confirmation of hsFLP-FRT based deletion for *spz* | | | | |
|---|---|---|---|---|
| **PCR Type** | **Left Primer** | **Right Primer** | **Expected Fragment Size When Hybrid Element Present** | **Expected Fragment Size When Hybrid Element Absent** |
| LHS two-sided | *GP fwd* | *Tn1 rev* | 354bp | * see legend |
| RHS two-sided | *Tn2 fwd* | *GP rev* | 670bp | |
| **Verification of *P{XP}spz$^{d00069}$* insertion** | | | | |
| **PCR Type** | **Left Primer** | **Right Primer** | **Expected Fragment Size When Transposon Present** | **Expected Fragment Size When Transposon Absent** |
| LHS two-sided | *GP fwd* | *Tn1 rev* | 354bp | No band |
| **Verification of *PBac{RB}e00046* insertion** | | | | |
| **PCR Type** | **Left Primer** | **Right Primer** | **Expected Fragment Size When Transposon Present** | **Expected Fragment Size When Transposon Absent** |
| RHS two-sided | *Tn2 fwd* | *GP rev* | 670bp | No band |
| **Primer Sequences** | | | | |
| **Name** | **Sequence (5' to 3')** | | | |
| *Tn1 rev* | CCT CGA TAT ACA GAC CGA TAA AAC | | | |
| *Tn2 fwd* | AAT GAT TCG CAG TGG AAG GCT | | | |
| *GP fwd* | GCC TTA TAG TCT GCC ACT GTT | | | |
| *GP rev* | ACA TGG CGA TTA CTT GCA GTG | | | |

Table 2.3 Primers for screening putative *spz* loss of function allelic stocks.
The left- and right-hand sides of the two-sided PCR must both give bands of expected sizes (354bp and 670bp) from an isolate fly line to determine that the hybrid element is present. **LHS:** left-hand side. **RHS:** right-hand side.

| Recovery of sequences flanking 5' end of *P{XP}d05170* insertion | | |
|---|---|---|
| **Primer Name** | **PCR Round** | **Sequence (5' to 3')** |
| *51A* | 1 | AAT GAT TCG CAG TGG AAG GCT |
| *51B* | 1 | CAC CCA AGG CTC TGC TCC CAC AAT |
| *52A* | 2 | TAC CAG TGG GAG TAC ACA AAC |
| *52B* | 2 | TTT ACT CCA GTC ACA GCT TTG |
| *XP-5SEQ* | sequencing | ACA CAA CCT TTC CTC TCA ACA |

Table 2.4 Primers for the recovery of sequences flanking 5' end of *P{XP}* elements. The primer names were given by Exelixis.

## 2.3 Immunohistochemistry

Wandering larvae were dissected for their CNS in cold phosphate buffered saline (PBS). Embryonic brains were dissected by Dr M. Losada and the dissected, unfixed brains were a gift to this project. For all immunostaining purposes, unless otherwise indicated, the following steps were observed: CNS were fixed in 4% formaldehyde solution with PEM buffer (0.1M PIPES; 2mM EGTA; 1mM $MgSO_4$) for 50 mins at room temperature (RT). After washing and permeabilising with 0.3% Triton X-100 in PBS (PBTx) for 30 mins at RT, CNS were blocked using 10% normal goat serum (Vector Laboratories) with 0.3% PBTx for at least 1 hr at RT or overnight at 4°C. Blocking was succeeded by the following sequence: incubation in primary antibody solution, washes, incubation in secondary antibody solution, and washes again. This sequence after blocking was repeated for any second immunolabelling required. Finally, immunostained CNS were mounted on microscope slides using mounting media of glycerol and $dH_2O$ in a 4:1 composition, before being covered with 18mm by 18mm borosilicate glass coverslips of thickness 0.08mm (VWR). In the case of immunostaining CNS with anti-nc82 (DSHB), the fixing and permeabilising steps were modified: CNS were fixed in 4% paraformaldehyde with PBS for 3 hrs on wet ice, and then permeabilised by 0.3% PBTx for 1 hr at RT. With anti-Toll7-AAQ staining, the wash buffer 0.3% PBTx was replaced by 0.3% Tween-20 in PBS (PBTw).

Table 2.5 and Table 2.6 list the primary and secondary antibodies used in the course of this project, respectively. Stocks of the primary and secondary antibodies were usually diluted in 10% normal goat serum with 0.3% PBTx for use in immunohistochemistry. In the case of anti-Toll7-AAQ, the antibody was diluted in 10% normal goat serum with 0.3% PBTw.

| Primary Antibody | Dilution | Donor | Source | Catalogue Number | Use |
|---|---|---|---|---|---|
| Anti-BP102 | 1:250 | Mouse | DSHB | BP 102 | CNS neuropile marker |
| Anti-Dcp1 | 1:500 | Rabbit | Cell Signaling Technology | 9578 | Apoptotic marker |
| Anti-DNT1-RRPQ | 1:100 | Rabbit | Davids Biotechnologie | | DNT1 protein distribution |
| Anti-DNT1-VRY | 1:100 | Rabbit | Davids Biotechnologie | | DNT1 protein distribution |
| Anti-DNT2-GYN | 1:100 | Rabbit | Davids Biotechnologie | | DNT2 protein distribution |
| Anti-DNT2-KRL | 1:100 | Rabbit | Davids Biotechnologie | | DNT2 protein distribution |
| Anti-DsRed | 1:100 | Rabbit | Clontech | 632496 | Larval expression profile |
| Anti-Ebony | 1:250 | Rabbit | Gift of S. Carroll | | Neuropile-associated glial marker |
| Anti-Elav | 1:250 | Rat | DSHB | 7E8A10 | Pan-neuronal marker |
| Anti- Fas-II | 1:250 | Mouse | DSHB | 1D4 | Axonal fascicle marker |
| Anti-GFP | 1:500 | Mouse | Life Technologies | A11120 | Larval expression profile |
| Anti-GFP | 1:1000 | Rabbit | Life Technologies | A11122 | Larval expression profile |
| Anti-GS2 | 1:250 | Mouse | Chemicon® Merck Millipore | MAB302 | Neuropile-associated glial marker |
| Anti-nc82 | 1:50 | Mouse | DSHB | nc82 | Active zone marker |
| Anti-pH3 | 1:250 | Rabbit | Upstate® Merck Millipore | 06-570 | Mitotic marker |
| Anti-Repo | 1:250 | Mouse | DSHB | 8D12 | Pan-glial marker, except midline glia |
| Anti-Spz-ASIK | 1:100 | Rabbit | Davids Biotechnologie | | Spz protein distribution |
| Anti-Spz-GLR | 1:100 | Rabbit | Davids Biotechnologie | | Spz protein distribution |
| Anti-Toll-d300 | 1:200; 1:250 | Rabbit | Santa Cruz Biotechnology | sc-33741 | Toll protein distribution |
| Anti-Toll7-AAQ | 1:10 | Guinea Pig | Davids Biotechnologie | | Toll7 protein distribution |

Table 2.5 Primary antibodies used for immunohistochemistry.

| Secondary Antibody | Dilution | Donor | Source | Catalogue Number |
|---|---|---|---|---|
| Alexa Fluor® 488 Anti-Guinea Pig | 1:250 | Goat | Life Technologies | A11073 |
| Alexa Fluor® 488 Anti-Mouse | 1:250 | Goat | Life Technologies | A11001; A11029 |
| Alexa Fluor® 488 Anti-Rabbit | 1:250 | Goat | Life Technologies | A11034; A11070 |
| Alexa Fluor® 488 Anti-Rat | 1:250 | Goat | Life Technologies | A11006 |
| Alexa Fluor® 647 Anti-Mouse | 1:250 | Goat | Life Technologies | A21236 |
| Alexa Fluor® 647 Anti-Rabbit | 1:250 | Goat | Life Technologies | A21245 |
| Alexa Fluor® 647 Anti-Rat | 1:250 | Goat | Life Technologies | A21247 |

Table 2.6 Secondary antibodies used for immunohistochemistry.

Anti-Ebony is a gift reagent from S. Carroll and it was used at dilution 1:250, the same dilution used by Kato *et al.* (2011) for anti-Ebony staining in larval brain tissue. The signal and specificity of anti-Toll-d300 (Santa Cruz Biotechnology), as well as those of custom-designed antibodies against the DNTs and Toll7 (Davids Biotechnologie), were first characterised in this project. The usefulness of anti-Toll-d300 and the custom-designed antibodies will be assessed in Chapter 3. Dilution series to optimise immunostaining signal and controls to establish specificity were not usually carried out in this project since the Hidalgo lab has extensive experience in using antibodies for immunostaining in the *Drosophila* CNS. Hence, the specificity of commonly used antibodies sourced from Clontech, DSHB, Life Technologies and Merck Millipore were well-established.

## 2.4 Microscopy

### 2.4.1 Image Acquisition

All images of *Drosophila* adult eyes were collected on a Zeiss Stemi 2000-C stereomicroscope equipped with an AxioCam ICc3 camera, which was controlled with the Zen lite 2012 software.

Phase contrast images of whole larval CNS were acquired from the Zeiss Axioplan 2 equipped with a 10x/0.3 Plan-Neofluar objective lens and an AxioCam HRc camera, which was controlled with Zen lite 2012 software. Alternatively, phase contrast images were viewed from the Zeiss Axio Observer equipped with a 10x/0.3 Plan-Neofluar objective lens and then acquired using Zen 2010 software.

Fluorescent, confocal images of larval CNS were taken from two systems: (1) the Leica TCS SP2 AOBS spectral confocal scanner mounted on a Leica DM IRE2 inverted fluorescent microscope; and (2) the Zeiss LSM710 spectral confocal scanner mounted on the Zeiss Axio Observer. The Leica was equipped with a 20x/0.7 Plan-Apochromat multi-immersion objective lens and a 40x/0.75 Plan-Apochromat oil lens. The Zeiss was fitted with a 25x/0.8 Plan-Apochromat oil objective lens and a 40x/1.3 Plan-Neofluar oil lens. Alexa Fluor® 488 was excited with the 488nm line from the 100mW argon (Ar) and 75mW argon-krypton (ArKr) lasers on the Leica system, and from the 25mW Ar laser on the Zeiss system. Alexa Fluor 647® was excited with the 633nm line from the 10mW helium-neon (HeNe) laser on the Leica and the 5mW HeNe on the Zeiss. Endogenous myristoylated tandem dimer Tomato (myr-tdTomato) and myr-RFP were excited with the 543nm line from the 1mW HeNe laser on the Zeiss.

### 2.4.2 Time-Lapse Recordings of Stabbed Samples

Two sets of Z-stack time-lapse recordings over the course of 10 to 15 hrs were carried out using the Leica confocal microscope with the 20x objective lens. Samples were maintained at 25ºC in a temperature controlled chamber (Life Imaging Services). One set of Z-stack time-lapse recording over the duration of 12 hrs was imaged by the Zeiss confocal using the 25x lens. Samples were maintained at 25ºC using the Zeiss heated stage controlled by the Zeiss TempModule. Endogenous green fluorescent protein (GFP) was excited using the 488nm line on both confocal systems. Z-stack imaging of step size 1 μm was carried out hourly.

### 2.4.3 Image Processing and Analysis

Every image was processed and analysed using ImageJ (version 1.44p or 1.49i) and Adobe Photoshop CS6 (64 bit). Images of RFP-positive RP2 neurons (Section 2.1.6) were processed in ImageJ according to Ou *et al.* (2008) for Sholl analysis. The pixels showing the cell soma and axon were removed manually from each focal point. Any background spot was removed by running the built-in Median Filter function at radius 1 pixel. After each focal plane was converted to a binary image by applying the Auto Threshold function, dendrites were then ready to be analysed by Sholl analysis using the plug-in written by Ferreira *et al.* (2014b) (Section 2.5.3) . Time-lapse images (Section 2.4.2) were processed by ImageJ plugins Turboreg and Stackreg to correct sample movement.

## 2.5 Phenotypic Analysis

### 2.5.1 Cuticle Preparations of Unhatched Embryos

The protocol for cuticle preparations of unhatched embryos was adopted from Stern and Sucena (2000). Females were allowed to lay their eggs in cages on grape juice agar plates for 24 hours. After 24 hours, the females were removed and the laid eggs left alone to develop on the grape juice agar plates for a further 24 hours. The eggs were then washed with tap water through an egg sieve. The egg sieve was placed in a small dish containing 50% bleach (12% sodium hypochlorite) until the eggs developed from dull white to having shiny appearance, indicating full dechorionation of embryos. The dechorionated embryos were then dried by blotting the egg sieve on dry paper towel. Using a wet paintbrush, the embryos were

transferred from the egg sieve into a 1.5mL microcentrifuge tube containing 500µL heptane and 500µL methanol. The microcentrifuge tube was shaken using a vortex mixer for 30 seconds to cause the vitelline membrane to pop. The heptane and methanol mixture was removed and replaced with 1mL of methanol for washing. Devitellised embryos were washed twice with methanol and then twice with 0.1% PBTx. Embryos were then transferred to a clean microscope slide. Excess liquid was absorbed by a piece of filter paper while avoiding the embryos. A drop of diluted lactic acid (75%) was placed on the embryos and a clean coverslip placed over the preparation. The preparation was cooked in an oven at 60°C for 27.5-28 hours. Cuticles were viewed by using low-power objectives (10x) with the condenser set in phase-contrast position for higher-powered objective (Ph3) as a substitute for dark-field illumination on the Zeiss Axioplan 2.

### 2.5.2 Measurements of CNS Size

Wandering larvae were dissected and CNS fixed for 30 minutes. CNS were then washed with 0.3% PBTx for 30 minutes, and finally suspended in 80% glycerol. Microscope slides were layered twice with cellotape and a small rectangle, around the centre of the slide, cut out with a razor. This rectangular area was where CNS were mounted and covered with a coverslip without being squashed. Mounting technique and quality was very consistent under the author's hands. Images were acquired immediately, or a day later at latest, to avoid tissue shrinkage. Measurements of CNS size were done in ImageJ by drawing region of interests (ROIs) separately for the brain area, VNC area and VNC length. Area and length measurements were derived from the built-in Measure function in ImageJ.

### 2.5.3 Sholl Analysis of RP2 Dendrites

Processed images of RFP-positive RP2 dendrites were used for Sholl analysis (Section 2.4.3). Before running the plugin, the centre of analysis was defined as the point where the axon intersected with the cell soma, and the centre was selected using the Point Selection Tool. Table 2.7 details the essential parameters used when running Sholl Analysis v3.4.3 plug-in for analysis of RFP-positive RP2 dendrites. The output of each Sholl Analysis for each neuron supplied a list of the x- and y-coordinates, with x-values being distance from cell soma and y-values being the number of intersections at each distance sampled. Each RP2 neuron was categorised into one of three groups: thoracic RP2, A1-3 RP2 or A6-7 RP2. In each genotype in each category, the associated y-values were summed up at each distance sampled before obtaining the mean number of intersections for statistical comparisons.

### 2.5.4 DeadEasy for Automatic Counting of Cells

DeadEasy Larval Glia (Forero *et al.*, 2012) is the software which was purposely written in Java as an ImageJ plugin to count automatically the number of all larval glia stained with anti-Repo and later acquired as confocal microscopy images. In the publication by both Forero *et al.* (2012) and Kato *et al.* (2011), confocal serial sections of anti-Repo staining were obtained with the BioRad Radiance 2000 upright confocal microscope as images of pixel size 0.5665μm and step size 1 μm. DeadEasy Larval Glia identifies stained cells first through each confocal slice in 2-dimensional shape (circular or elliptical), and then throughout the stack in 3-dimensions based on mimimum and maximum volume as well as pixel intensity. The software creates a stack of processed images in which the identified objects reproduce those

| Definition of Shells | | |
|---|---|---|
| **Parameter** | **Input** | **Use** |
| **Starting radius** | 5.0µm (thoracic and A1-3 RP2 neurons)<br>2.5 µm (A6-7 RP2 neurons) | This input defines the radius of the first concentric spherical shell, and thus the first discrete measurement from the centre of analysis. |
| **Ending radius** | NaNµm | "NaN" stands for "Not a Number". This input instructs the program to sample the entire Z-stack image. |
| **Radius step size** | 5.0µm (thoracic and A1-3 RP2 neurons)<br>2.5 µm (A6-7 RP2 neurons) | This input defines the radius of the second and subsequent concentric spherical shells. By having the step size the same as the starting radius, the discrete sampling is incremented equally. |
| **Descriptors and Curve Fitting** | | |
| **Parameter** | **Input** | **Use** |
| **Enclosing radius cutoff** | 1 | This input instructs the program to use one intersection in defining the last and widest shell. |
| **Primary branches** | 1 | An RP2 neuron has one axon only leaving the cell body and thus the number of primary branches is 1. |
| **Sholl Methods** | | |
| **Parameter** | **Input** | **Use** |
| **Linear** | Tick the box | This input instructs the program to supply a graph of number of intersections by shells versus radius length for each neuron. This graph will be supplied with a list of x- and y-coordinates which can be saved manually. |
| **Polynomial** | Best fitting degree | The linear profile will include the line of best fit in the graph of number of intersections versus radius length for each neuron. |
| **Output Options** | | |
| **Parameter** | **Input** | **Use** |
| **Create intersections mask** | Tick the box | This input instructs the program to supply a maximum intensity projection of the neuron analysed, in which the measured dendrites is painted according to its linear Sholl profile using a rainbow color map. |
| **Save results in image directory** | Tick the box | This input allows Sholl plots, associated coordinates and Sholl intersection mask to be saved directly and automatically. |

Table 2.7 Parameters used when running Sholl Analysis v3.4.3 (Ferreira *et al.*, 2014b) to analyse dendrites of RP2 neurons.

of the Repo-positive glia in the raw images (Figure 2.14), enabling comparisons and validation. Validation by Forero *et al.* (2012) was carried out through counting the number of false positive objects and false negative cells using 10 different confocal image stacks. False positive objects are those which DeadEasy Larval Glia identified incorrectly as Repo-positive glia while false negative cells are those which incorrectly escape identification as Repo-positive glia. A total of 947 real cells were counted after verifying each cell between the raw and DeadEasy-processed images. DeadEasy Larval Glia identified 907 cells with an accuracy of 0.11% false positive and 4.33% false negative (Forero *et al.*, 2012). In this project, confocal serial sections were obtained with the Zeiss LSM 710 microscope due to the breakdown of the BioRad Radiance 2000 upright confocal microscope. The pixel size was 0.664μm and the step size 1 μm. Validation through counting the number of false positive objects and the false negative cells was carried out from 21 different confocal image stacks in ImageJ using Cell Counter. The accuracy of DeadEasy Larval Glia when switching from the BioRad to the Zeiss system was 0.3% false positive and 3.9% false negative.

Before running DeadEasy Larval Glia, ROIs must be selected (Figure 2.15). Peripheral nerves exiting the VNC were excluded from the ROI. For the abdominal VNC, the ROI was defined according to Kato *et al.* (2011) as the area starting from the posterior of a pair of Repo-positive ventral interface glia (vIG) in the last thoracic segment (T3) to the posterior tip of the ventral nerve cord (Figure 2.15). The thoracic ROI was defined by the adjacent area anterior to the abdomen and which encompasses three pairs of interface glia in unique C-shaped arrangements in the ventral side of the nerve cord (Figure 2.15).

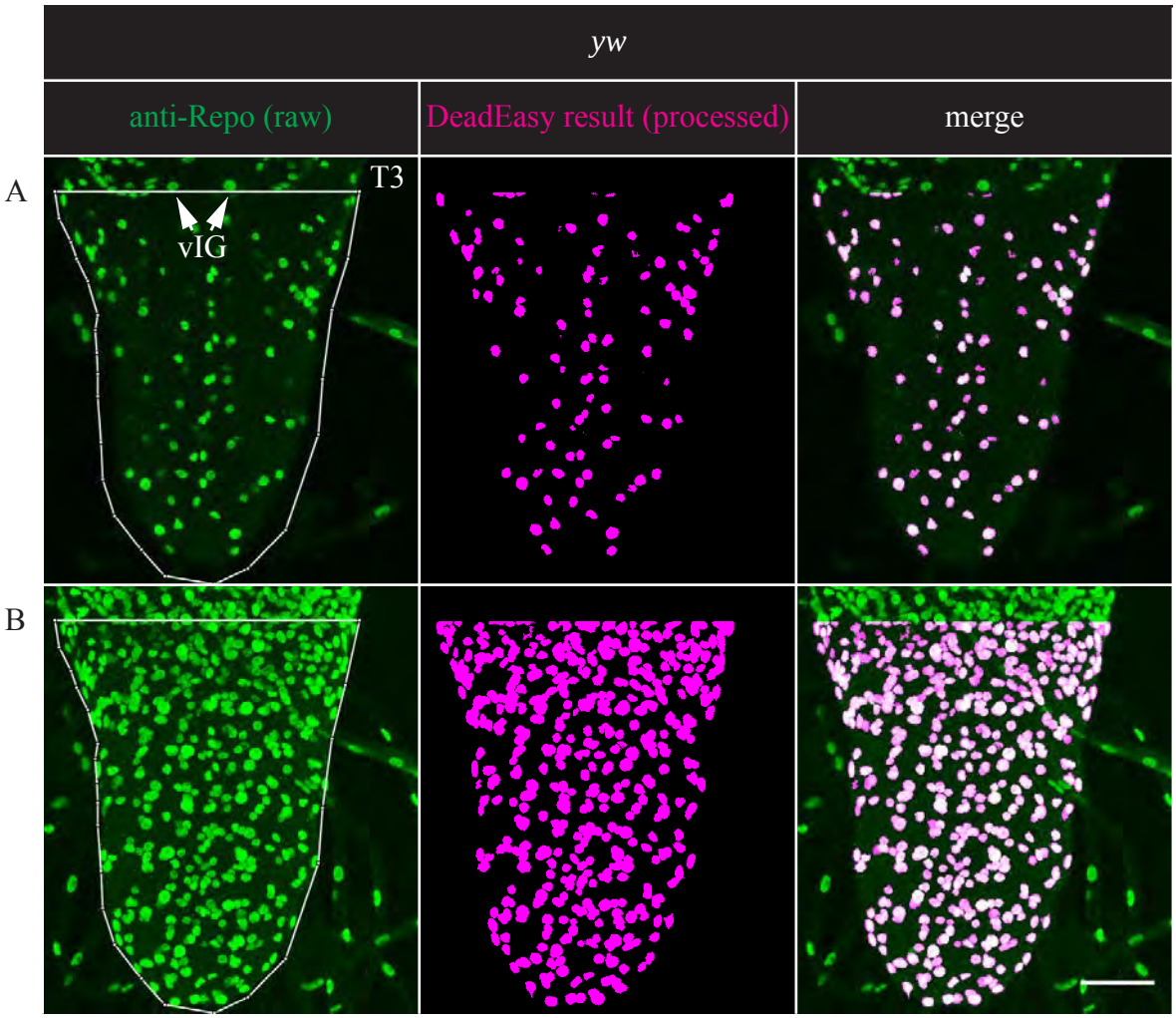


**Figure 2.14** DeadEasy Larval Glia processes raw images of anti-Repo staining. **(A)** Maximum projections of 10 confocal slices to show the ventral interface glia of the third thoracic segment (T3 vIG). **(B)** Maximum projections of whole Z-stack of the same sample as in (A). DeadEasy results are in pseudocolor magenta. **White solid line:** ROI boundary drawn for DeadEasy to process. Scale bar represents 50μm.

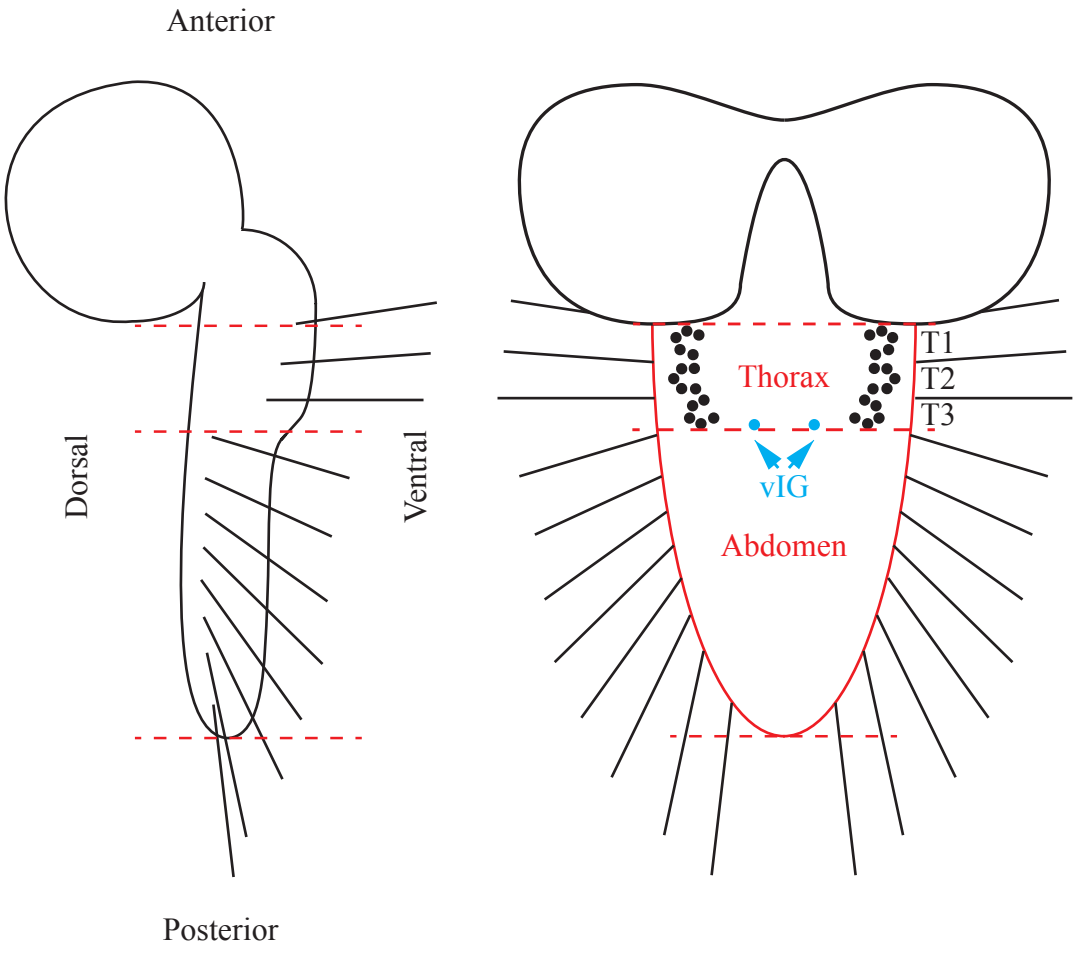


**Figure 2.15** Defining abdominal and thoracic VNC areas as ROIs in anti-Repo staining. The ventral interface glia (vIG) of the last thoracic segment (T3) must first be identified in longitudinal view through the Z-stack of confocal serial sections. The abdominal ROI according to anti-Repo staining is defined as the posterior end of the VNC beginning from the T3 vIG. The thoracic ROI according to the same staining is defined as the anterior region to T3 vIG and includes three pairs of interface glia in unique C-shaped arrangements.

### 2.5.5 Stabbing Injury to the Larval VNC

Stabbing was done in sterile conditions according to the injury paradigm which was set up by Kato *et al.* (2011) and described with more details Kato and Hidalgo (2013) in the Journal of Visualized Experiments. CNS were dissected from staged 96h AEL old larva in Shields and Sang M3 insect culture medium (Sigma) and transferred to fresh culture medium where they were pooled until the dissecting period of a maximum of 20 mins was over. Once dissection was finished, each pooled CNS had their abdominal VNCs stabbed from the dorsal side (Figure 2.16). The instrument of choice was a fine tungsten needle of 0.5mm diameter at the base and 1µm diameter at the tip (Roboz Surgical Instrument Co.).

For time-lapse imaging of stabbed genotype *G9*, in which endogenous GFP labels all the neuropile axons, stabbed samples were transferred and placed dorsal side down in a 35mm glass-based dish (Iwaki), previously coated with 0.01% poly-L-lysine (Sigma) and containing 1mL Shields and Sang M3 insect medium supplemented with 7.5% fetal bovine serum (Sigma) as well as1% penicillin-streptomycin (Sigma). The sample with the highest shape integrity upon being attached to the dish was used for time-lapse imaging. The glass-based dish was lid-covered throughout imaging to prevent evaporation.

For immunohistochemistry, stabbed samples were transferred and cultured separately for 20 to 24 hrs at 25ºC in a 24-well plate (Corning) containing 500µL culture medium with 7.5% fetal bovine serum and 1% penicillin-streptomycin mix. Control samples were dissected, pooled and cultured similarly to stabbed samples, but without applying the needle for injury. Following culture, the samples were checked under the Leica MZ8 stereomicroscope for

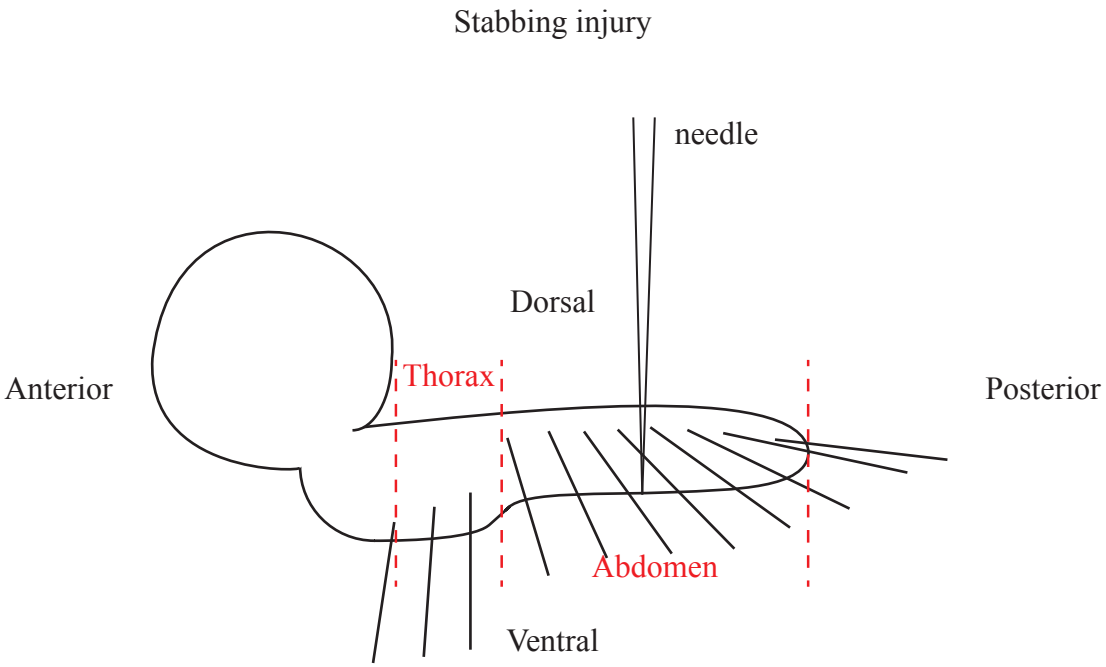


**Figure 2.16** Applying a stabbing injury to the larval VNC. Dissected CNS in Shields and Sang M3 insect medium was pierced through the abdomen from the dorsal side by a fine tungsten needle of 0.5mm diameter at the base and 1μm diameter at the tip (not drawn to scale).

either the retainment of normal shape and size or the attainment of abnormal gross morphology characterised by a cauliflower-like appearance. Samples with normal integrity were selected to be fixed for anti-GS2 immunolabelling while abnormal samples were discarded due to severe tissue degradation.

### 2.5.6 Measurement of Neuropile Wound Size

Wound area was visualised either by GFP in genotype *G9* or by anti-GS2 staining. The area was measured according to Kato *et al.* (2011) on longitudinal Z-stack images of the neuropile acquired using confocal microscopy. The largest outline of the wound throughout the stack of images (that is, the neuropile) was set as the ROI in ImageJ, and the area measured in $\mu m^2$.

## 2.6 Statistical Methods

All data were collated and analysed using Excel 2010 (Microsoft). All statistical tests were carried out using SPSS Statistics 21 (IBM). In all cases, the null hypothesis was that there was no difference between test samples and controls. In all results, whenever the p-value was less than 0.05 ($p<0.05$), the null hypothesis of the test was rejected. The * symbol in statistical results indicates $p<0.05$, ** meaning $p<0.01$ and *** $p<0.001$. Comparisons which are not statistically significant are denoted by 'ns'.

The data for survival index assays were categorical (Section 2.1.5), and all categorical data were tested using Pearson's chi-square test ($\chi^2$). Whenever multiple comparisons among different genotypes were made, a Bonferroni correction was applied to the $\chi^2$ test by

multiplying the p-value with the number of comparisons. When categorical data such as survival index were plotted in bar charts, error bars were not applicable.

Continuous data were obtained from experiments involving area measurements (Section 2.5.2; Section 0), cell counting (Section 2.5.4) and Sholl analysis (Section 2.5.3). The data sets were tested for normality using kurtosis and skewness, as well as the Kolmogorov-Smirnov and Shapiro-Wilk tests. Data were treated as normally distributed when absolute kurtosis and absolute skewness was less than 1.96 of the standard error kurtosis and skewness, respectively. According to the Kolmogorov-Smirnov and Shapiro-Wilk tests of normality, data were normally distributed when p-value was greater than 0.05 ($p>0.05$).

If data were not normally distributed, medians would be considered. For two samples, the medians would be compared using the Mann-Whitney U test. For three or more samples, the medians would be tested using the Kruskal-Wallis one-way ANOVA, with post hoc multiple comparisons performed using the Dunn method.

Normally distributed data from different samples were tested for the homogeneity of variances. Variances of the data from different samples were considered equal if Levene's Test resulted in $p>0.05$. For two samples having equal variances, the means were compared using the independent samples t-test for equality of means. For three or more samples having equal variances, the means were compared using the one-way ANOVA, after which post hoc multiple comparisons were applied using the Dunnett or Bonferroni method. The Dunnett method compares all the means of test samples to the control mean, while the Bonferroni compares all means to each other. For normally distributed data of different samples having

unequal variances (Levene's Test, $p<0.05$), Welch ANOVA was applied instead. In turn, the post hoc multiple comparison was performed using the Games-Howell method, which compares all means to each other.

When continuous data such as area and length were plotted in bar charts, error bars representing standard deviation (SD) were used instead of standard error (SE). All statistical reports for this project have been included in the appendix (Section 9).

# Chapter 3

# 3 Expression and Distribution of DNTs, Toll, Toll6 and Toll7

## 3.1 Introduction

This chapter is about determining whether or not the DNTs remain biologically relevant in the larval CNS after embryonic stages.

### 3.1.1 Known Expression Patterns of DNTs, Toll, Toll6 and Toll7 in Larval CNS

Previously in the Hidalgo lab, expression patterns of *dnt* genes in embryos were described from localised mRNA expression using the *in situ* hybridisation technique (Zhu *et al.*, 2008). In the larva, transcripts for *dnt1*, *dnt2* and *spz* were expressed in the body-wall musculature (Sutcliffe *et al.*, 2013). *Dnt1* transcripts were detected in the larval optic lobe and diffusely throughout the central brain and thoracic cortex (Sutcliffe, 2011; Zhu *et al.*, 2008). *Dnt2* transcripts were restricted the larval eye-antenna disc (Sutcliffe, 2011). *Spz* transcripts were detected in the larval optic lobe, diffusely throughout the central brain and VNC, and in higher levels in cells within the central brain and VNC (Sutcliffe, 2011).

*Toll6* and *Toll7* transcripts were shown to be expressed in the larval optic lobes, central brain and VNC (McIlroy, 2012). GAL4 reporter lines for *Toll*, *Toll6* and *Toll7* showed GFP expression in the CNS (McIlroy, 2012; Sutcliffe, 2011). Although Toll is the well-known receptor of Spz, and *spz* transcripts were found in the larval CNS (Sutcliffe, 2011), whether or

not *Toll* is expressed in the larval CNS has yet to be discovered, primarily because the research focus has mainly centred around the role of *Toll* in embryonic dorsal-ventral patterning and in immunity.

### 3.1.2 GAL4 Reporters for *dnt* Genes

There are four available GAL reporters for *dnt1* which were generated by Dr B. Zhu of the Hidalgo lab (Figure 3.1A). The regulatory sequence upstream of *dnt1* used for *Dnt1-I*'s construct was derived from the 2.3kb genomic region between *dnt1* and its adjacent gene *tie* (Figure 3.1A). At 4.8kb, *dnt1-II*'s construct was the longest and was an extension of *dnt1-I*'s construct length, encompassing the first exon of *dnt1*, up to and including the first intron of *dnt1* (Figure 3.1A). *Dnt1-III*'s 2.5kb construct was cloned from the first exon and first intron of the *dnt1* gene (Figure 3.1A). The fourth *dnt1-GAL4* construct used the first intron only (Figure 3.1A). Put together, the four *dnt1-GAL4* transgenic constructs had covered all the non-coding genomic regions between the *dnt1* and *tie* genes, both fully and at divided lengths, for which their suitability as drivers to express *dnt1* patterns were tested.

Dr S. Alahmed generated a *dnt2-GAL4* transgenic based on cloning approximately 2.5-6.0kb of the region upstream of the *dnt*2 coding region (Dr S. Alahmed, personal communication).The *spz-GAL4* construct was generated in the lab by cloning approximately 3kb of the regulatory region upstream of the coding region of the *spz* gene (Dr S. Alahmed, personal communication).

### 3.1.3 *Mi{MIC}*-EGFP Protein Traps for *spz* and *Toll6*

Gene expression patterns can also be visualised with protein traps (Venken *et al.*, 2011a). Protein traps depend on the presence of transposons, such as *Minos*, in the gene of interest (Venken *et al.*, 2011a). The *Minos*-mediated integration cassette (*Mi{MIC}*) incorporates an enhanced green fluorescent protein (EGFP) tag into genes (Venken *et al.*, 2011b), and there are *Mi{MIC}* lines containing EGFP tags available for *spz* (Figure 3.13A) and *Toll6* genes (Figure 3.27A).

### 3.1.4 Antibodies for DNTs, Toll and Toll7

The Hidalgo lab generated antibodies to the DNTs, Toll6 and Toll7 using peptides that were designed by the collaborators, Dr J. Aurikko and Prof N. Gay, and by Davids Biotechnologie. Commercially available antibodies against Toll are available (Table 2.5).

Two different antibodies were raised against DNT1. They were raised against the peptides, RRPQ and VRY. The RRPQ peptide is a 21-mer amino acid sequence (RRPQHSEARLDLD LAPSETHS) within the DNT1 C-terminus tail (Figure 3.4A). This portion of the C-terminus exists in four out of seven DNT1 isoforms annotated in FlyBase. The VRY peptide is an 18-mer amino acid sequence (VRYARPQKAKSASGEWKY) within the DNT1 CysKnot domain (Figure 3.5A).

Three peptides were designed for the purpose of raising antibodies against DNT2. These peptides are DNT2-ALN, DNT2-GYN and DNT2-KRL. Their amino acid sequences are

situated in the CysKnot domain (Figure 3.8B). The ALN peptide is a 23-mer long amino acid sequence (ALNSRGNWMFVVNEQNTARQMVK). The GYN peptide is 18-mer long (GYNSRCEQKFVQKRLIAL) and its last 6 amino acid seqeuence overlaps with the KRL peptie, which is a 12-mer amino acid sequence (KRLIALQGNGQN).

Two antibodies were raised against amino acid sequences within the CysKnot domain of the Spz protein (Figure 3.14A). The amino acid sequence of Spz-GLR, which is 14-mer long, is GLRADDTWQLIVNN, while Spz-ASK's 9-mer sequence is ASIKSDGEL.

### 3.1.5 Specific Aims

The specific aims of this chapter are:

- To characterise reporter patterns of *dnt1*-, *dnt2*- and *spz-GAL4* in the larval VNC.
- To characterise larval VNC EGFP patterns of *Mi{MIC}* insertions into the *spz* and *Toll6* gene.
- To characterise immunostaining patterns of anti-DNT1, anti-DNT2 and anti-Spz antibodies in the larval VNC.
- To characterise immunostaining patterns on anti-Toll and anti-Toll7 antibodies in the larval VNC.

### 3.1.6 Methods in Brief

*Dnt-GAL4* lines were crossed to *UAS-GAP-GFP*, *UAS-mCD8-GFP* and *10xUAS-myr-tdTomato*. GAP-GFP is a fusion of the myristoylation sequence from *GAP43* gene to GFP,

and it is membrane-targeted. The mCD8-GFP is a protein fusion between the murine lymphocyte receptor CD8 and EGFP, and it is also membrane targeted. Myristoylated tandem dimer Tomato (tdTomato) fluorescent protein is membrane targeted too.

*Elav-GAL4* were crossed to *UAS-DNT1-CK3'+* for pan-neuronal overexpression of activated DNT1 in the form of CysKnot with 3' tail (genotype: *elav>DNT1-CK3'+*). *Pdf-GAL4* were crossed to *UAS-DNT2-CK-6A* (genotype: *pdf>DNT2-CK-6A*) to overexpress the CysKnot form of DNT2 in laternal neurons (LN) in the brain. *Repo-GAL4* crossed to *UAS-actSpz(2)* overexpress activated Spz in all glia, except midline glia (*repo>actSpz(2)*). The genotype $spz^{HMS01178}$ is a fly stock used to knockdown *spz* (stock no. 29, Table 2.1).

The antibodies used in this chapter are listed in Table 2.5 and Table 2.6. Antibodies against Toll6 failed to be optimised for immunohistochemistry and will not be discussed here.

Z-stack confocal images of larval CNS were acquired in longitudinal view. Images in transverse view were reconstructed from acquired Z-stacks in ImageJ. Pixel width and height do not match voxel depth in most cases.

## 3.2 Results

### 3.2.1 Expression Pattern of *dnt1* in the Larval CNS

#### 3.2.1.1 Patterns of *dnt1-GAL4*

*Dnt1-I-GAL4* and *dnt1-III-GAL4* transgenic flies were crossed to *UAS-GAP-GFP*, and the larval CNS stained with anti-GFP antibody. Between *dnt1-I-* and *dnt1-III-GAL4*, the expression patterns of GAP-GFP in the larval VNC were similar (Figure 3.1B and C). GAP-GFP was found in the neurohemal organs (NHOs) in the abdomin (n=7, Figure 3.1B; n=7, Figure 3.1C). The neurohemal organ was identified as part of the abdomen because the stalk-like structure at the segment border of neuromeres bifurcates and thoracic neurohemal organ do not exhibit bifucation (Ito *et al.*, 1995).The GAP-GFP was also found in a pair of axons running along the midline (or close to the midline) between the anterior subesophageal ganglion (SEG/SubGgl) and the peripheral nerves of the posterior caudal neuromere, A8/9 (n=7, Figure 3.1B). The cytoplasm of three cell soma pairs in the anterior half of the abdomen, relatively ventral in the nerve cord, carried abundant GFP signal (n=7, Figure 3.1B; n=7, Figure 3.1C). Anterior to the nerve cord, GFP was detected in the ring gland and, below the ring gland, in a pair of cell bodies together with their projections (n=1, Figure 3.1C).

The crossings of *dnt1-I-* and *dnt1-III-GAL4* to *UAS-GAP-GFP* were done in parallel with Dr S. Alahmed of the Hidalgo Lab. When using *GAL4* lines other than *dnt1-GAL4*, Dr S. Alahmed observed similar GAP-GFP patterns to those shown in B and C (personal communication). Her GAP-GFP was seen in the pair of axons running close to the midline along the VNC and in the three pairs of ventral cell bodies (personal communication). The said GAP-GFP pattern had turned up in a sufficient number of occasions such that the legitimacy of the *UAS-GAP-GFP* transgenic stock was doubted and eventually checked (Hidalgo Lab, personal communication). Despite the absence of GAL4, Dr S. Alahmed detected endogenous GFP in *UAS-GAP-GFP* using anti-GFP antibodies (n=2, Figure 3.2A; raw data provided by Dr S. Alahmed). Furthermore, the anti-GFP pattern (Figure 3.2A) was

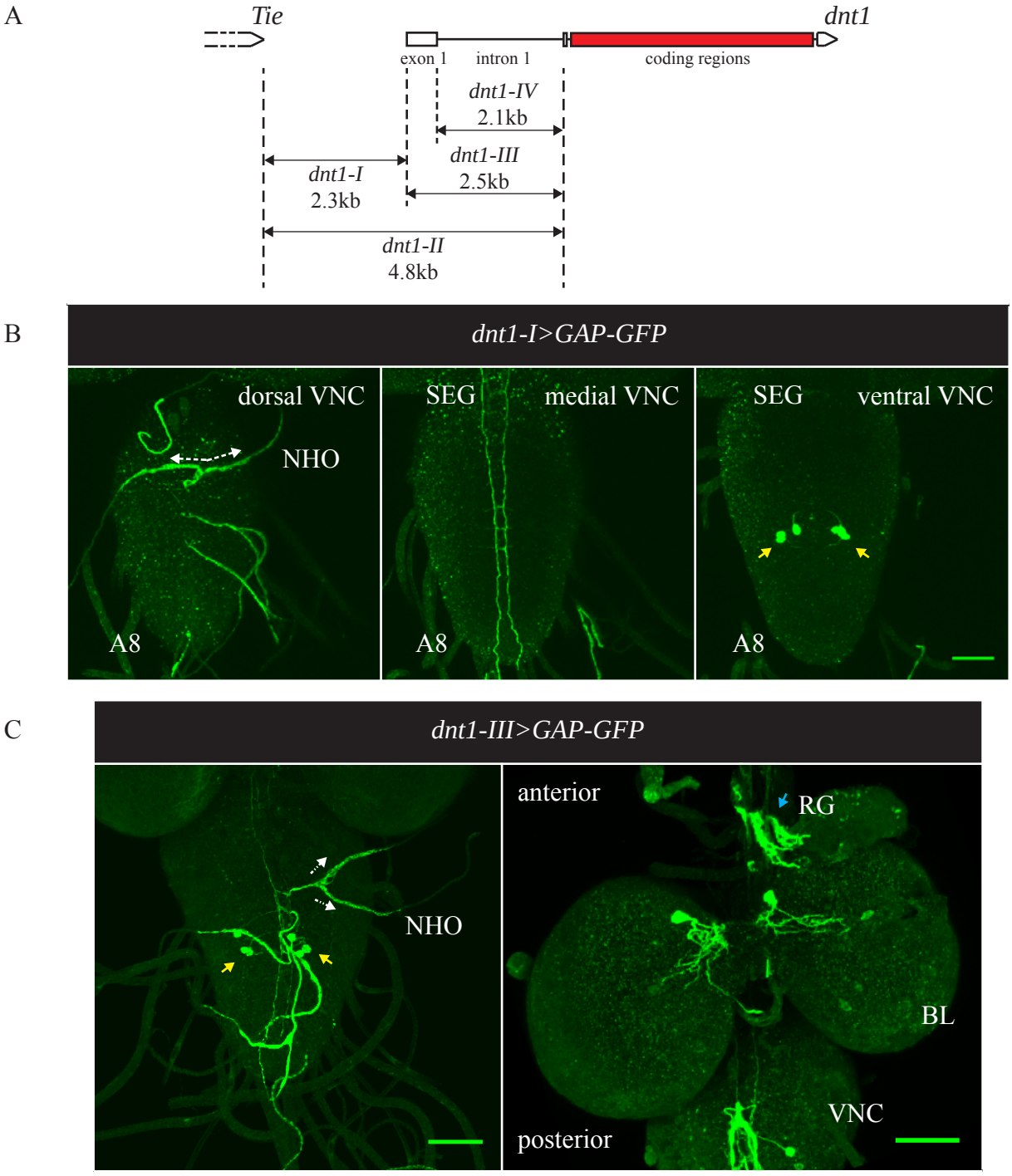


**Figure 3.1** Expression of GAP-GFP in the larval CNS as revealed by *dnt1-GAL4*. **(A)** Four genomic sequences cloned as possible promoters of *dnt1* and spanning from *dnt1*'s coding region to *Tie*. *Dnt1* and *Tie* genes are illustrated here in 5' to 3' orientation, although both genes are in the minus strand and *Tie* lies upstream of *dnt1*. **(B)** Expression of GAP-GFP driven by *dnt1-I-GAL4* in the larval VNC (n=7). **(C)** Expression of GAP-GFP driven by *dnt1-III-GAL4* in the larval VNC (left: n=7) and BLs (right: n=1). Signal of endogenous GFP in (B) and (C) was amplified by labelling with anti-GFP and Alexa Fluor® 488 antibodies. **White arrows:** Bifurcation of NHO. **Yellow arrowheads:** Ventral cell bodies. **Cyan arrowhead:** GFP in RG. Scale bars in (B) and (C) represent 50µm.

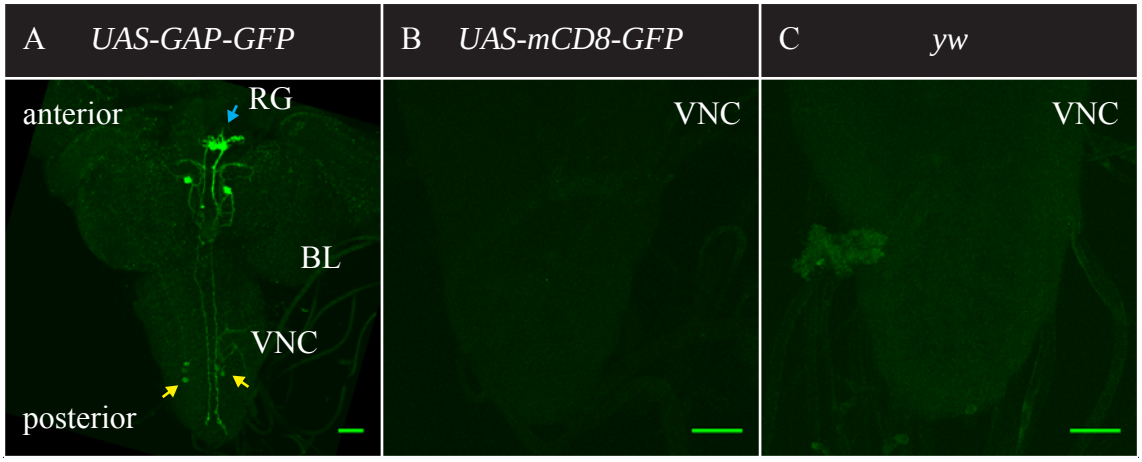


**Figure 3.2** Checking of *UAS-GAP-GFP* and *UAS-mCD8-GFP*. Anti-GFP and Alexa Fluor® 488 labelling in **(A)** *UAS-GAP-GFP* alone without GAL4 (maximum projections of larval CNS; n=2, raw images provided by Dr S. Alahmed), **(B)** *UAS-mCD8-GFP* alone without GAL4 (maximum projections of larval VNC; n=2), and **(C)** *yw* without GAL4 and UAS (maximum projections of larval VNC; n=2). **Yellow arrowheads:** Ventral cell bodies. **Cyan arrowhead:** GFP in RG. Scale bars in (A) to (C) represent 50µm.

similar to those in *UAS-GAP-GFP* under the control of *dnt1-I-* and *dnt1-III-GAL4* (Figure 3.2B and C). In effect, expression pattern data collected from fly crosses which used *UAS-GAP-GFP* were invalid. However, any expression pattern data from crosses with *UAS-mCD8-GFP* remained valid because the presence of GAL4 was proven to be required for the expression of mCD8-GFP (n=2, Figure 3.2B). Lack of GAL4 proteins did not yield reporter signal in *UAS-mCD8-GFP* (Figure 3.2B), and the background signal in *UAS-mCD8-GFP* was similar to the baseline level in *yw*, a genotype without *GAL4* and *UAS* transgenes (n=2, Figure 3.2C).

*Dnt1-GAL4* flies were crossed to *UAS-mCD8-GFP*, and the larval CNS stained with anti-GFP antibody. *Dnt1-I-GAL4* drove mCD8-GFP expression in two regions: in a punctate fashion along the longitudinal axis of the neuropile at the dorsal edge, and in a narrow tract along the longitudinal axis of the ventral neuropile (n=19, Figure 3.3A). The punctate mCD8-GFP expression was strongest under *dnt1-I-GAL4* (n=19, Figure 3.3A) and was variable in strength from weakly, with *dnt1-II* (n=20, Figure 3.3B) and *dnt1-III*-GAL4 (n=5, Figure 3.3C), to virtually non-existing with *dnt1-IV-GAL4* (n=10, Figure 3.3D). Across the four *dnt1-GAL4* lines, the narrow tract pattern of mCD8-GFP was more consistent and more prominent than the punctate expression (Figure 3.3A-D). The prominent longitudinal tracts also have lateral GFP-positive axons in most segments of the nerve cord (Figure 3.3, top panel). These lateral GFP axons appear to connect the tracts in the neuropile with the edge of the nerve cord, particularly at the intersection with peripheral nerves (Figure 3.3, bottom panel). Collectively, the four *dnt1-GAL4* transgenes, irrespective of their promoter length, reported similar EGFP patterns in the larval CNS, which means the regulatory region for *dnt1* is most likely to be within the first intron of *dnt1* (Figure 3.1A).

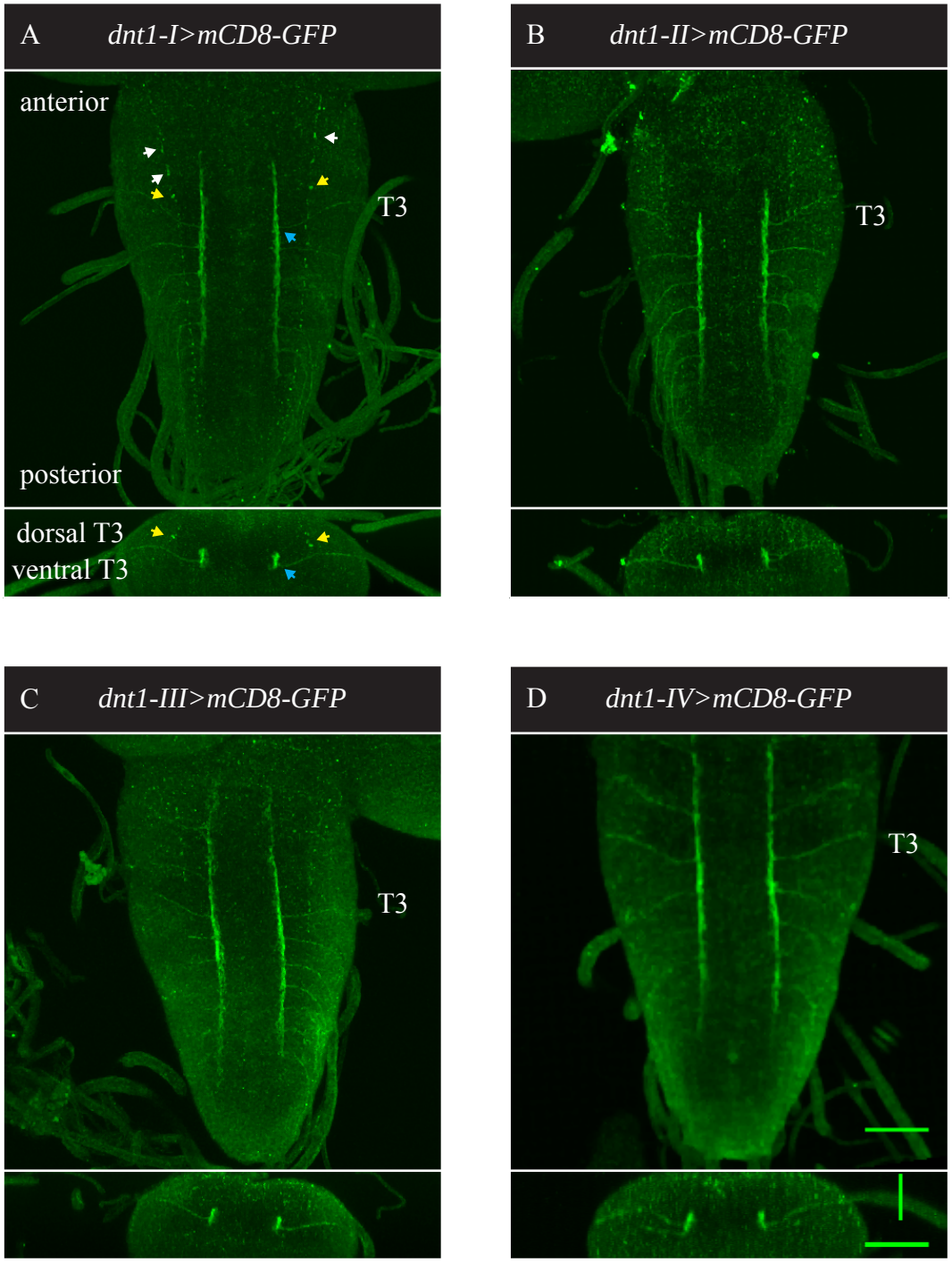


**Figure 3.3** Expression of mCD8-GFP under GAL4 driven by **(A)** *dnt1-I*- (n=19), **(B)** *dnt1-II*- (n=20), **(C)** *dnt1-III*- (n=5) and **(D)** *dnt1-IV-GAL4* (n=10). Signal of endogenous mCD8-GFP was amplified by labelling with anti-GFP and Alexa Fluor® 488 antibodies. **Top panel:** Maximum projections of VNC in longitudinal view. **Bottom panel:** Maximum projections of thoracic segment T3 in reconstructed transverse view. **White arrowheads:** Punctate GFP. **Yellow arrowheads:** Corresponding punctate GFP in longitudinal and transverse views. **Cyan arrowheads:** Corresponding tract in longitudinal and transverse views. Scale bar in top panel represents 50µm. Scale bars along x- and y-axes in bottom panel represent 50µm.

#### 3.2.1.2 Immunostainings of Anti-DNT1 Antibodies

Staining *yw* CNS with anti-DNT1-RRPQ antibody (Figure 3.4A) revealed signal in two pairs of cell bodies in the central brain area, in lateral cells in the VNC and in most areas of the neuropile (n=5, Figure 3.4B). These signal were also detected in the transheterozygous null genotype *dnt1*$^{41}$*/Df(3L)Exel6101* (n=3, Figure 3.4B), indicating anti-DNT1-RRPQ is not a specific antibody.

In *yw* CNS, anti-DNT1-VRY (Figure 3.5) stained the ring gland, the outer proliferation centre (OPC), the inner proliferation centre (IPC) and a pair of cell bodies in the anterior edge of the brain lobes (n=6, Figure 3.6B). There are punctate signals in the *yw* central brain and VNC neuropile (Figure 3.6B). The puncta are contiguous along the longitudinal axis in the thoracic neuropile, relatively ventral. These described patterns in the *yw* were reproduced in *dnt1*$^{41}$*/Df(3L)Exel6101* (n=6, Figure 3.6B). In *elav>DNT1-CK-3'+* CNS, signal came up in the ring gland and brain lobes too (n=4, Figure 3.6B). Most particularly, ectopic signal in multiple cell bodies in the lateral and ventral cortex were detected (Figure 3.6B).

### 3.2.2 Expression Pattern of *dnt2* in the Larval CNS

#### 3.2.2.1 Patterns of *dnt2-GAL4*

*Dnt2-GAL4* flies were crossed to *10xUAS-myr-tdTomato*, and the larval CNS stained with anti-DsRed antibody. The *10xUAS-myr-tdTomato* reporter might drive stronger expression than *UAS-mCD8-GFP*. At best, the myr-tdTomato expression under *dnt2-GAL4* control was

A

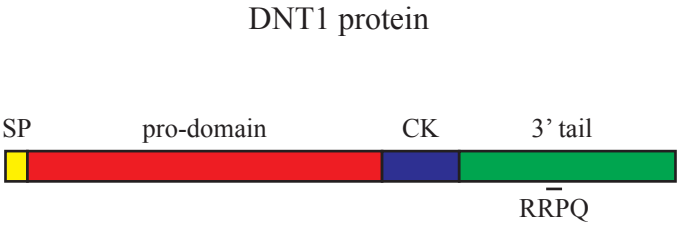


B

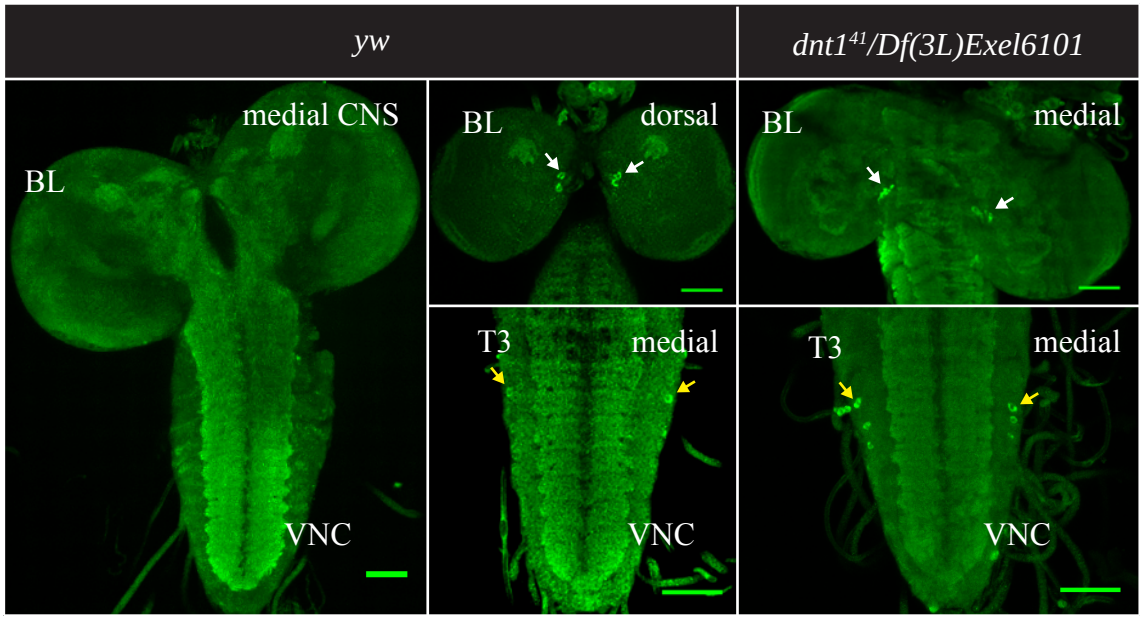


**Figure 3.4** Staining of larval CNS with anti-DNT1-RRPQ antibodies. **(A)** DNT1 protein illustrated in the direction of N-terminus to C-terminus. SP: signal peptide. CK: CysKnot domain. RRPQ is a 21-mer amino acid sequence in the C-terminus tail. **(B)** Detection of DNT1 protein using anti-DNT1-RRPQ in *yw* control larvae (n=5) and *dnt1*$^{41}$*/Df(3L)Exel6101* transheterozygous null mutant larvae (n=3). Images were acquired using the 488nm laser with identical laser power and PMT settings, then processed using ImageJ and Photoshop. **White arrowheads:** Note signal in cell bodies in BLs. **Yellow arrowheads:** Note signal in cell bodies in VNCs. Scale bars in (B) represent 50µm.

A

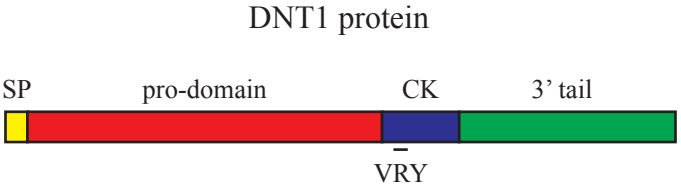


B

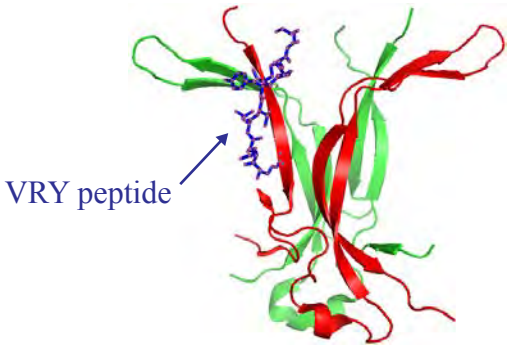


**Figure 3.5** Raising polyclonal antibodies against DNT1 using the VRY peptide. **(A)** DNT1 protein illustrated in the direction of N-terminus to C-terminus. SP: signal peptide. CK: CysKnot. VRY is an 18-mer amino acid sequence in the CysKnot domain. **(B)** Model of DNT1 protein by J. Aurikko and N. Gay. The quaternary structure is made of two DNT1 monomers, one in green and one in red. In the red monomeric structure, the ball and stick model represents the VRY peptide in context of the DNT1 protein.

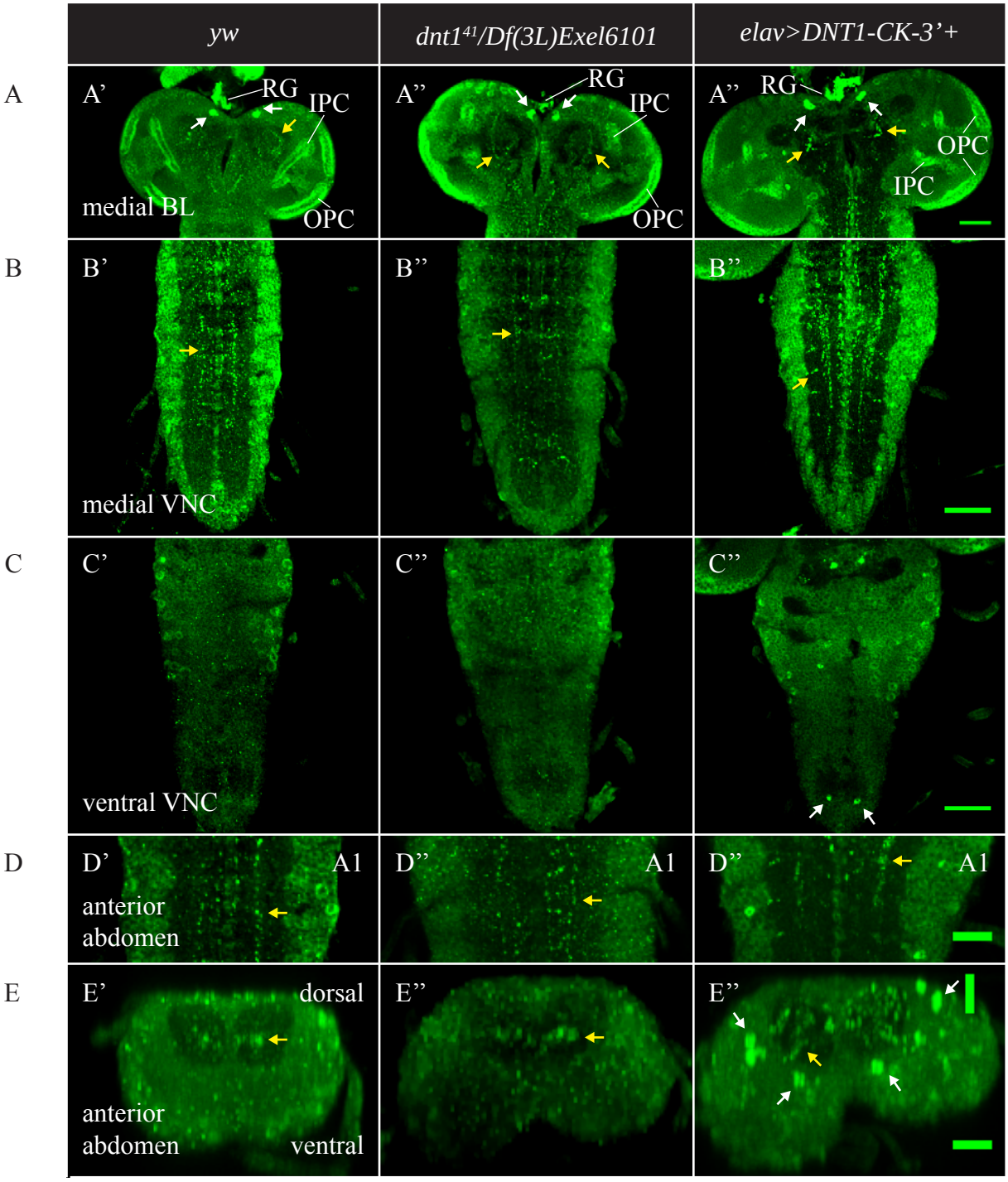


**Figure 3.6** Detection of DNT1 protein using anti-DNT1-VRY antibodies. Maximum projections of: **(A)** medial BLs in longitudinal view, **(B)** medial VNCs in longitudinal view, **(C)** ventral VNCs in longitudinal view, **(D)** anterior abdomens in medial and longitudinal views, and **(E)** anterior abdomen in reconstructed transverse view. Genotypes: *yw* (n=6), *dnt1*$^{41}$*/Df(3L)Exel6101* (n=6) and *elav>DNT1-CK-3'* (n=4). Images were acquired using the 488nm laser with identical laser power and PMT settings, then processed using ImageJ and Photoshop. **White arrowheads:** Note signal in cell bodies. **Yellow arrowheads:** Note punctate signals. Scale bars in (A) to (C) represent 50µm. Scale bars in (D) and (E) represent 25µm.

detected only in the ring gland (n=1, Figure 3.7).

#### 3.2.2.2 Immunostainings of Anti-DNT2 Antibodies

Dr A. Hidalgo, Dr J. Wentzell and the author started out immunohistochemistry work using anti-DNT2s in embryonic, adult and larval CNS, respectively. Immunostaining in embryos turned up with signal from all three anti-DNT2 antibodies (Figure 3.8), of which the most meaningful result came from staining with anti-DNT2-GYN. Anti-DNT2-GYN revealed revealed signal in the CNS, muscle, epidermal stripes and trachea (Dr A. Hidalgo & Dr J. Wentzell, personal communication). In the larval CNS, wisplike tracheal ganglionic branch (GB) was observed in the brain lobes and VNC (n=3, Figure 3.9C). No signal was observed in the adult brain by Dr J. Wentzell (personal communication). For the remaining two antibodies, anti-DNT2-ALN and anti-DNT2-KRL, immunohistochemical attempts had been made in the adult brain. Anti-DNT2-ALN did not yield signal while anti-DNT2-KRL revealed brain signal (Dr J. Wentzell, personal communication). Anti-DNT2-ALN staining revealed signal in the embryonic CNS, muscle and fat body. In the larval neuropile of *yw* central brain and VNC, anti-DNT2-KRL revealed strong puncta (n=3, Figure 3.10A' and B'). There were also signal surrounding the surface edges of the CNS. The puncta and CNS surface signals were reproduced in the VNC neuropile of $dnt2^{37}/Df(3L)Exel6092$, indicating that anti-DNT2-KRL is not specific (n=1, Figure 3.10B''). In genotype *pdf>DNT2-CK-6A*, ectopic symmetrical pair of cells furthest from the brain lobe commissure were detected (n=9, Figure 3.10A''), indicating that anti-DNT2-KRL can detect endogenous DNT2.

Next, *yw* CNS was stained with anti-DNT2-KRL and commercial anti-Fasciclin-II (anti-FasII)


**Figure 3.7** Expression of myr-tdTomato under *dnt2-GAL4*. Signal of endogenous myr-tdTomato was amplified by labelling with anti-dsRed and Alexa Fluor 647® antibodies (n=1). Scale bar represents 50µm.

A

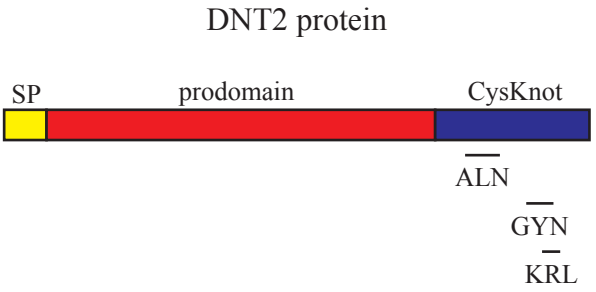


B

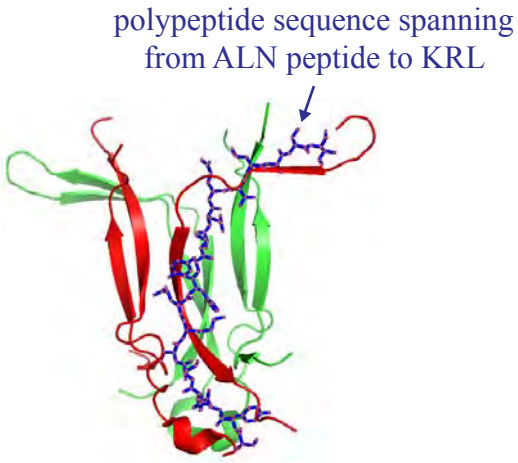


**Figure 3.8** Raising polyclonal antibodies against DNT2 using ALN, GYN and KRL peptides. **(A)** DNT2 protein illustrated in the direction of N-terminus to C-terminus. SP: signal peptide. ALN, GYN and KRL are 23-, 18- and 12-mer amino acid sequences in the CysKnot domain, respectively. **(B)** Model of DNT2 protein by J. Aurikko and N. Gay. The quaternary structure is made of two DNT2 monomers, one in green and one in red. In the red monomeric structure, the ball and stick model represents the polypeptides from sequences of the ALN peptide to those of KRL.

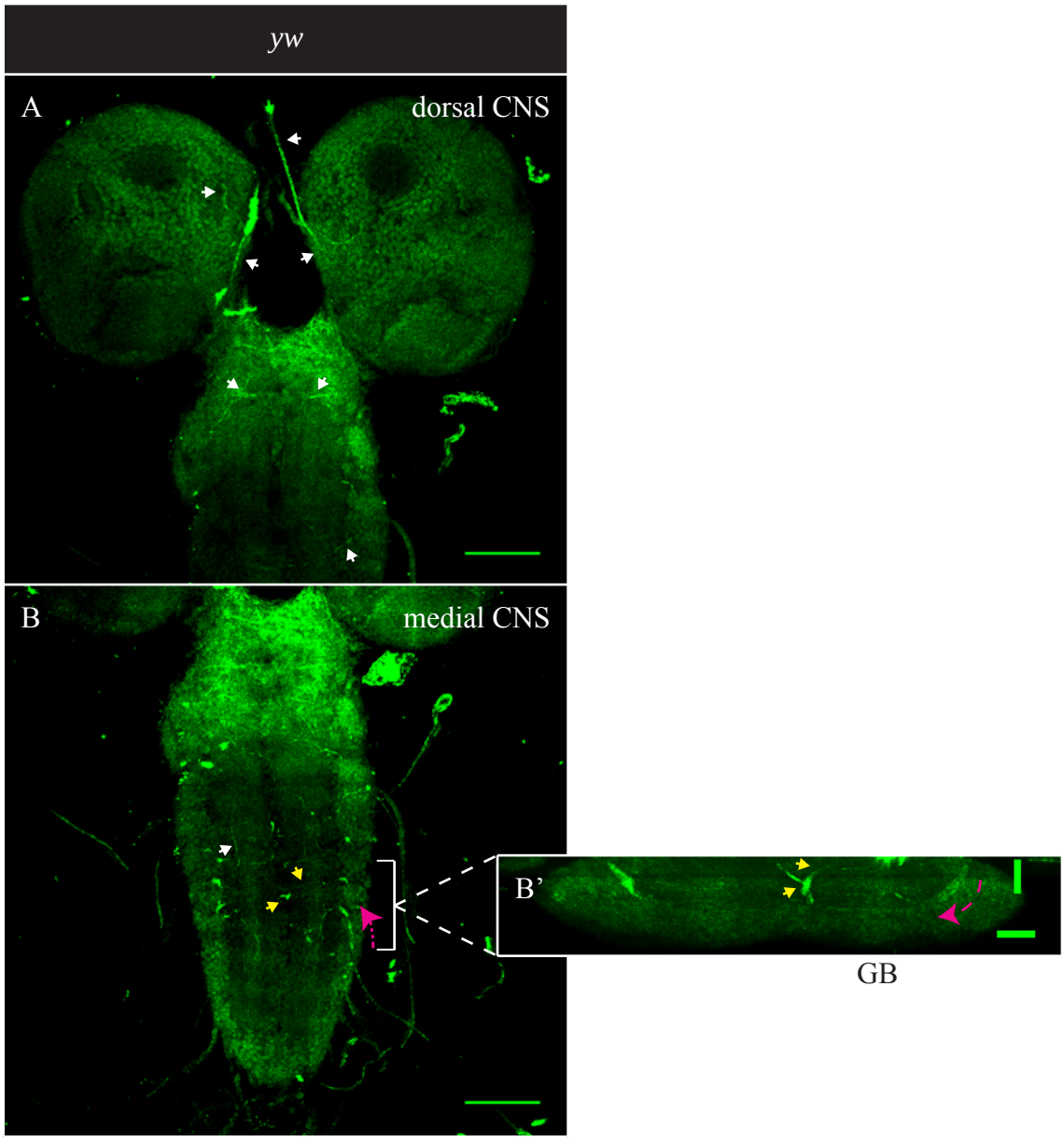


**Figure 3.9** Staining of larval CNS with anti-DNT2-GYN antibodies. **(A)** Maximum projections of dorsal CNS in longitudinal view. **(B)** Maximum projections of medial CNS in longitudinal view. **(B' inset)** Maximum projections of abdominal VNC in reconstructed transverse view. Genotype: *yw* (n=3). **White arrowheads:** Tracheal signal. **Yellow arrowheads:** Corresponding tracheal ganglionic branching in the VNC. **Cyan dashed path:** Trace of a tracheal branch. Scale bars in (A) and (B) represent 50µm. Scale bars along x- and y-axes in (B') represent 10 and 25µm, respectively.

Anti-DNT2-KRL staining

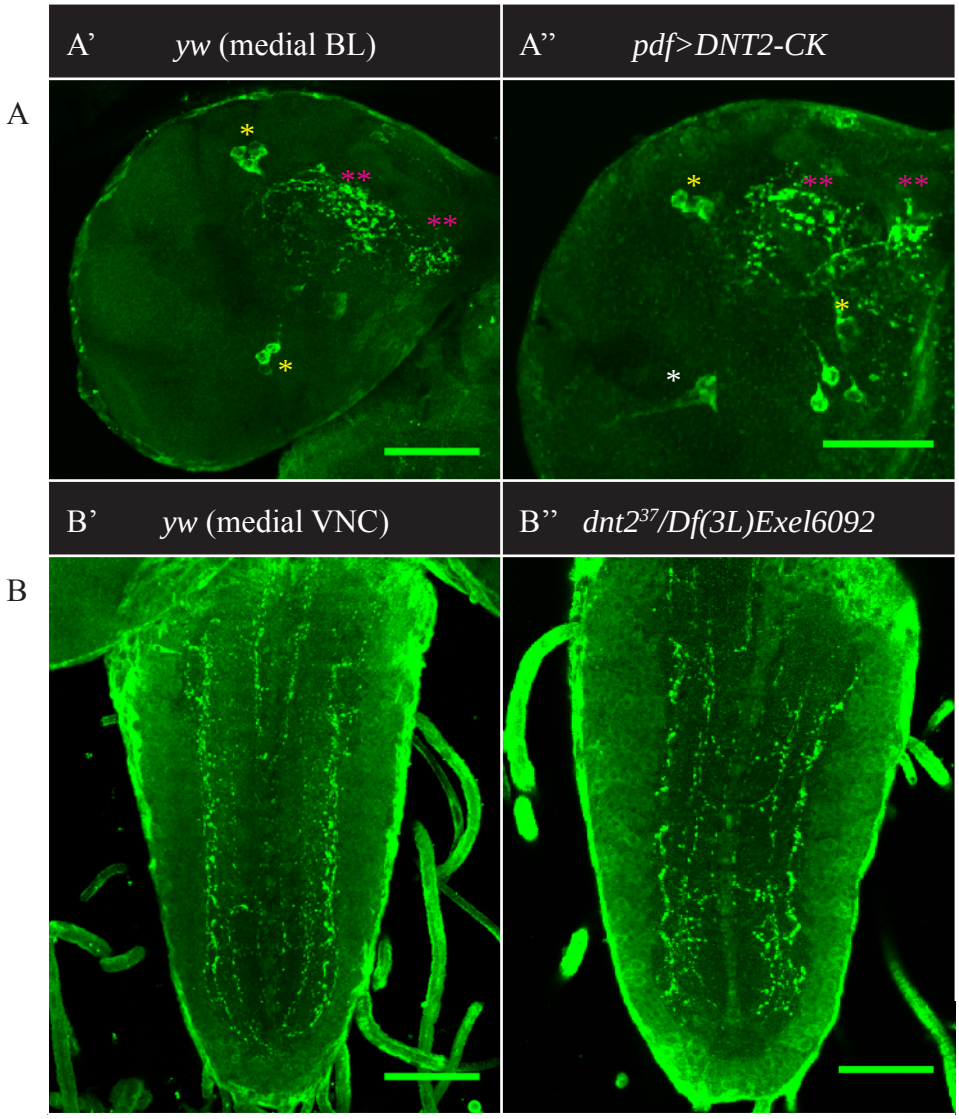


**Figure 3.10** Detection of DNT2 protein using anti-DNT2-KRL antibodies. Maximum projections of: **(A)** medial BLs in longitudinal view, and **(B)** medial VNC in longitudinal view. Genotypes: *yw* (n=3), *dnt2*$^{37}$*/Df(3L)Exel6092* (n=1) and *pdf>DNT2-CK* (n=9). Images were acquired using the 488nm laser with identical laser power and PMT settings, then processed using ImageJ and Photoshop. **White asterisk:** Ectopic signal. **Yellow asterisks:** Corresponding cell clusters. **Magenta asterisks:** Corresponding punctate clusters. Scale bars in (A) and (B) represent 50μm.

to characterise and map the antibody pattern (Landgraf *et al.*, 2003). DNT2 protein was distributed along the dorsal-lateral (DL) and dorsal-median (DM) neurons (n=2, Figure 3.11A and B). The puncta longitudinally along the DL is adjacently ventral to the DL tracts in the first two abdominal segments (Figure 3.11C). Most of the puncta are deposited along the centre axis of the neuropile in the transverse section (Figure 3.11C). The medial puncta clustered with the DM as well as the dorsal split of the ventral median fascicles (VMd) (Figure 3.11C).

### 3.2.3 Expression Pattern of *spz* in the Larval CNS

#### 3.2.3.1 Patterns of *spz-GAL4*

The *10xUAS-myr-dTomato* reporter signal under the control of *spzGAL4* (n=2) was stronger than *UAS-mCD8-GFP* (n=2), as exemplified by the signal intensity in the surface perineurium layer (Figure 3.12A). The perineurium layer was revealed all over the surface of the CNS except where the optic stalk enters the brain lobes (Figure 3.12B'''). Also, the neuropile signal in the central brain and thorax appeared sparser than that in the abdomen (Figure 3.12B'). The transverse view revealed that the denser neuropile signal in the abdomen than in both the thorax and central brain visually correlated with the increase of labelled cell bodies (Figure 3.12B'').

#### 3.2.3.2 Patterns of $spz^{Mi08633}$

There are two *Mi{MIC}* insertions into *spz*, one into the first intron and another into the 3'

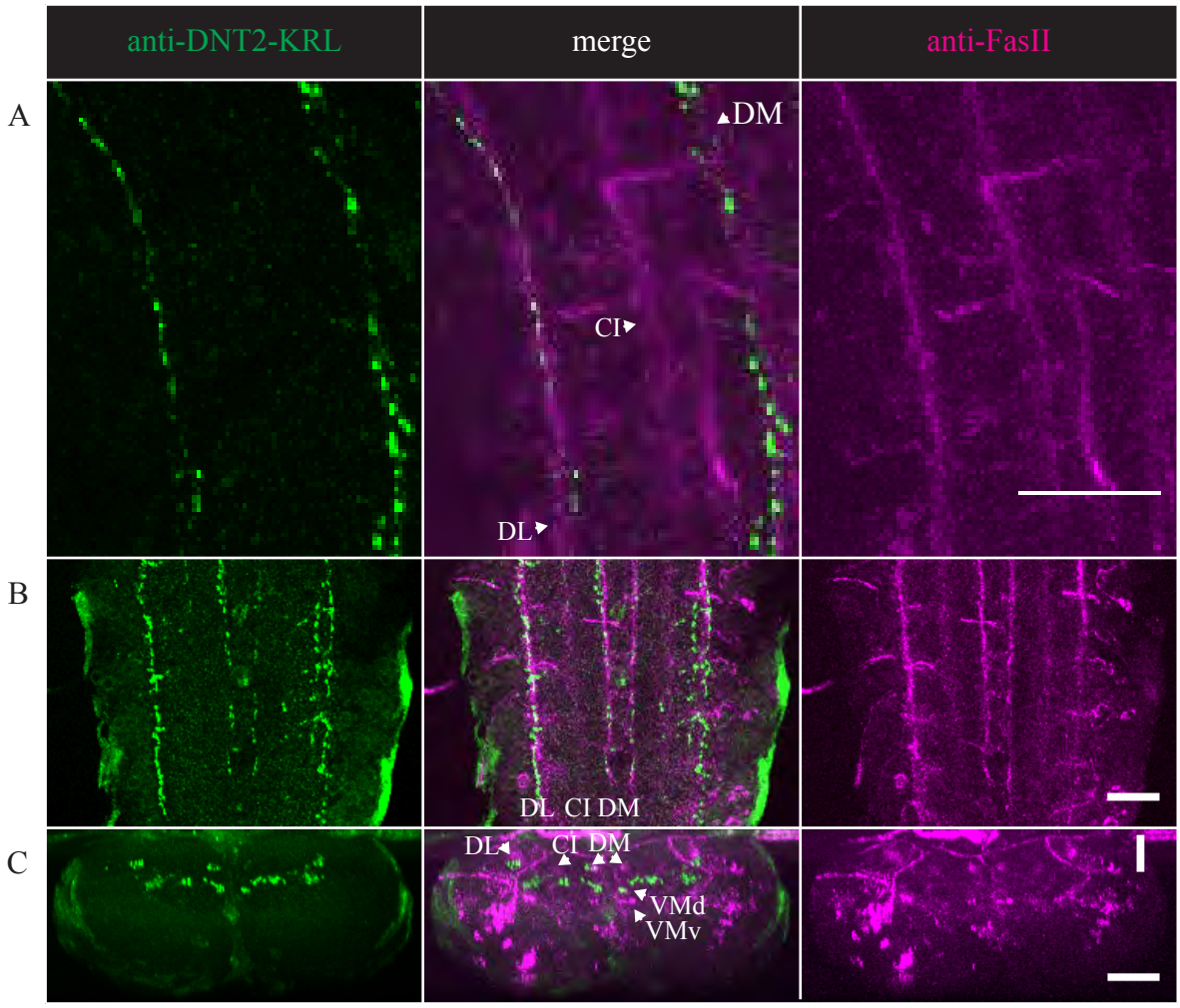


**Figure 3.11** Staining of anti-DNT2-KRL with anti-FasII. Maximum projections of: **(A)** thoracic VNCs in longitudinal view, **(B)** abdominal VNCs in longitudinal view, and **(C)** abdominal VNCs in reconstructed transverse view. Genotype: *yw* (n=2). D, d=dorsal; C=centre; V, v=ventral; L=lateral; I=intermediate; M=median. Scale bars in (A) to (C) represent 25µm.

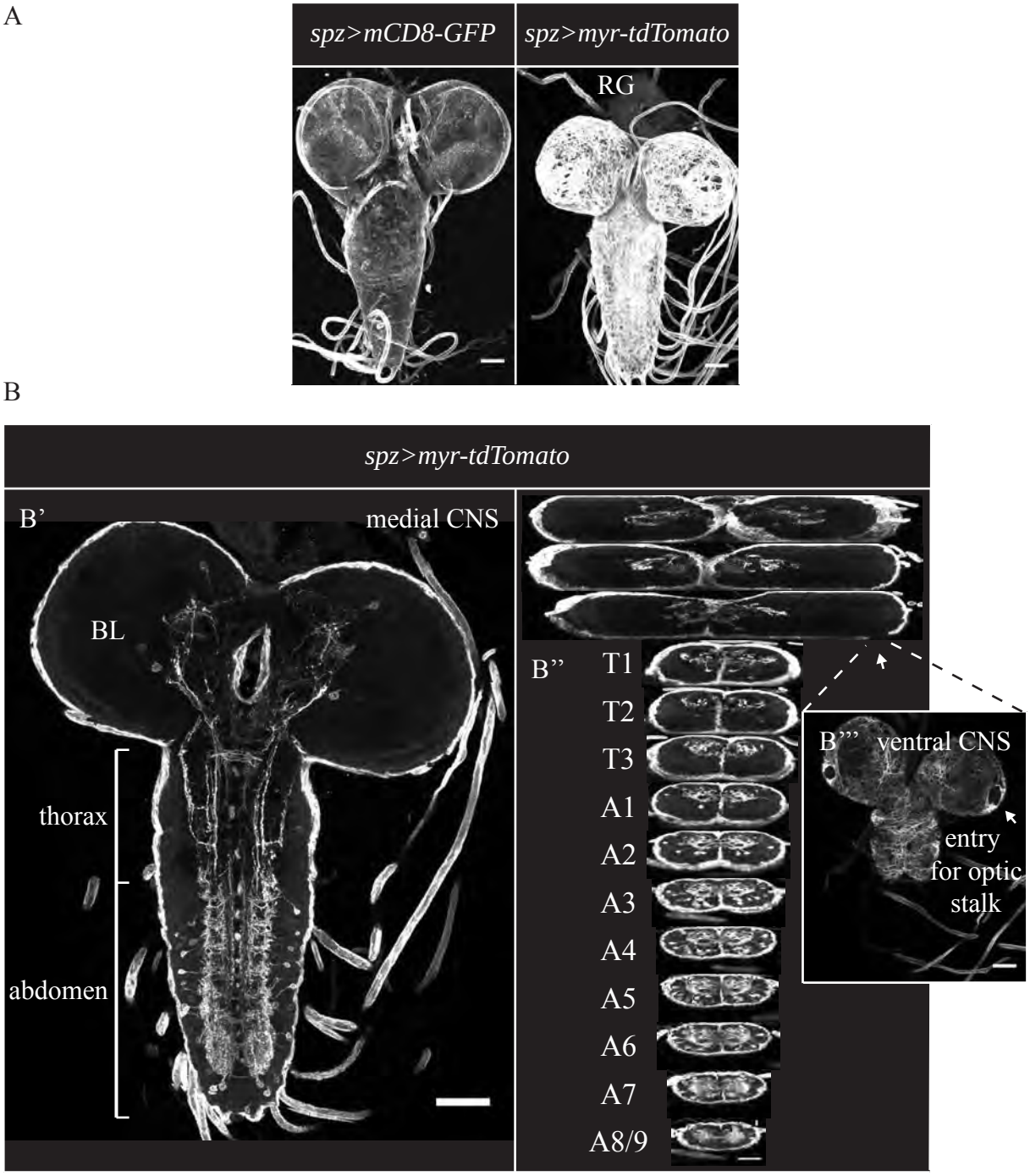


**Figure 3.12** Expression of mCD8-GFP and myr-tdTomato under *spz-GAL4*. **(A)** Maximum projections of whole stack larval CNS. Genotypes: *spz>mCD8-GFP* (n=2) and *spz>myr-tdTomato* (n=2). Signal of endogenous GFP and myr-tdTomato were amplified by labelling with anti-GFP+Alexa Fluor 488® and anti-dsRed+Alexa Fluor 647® antibodies, respectively. **(B)** Maximum projections of *spz>myr-tdTomato* in **(B')** medial longitudinal, **(B'')** reconstructed transverse, and **(B''')** ventral longitudinal views. In (B''), the volume occupied by the squashed brain lobes reflects the distance between the coverslip and microscope slide, accounting for the deformed look of the brain lobes in comparison to the VNC (T1-T3, A1-A8/9). Scale bars in (A), (B') and (B''') represent 50µm. Scale bars along x- and y-axes in (B'') represent 25 and 15µm, respectively.

untranslated region (UTR) (Figure 3.13A). EGFP was found in some cell bodies in the brain lobes and VNC, particularly obvious in the dorsal planes (n=2, Figure 3.13B). The strongest GFP signal was in the VNC neuropile in a tract-like manner while EGFP appeared to be absent from the optic lobe region (Figure 3.13B). The EGFP tract was located contiguously in the ventral neuropile (Figure 3.13B). The tract is connected to the peripheral nerves, suggested by the presence of EGFP in lateral nerves relatively ventral in the lateral thoracic cortex and relatively more dorsal in the lateral abdominal cortex (Figure 3.13B and C).

#### 3.2.3.3 Immunostainings of Anti-Spz Antibodies

No specific signal was obtained from anti-Spz-ASIK staining (n=1, Figure 3.14 and Figure 3.15). With anti-Spz-GRL (Figure 3.14), a pair of cells in the brain lobes as well as tracts within the neuropile of the VNC and SEG were detected (n=3, Figure 3.16A). The prominent tract signal derived from anti-Spz-GRL persisted in the genotype $spz^{MA05}/Df(3R)Exel6205$ (n=1, Figure 3.16B). It also persisted in knockdowns of *spz* (genotype: $elav>spz^{HMS01178}$ and $repo>spz^{HMS01178}$ (n=1, Figure 3.16C; n=1, Figure 3.16D). There was an absence of any obvious ectopic signal in larval overexpression of activated Spz (*actSpz(2)*) using *repo-GAL4* (n=2, Figure 3.16E).

#### 3.2.3.4 Combination of GAL4 Reporter, *Mi{MIC}*-EGFP and Antibody Patterns

Using *spz>myr-tdTomato*, most of the reporter signal in the neuropile overlapped with BP102-positive areas (n=6, Figure 3.17). There was a lack of signal in a specific area of the larval neuropile, which was also unstained by anti-BP102 (Figure 3.17B and D). Anti-Spz-

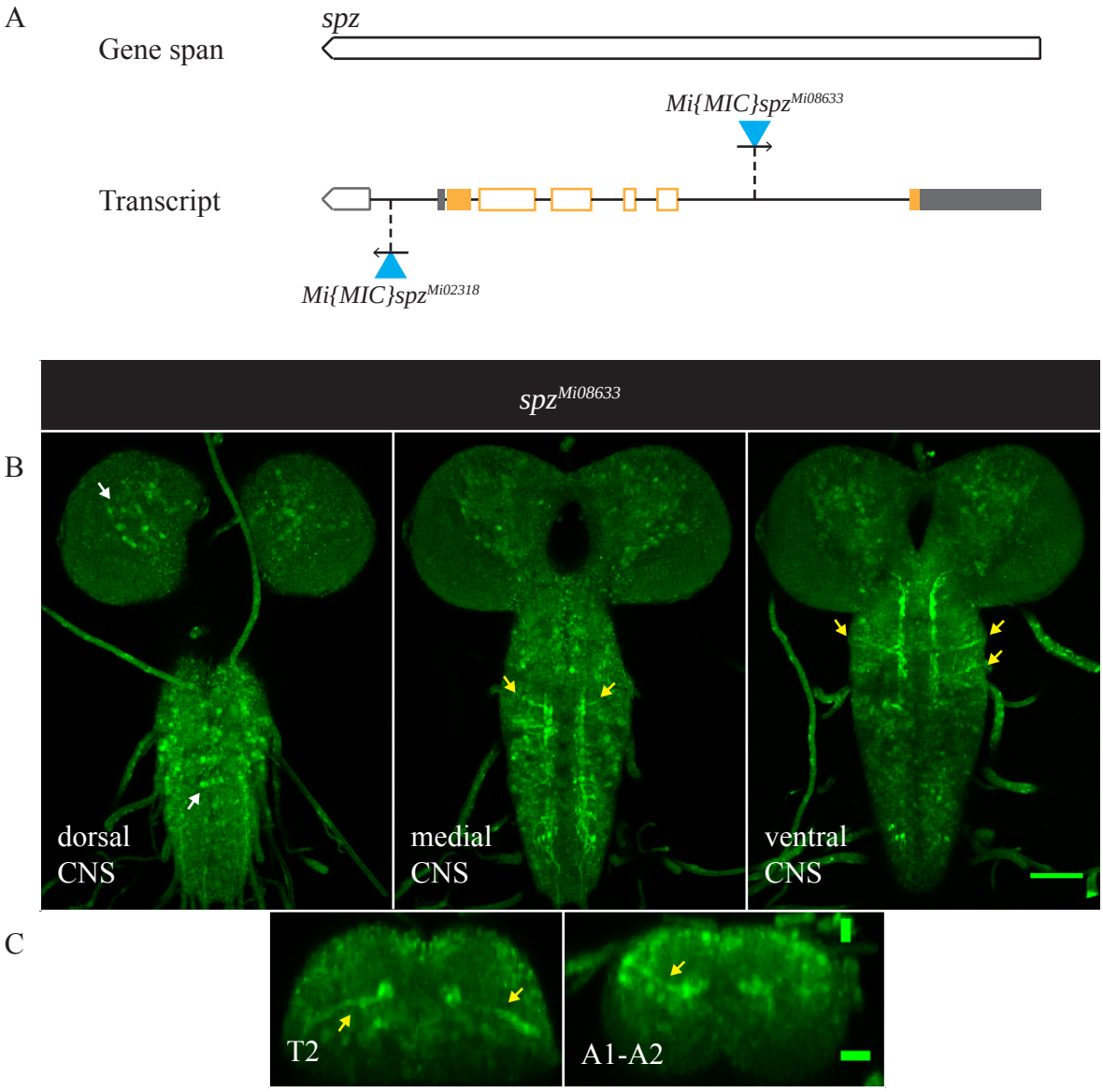


**Figure 3.13** Detection of GFP signal in *spz*$^{Mi08633}$. **(A)** Illustration of the *spz* gene and transcript adapted from FlyBase. *Spz* is oriented in minus orientation along the 5' to 3' chromosomal strand. The *Mi{MIC}* insertion of *spz*$^{Mi08633}$ took place into the first intron of the coding region of *spz* in minus direction to the gene. *Mi{MIC}* of *spz*$^{Mi02318}$ was into the 3' UTR in plus orientation. FlyBase reports that the *Spz* transcript exists in eight isoforms with four exons having their length conserved across all eight isoforms and the remaining exons differing in splicing locations. Grey pentagon=variable length in UTR. Filled grey rectangle= fixed length in UTR. Filled orange rectangle=length of exon conserved across the eight isoforms. Unfilled orange rectangle=exonic regions which are subjected to alternative splicing. GFP pattern in maximum projections of **(B)** longitudinal view, and **(C)** reconstructed transverse view. Signal of endogenous GFP was amplified by labelling with anti-GFP and Alexa Fluor 488® antibodies (n=2). T=thoracic segment, A=abdominal segment. **White arrowheads:** GFP signal in cell bodes. **Yellow arrowheads:** GFP signal projecting laterally. Scale bar in (B) represents 50µm. Scale bars along x- and y-axes in (C) represent 15µm.

A

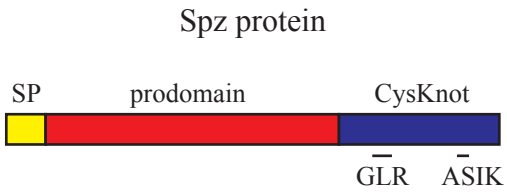


B

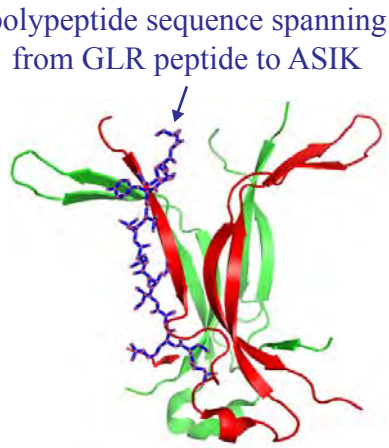


**Figure 3.14** Raising polyclonal antibodies against Spz using ASIK and GLR peptides. **(A)** Spz protein illustrated in the direction of N-terminus to C-terminus. SP: signal peptide. GLR and ASIK are 14- and 9-mer amino acid sequences in the CysKnot domain, respectively. **(B)** Model of Spz protein by J. Aurikko and N. Gay. The quaternary structure is made of two Spz monomers, one in green and one in red. In the red monomeric structure, the ball and stick model represents the polypeptides from sequences of the GLR peptide to those of ASIK.

Anti-Spz-ASIK staining

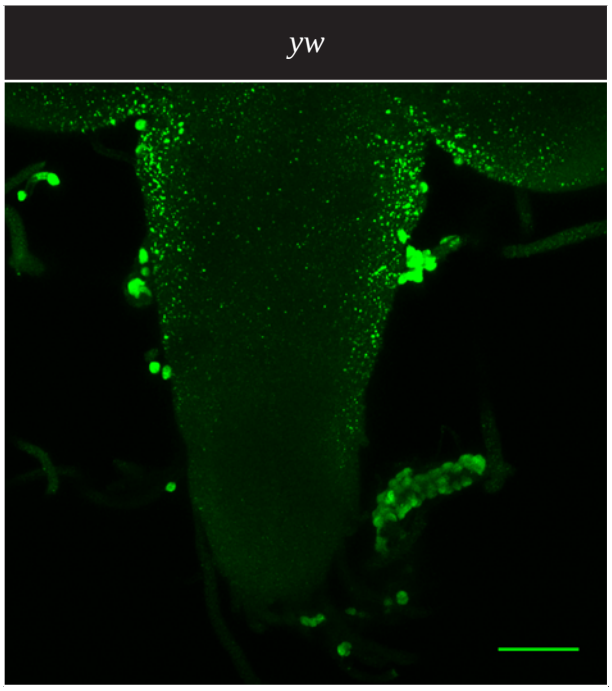


**Figure 3.15** Staining of larval CNS with anti-Spz-ASIK antibodies. Maximum projections of *yw* medial CNS in longitudinal view (n=1). Scale bar represents 50µm.

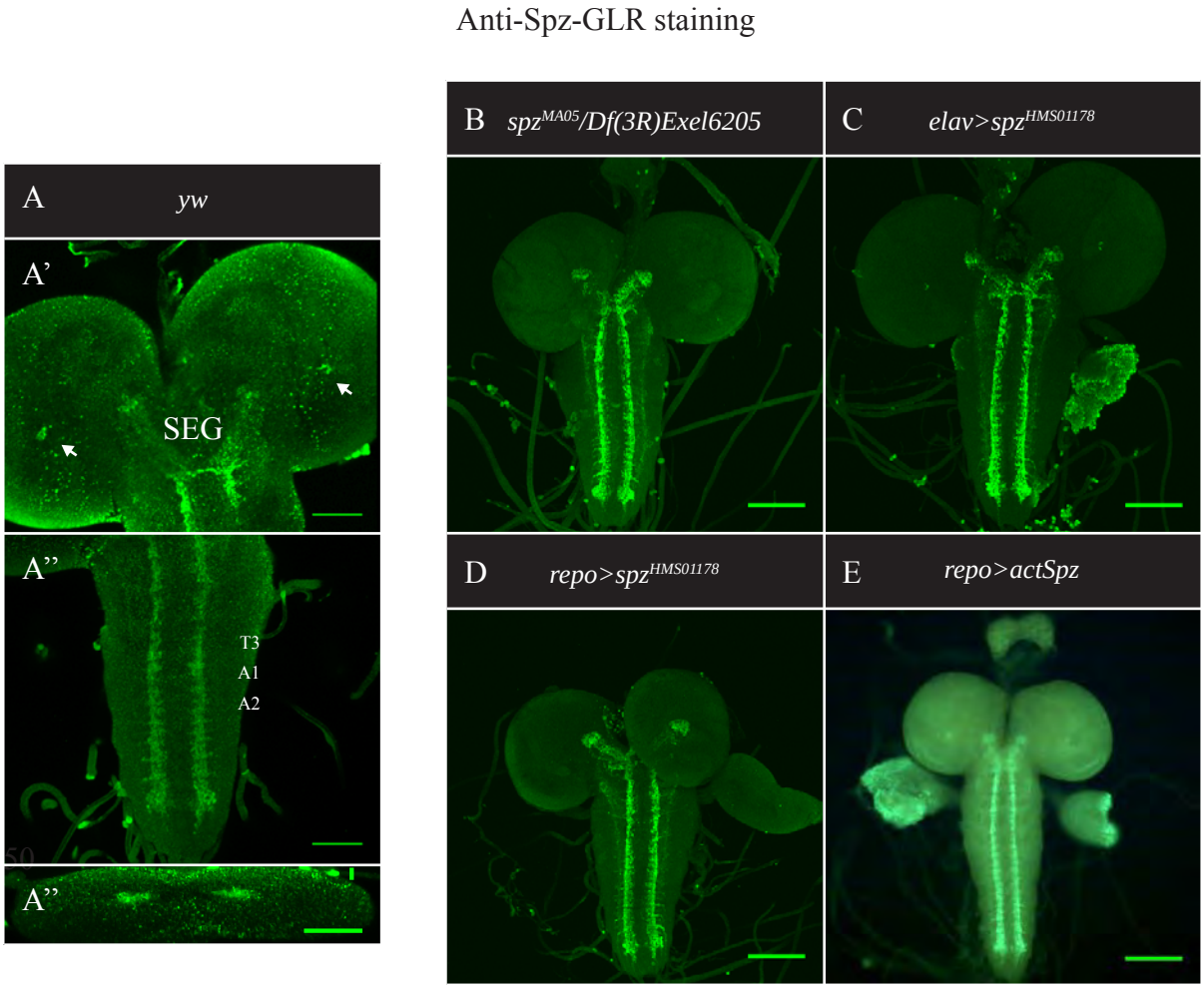


**Figure 3.16** Detection of Spz protein using anti-Spz-GLR antibodies. **(A)** Anti-Spz-GLR staining in *yw* (n=3). Maximum projections of **(A')** medial BLs in longitudinal view, **(A'')** medial VNC in longitudinal view, and **(A''')** abdominal segments A1 and A2 in reconstructed transverse view. Anti-Spz-GLR staining in **(B)** *spz$^{MA05}$/Df(3R)Exel6205* (n=1, confocal image), **(C)** *elav>spz$^{HMS01178}$* (n=1, confocal image), **(D)** *repo>spz$^{HMS01178}$* (n=1, confocal image) and **(E)** *repo>actSpz* (n=2, non-confocal image). Confocal images were acquired using the 488nm laser with identical laser power and PMT settings, then processed using ImageJ and Photoshop. **White arrowheads:** signal in cell bodies. Scale bars in (A') and (A'') represent 50µm. Scale bars Scale bars along x- and y-axes in (A'') represent 25µm and 15µm, respectively. Scale bars in (B) to (E) represent 100µm.

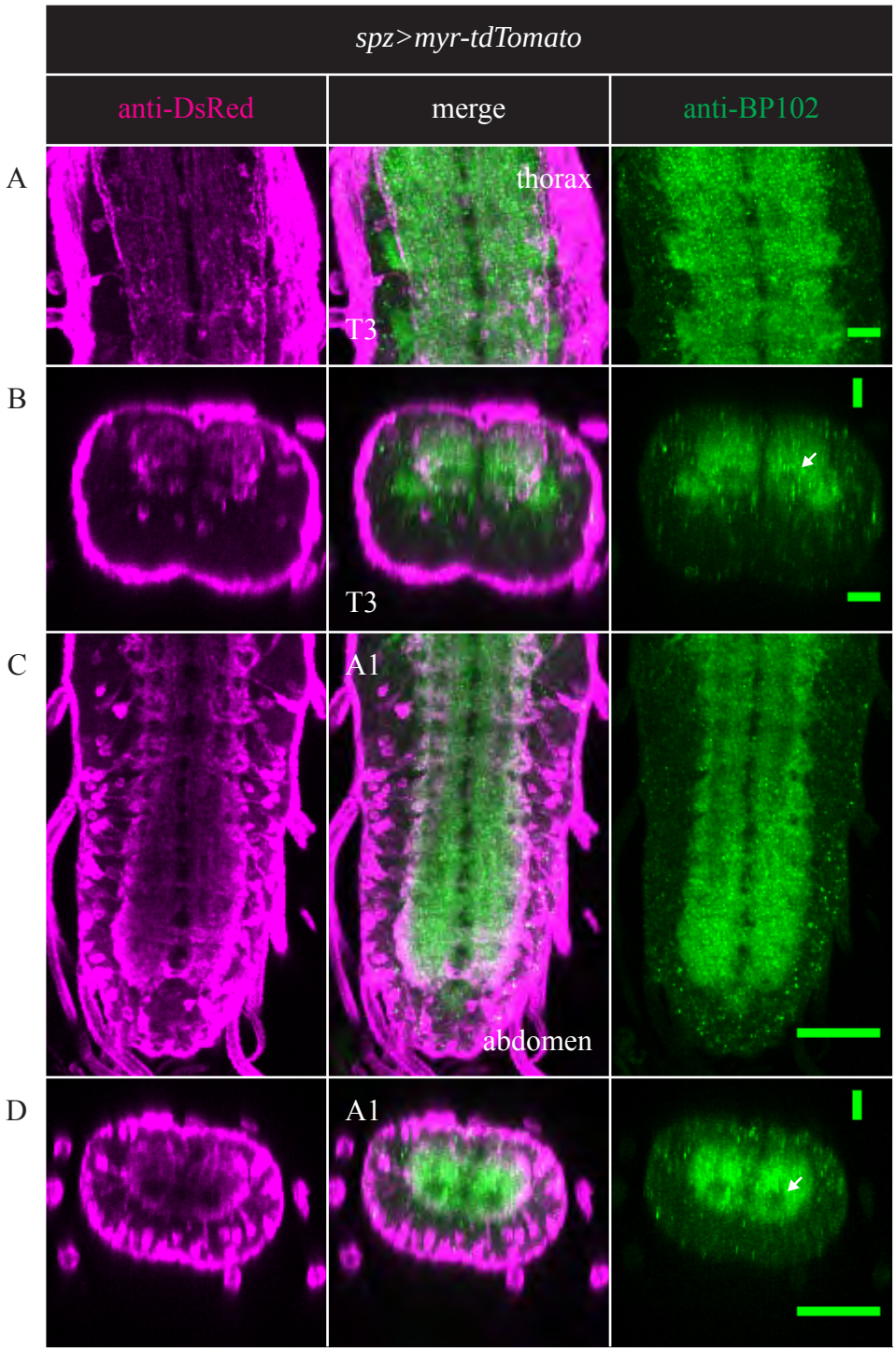


**Figure 3.17** Characterising *spz>myr-tdTomato* with anti-BP102 staining. Signal of endogenous myr-tdTomato was amplified by labelling with anti-DsRed and Alexa Fluor 647® antibodies (n=6). Maximum projections of **(A)** medial thoracic VNC in longitudinal view, **(B)** thoracic segment T3 in reconstructed transverse view, **(C)** medial abdominal VNC in longitudinal view, and **(D)** abdominal segment A1 in reconstructed transverse view. **White arrowheads:** BP102-negative areas in the ventral neuropile, which corresponds to the central input areas of the mechanosensory axon terminals. Scale bars in (A) and (B) represent 20µm. Scale bars along x- and y-axes in (C) and (D) represent 50µm and 20µm, respectively.

GLR pattern in the neuropile complemented anti-BP102 staining (n=2, Figure 3.18). Anti-Spz-GLR also complemented the neuropile signal in *spz>myr-tdTomato* (n=2, Figure 3.19). EGFP of $spz^{MI08633}$ fit into the areas unoccupied by myr-tdTomato in *spz>myr-tdTomato* (n=3, Figure 3.20).

In the thorax of *spz>myr-tdTomato*, the myr-tdTomato fascicles run alongside the dorsal-lateral (DL) and centre-intermediate (CI) neurons (n=4, Figure 3.21). No myr-tdTomato cells appeared to be FasII+ cells (Figure 3.21). In the abdomen, the area lacking myr-tdTomato signal in the ventral neuropile is below the centre axis (Figure 3.21B and D) Anti-Spz-GLR could cluster with CI neurons in the thorax (n=4, Figure 3.22B) but this was not obvious in the abdomen (Figure 3.22D). It is clear from the abdominal sections that the Spz protein distribution was below the centre axis of the neuropile, and in between the ventral lateral (VL) and ventral-median (VM) fascicles (Figure 3.22D).

Anti-Spz-GLR signal was distributed in synaptic rich zones which were labelled with anti-nc82, the antibody targeting Bruchpilot, an active zone protein (n=2, Figure 3.23). In *alrm>mCD8-GFP,* in which the interface glia (IG) was labelled, anti-Spz-GLR signal appeared to be distributed directly above the ventral IG (vIG) cells in both the thorax and abdomen (Figure 3.24B and D). Anti-Spz-GLR signal also met where vIG processes project into the neuropile (Figure 3.24B and D).

Anti-GS2 staining of genotype *spz>myr-Tomato*, the interface between the dorsal neuropile and perineurium was clearly distinguished (n=3, Figure 3.25B and D). Additionally, it was

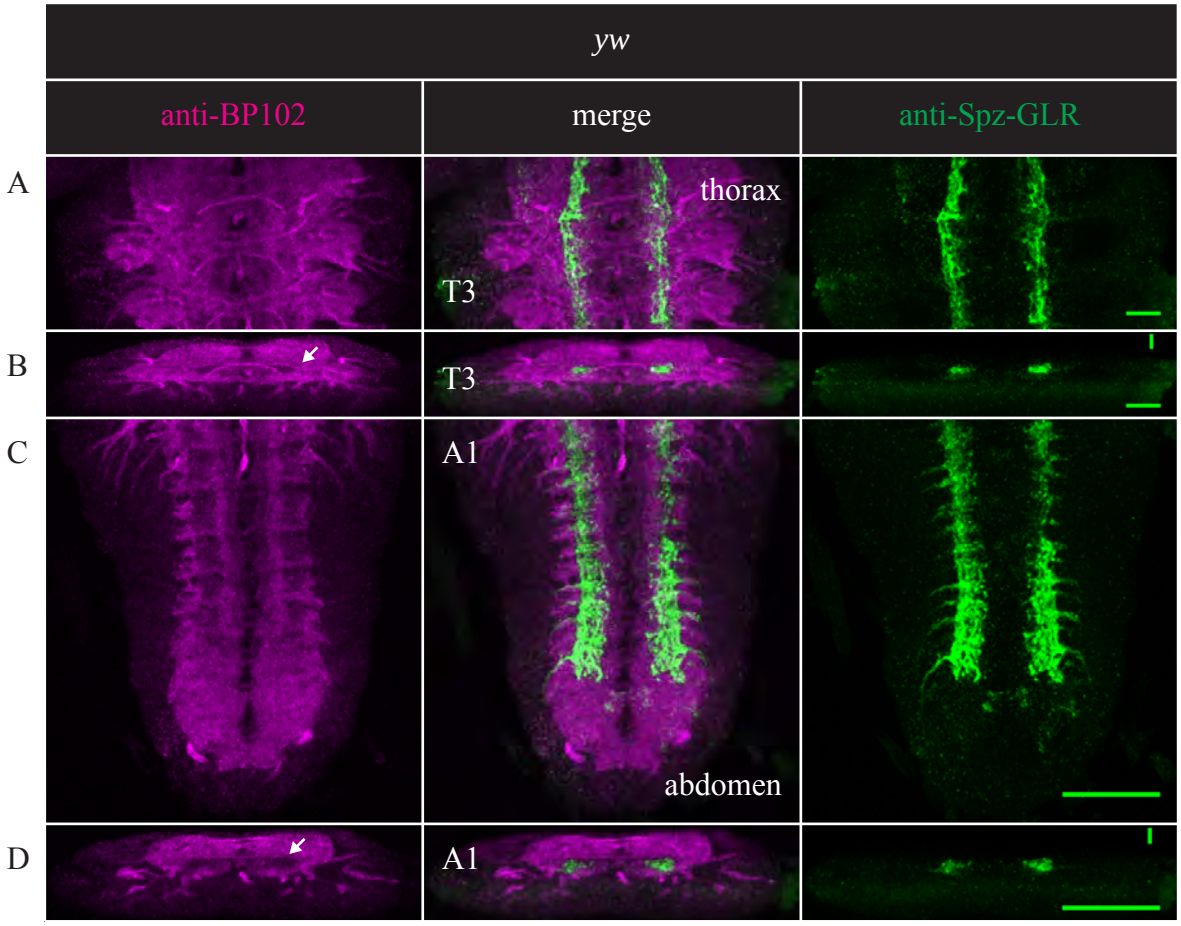


**Figure 3.18** Characterising anti-Spz-GLR pattern with anti-BP102 staining. Maximum projections of **(A)** medial thoracic VNC in longitudinal view, **(B)** thoracic segment T3 in reconstructed transverse view, **(C)** medial abdominal VNC in longitudinal view, and **(D)** abdominal segment A1 in reconstructed transverse view. Genotype: *yw* (n=2). **White arrowheads:** BP102-negative areas in the ventral neuropile, which corresponds to the central input areas of the mechanosensory axon terminals. Scale bars in (A) and (B) represent 20µm. Scale bars along x- and y-axes in (C) and (D) represent 50µm and 20µm, respectively.

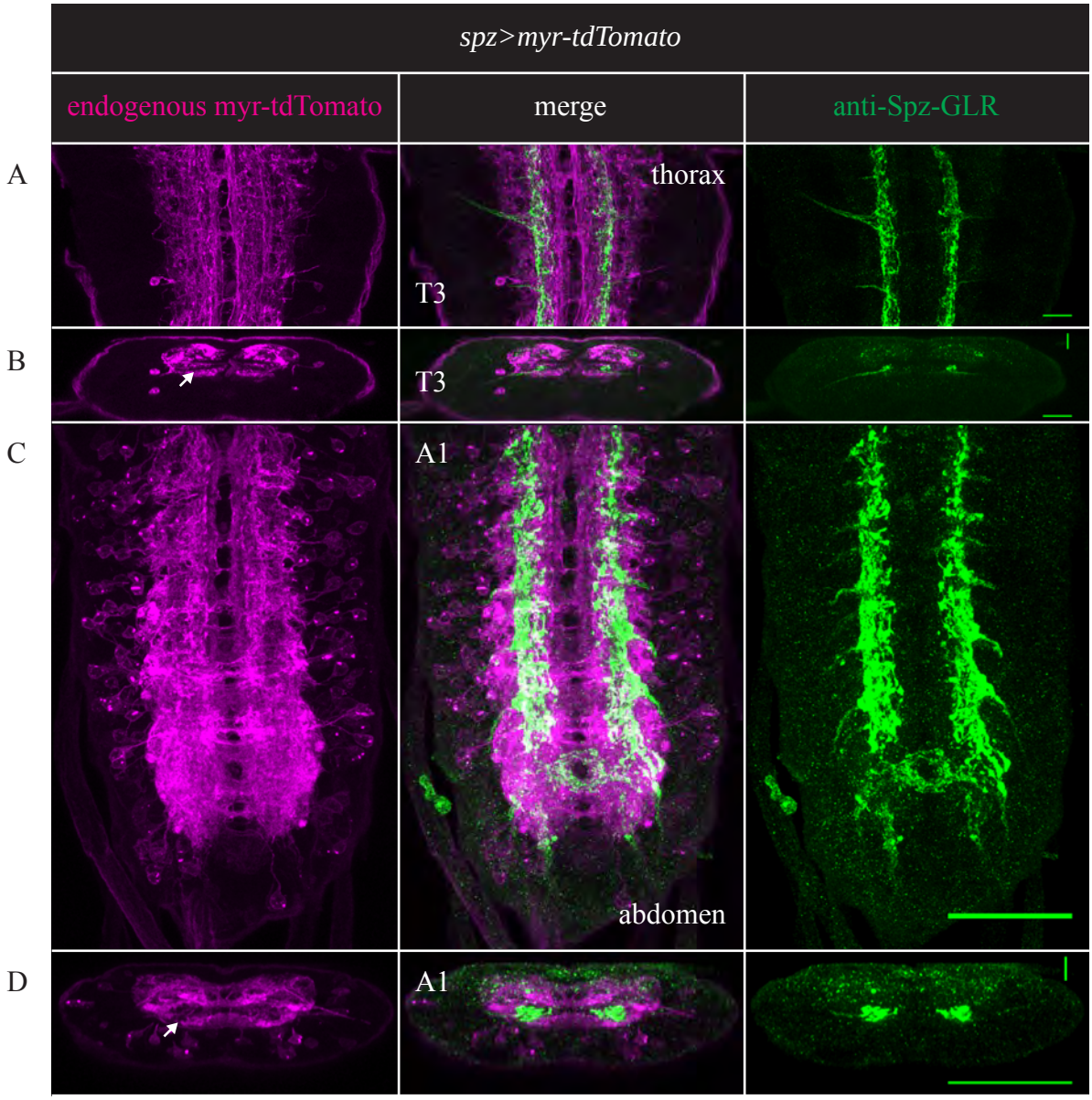


**Figure 3.19** Characterising *spz>myr-tdTomato* with anti-Spz-GLR staining. Maximum projections of **(A)** medial thoracic VNC in longitudinal view, **(B)** thoracic segment T3 in reconstructed transverse view, **(C)** medial abdominal VNC in longitudinal view, and **(D)** abdominal segment A1 in reconstructed transverse view. Genotype: *spz>myr-tdTomato* (n=2). **White arrowheads:** Areas in the ventral neuropile in which endogenous myr-tdTomato signal was absent. Scale bars in (A) and (B) represent 20µm. Scale bars along x- and y-axes in (C) and (D) represent 50µm and 20µm, respectively.

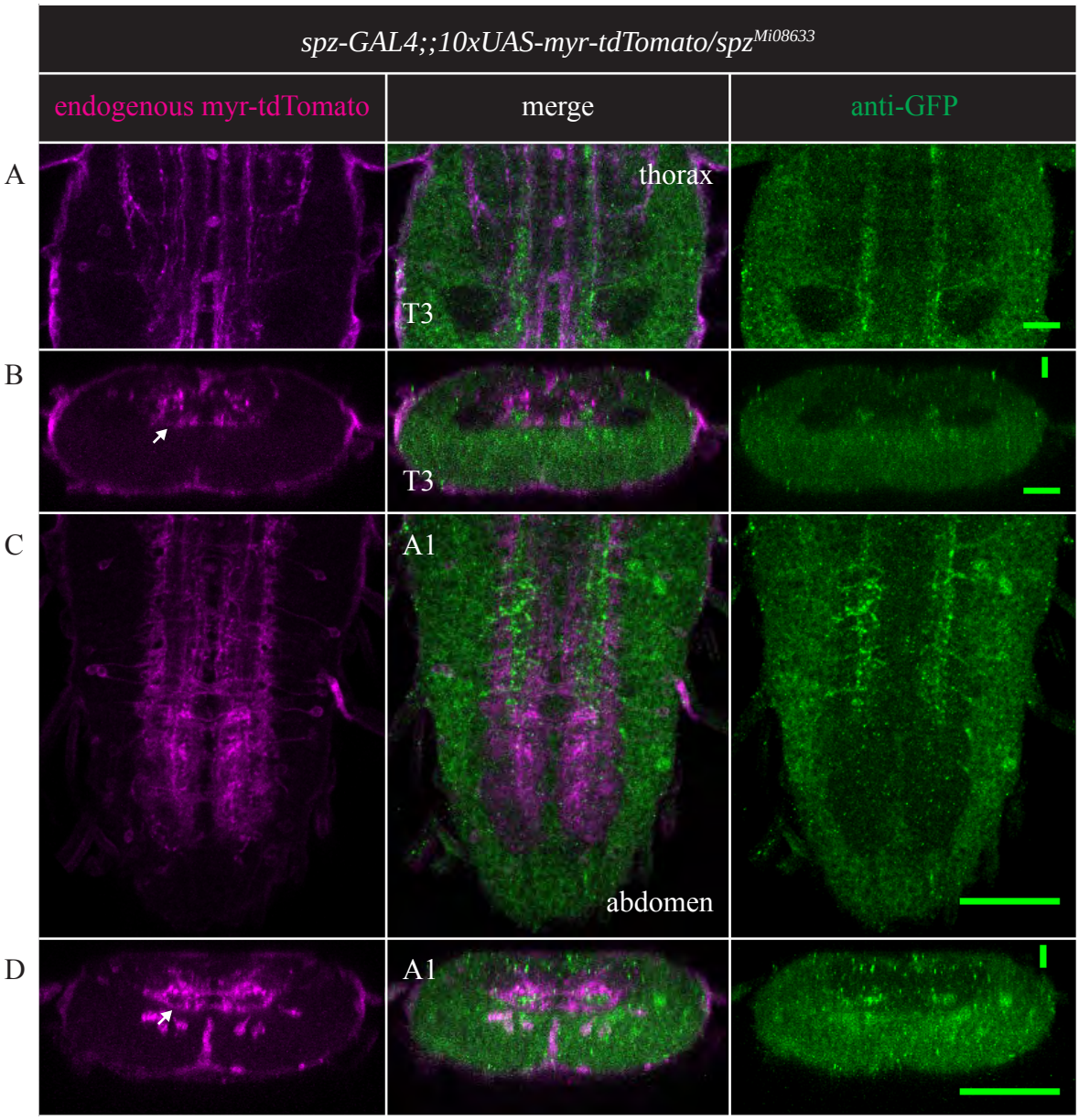


**Figure 3.20** Characterising *spz>myr-tdTomato* with *spz*$^{Mi08633}$. Signal of endogenous GFP was amplified by labelling with anti-GFP and Alexa Fluor 488® antibodies (n=3). Maximum projections of **(A)** medial thoracic VNC in longitudinal view, **(B)** thoracic segment T3 in reconstructed transverse view, **(C)** medial abdominal VNC in longitudinal view, and **(D)** abdominal segment A1 in reconstructed transverse view. **White arrowheads:** Areas in the ventral neuropile in which endogenous myr-tdTomato signal was absent, and which also coincide with the GFP+ mechanosensory domain. Scale bars in (A) and (B) represent 20µm. Scale bars along x- and y-axes in (C) and (D) represent 50µm and 20µm, respectively.

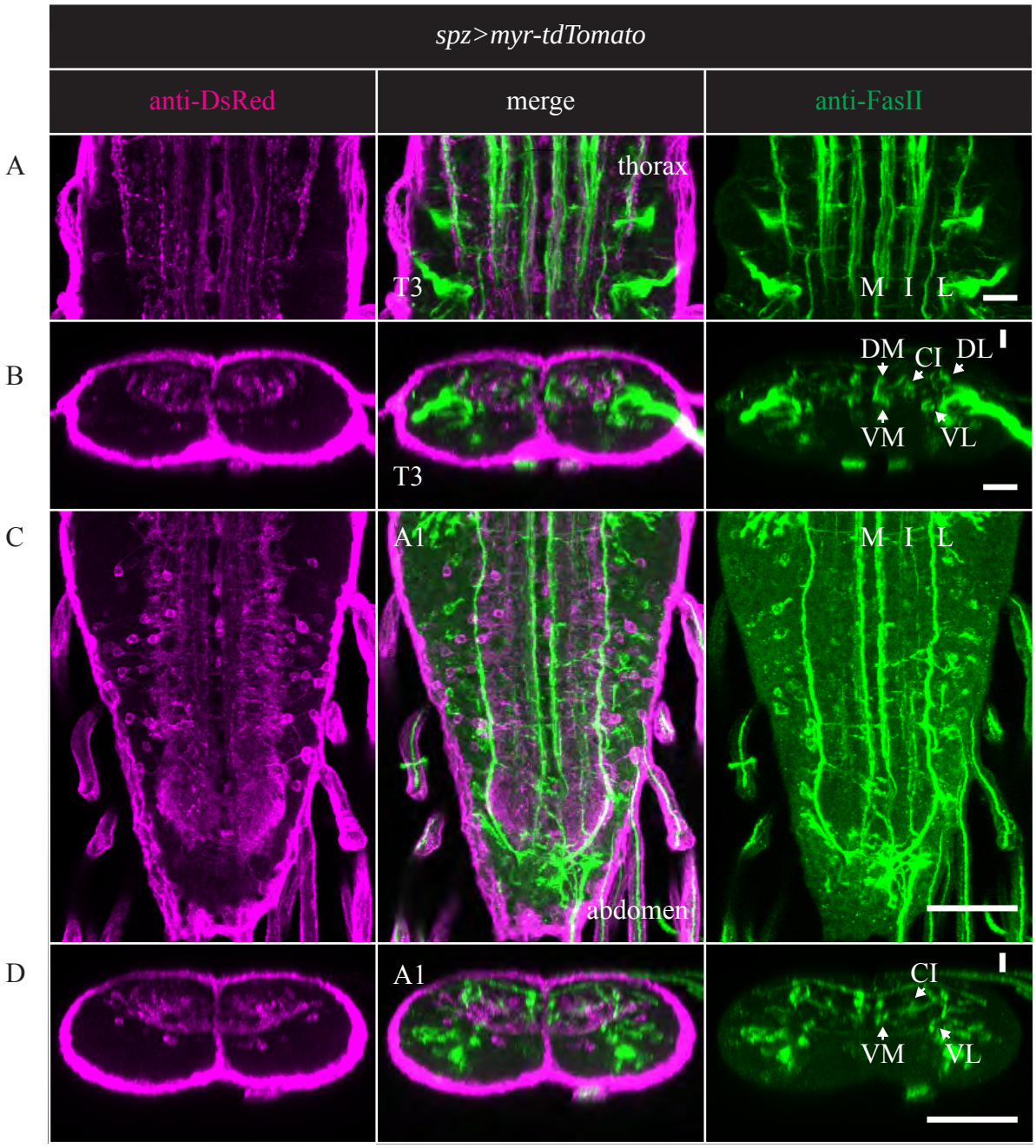


**Figure 3.21** Characterising *spz>myr-tdTomato* with anti-FasII staining. Signal of endogenous myr-tdTomato was amplified by labelling with anti-DsRed and Alexa Fluor 647® antibodies (n=4). Maximum projections of **(A)** medial thoracic VNC in longitudinal view, **(B)** thoracic segment T3 in reconstructed transverse view, **(C)** medial abdominal VNC in longitudinal view, and **(D)** abdominal segment A1 in reconstructed transverse view. D=dorsal; C=centre; V=ventral; L=lateral; I=intermediate; M=median. Scale bars in (A) and (B) represent 20µm. Scale bars along x- and y-axes in (C) and (D) represent 50µm and 20µm, respectively.

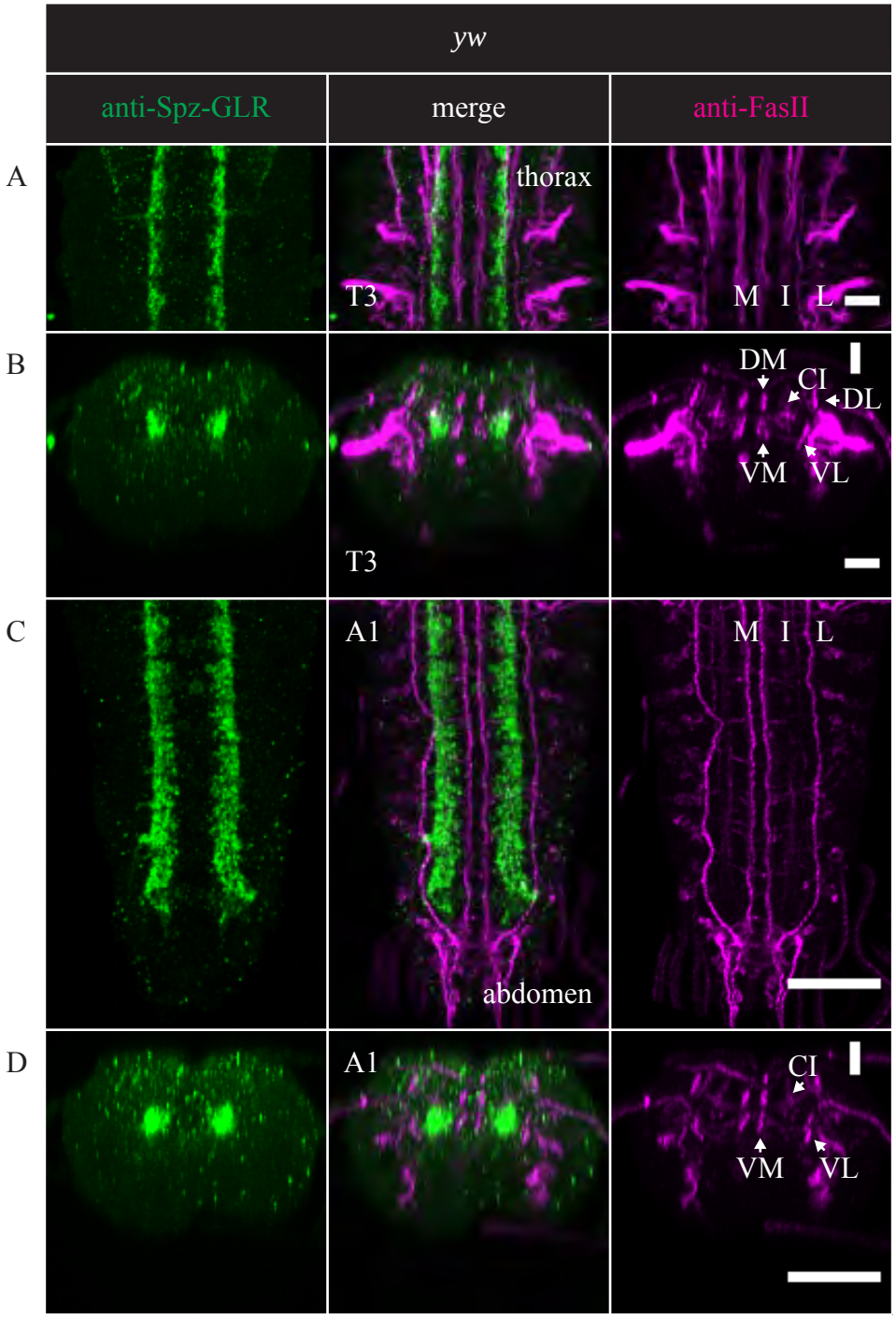


**Figure 3.22** Characterising anti-Spz-GLR pattern with anti-FasII staining. Maximum projections of **(A)** medial thoracic VNC in longitudinal view, **(B)** thoracic segment T3 in reconstructed transverse view, **(C)** medial abdominal VNC in longitudinal view, and **(D)** abdominal segment A1 in reconstructed transverse view. Genotype: *yw* (n=4). D=dorsal; C=centre; V=ventral; L=lateral; I=intermediate; M=median. Scale bars in (A) and (B) represent 20µm. Scale bars along x- and y-axes in (C) and (D) represent 50µm and 20µm, respectively.

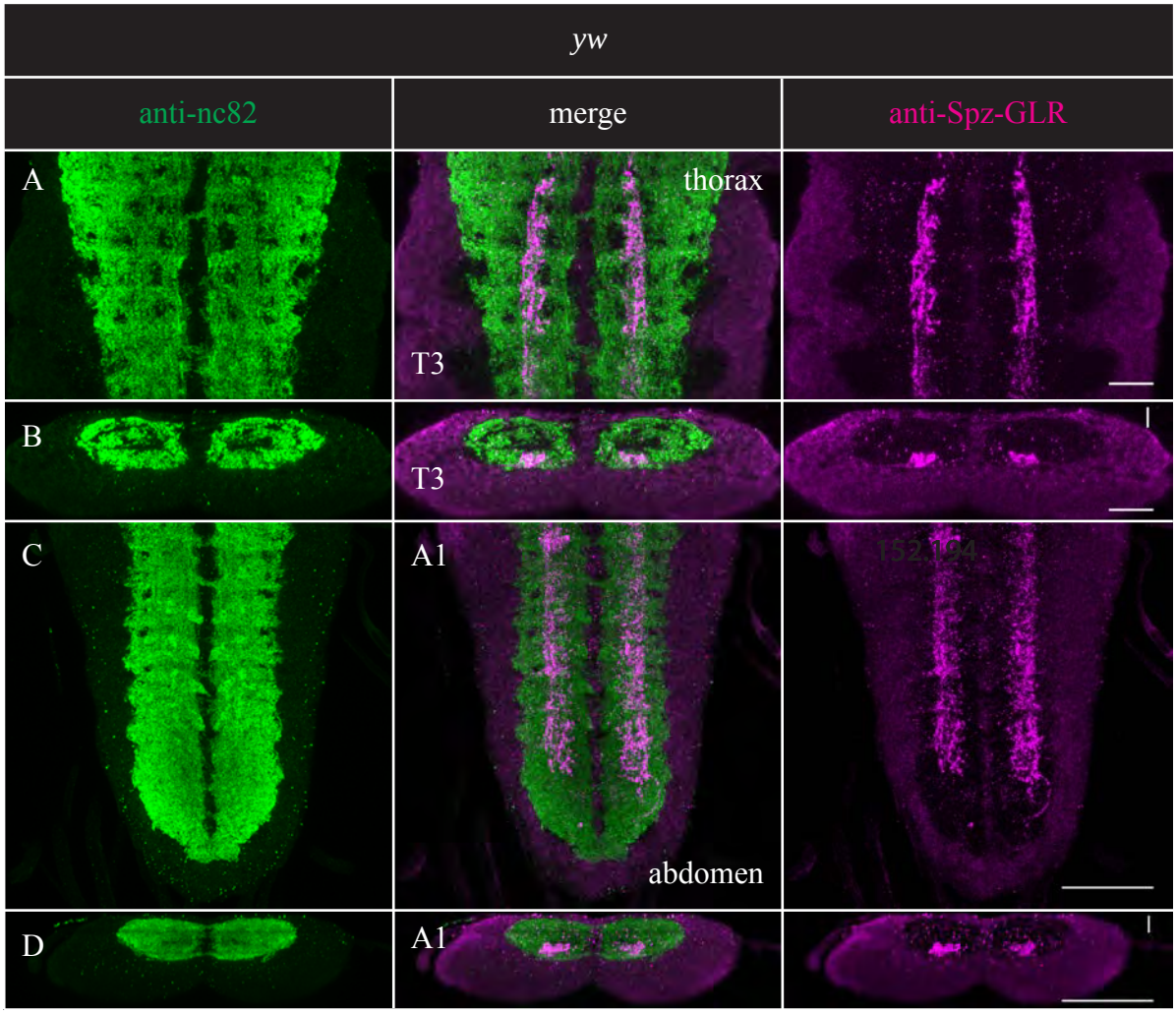


**Figure 3.23** Characterising anti-Spz-GLR pattern with anti-nc82 staining. This shows that the anti-Spz-GLR signal in the mechanosensory domain is a synaptic area. Maximum projections of **(A)** medial thoracic VNC in longitudinal view, **(B)** thoracic segment T3 in reconstructed transverse view, **(C)** medial abdominal VNC in longitudinal view, and **(D)** abdominal segment A1 in reconstructed transverse view. Genotype: *yw* (n=2). Scale bars in (A) and (B) represent 20µm. Scale bars along x- and y-axes in (C) and (D) represent 50µm and 20µm, respectively.

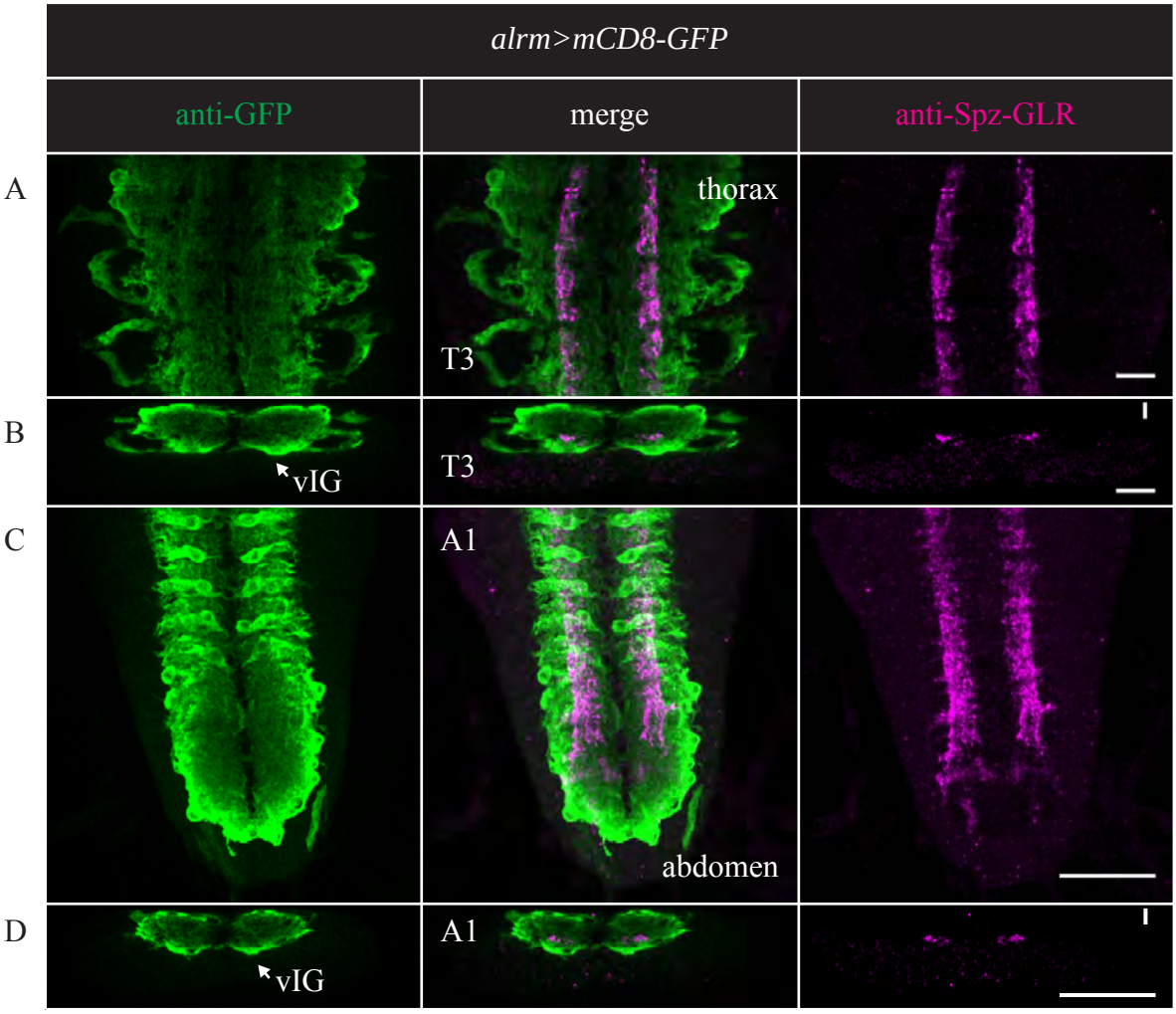


**Figure 3.24** Characterising *alrm>mCD8-GFP* with anti-Spz-GLR staining. This shows that the anti-Spz-GLR signal is in neurons, not glia, and deep in neuropile. Signal of endogenous GFP was amplified by labelling with anti-GFP and Alexa Fluor 488® antibodies (n=2). Maximum projections of **(A)** medial thoracic VNC in longitudinal view, **(B)** thoracic segment T3 in reconstructed transverse view, **(C)** medial abdominal VNC in longitudinal view, and **(D)** abdominal segment A1 in reconstructed transverse view. **White arrowheads:** Signal in ventral interface glia (vIG). Scale bars in (A) and (B) represent 20µm. Scale bars along x- and y-axes in (C) and (D) represent 50µm and 20µm, respectively.

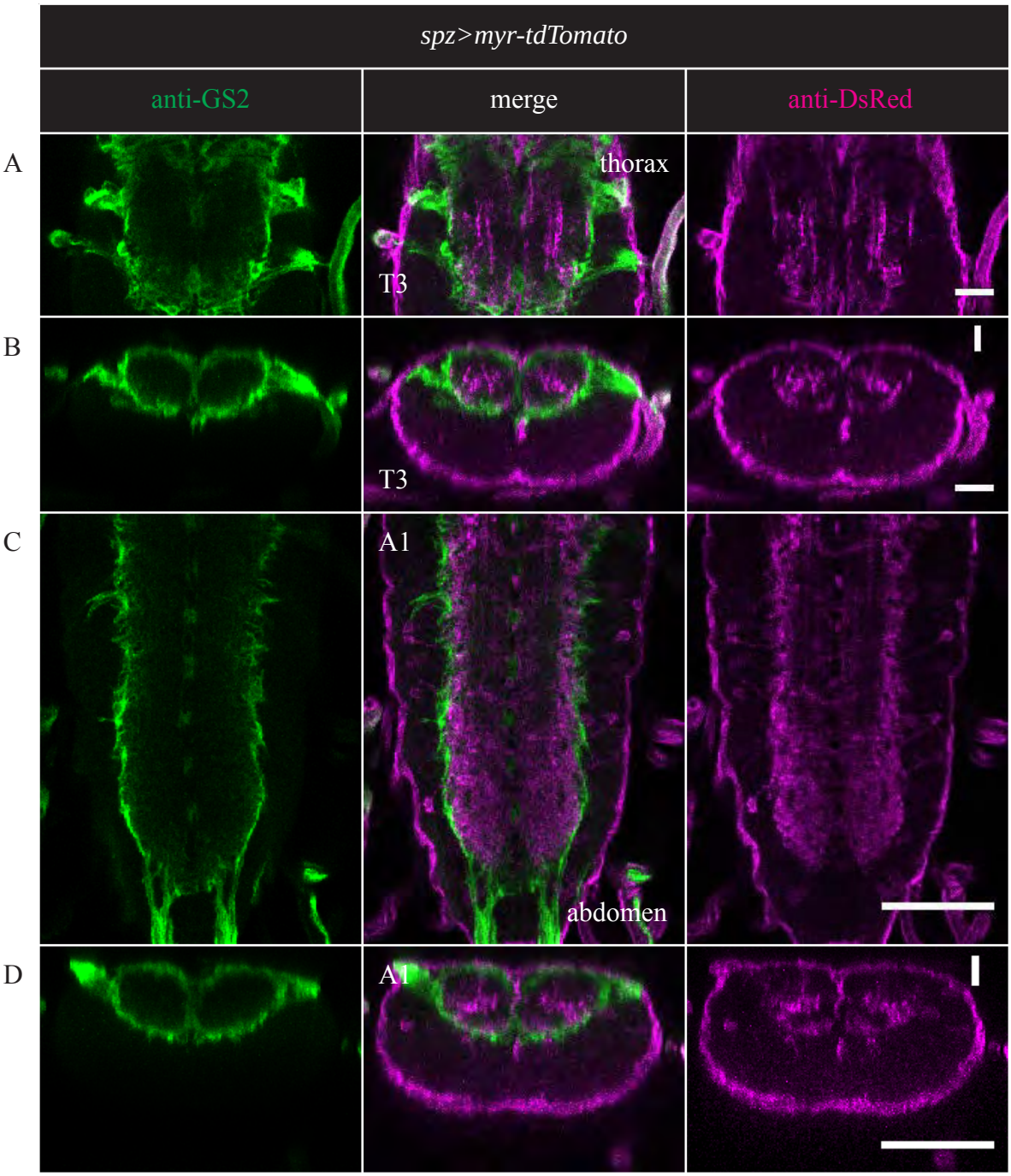


**Figure 3.25** Characterising *spz>myr-tdTomato* with anti-GS2 staining. This shows that the myr-tdTomato signal is not expressed in glia, and is instead in neurons and within neuropile. Signal of endogenous myr-tdTomato was amplified by labelling with anti-DsRed and Alexa Fluor 647® antibodies (n=3). Maximum projections of **(A)** medial thoracic VNC in longitudinal view, **(B)** thoracic segment T3 in reconstructed transverse view, **(C)** medial abdominal VNC in longitudinal view, and **(D)** abdominal segment A1 in reconstructed transverse view. Scale bars in (A) and (B) represent 20µm. Scale bars along x- and y-axes in (C) and (D) represent 50µm and 20µm, respectively.

clear that myr-Tomato was within the confines of the neuropile boundary marked by anti-GS2 (Figure 3.25C).

### 3.2.4 Expression Pattern of Toll, Toll6 and Toll7 in the Larval CNS

Wandering larvae of *G9*, in which all axons are labelled with GFP, was stained with anti-Toll-d300. In the brains lobes, anti-Toll-d300 revealed an unidentified cell cluster on the dorsal side, the outer proliferation centre (OPC) and the inner proliferation centre (IPC) (n=4, Figure 3.26A). Within the thorax, there was signal in 3 pairs of single isolated processes. Staining in *yw* embryonic stage 17 brains revealed only a cluster consisting of four cells in each brain lobe (n=11, Figure 3.26B).

Immunoreactivity against EGFP in $Toll6^{Mi02127}$ revealed cortex cells in the VNC and signal in the central brain (n=5, Figure 3.27). The immunoreactivity against Toll7 using anti-Toll7-AAQ revealed neuropile signal in the VNC, central brain, lamella/medulla and ring gland (n=5, Figure 3.28)

## 3.3 Discussion

Three tools were used to visualise gene expression patterns in this chapter: (1) GAL4 reporter lines, (2) *Mi{MIC}*-EGFP lines, and (3) a set of antibodies against all the protein of interests, which are *dnt1*, *dnt2*, *spz*, *Toll*, *Toll6* and *Toll7*.

Anti-Toll-d300 staining

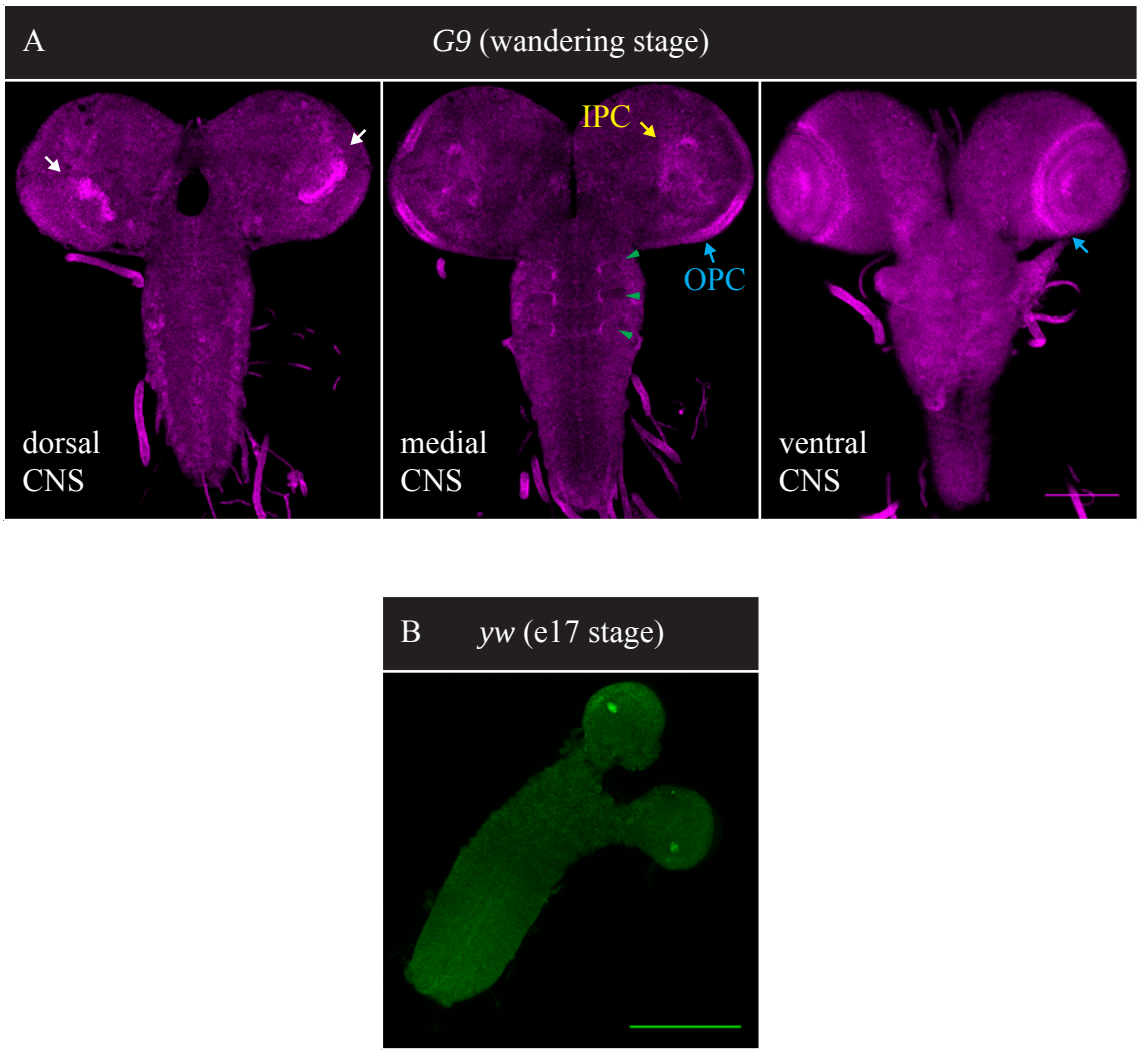


**Figure 3.26** Staining of larval CNS with anti-Toll-d300 antibodies. **(A)** Anti-Toll-d300 pattern in maximum projections of longitudinal view. Genotype: *G9* (n=4, wandering stage). **(B)** Anti-Toll-d300 pattern in maximum projection of whole stack CNS in longitudinal view. Genotype: *yw* (n=11, embryonic stage 17). Dissected embryonic brains were a gift of Dr M. Losada. **White arrowheads:** Signal in unidentified cell cluster. **Yellow arrowhead:** Signal in IPC. **Cyan arrowheads:** Signal in OPC. **Green arrowheads:** Signal in isolated unbranched processes. Scale bars in (A) and (B) represent 100µm.

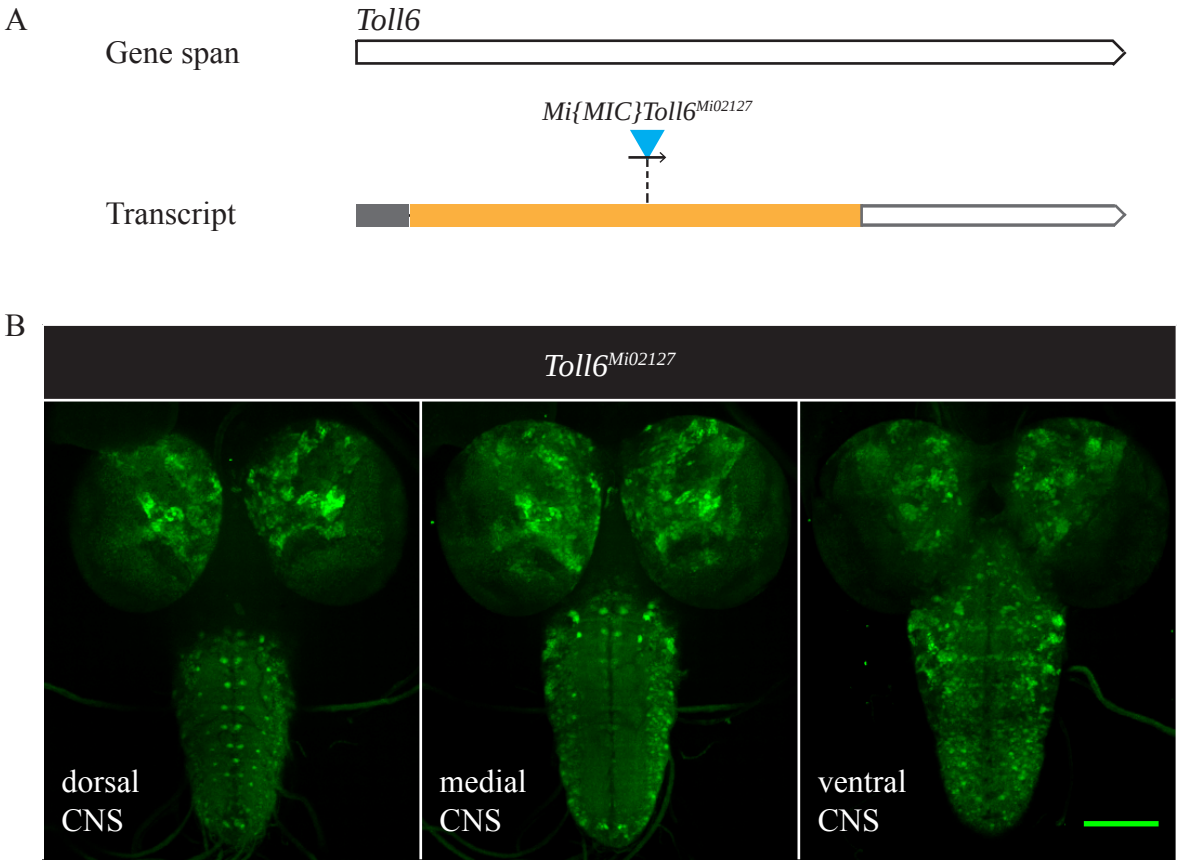


**Figure 3.27** Detection of GFP signal in *Toll6*$^{Mi02127}$. **(A)** Illustration of the *Toll6* gene and transcript adapted from FlyBase. *Toll6* is oriented in plus orientation along the 5' to 3' chromosomal strand. The *Mi{MIC}* insertion of *Toll6*$^{Mi02127}$ took place into the exon of *Toll6* in plus direction to the gene. Flybase reports that the *Toll6* transcript exists in three isoforms with the 5' UTR and exon lengths conserved across all three isoforms. Grey pentagon= variable length in 3' UTR. Filled grey rectangle=fixed length in 5' UTR. Filled orange rectangle=length of exon conserved across the three isoforms. **(B)** GFP pattern in maximum projections of longitudinal view. Signal of endogenous GFP was amplified by labelling with anti-GFP and Alexa Fluor 488® antibodies (n=5). Scale bar in (B) represents 100µm.

Anti-Toll7-AAQ staining

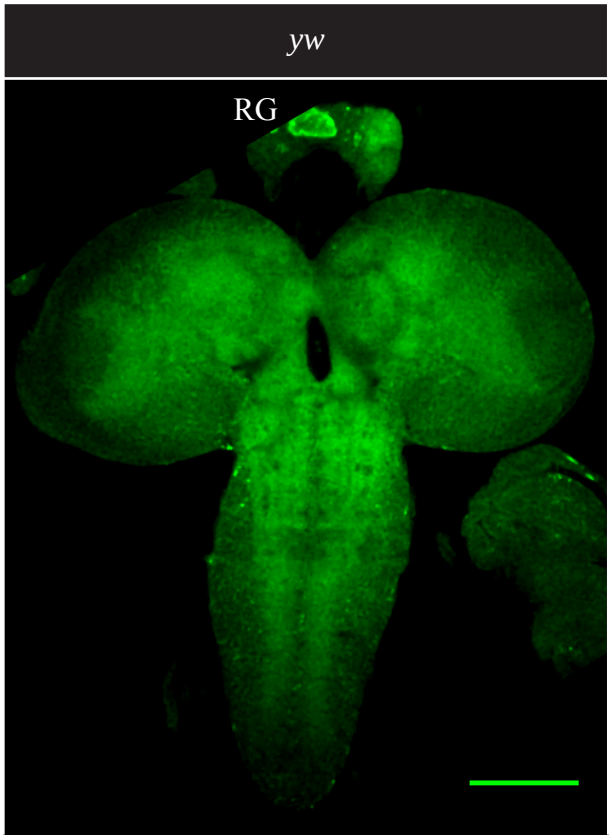


**Figure 3.28** Staining of larval CNS with anti-Toll7-AAQ antibodies. Maximum projections of *yw* medial CNS in longitudinal view (n=5). Scale bar represents 100µm.

### 3.3.1 Limitations of GAL4 Reporters

The following GAL4-UAS crosses were set up: *dnt1>mCD8-GFP*, *dnt2>myr-tdTomato*, *spz>myr-tdTomato*. In each case, there was reporter signal.

Under the regulatory sequences of *dnt1*, GFP were detected in the ventral neuropile as longitudinal tracts. This GFP tract pattern would not match the diffused *dnt1* transcript signal in the thoracic cortex (Sutcliffe, 2011; Zhu *et al.*, 2008). Other than background signal in the VNC, myr-tdTomato reporter was detected strongly in the ring gland under the regulatory control of *dnt2*. So far *dnt2* transcripts have been reported to be restricted to the larval eye-antenna disc attached outside of the CNS (Sutcliffe, 2011). Therefore, the results from *dnt2-GAL4* and *dnt2* mRNA so far matched.

There was abundant myr-tdTomato signal in the neuropile and surface CNS under the regulatory control of *spz*. This would match the *spz* transcript localisation in the central brain and VNC, except virtually no reporter signal was observed under *spz-GAL4* in the larval optic lobe, where *spz* transcripts have been detected (Sutcliffe, 2011).

The use of GAL4 reporters can either be as an enhancer construct line or as an enhancer trap line. *Dnt1-*, *dnt2-* and *spz-GAL4* are examples of enhancer trap line. The full working knowledge of all the enhancer elements for *dnt1*, *dnt2* and *spz* are yet fully known. The intergenic region betweent *dnt1* and *tie* were fully cloned, but this was not the case for *dnt2* and *spz*. Regulatory elements for *dnt2* and *spz* which might have been missed could be outside of the cloned region. Although this is not the case for *dnt1*, it is conceivable that there could

be regulatory elements elsewhere and also in the intronic regions of *dnt1*, of which *dnt1* has at least three introns in four out of seven of its isoforms.

Following transformation of the enhancer construct into the fly genome, the expression of *GAL4* is subjected to a positional effect, whereby identical constructs have different levels of expression according to their genomic insertion sites. Different levels of expression could arise due to each genomic locus displaying its own transcriptional base-level as well as degree of chromosomal condensation. Effectively, the regulation of the gene of interest could be lost and no longer applicable to the regulation of the enhancer construct *GAL4*.

*GAL4* could be designed to be incorporated into the locus of the gene of interest, downstream of the enhancer element and upstream of the gene of interest, that is, to design an enhancer trap line, but this could with its own drawback that the inserted construct might disrupt expression of the gene of interest.

### 3.3.2 Limitations on *Mi{MIC}-EGFP* Lines

Despite the claim that *Mi{MIC}* insertions do not appear to disturb protein function much (Venken *et al.*, 2011a), there is no empirical evidence for this. For example, in the case of the *Mi{MIC}* insertion in $Toll6^{Mi02127}$, the insertion took place into an intronless gene. However, for the purpose of GFP expression from the endogenous loci of *Toll6* and *spz*, the use of *Mi{MIC}-EGFP* is justifiable.

EGFP expressed in *spz*$^{Mi08633}$ is restricted to the central brain in the brain lobes, some cells on the dorsal side of the VNC and a pair or ventral tracts in the VNC neuropile (Figure 3.13). The fly line *spz*$^{Mi02318}$ has yet to be purchased and tested.

The EGFP from the *Toll6* locus in *Toll6*$^{Mi02127}$ belonged to cortex cells in the VNC and signal in the central brain (Figure 3.27). By comparing the EGFP pattern of *Toll6*$^{Mi02127}$ to DsRed signal under the control of *D42-GAL4* motoneuron reporter, the author found EGFP and DsRed to colocalised in the aCC motorneurons on the dorsal-median side of the VNC (McIlroy *et al.*, 2013).

### 3.3.3 Summary on Anti-DNT1 Antibodies

Anti-DNT1-RRPQ was not a specific antibody (Figure 3.4). Neither was anti-DNT1-VRY (Figure 3.6). Nonetheless, the anti-DNT1-VRY pattern resembled the *dnt1-GAL4* pattern more than the anti-DNT1-RRPQ pattern. Additionally, anti-DNT1-VRY detected overexpressed DNT1-CK-3'+ protein in an over-expression genotype. Therefore, anti-DNT1-VRY was more likely to reveal the endogenous pattern of DNT1 than anti-DNT1-RRPQ.

Ideally, in the testing of antibody specificity, an optimised signal is obtained in a positive control while the optimised signal is lost in a negative control. In embryonic wild-type, anti-DNT1-VRY reproduced the endogenous pattern of *dnt1* transcripts in the ventral midline and muscle. These patterns were absent from anti-DNT1-VRY embryonic stainings in the homozygous null mutant *dnt1*$^{41}$ (McIlroy *et al.*, 2013). It is not understood why *dnt1*$^{41}$/ *Df(3L)Exel6101* larval CNS retained the optimised anti-DNT1-VRY staining, which was

acquired using identical laser power and PMT settings to the *yw* control. One possibility which has yet to be eliminated is whether or not the *Df(3L)Exel6101* chromosome truly do not carry the *dnt1* gene. This is because the genotype of *Df(3L)Exel6101* has yet to be verified by PCR or inverse PCR in the Hidalgo lab. A similar situation presented itself with anti-DNT2-KRL larval staining in genotype $dnt2^{37}$*/Df(3L)Exel6092*. *Df(3L)Exel6092* has yet to be verified too.

### 3.3.4 Summary on Anti-DNT2 Antibodies

Anti-DNT2-GYN stained for the trachea in embryos and in larva. In the VNC, the tracheal ganglionic branch (GB) was identified by the anti-DNT2-GYN (Figure 3.9), because the signal pattern matched a well-characterised route in tracheal patterning in the *Drosophila* nervous system (Englund *et al.*, 1999; Pereanu *et al.*, 2007; Uv *et al.*, 2003). The GB migrates into the VNC via peripheral nerves and then extends along the ventral neuropile. At the ventral midline, the GB turns and migrates dorsally. Upon reaching the dorsal side of the neuropile, GB then extends laterally or posteriorly or both.

Anti-DNT2-ALN staining was not done on larval samples. The anti-DNT2-KRL antibody revealed signal in the neuropile of the central brain and VNC as well as in small cell clusters in the brain (Figure 3.10). Anti-DNT2-KRL signal also surrounded the surface of the CNS, which could be the acellular neural lamella of the perineurium, but not the surface-associated glia.

The pattern revealed by anti-DNT2-GYN and anti-DNT2-KRL in the larval CNS were different from each other. However, given that anti-DNT2-KRL could detect ectopic signal in an overexpressing gain-of-function genotype (*pdf>DNT2-CK-6A*), this would suggest that it is the most likely antibody to reval the endogenous protein. Double staining of anti-DNT2-KRL with anti-FasII revealed that DNT2 was distributed partly along mapped neurons and partly along other as yet unidentified neurons (Figure 3.11).

The CysKnots of DNT1 and DNT2 were detected by anti-DNT1-VRY and anti-DNT2-KRL in a punctate manner in the neuropile. The punctate pattern was not observed in anti-Spz-GLR staining of Spz CysKnot.

### 3.3.5 Summary on Anti-Spz Antibodies

The *spz>myr-tdTomato* reporter showed cells which appear to send projections into most areas of the neuropile except for the innervation area of sensory chordotonal neurons (Figure 3.12 and Figure 3.17). The lack of innervation in a specific area of the larval neuropile could make the *spz-GAL4* an interesting transgenic for mapping nervous system circuitry.

Similar to anti-DNT1-VRY and anti-DNT2-KRL, anti-Spz-GLR revealed signal in transheterozygous loss of function and knockdown mutants (Figure 3.16). However, anti-DNT1-VRY and anti-DNT2-KRL were able to recognise overexpressed DNT1 and DNT2 CysKnot epitopes, whereas anti-Spz-GLR did not reveal signal of overexpressed activated Spz (Figure 3.16). Despite this limitation, anti-Spz-GLR pattern instead matched the EGFP

pattern in *spz*$^{MI08633}$ (Figure 3.19 and Figure 3.20). Therefore, anti-Spz-GLR probably represents the endogenous distribution of Spz.

The anti-BP102 and anti-Spz-GLR patterns were complementary to each other (Figure 3.18). So were the *spz>myr-tdTomato* and anti-Spz-GLR patterns (Figure 3.19). Anti-Spz-GLR signal was found in synaptic rich area in the neuropile, and this reveals that anti-Spz-GLR detected a secreted protein (Figure 3.23). The myristoylated tdTomato reporter targets to the the membrane. Therefore, it remains possible that *spz-GAL4* and anti-Spz-GLR are both compatible with the endogenous pattern of Spz. The Anti-Spz-GLR signal also met where vIG processes project into the neuropile (Figure 3.24), and this provides an interesting link to interactions between glia and mechanosensory neurons.

### 3.3.6 Summary on Toll, Toll6 and Toll7

Commercial anti-Toll-d300 staining in the CNS of the wandering larvae revealed the neuroepithelia at the inner and outer proliferation centres, a mass of unidentified cells on the dorsal side of the brain and a set of simple processes in the thoracic VNC (Figure 3.26). The set of simple process is akin to the pattern of the R15D11 *GAL4* driver in Li *et al.* (2014). R15D11 revealed immature neuronal cells in arrest, which act as stockpile for future use in the adult (Li *et al.*, 2014). The anti-Toll-d300 staining is not complementary with the anti-Spz-GLR pattern.

The anti-Toll-d300 staining in the embryonic stage 17 CNS was limited to a cluster of four cells in each brain lobe (Figure 3.26). This pattern differs from the published anti-Toll

staining of axon neuropile and midline glia in embryonic stage 15 CNS (Zhu *et al.*, 2008). Other than the difference in development time, another reason which could account for the difference in staining pattern is that the published staining used a different anti-Toll antibody, which was a gift from Prof N. Gay.

Anti-Toll7-AAQ staining in *yw* larval CNS revealed signal in the VNC, central brain, lamella/medulla and ring gland. The distribution of anti-Toll7-AAQ staining in the neuropile VNC and central, as well as the lamella/medulla, matched the expression pattern of *Toll7* transcripts, indicating that the protein pattern likely represent the distribution of the endogenous *Toll7* receptor (McIlroy, 2012; McIlroy *et al.*, 2013). Anti-Toll7-AAQ is specific because no signal could be detected in *Toll7* null embryos or in deficiency embryos which lack the *Toll7* gene (McIlroy *et al.*, 2013). The anti-Toll-7 staining is compatible with the anti-Spz-GLR pattern.

### 3.3.7 Assessing Antibody Quality

The antibodies against the CysKnots of DNT1, DNT2 and Spz were not specific. Their use in immunohistochemistry on CNS tissue for the purpose of characterising endogenous distribution of proteins is not accurate. Whether or not these antibodies would be useful in *in vitro* assays, for example, to detect proteins in western blots, remains to be tested.

The specificity of commercial anti-Toll-d300 will require further testing on negative controls. There is also another commercial anti-Toll antibody available from Santa Cruz Biotechnology. Anti-Toll-dY was purified from goat and remains to be tested.

# Chapter 4

## 4 Generation and Characterisation of *dnt2* and *spz* Mutant Alleles

### 4.1 Introduction

#### 4.1.1 Existing *dnt2* and *spz* Loss of Function Alleles

There are existing suitable null stocks for *dnt1* for studying loss of function effects, but none for *dnt2* and *spz*. $Dnt1^{41}$ and $dnt1^{55}$ are null mutant alleles previously generated by homologous recombination, and it is homozygous viable (Zhu *et al.*, 2008). $Dnt2^{e03444}$ is a homozygous viable hypomorphic allele with a large 5.9kb transposon insert in its intronic region, after the exon encoding the signal peptide (Dos Santos *et al.*, 2015). There is a possibility of the transposon insert being spliced out and excluded from the mature RNA for protein translation, effectively creating functional DNT2 protein. $Spz^2$, $spz^3$, and $spz^4$ arose by the application of ethyl methanesulfonate (EMS) which resulted in point mutations in Spz (Tearle and Nusslein-Volhard, 1987; Weber *et al.*, 2007). According to FlyBase, there is at least one secondary mutation annotated with each *spz* allele due to the unspecific mutagenic effect of EMS: "$ca^1$" with $spz^2$, "$ru^1st^1ea^{14}ca^1$" with $spz^3$, and "$ru^1Diap^1st^1kni^{ri\text{-}1}rn^{roe\text{-}1}p^pe^1$" with $spz^4$. $Spz^2ca^1$ is homozygous semi-lethal, while $ru^1st^1ea^{14}spz^3ca^1$ and $ru^1Diap^1st^1kni^{ri\text{-}1}rn^{roe\text{-}1}p^pe^1spz^4$ are homozygous fully lethal (Zhu *et al.*, 2008). Here, this chapter is about the generation of new loss of functions alleles for *dnt2* and *spz*.

### 4.1.2 Exelixis hsFLP-FRT Deletion

The strategy adopted to generate null mutant alleles of *dnt2* and *spz* is based on the *Drosophila* genome deletion strategy developed by Exelixis (Parks *et al.*, 2004; Thibault *et al.*, 2004). The deletion works on the principle that transposons, which carry flippase recognition target (FRT) sites, the substrates of yeast flippase recombinase (FLP), are used to efficiently cause deletions with precise endpoints defined by the FRT sites (Golic and Golic, 1996). The Exelixis transposons available for precise *Drosophila* genome deletion are the *P-element* (*P{XP}*), *piggyBac RB* (*PBac{RB}*) and *piggyBac WH* (*PBac{WH}*) insertion lines (Parks *et al.*, 2004). These 3 transposons differ among each other in terms of the following: (i) the number of FRT sites carried (either 1 or 2), (ii) the orientation of the FRT site(s) relative to the *mini-white* ($w^{+m}$) construct within the transposon; and (iii) whether or not there is a *UAS* construct (Thibault *et al.*, 2004). According to Parks *et al.* (2004), there is a selection criteria to meet in choosing the type of transposons (*P{XP}*/*PBac{RB}*/*PBac{WH}*) to flank the genomic region to be deleted, that is, the allowable pairs of Exelixis transposons must both have the FRT sites in the same orientation to each other for heat shock FLP (hsFLP) to act on. Successful genome deletion is accompanied by a leftover hybrid transposon (Figure 2.13A). Allowable pairwise combinations will ultimately result in either red- or white-eyed flies depending on whether or not the $w^{+m}$ was removed from the genome (Parks *et al.*, 2004). Confirmation of successful genome deletion is provided by PCR (Figure 2.13B). Parks *et al.* (2004) estimated 5 white-eyed and 50 red-eyed fly lines to be screened by PCR to obtain 4 confirmed deletions each.

### 4.1.3 *Spz* Loss of Function Alleles Affect Embryonic Dorsal-Ventral Polarity

Spz is found in the perivitelline fluid space that surrounds a developing embryo (Morisato and Anderson, 1994; Schneider *et al.*, 1994). The spz signal transduces across the cell membrane by binding and activating the Toll receptor, henceforth establishing the signalling which culminate in generating the dorsal-ventral (DV) polarity axis of the developing embryo (Morisato and Anderson, 1995; Weber *et al.*, 2003). Females lacking *spz* activity produce dorsalised embryos that miss ventral and lateral structures in the cuticles (Anderson and Nusslein-Volhard, 1984; Morisato and Anderson, 1994). Therefore, to demonstrate if newly generated *spz* alleles are truly loss of function in nature, an assessment of embryonic DV polarity is necessary.

### 4.1.4 Specific Aims

The specific aims of this chapter are:

- To generate a loss of function allele of *dnt2* and *spz* by hsFLP-FRT deletion.
- To classify any newly generated *spz* allele.
- To characterise the viability of any newly generated *dnt2* and *spz* allele.

### 4.1.5 Methods in Brief

The genetic protocols to generate a null mutant allele of *dnt2* and *spz* were supplied in Figure 2.10 and Figure 2.11, and these protocols were based on the genetic scheme designed by Parks *et al.* (2004) for hsFLP-FRT deletion of the *Drosophila* genome (Section 2.1.4). For

generation of a *dnt2* loss of function mutant allele, the allowable pairwise combination of Exelixis transposons chosen was between *PBac{RB}dnt2*$^{e03444}$ at the lower coordinate and *P{XP}d05170* at the upper coordinate (Figure 4.1). For new *spz* allele, the combination consisted of the *P{XP}spz*$^{d00069}$ and *PBac{RB}e04446* at the lower and upper coordinate, respectively (Figure 4.2). Putative transposon hybrids *dnt2*$^{e03444/d05170}$ and *spz*$^{d00069/e04446}$ were tested by PCR (Section 2.2.2).

To determine whether or not any newly generated *spz* allele results in loss of function, cuticle preparations of unhatched embryos were made to observe dorsal-ventral polarity (Section 2.5.1).

The viability of any newly generated *dnt2* and *spz* allele were examined using survival index (Section 2.1.5). Chi-square test ($\chi^2$) was used to compare the observed ratio of $Tb^+$ and $Tb^-$ pupal cases to the expected Mendelian ratio, as well as the observed ratios of $Tb^+$ and $Tb^-$ from two test crosses (Section 9.1). For $\chi^2$ test between two crosses, Bonferroni post hoc correction was applied to any $\chi^2$ p-value of less than 0.05 (Section 9.1).

## 4.2 Results

### 4.2.1 Generating a *dnt2* Loss of Function Allele

A total of 21 putative hybrid *dnt2*$^{e03444/d05170}$ fly lines were established (Figure 2.10). Of these lines, 14 were homozygous viable while the remaining 7 were homozygous lethal. The first

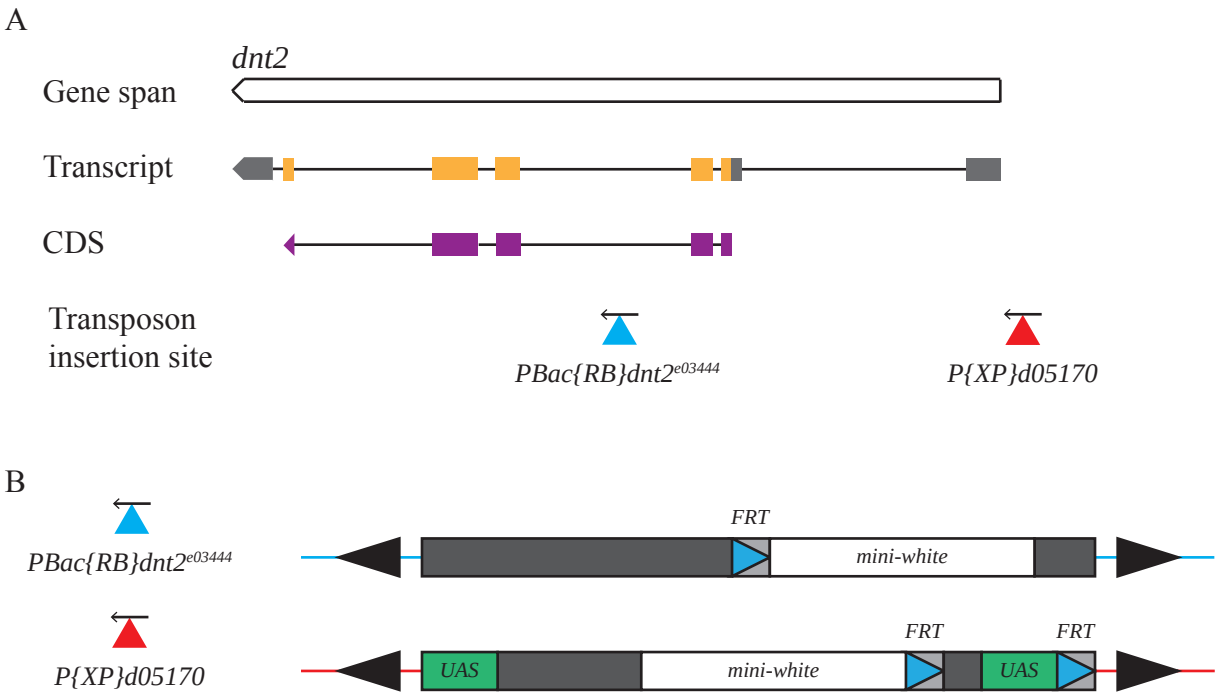


**Figure 4.1** Exelixis transposons for generating a *dnt2* loss of function mutant allele (adapted from FlyBase, Parks *et al*. (2004) and Thibault *et al*. (2004). **(A)** The *dnt2* gene, in minus orientation, is located along chromosomal arm 3L in cytogenetic location 63A1 from sequence 2,883,638 to 2,892,164. *PBac{RB}dnt2*$^{e03444}$ and *P{XP}d05170* were selected as the flanking pair of starting insertions to delete the genomic region between them. Such a deletion will remove the start codon of the coding sequence (CDS). *PBac{RB}dnt2*$^{e03444}$ is the lower coordinate transposon between the two; it is inserted into the intronic region of *dnt2* at sequence 2,887,990 while *P{XP}d05170* is inserted into the genome outside of *dnt2*'s gene span at sequence 2,892,453. Flybase reports only one isoform for the *dnt2* gene. **(B)** *PBac{RB}dnt2*$^{e03444}$ and *P{XP}d05170* are transposons inserted the fly genome in minus orientation. The *cis* recombination in P-element *XP* occurs earlier than the *trans* recombination between *XP* and piggyBac element *RB* (Parks *et al*., 2004). Their genomic orientation and position of the *mini-white* ($w^{+m}$) gene allows for deletion to be initially screened by collecting white-eyed progeny.

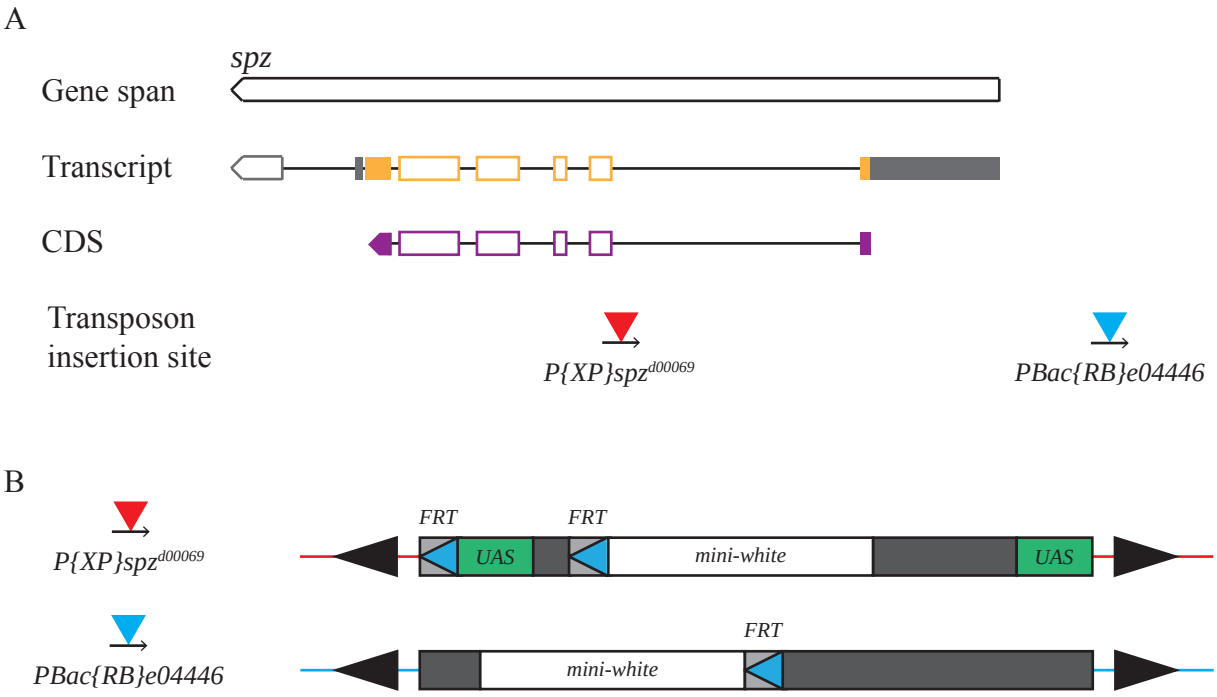


**Figure 4.2** Exelixis transposons for generating a *spz* loss of function mutant allele (adapted from FlyBase, Parks *et al*. (2004) and Thibault *et al*. (2004). **(A)** The *spz* gene of minus orientation is located along chromosomal arm 3R in cytogenetic location 97E1 from sequence 22,890,712 to 22,895,792. *P{XP}spz*$^{d00069}$ and *PBac{RB}e04446* were chosen to be recombined to delete the genomic region spanning between them, including the start codon of the coding sequence (CDS). *P{XP}spz*$^{d00069}$ and *PBac{RB}e04446* are inserted into the intronic region of *spz* at sequence location 22,893,329 and outside of *spz*'s gene span at 22,896,645, respectively. Flybase reports that *Spz* transcript exists in eight isoforms. Grey pentagon=variable length in UTR. Filled grey rectangle=fixed length in UTR. Filled orange rectangle=length of exon conserved across the eight isoforms. Unfilled orange rectangle= exonic regions which are subjected to alternative splicing.**(B)** Due to *P{XP}spz*$^{d00069}$ and *PBac{RB}e04446* both being inserted in plus orientations, deletion can be screened by collecting white-eye progeny which have lost the *mini-white* ($w^{+m}$) gene.

step undertaken was to eliminate as many non-hybrid lines as possible, and so the homozygous viable lines were tested by PCR first. Internal PCR was possible in homozygous flies only, whereby primers *deleteGP fwd* and *deleteGP rev* bind to the genomic region in between the *PBac{RB}dnt2*$^{e03444}$ and *P{XP}d05170* insertions (Table 2.2; Figure 4.3A). HsFLP-FRT deletion would have been unsuccessful if the genomic region between *PBac{RB}dnt2*$^{e03444}$ and *P{XP}d05170* was still present in the fly line – this would be shown by the presence of a 195bp band amplified between primers *deleteGP fwd* and *deleteGP* (Table 2.2; Figure 4.3A). The 195bp band was detected in all the 14 homozygous viable fly lines so these stocks were thrown away (Figure 4.3B).

Internal PCR cannot be used to confirm deletions in the remaining 7 homozygous lethal lines because of the presence of the balancer chromosome, so other PCR strategies detailed in Figure 2.13 were adopted. Hybrid PCR using primers *Tn1 fwd* and *Tn2 rev* under a gradient temperature PCR program yielded either absent or spurious bands of unexpected fragment sizes (data not shown; Table 2.2). Genomic PCR using primers *GP fwd* and *GP rev* gave rise to a 5.2kb band across all the 7 remaining fly lines (Figure 4.3C). The 5.2kb bands were derived from the balancer chromosome and were expected to be present, but 3.1kb bands, which would have been obtained if hsFLP-FRT deletion had been successful, were missing (Figure 4.3C; Table 2.2). This suggests that there were no successful hsFLP-FRT deletion to generate the hybrid *dnt2*$^{e03444/d05170}$.

Despite the results of the genomic PCR on the putative hybrid *dnt2*$^{e03444/d05170}$ fly lines, further investigation using two-sided and genomic PCR were done on the Exelixis lines *PBac{RB}dnt2*$^{e03444}$ and *P{XP}d05170* (Figure 4.4A; Table 2.2), especially since the hsFLP-

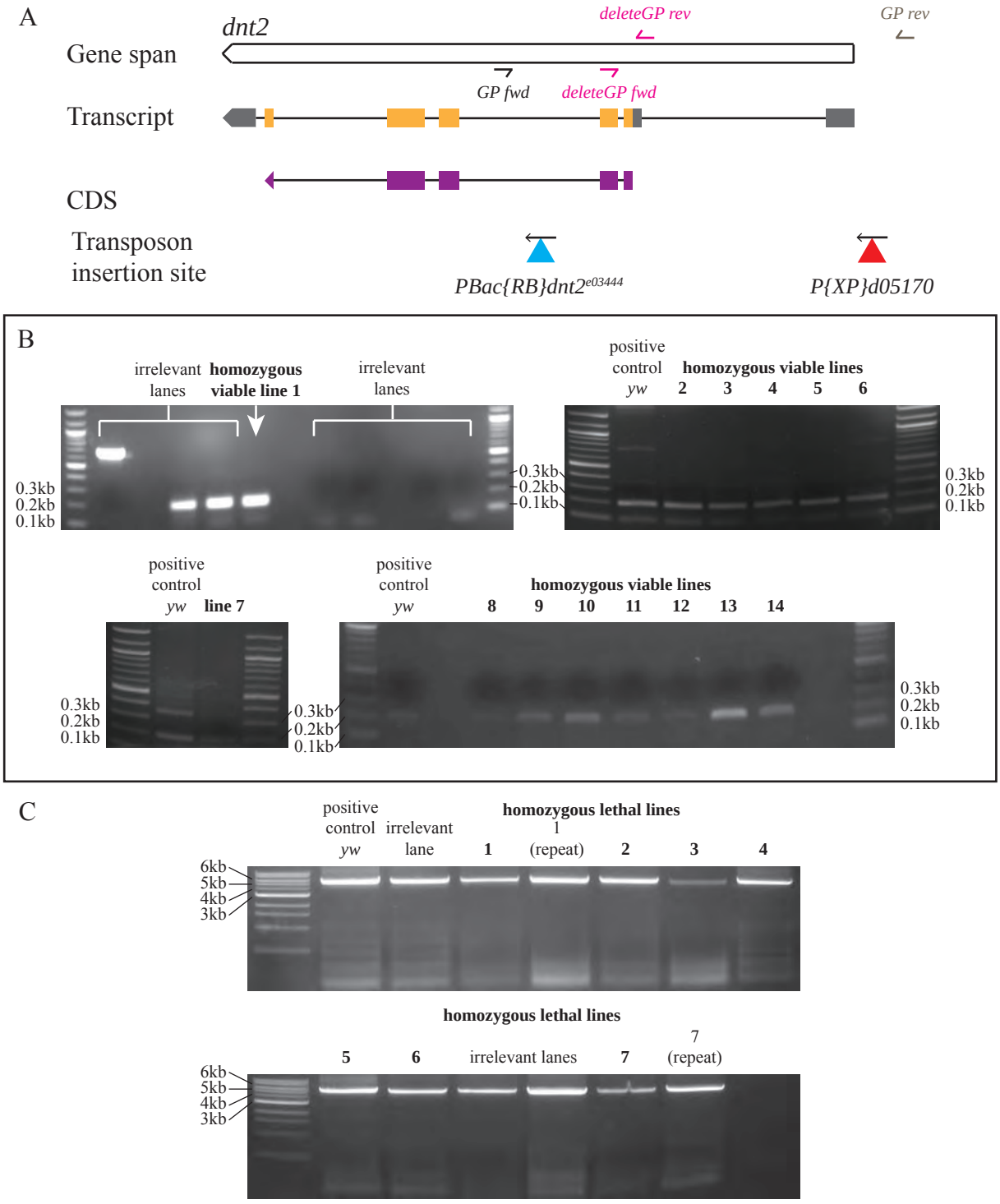


**Figure 4.3** PCR confirmation of putative *dnt2*$^{e03444/d05170}$ loss of function alleles. **(A)** Primer sites of *deleteGP fwd*, *deleteGP rev*, *GP fwd* and *GP rev* (Table 2.2). **(B)** Internal PCR using primers *deleteGP fwd* and *deleteGP rev* on homozygous viable lines 1-14. There were irrelevant lanes present because of different PCR experiments occupying the same gel. The 100bp DNA ladder (New England Biolabs) were used throughout gels. **(C)** Genomic PCR using primers *GP fwd* and *GP rev* on homozygous lethal lines 1-7. There were irrelevant lanes due to the DNA template being extracted and used for PCR before the fly lines died and cease to exist. The 1kb DNA ladder (New England Biolabs) were used.

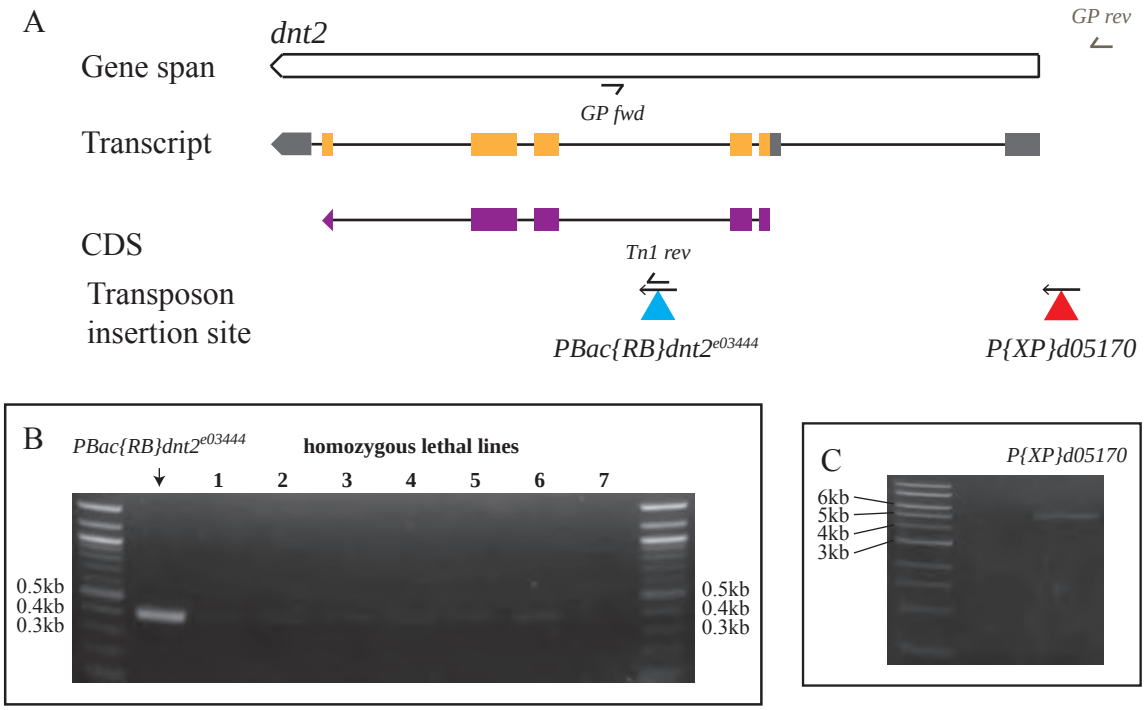


**Figure 4.4** Verification of transposon insertion at the correct location for the Exelixis lines that were selected for the purposes of generating a *dnt2* FLP-FRT-based deletion allele. **(A)** Primer sites of *GP fwd*, *Tn1 rev* and *GP rev* (Table 2.2). **(B)** Left-hand side of two-sided PCR using primers *GP fwd* and *Tn1 rev* on putative $dnt2^{e03444/d05170}$ homozygous lethal lines 1-7. The 100bp DNA ladder (New England Biolabs) was used. **(C)** Genomic PCR using primers *GP fwd* and *GP rev* on *P{XP}d05170*. The 1kb DNA ladder (New England Biolabs) was used.

FRT based deletion strategy has proven to be predictable, precise and efficient (Parks *et al.*, 2004). As observed by Parks *et al.* (2004), it was supposedly sufficient to test 5 putative $w^-$ lines. The *PBac{RB}dnt2*$^{e03444}$ flies were shown to carry its *piggyBac* element in the correct location as evidenced by the left-hand side of the two-sided PCR (Figure 4.4B). All the homozygous lethal lines carried the *piggyBac* element too (Figure 4.4B).

Genomic PCR of DNA extracted from *P{XP}d05170* flies yielded a 5.2kb band, suggesting that the *P-element XP* was not inserted outside of *dnt2*'s gene span at sequence 3L: 2,887,453 (Figure 4.4A; Table 2.2). To confirm the whereabouts of the *P-element XP* insertion, inverse PCR was deployed by directing nested primer pairs against circular fragments of *P{XP}d05170* DNA (Figure 4.5A; Section 2.2.3). There were two rounds of PCR: the first used primers *51A* and *51B*, and the second *52A* and *52B* (Figure 4.5A; Table 2.4). The resulting single specific PCR band was extracted, purified and sent for sequencing with sequencing primer *XP-5SEQ* (Figure 4.5A and B; Table 2.4). The sequencing output was used as a query in BLAST against the *D. melanogaster* genome (Figure 4.5C). *P-element XP* of Exelixis line *P{XP}d05170* was reported in FlyBase to be inserted in cytogenetic location 63A1 along chromosomal arm 3L. However, BLAST returned significantly matching sequence within the *Ectoderm-expressed 4* (*Ect4*) gene at cytogenetic location 66B5 of the same chromosomal arm (Figure 4.5D), at least 5 million nucleotides away from *dnt2*. The sequences were found flanking the *P{XP}Ect4*$^{d04977}$ transposon element instead. To conclude, no new *dnt2* allele was generated in this project because the Exelixis *P{XP}d05170* fly line had been incorrectly annotated.

A

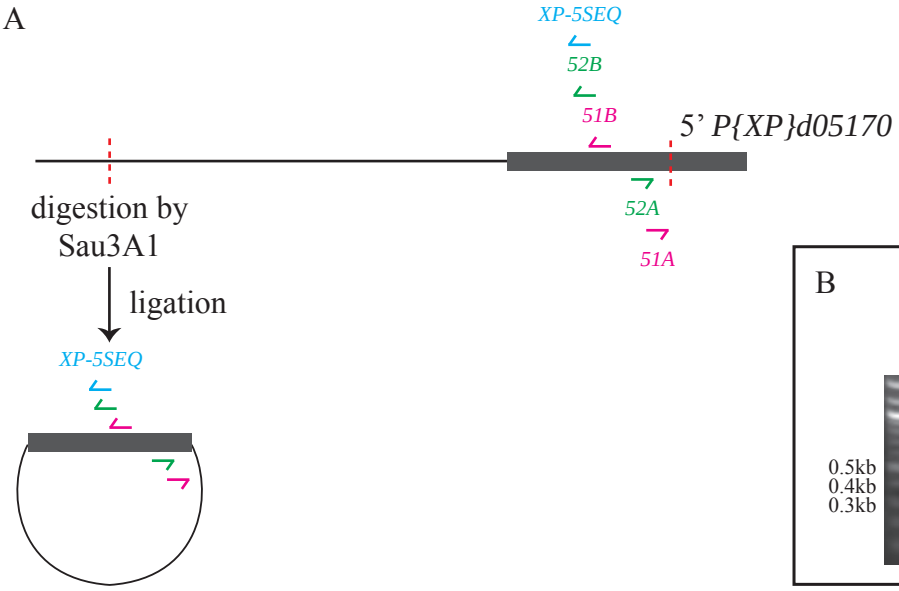


B

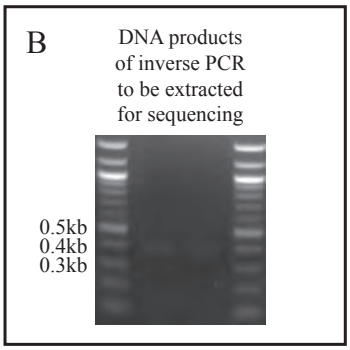


C Sequencing result:

TGA TAA GTG TAT ACT TCG GTA AGC TTC GGC TAT CGA CGG GAC
CAC CTT ATG TTA TTT CAT CAT GCG TGG GAG CTT GGC AGC TCG
AGA GCT TTT TCA TTG CGG TCG CGT CGC TGC CGG CGT CGT TTT
AAA GTG CGA TCT CTG CAG CCC GGG AGG ACC TAA CGC ACA GTC
ACG TTA TTG TTT ACA TAA ATG ATT TTT TTT ACT ATT CAA ACT
TAC TCT GTT TGT GTA CTC CCA CTG GTA

BLAST result:

```
Query:   64        GCGTGGGAGCTTGGCAGCTCGAGAGCTTTTTCATTGCGGTCGCGTCGCTGCCGGCGTCGT   123
                   ||||||||||||||||||||||||||||||||||||||||||||||||||||||||||||
Subject: 8096481   GCGTGGGAGCTTGGCAGCTCGAGAGCTTTTTCATTGCGGTCGCGTCGCTGCCGGCGTCGT   8096422

Query:   124       TTTAAAGTGCGATC   137
                   ||||||||||||||
Subject: 8096421   TTTAAAGTGCGATC   8096408
```

D

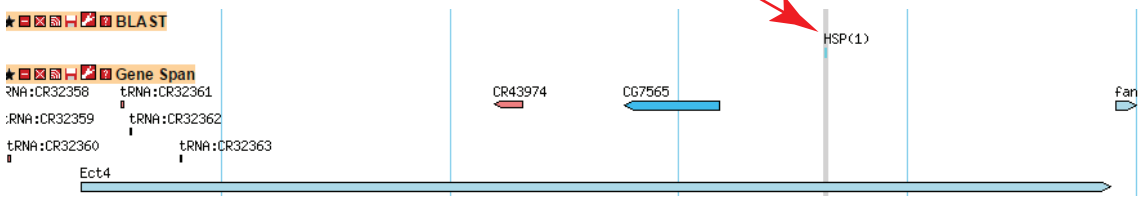


**Figure 4.5** Inverse PCR of the 5' end of *P{XP}* elements. **(A)** Primers used for inverse PCR to recover the sequences flanking the 5' end of *P{XP}d05170* (Table 2.4). **(B)** Preparative gel electrophoresis of DNA products after inverse PCR. The 100bp DNA ladder (New England Biolabs) was used.(**C**) Sequencing output used as the query in BLAST. (**D**) Screenshot of the genome browser view from FlyBase for *D. melanogaster*. BLAST match the sequence flanking the 5' end of *P{XP}d05170* to the *Ectoderm-expressed 4* (*Ect4*) gene.

### 4.2.2 Generating a *spz* Loss of Function Allele

Learning from experience, prior to setting up genetic crosses to generate a new *spz* allele (Figure 2.11), Exelixis flies *P{XP}spz*$^{d00069}$ and *PBac{RB}e04446* were first verified for insertions at correct locations by two-sided PCR (Figure 4.6A). Using primers *GP fwd* and *Tn1 rev* on DNA template extracted from *P{XP}spz*$^{d00069}$, a DNA band of 354bp was expected to be amplified (Figure 4.6A, Table 2.3). With primers *Tn2 fwd* and *GP rev* on DNA from *PBac{RB}e04446*, a band of 670bp was expected (Figure 4.6A, Table 2.3). The expected band sizes were obtained using conventional PCR for both *P{XP}spz*$^{d00069}$ and *PBac{RB}e04446* (Figure 4.6B). Subsequently, the conditions for two-sided PCR in amplifying the 354 and 670bp bands from *P{XP}spz*$^{d00069}$ and *PBac{RB}e04446* DNA were used as positive controls to determine the generation of the hybrid *spz*$^{d00069/e04446}$. Out of the 17 putative hybrid *spz*$^{d00069/e04446}$ fly lines, 15 of these yielded positive bands of the correct sizes for two-sided PCR (Figure 4.6C). Therefore, 15 fly lines were confirmed to have the hybrid *spz*$^{d00069/e04446}$. 3 out of the 15 fly lines were kept and maintained as fly stocks and given the following genotype labels: *w*$^{-}$*;;spz*$^{MA05}$*/TM6B* (stock no. 24, Table 2.1), *w*$^{-}$*;;spz*$^{MA10}$*/TM6B* (stock no. 25, Table 2.1) and *w*$^{-}$*;;spz*$^{MA12}$*/TM6B* (stock no. 26, Table 2.1).

### 4.2.3 Cuticle Prep to Test for *spz* Loss of Function Phenotype

In unhatched *yw* embryos, the normal anterior-posterior and dorsal-ventral axes were established (Figure 4.7A). Segmentation of the larval body wall into thoracic and abdominal segments was also normal as indicated by the presence of the ventral denticle bands. Females of genotypes *spz*$^{2}$*ca*$^{1}$*/ru*$^{1}$*Diap*$^{1}$*st*$^{1}$*kni*$^{ri-1}$*rn*$^{roe-1}$*p*$^{p}$*e*$^{1}$*spz*$^{4}$, *spz*$^{2}$*ca*$^{1}$*/Df(3R)Exel6205* and

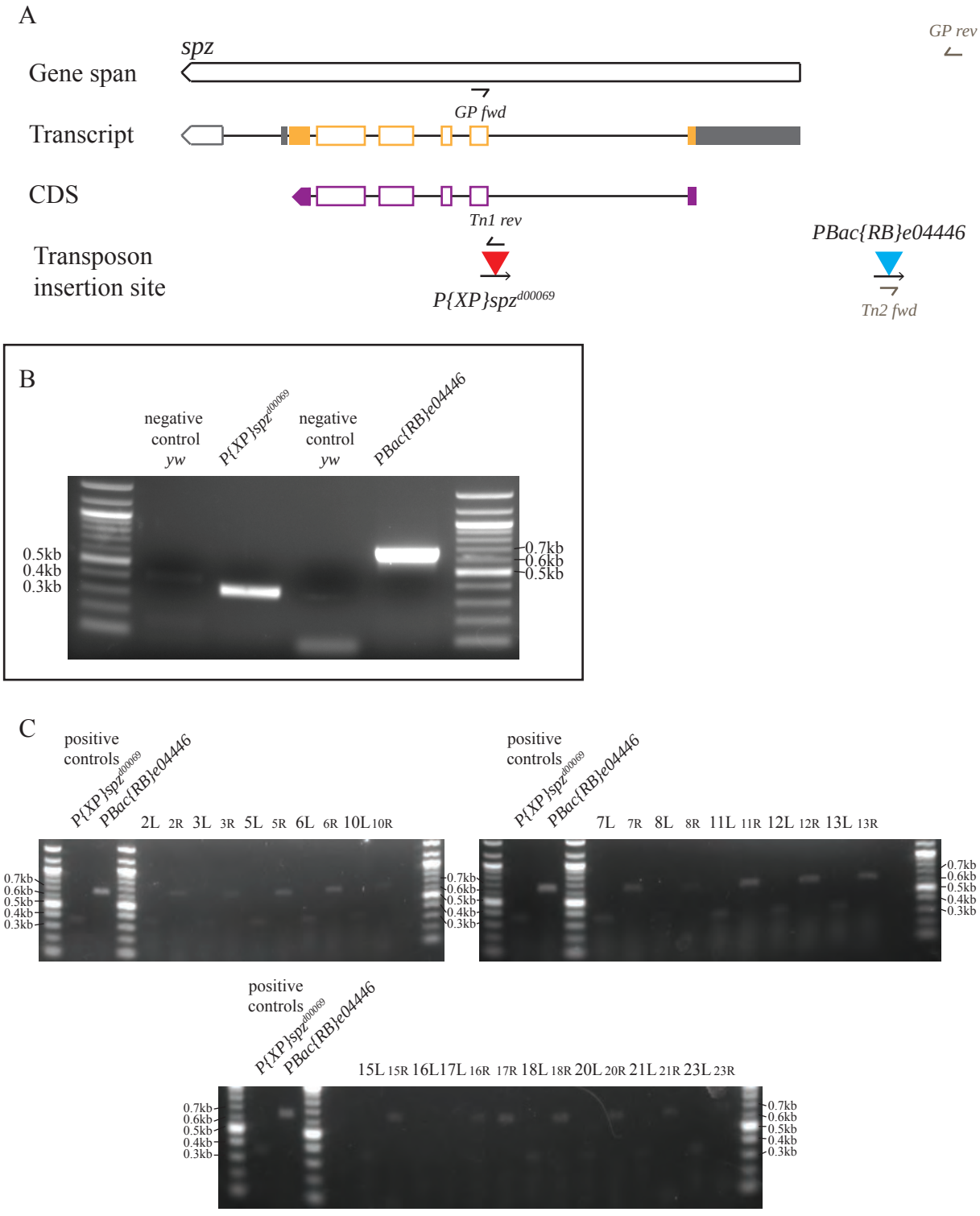


**Figure 4.6** Determination of putative *spz*$^{d00069/e04446}$ loss of function alleles. **(A)** Primer sites of *GP fwd*, *Tn1 rev*, *Tn2 fwd* and *GP rev* (Table 2.3). **(B)** Verification of transposon insertion at the correct location using two-sided PCR. The left-hand side was used for *P{XP}spz*$^{d00069}$ and the right side for *PBac{RB}e04446*. **(C)** Two-sided PCR confirmation of 17 fly lines with putative genotype *spz*$^{d00069/e04446}$. The 100bp DNA ladder (New England Biolabs) was used in (B) and (C).

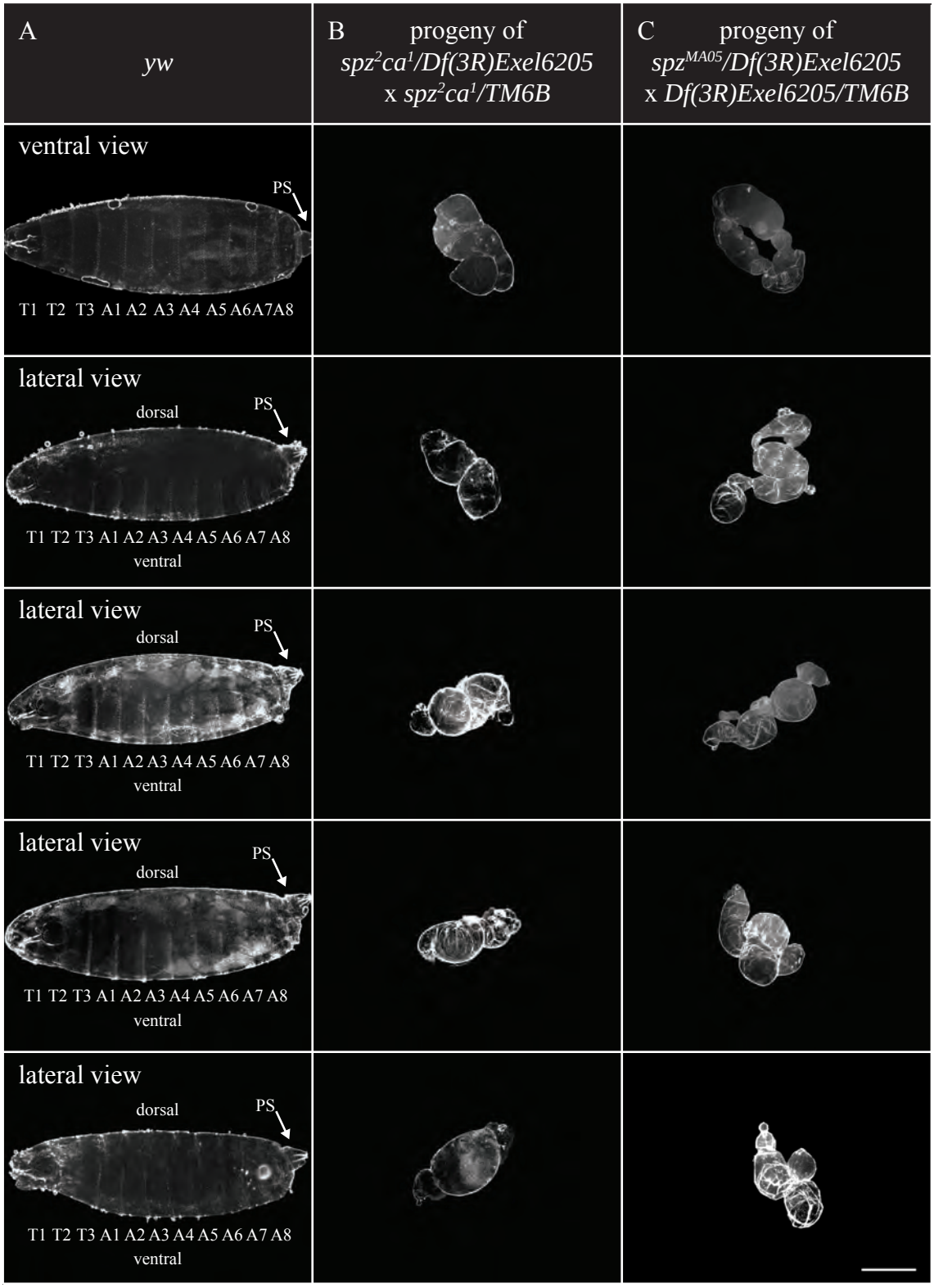


**Figure 4.7** Cuticle preparations to observe dorsal-ventral phenotype. **(A)** 5 individuals of positive control *yw*. **PS:** posterior spiracles. **(B)** 5 unviable individuals of the $F_2$ generation originating from $F_1$ *spz²ca¹/Df(3R)Exel6205* females crossed to *Df(3R)Exel6205/TM6B* males. **(C)** 5 unviable $F_2$ individuals as a result of $F_1$ *spz$^{MA05}$/Df(3R)Exel6205* females crossed to *Df(3R)Exel6205/TM6B* males. Scale bar represents 250µm.

*spz*$^{MA05}$*/Df(3R)Exel6205* were viable and were able to lay eggs, but the eggs never hatch. Unhatched offspring of *spz*$^{2}$*ca*$^{1}$*/Df(3R)Exel6205* females exhibited perturbed morphology with respect to their DV polarity (Figure 4.7B). There were virtually no clear denticle bands because the embryos were dorsalised. Unhatched offspring of *spz*$^{MA05}$*/Df(3R)Exel6205* females also exhibited perturbed polarity lacking denticle bands (Figure 4.7C). The embryos differentiated an elongated hollow tube of dorsalised cuticle akin to those laid by *spz*$^{2}$*ca*$^{1}$*/Df(3R)Exel6205* females. To conclude, both *spz*$^{2}$ and *spz*$^{MA05}$ are loss of function alleles.

### 4.2.4 Lethality of *spz*$^{2}$ and *spz*$^{MA05}$ Allele

The survival index (SI) of *spz*$^{2}$*ca*$^{1}$ over *TM6B* was 0.14 (Figure 4.8), indicating that the alleles were homozygous semi-lethal (n=1393, $\chi^2(1)=455.088$, $p<0.001$), and that the alleles reduced the viability of larval homozygotes surviving. Only 6.4% of larval population survive as homozygotes into pupal stages. When heterozygote *spz*$^{2}$*ca*$^{1}$ females were crossed to heterozygote *ru*$^{1}$*st*$^{1}$*ea*$^{14}$*spz*$^{3}$*ca*$^{1}$ males, the SI of *spz*$^{2}$*ca*$^{1}$ larvae was 1.06 (n=876, $\chi^2(1)=0.622$, $p=0.430$), indicating that the alleles were rescued and corresponded to the Mendelian segregation of wild-type chromosome. Heterozygote *spz*$^{2}$*ca*$^{1}$ crossed to heterozygote *ru*$^{1}$*Diap*$^{1}$*st*$^{1}$*kni*$^{ri\text{-}1}$*rn*$^{roe\text{-}1}$*p*$^{p}$*e*$^{1}$*spz*$^{4}$ improved SI to 1.36, significantly beyond rescued levels (n=250, $\chi^2(1)=5.618$, $p<0.05$). The *spz*$^{2}$*ca*$^{1}$ alleles were again rescued when heterozygote *spz*$^{2}$*ca*$^{1}$ females were crossed to heterozygote *spz*$^{MA05}$ males (n=685, $\chi^2(1)=0.292$, $p=0.589$) and heterozygote *Df(3R)Exel6205* males (n=662, $\chi^2(1)=1.208$, $p=0.272$).

In constrast to *spz*$^{2}$*ca*$^{1}$, *spz*$^{MA05}$ over TM6B was observed to be fully lethal with a SI of 0 (Figure 4.8). Heterozygote *spz*$^{MA05}$ females crossed to heterozygote *spz*$^{2}$*ca*$^{1}$ males gave a rescued SI of 0.88 (n=473, $\chi^2(1)=1.526$, p=0.217). This SI of 0.88 replicated the result of an earlier SI when heterozygote *spz*$^{2}$*ca*$^{1}$ females were crossed to heterozygote *spz*$^{MA05}$males ($\chi^2(1)=1.692$, p=0.193). When heterozygote *spz*$^{MA05}$ were crossed to heterozygotes *ru*$^{1}$*st*$^{1}$*ea*$^{14}$*spz*$^{3}$*ca*$^{1}$ and *ru*$^{1}$*Diap*$^{1}$*st*$^{1}$*kni*$^{ri-1}$*rn*$^{roe-1}$*p*$^{p}$*e*$^{1}$*spz*$^{4}$, the *spz*$^{MA05}$ allele was rescued with SI 1.24 (n=222, $\chi^2(1)=2.453$, p=0.117) and 0.95 (n=375, $\chi^2(1)=0.192$, p=0.661), respectively. Heterozygote *spz*$^{MA05}$ crossed to heterozygote *spz*$^{MA10}$ also rescued SI to 0.92 (n=321, $\chi^2(1)=0.505$, p=0.477), but when crossed to heterozygote *spz*$^{MA12}$, SI was 0. The cross between heterozygotes *spz*$^{MA05}$ and *Df(3R)Exel6205* resulted in a SI of 0.74, indicating that the allele was not fully rescued (n=719, $\chi^2(1)=12.487$, p<0.001). This was also the case when heterozygotes *Df(3R)Exel6205* were crossed to *spz*$^{MA10}$ to yield a SI of 0.55 (n=280, $\chi^2(1)=17.857$, p<0.001), and when crossed to *spz*$^{MA12}$ to give SI 0.53 (n=238, $\chi^2(1)=16.269$, p<0.001). Crosses between *Df(3R)Exel6205* with *spz*$^{MA05}$ and *spz*$^{MA12.}$gave SI which were not statistically different to each other ($\chi^2(1)=3.508$, p=0.061).

### 4.2.5 Lethality of *dnt2*$^{37}$ Allele

As mentioned in Section 4.2.1, there was no new *dnt2* allele generated in this project. Instead, new *dnt2* alleles were generated by Dr J. Wentzell by hsFLP-FRT deletion using *PBac{RB}dnt2*$^{e03444}$ and *PBac{WH}Shab*$^{f05893}$ (personal communication). Dr J. Wentzell generated fly stocks *;;dnt2*$^{18}$ (stock no. 36, Table 2.1) and *;;dnt2*$^{37}$*/(TM6B)* (stock no. 37, Table 2.1). The *dnt2*$^{18}$ allele exists in homozygosis but *TM6B* is required for survival index assays, so only the *dnt2*$^{37}$ allele was characterised (Figure 4.9).

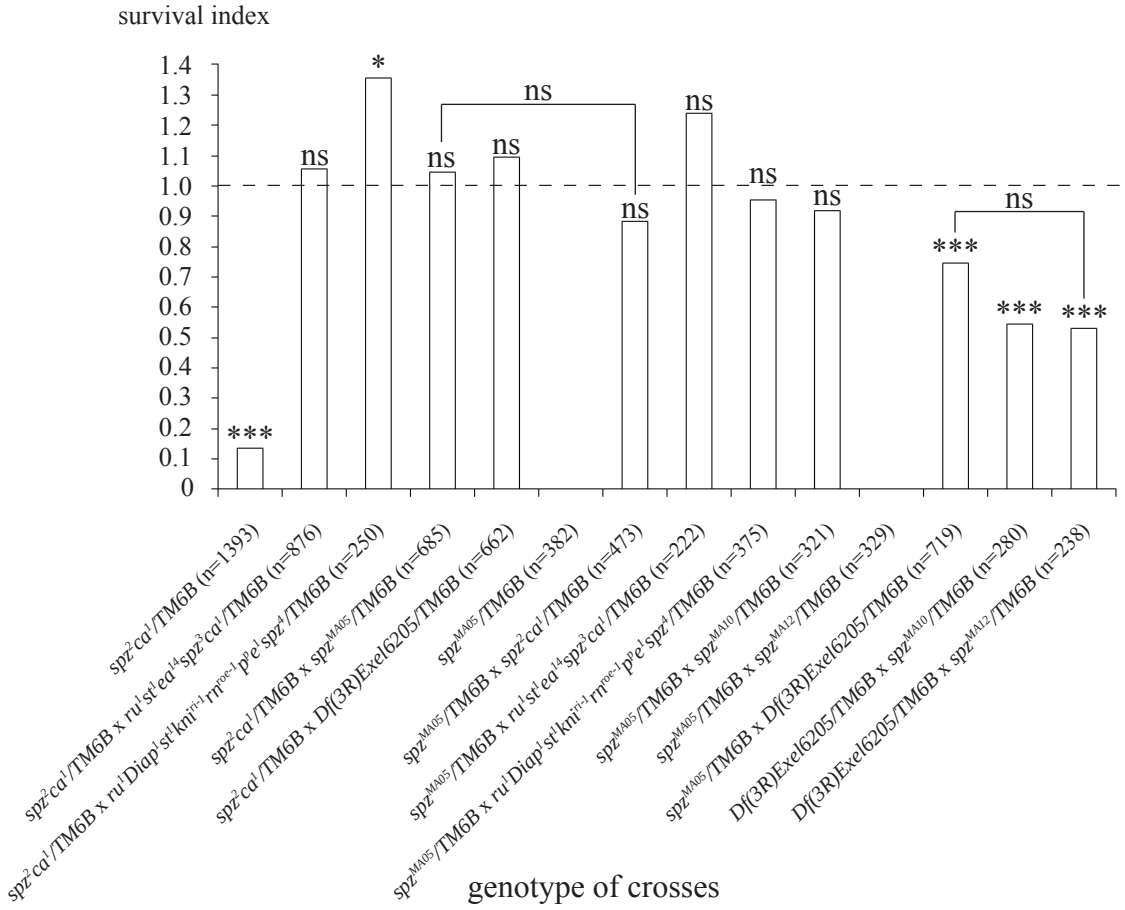


**Figure 4.8** Survival indexes of the *spz*$^{2}$ and *spz*$^{MA05}$ allele. Expected survival index of wild-type chromosome is 1.0. Statistical results on top of each bar in the chart above were results of the comparisons between test genotypes and expected values according to Mendelian segregation of wild-type chromosomes.

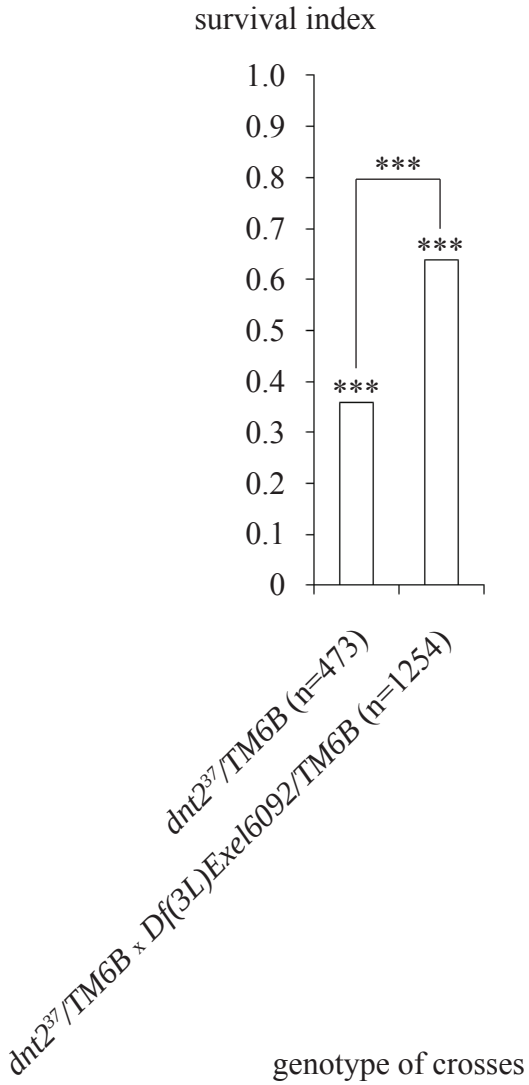


**Figure 4.9** Survival indexes of the *dnt2*$^{37}$ allele. Expected survival index of wild-type chromosome is 1.0. Statistical results on top of each bar in the chart above were results of the comparisons between test genotypes and expected values according to Mendelian segregation of wild-type chromosomes.

The *dnt2*$^{37}$ allele is semi-lethal with SI of 0.36 (n=473, $\chi^2(1)=69.819$, $p<0.001$). 15.2% of the larval population survive as homozygotes into pupal stages. When heterozygote *dnt2*$^{37}$ females were crossed to heterozygote *Df(3L)Exel6092*, the SI of *dnt2*$^{37}$ larvae was 0.64 (n=1254, $\chi^2(1)=47.458$, $p<0.001$). Although this SI value of 0.64 indicates that the allele was not rescued, it was significantly higher than the SI of 0.36 from the heterozygote sibling cross ($\chi^2(1)=16.150$, $p<0.001$).

## 4.3 Discussion

Before this project, the alleles used for studying the loss of DNT function were *dnt1*$^{41}$, *dnt1*$^{55}$, *dnt2*$^{e03444}$, *spz*$^{2}$, *spz*$^{3}$ and *spz*$^{4}$ (Sutcliffe *et al.*, 2013; Weber *et al.*, 2007; Zhu *et al.*, 2008). *Dnt1*$^{41}$ and *dnt1*$^{55}$ are null mutant alleles while *dnt2*$^{e03444}$ is hypomorphic with a 5.9kb *PBac* insertion (Dos Santos *et al.*, 2015; Zhu *et al.*, 2008). *Spz*$^{2}$, *spz*$^{3}$ and *spz*$^{4}$ are point mutant alleles (Tearle and Nusslein-Volhard, 1987; Weber *et al.*, 2007). Due to the generation of *spz*$^{2}$, *spz*$^{3}$ and *spz*$^{4}$ by EMS, the point mutant alleles exist with secondary mutations of other genes in the same chromosome. Therefore, the work of this chapter aims to generate new loss of function alleles for *dnt2* and *spz*.

### 4.3.1 Generation and Characterisation of *dnt2*$^{37}$ Allele

Despite the aims of this chapter, no new *dnt2* alleles were generated by hsFLP-FRT deletion. This was due *P{XP}d05170* flies not carrying the *P{XP}* transposon element at its reported insertion site. By using inverse PCR to identify the location of the *P{XP}* element in DNA extracted from *P{XP}d05170* flies, the nucleotide sequences were found to flank

*P{XP}Ect4*$^{d04977}$ instead. *P{XP}Ect4*$^{d04977}$ was inserted into the *Ect4* gene in plus orientation about 5 million nucleotides away from *dnt2,* and would not be an allowable partner to pair with *PBac{RB}dnt2*$^{e03444}$ for hsFLP-FRT deletion of the *dnt2* locus (Figure 4.1B). So, new *dnt2* alleles were generated by Dr J. Wentzell using hsFLP-FRT deletion between *PBac{RB}dnt2*$^{e03444}$ and *PBac{WH}Shab*$^{f05893}$*,* the next allowable partner inserted downstream of *dnt2*, into the 5' untranslated region (UTR) of the *Shaker cognate b* (*Shab*) gene. The new *dnt2* alleles were called *dnt2*$^{18}$ and *dnt2*$^{37}$ (Dr J. Wentzell, personal communication).

The *dnt2*$^{37}$ fly stock exists in heterozygosis over *TM6B* with SI of 0.36, indicating that *dnt2*$^{37}$ was homozygous semi-lethal, with 15.2% of the larval population surviving as homozygotes into pupal stages. When heterozygote *dnt2*$^{37}$ females were crossed to heterozygote *Df(3L)Exel6092*, the resulting SI value of 0.64 was significantly higher than the SI of 0.36 from the heterozygote *dnt2*$^{37}$ sibling cross. The improved viability of the non-tubby larval genotype *dnt2*$^{37}$/*Df(3L)Exel6092* over *dnt2*$^{37}$/*dnt2*$^{37}$ could be accounted by rescue of the set of genes deleted in the *Df(3L)Exel6092*. Although the viability of *dnt2*$^{37}$/*Df(3L)Exel6092* was improved, the improvement was not comparable to SI of 1, and thus the improved viability was not a full rescue. This suggests that the *dnt2*$^{37}$ allele in homozygosis, or in *trans* with the *Df(3L)Exel6092* background, reduced the viability of larvae reaching pupal stages. However, the *dnt2*$^{18}$ fly stock exists in homozygosis. The difference in viability between the *dnt2*$^{18}$ and *dnt2*$^{37}$ allele is not yet understood, and there is a possibility that the *dnt2*$^{37}$ stock could require more time to achieve stable homozygosis.

### 4.3.2 Generation and Characterisation of *spz*$^{MA05}$ Allele

In this chapter, only new *spz* alleles were generated by hsFLP-FRT deletion. The new *spz* alleles were called $spz^{MA05}$, $spz^{MA10}$ and $spz^{MA12}$.

The females of $spz^{MA05}/Df(3R)Exel6205$ laid embryos with dorsalised phenotype. A dorsalised phenotype is a well-known loss of function phenotype for the lack of *spz* activity (Anderson and Nusslein-Volhard, 1984; Carroll *et al.*, 1987; DeLotto and DeLotto, 1998). This concludes that $spz^{MA05}$ is a loss of function allele. The $spz^{2}$ allele is also a loss of function allele. Here, $spz^{2}ca^{1}/Df(3R)Exel6205$ females laid dorsalised embryos, a result matching dorsalised embryos laid by $spz^{2}/spz^{2}$ females (DeLotto and DeLotto, 1998). The cuticles of unviable embryos laid by $spz^{2}ca^{1}/ru^{1}Diap^{1}st^{1}kni^{ri\text{-}1}rn^{roe\text{-}1}\ p^{p}e^{1}spz^{4}$ were not prepared because $spz^{4}$ was previously shown to produce embryos with dorsalised cuticle (Morisato and Anderson, 1994).

The survival index of $spz^{MA05}$ over *TM6B* differs from that of $spz^{2}ca^{1}$. The $spz^{MA05}$ allele is fully lethal while $spz^{2}ca^{1}$ alleles together are semi-lethal. The SI of $spz^{2}ca^{1}$ over *TM6B* was 0.14, with 6.4% of the larval population surviving as homozygotes into pupal stages. This percentage was comparable to the observed 7.1% of pupal population eclosing as homozygote fly adults (Sutcliffe *et al.*, 2013; Zhu *et al.*, 2008).

When heterozygotes $spz^{MA05}$ and $spz^{2}ca^{1}$ were crossed with each other in two independent crosses, the resulting SI were 1.04 and 0.88. These two SI values were not significantly different from each other and they indicate that the non-tubby larval genotype $spz^{MA05}/spz^{2}ca^{1}$ was fully viable. Other non-tubby larval genotypes which were fully viable includes:

$spz^{MA05}/ru^1st^1ea^{14}spz^3ca^1$, $spz^2ca^1/ru^1st^1ea^{14}spz^3ca^1$, $spz^{MA05}/ru^1Diap^1st^1kni^{ri-1}rn^{roe-1}p^pe^1spz^4$, $spz^2ca^1$/*Df(3R)Exel6205* and $spz^{MA05}/^{MA10}$.

The resulting SI of heterozygote $spz^2ca^1$ crossed to $ru^1Diap^1st^1kni^{ri-1}rn^{roe-1}p^pe^1spz^4$ was 1.36, which is a SI value significantly above 1. This indicates that there were more $spz^2ca^1/ru^1Diap^1st^1kni^{ri-1}rn^{roe-1}p^pe^1spz^4$ larvae surviving into pupal stages than would be expected for wild-type rescue. The $spz^2ca^1/ru^1Diap^1st^1kni^{ri-1}rn^{roe-1}p^pe^1spz^4$ larvae could possibly be out-competing the heterozygote population.

While heterozygote $spz^2ca^1$ crossed to *Df(3R)Exel6205* produce fully viable non-tubby larvae with SI of 1.09, this was not the case for when $spz^{MA05}$ was crossed to *Df(3R)Exel6205*, in which the SI of non-tubby larvae was 0.74. This suggests that the $spz^{MA05}$ allele in *trans* over *Df(3L)Exel6205* reduced the viability of larvae reaching pupal stages. The $spz^{MA10}$ and $spz^{MA12}$ alleles in trans over *Df(3L)Exel6205* also reduced larval viability to the same extent as $spz^{MA05}$/*Df(3R)Exel6205*. It is not clear why heterozygote $spz^{MA05}$ crossed to $spz^{MA10}$ produced fully viable larvae and yet no $spz^{MA05}/spz^{MA12}$ larvae reached pupal stages.

Put together, when $spz^2ca^1$ was in *trans* over other *spz* alleles and *Df(3R)Exel6205*, the viability of the non-tubby larval progeny were rescued, except when the non-tubby larval genotype was $spz^2ca^1/ru^1Diap^1st^1kni^{ri-1}rn^{roe-1}p^pe^1spz^4$. When $spz^{MA05}$ was in *trans* over other *spz* alleles, the viability of non-tubby larvae were also rescued, except when the larval genotype was $spz^{MA05}/spz^{MA12}$. Lastly, when all *spz* alleles generated by hsFLP-FRT were in *tans* over *Df(3R)Exel6205*, the viability of non-tubby progeny reaching pupal stages were lowered.

# Chapter 5

# 5 Developmental Functions of DNTs and Their Toll Receptors

## 5.1 Introduction

This chapter is about analysing DNT function in the third instar larval stage. Whereas Sutcliffe (2011) characterised DNT roles in the larval neuromuscular junction, the author investigated the roles of DNTs in organ size and cell numbers in the CNS.

### 5.1.1 The *spz$^{2}$ca$^{1}$/TM6B* Fly Stock

The *spz$^{2}$ca$^{1}$/TM6B* stock co-exists with *ca$^{1}$*, a recessive and eye-colour defective allele of the *claret* gene (Silva and Mensua, 1985; Yamamoto *et al.*, 1989). The *claret* gene codes for the protein Rab32-GEF, that is, a guanine nucleotide exchange factor (GEF) which switches the GTPase Rab32 from its inactive to active form (Ma *et al.*, 2004; Wang *et al.*, 2012). In order to address whether or not *ca$^{1}$/ca$^{1}$* interacts with *spz$^{2}$/spz$^{2}$*, the eye-colour defective *ca$^{1}$* allele in the fly stock *spz$^{2}$ca$^{1}$/TM6B* was recombined out to generate *spz$^{2}$ca$^{+}$/TM6B*, bearing a *ca$^{+}$* wild-type allele. If *ca$^{1}$* is an interacting factor with *spz$^{2}$* that results in a small CNS phenotype, the outcome of replacing *spz$^{2}$ca$^{1}$/spz$^{2}$ca$^{1}$* with *spz$^{2}$ca$^{+/}$spz$^{2}$ca$^{+}$* is hypothesised to return the CNS phenotype to control size.

### 5.1.2 Rescue of *spz$^{2}$ca$^{1}$* with Tolls

Previously, Sutcliffe *et al.* (2013) and McIlroy *et al.* (2013) showed that the semi-lethality in $spz^{2}$ animals (SI=0.08 and SI=0.17, respective papers) was rescued by pan-neuronal expression of constitutively active Toll, $Toll^{10bB}$ (SI=0.92 and SI=0.60, respectively). The rescue was replicated with the overexpression of $Toll6^{CY}$ and $Toll7^{CY}$ in McIlroy *et al.* (2013) (SI=0.39 and SI=0.38, respectively), but with lesser degree of viability.

Here, the viability experiment will be extended by looking into the effect $Toll^{10bB}$, $Toll6^{CY}$ and $Toll7^{CY}$ have on homozygous $spz^{2}$ CNS size through *elav-GAL4* and *repo-GAL4*, with the idea of testing whether or not Toll6 and Toll7 could be potential receptors of Spz.

### 5.1.3 Overexpression Different Forms of Spz

The *spz-GAL4* line crossed to *myr-tdTomato* reporter revealed complementary patterns with anti-Spz-GLR staining in the VNC neuropile. Spz was previously suggested to be secreted into the mechanosensory domain. In this chapter, the use of *spzGAL4* to overexpress Spz presumed increasing base level of Spätzle protein production in cells with active *spz* promoter.

### 5.1.4 Interaction between DNTs and Notch

In the *Drosophila* larval CNS, there are mostly neurons and glia. Trophic factors could be secreted from neurons or glia or both. Pan-neuronal overexpression of the intracellular domain of Notch fragment ($Notch^{ICD}$) affects cell fate decision in embryogenesis (Le Gall *et al.*, 2008; Lehmann *et al.*, 1983), and is fully lethal with no single larvae hatching from eggs

(personal observation). However, *repo-GAL4* overexpression of the intracellular domain throughout embryogenesis and up to wandering third instar larval life will result in CNS with a long VNC with abdominal glia numbers higher than in *yw* (Kato *et al.*, 2011). Due to injury-induced apoptosis being rescued by *repo>Notch$^{ICD}$*, this suggest the genotype could produce a trophic factor that protects cells from apoptosis. This chapter will test for an interaction between the DNTs and Notch.

### 5.1.5 Regulation of Cell Numbers

DNT1, DNT2 and Toll maintain neuronal survival in embryos (Zhu *et al.*, 2008). Whether or not they maintain cell survival in the larval VNC remains unknown.

### 5.1.6 *Bdnf$^{Met66}$* and *spz$^{2}$*

Hippocampal neurons of *bdnf$^{Met66}$* knock-in mice were analysed by Sholl analysis and were shown to display decreased dendritic arbor complexity (Chen *et al.*, 2006). Using FLP technique to visualise single cells, it is possible to analyse the dendrites of RP2 neurons for the *spz$^{2}$* allele.

### 5.1.7 Specific Aims

The specific aims of this chapter are:

- To characterise *spz$^{2}$ca$^{1}$* and *spz$^{2}$ca$^{+}$* in terms of CNS size.
- To test *Toll6* and *Toll7* as putative receptors of *spz* using SI assays.

- To test *Toll6* and *Toll7* as putative receptors of *spz* using CNS size.
- To characterise the CNS size when *spz* is overexpressed by *spz-GAL4*.
- To test for an interaction between DNTs and Notch using VNC size phenotype.
- To investigate if Spz, DNT1, DNT2, Toll, Toll6 and Toll7 affect Repo+ cell number.
- To investigate if Spz, DNT1, DNT2, Toll, Toll6 and Toll7 affect pH3+ cell number.
- To investigate if Spz, DNT1, DNT2, Toll, Toll6 and Toll7 affect Dcp1+ cell number.
- To characterise the dendrites of $spz^2$ RP2 neurons according to Sholl analysis.

### 5.1.8 Methods in Brief

For CNS size experiments, absolute measurements were used and there was no normalising of VNC length measurements to body length. This was because only wandering larvae were sampled and all test genotypes did not exhibit any obvious differences in body size. There was only 1 CNS sample collected for the genotype $spz^{MA05}/TM6B$ because the project ran out of time and the data collection was disappointingly left unfinished (Figure 5.1). The sample will be used for showing the ROIs of brain area, VNC area and VNC length (Figure 5.1A).

The genetic protocol for recombining $ca^1$ with $ca^+$ was provided in Figure 2.8 (Section 2.1.3). Screening details were provided in Figure 2.9. During screening, SI assays on the test genotypes were undertaken. Ultimately, 2 out of 15 lines tested positive for the presence of $spz^2$ (genotypes: $w^+;;spz^2ca^+.33/TM6B$, stock no. 20; $w^+;;spz^2ca^+.56/TM6B,LacZ$, stock no. 21, Table 2.1). The two genotypes arose from the same genetic scheme but both could be chromosomally different products. The remaining 13 were thrown out after screening because the purpose of the genetic protocol was to retrieve genotype $spz^2ca^+/TM6B$. During screening,

SI was recorded. Observations were made on locomotion and life span defects too. Locomotion was classed defective when flies could not stand upright after falling. Shorten life spans were detected through flies found dead half-way emerged from their pupal case or via young flies with wings remaining folded.

Occasionally, the aberrant chromosomes of fly deficiency lines *Df(3R)Exel6205*, *Df(3L)Exel6101* and *Df(3L)Exel6092* were abbreviated to *Df6205*, *Df6101* and *Df6092*. All "CK" symbols refer to the activated form of Spz (*actSpz(2)*), DNT1 (*DNT1-CK-3'+*) and DNT2 (*DNT2-CK-6A*) fused to UAS construct. All "FL" symbols refer to full length form of Spz (*spz-FL*), DNT1 (*DNT1-FL*) and DNT2 (*DNT2-FL-47C*) fused to UAS construct. *UAS-spz$^{2}$-E1* refers to the *UAS* construct fused to the full length form of the *spz$^{2}$* allele, a construct generated by M. Rai. *Toll$^{10b}$* refers to the activated form of Toll fused to UAS. *UAS-Toll$^{10bA}$* and *UAS-Toll$^{10bB}$* refers to the same transgenic construct, but they were inserted into chromosome 3 and 2, respectively. To avoid any positional effects, the same insertion (*UAS-Toll$^{10bB}$*) was used every time. The *p35* in fly stock *UAS-p35,spz$^{2}$/TM6B,LacZ* (stock no. 50, Table 2.1) refers to the viral protein highly adapted to inhibit caspase.

To address the effect of *ca$^{1}$* independently of *spz$^{2}$*, the fly stock *ru$^{1}$h$^{1}$th$^{1}$st$^{1}$cu$^{1}$sr$^{1}$e$^{s}$ca$^{1}$* was used (stock no. 42, Table 2.1). This stock was an alternative to "*ca$^{1}$*" due to logistic problems with purchasing from Kyoto *Drosophila* Genetic Resource Centre (Kyoto DGRC) at the time of experiment.

*Toll*$^{r3}$ is a loss of function allele which is temperature sensitive. For experiments which use *Toll*$^{r3}$, the permissive temperature for normal embryogenesis was 18°C and the restrictive temperature for loss of function study in larval life was 29°C.

To count the number of glia in the VNC, anti-Repo antibodies were used. Cells undergoing mitosis were marked by anti-pH3, an antibody targeting phosphorylated histone H3. Cells undergoing apoptosis were labelled by anti-Dcp1, an antibody targeting cleaved *Drosophila* Death caspase 1, an effector caspase with determines the rate of cell death (Florentin and Arama, 2012). Glial, mitotic and apoptotic cells were automatically counted with DeadEasy Larval Glia. Mitotic and apoptotic cell counting using DeadEasy Larval Glia were validated the same way as for glial cell counting (Section 2.5.4). Details for ROI selection were covered in Section 2.5.4 (Figure 2.15). More consideration towards experiments collecting number of mitotic cells included recognising that the abdominal VNC stained with anti-pH3 will produce a staining pattern illustrated by Figure 5.26. To account for the possibility that there could be genetic effects affecting the mitotic and non-mitotic zone differently, the number of pH3+ cells in the non-mitotic zone were independently treated too. The number of pH3+ cells in the non-mitotic zone were categorised into number of VNC having less than or equal to 5 cells and number of VNC having more than 5 cells undergoing mitosis. Abdominal VNC stained with anti-Dcp1 also produced similar zones of dense Dcp1+ (apoptotic zone) and sparse Dcp1+ cells (non-apoptotic zone).

All Ebony+ cells were counted using the Cell Counter tool in ImageJ. Z-stack images were opened in ImageJ and initialised by the Cell Counter tool. Once initialised, Ebony+ Repo+ cells were manually identified throughout the Z-stack and marked by clicking which Cell

Counter automatically tallies. Pairings of Ebony+ ventral interface glia (vIG) were manually counted and categorised.

All mean values were quoted with standard deviation. For reference to full statistical reports, please refer to Appendix (Section 9). Scatter plots were given to provide information on raw data in the interest of creating transparency. Box plots were provided to analyse outliers. Bar charts were included because statistical tests of normalise data compared means.

## 5.2 Results

### 5.2.1 Homozygous *spz²ca¹* and CNS Size

Homozygous *spz²ca¹* CNS were significantly smaller than *yw* in brain and VNC areas (Table 5.1, Figure 5.1). In addition, the VNC length of *spz²ca¹* was significantly shorter than *yw* (Table 5.1, Figure 5.1). Meanwhile, the CNS of heterozygous *spz²ca¹* allele over its deficiency *Df(3R)Exel6205* were surprisingly akin to those of *yw* (Table 5.1, Figure 5.1). Accordingly, *spz²ca¹/Df(3R)Exel6205* had CNS significantly larger and longer from the CNS of *spz²ca¹*. Data collected from *spz$^{MA05}$/Df(3R)Exel6205* was inconclusive.

| | Brain Area | | | VNC Area | | | VNC Length | | |
|---|---|---|---|---|---|---|---|---|---|
| Genotype | N | Mean ($x10^5 \mu m^2$) | SD ($x10^5 \mu m^2$) | N | Mean ($x10^4 \mu m^2$) | SD ($x10^4 \mu m^2$). | N | Mean (μm) | SD (μm) |
| *yw* | 25 | 1.70 | ±0.23 | 25 | 7.0 | ±0.8 | 25 | 372 | ±25 |
| *spz²ca¹* | 15 | 0.68 | ±0.13 | 15 | 5.8 | ±0.6 | 15 | 333 | ±18 |
| *spz²ca¹/Df6205* | 8 | 1.67 | ±0.11 | 9 | 7.3 | ±0.5 | 9 | 378 | ±22 |
| *spz$^{MA05}$/Df6205* | 1 | 1.01 | - | 1 | 5.5 | - | 1 | 355 | - |

Table 5.1 Brain and VNC size quantification for genotypes *yw*, *spz²ca¹*,*spz²ca¹/Df(3R)Exel 6205* and *spz$^{MA05}$/Df(3R)Exel6205*.

**Figure 5.1** Brain and VNC size characteristics for genotypes *yw*, *spz$^{2}$ca$^{1}$*, *spz$^{2}$ca$^{1}$/ Df(3R)Exel6205* and *spz$^{MA05}$/Df(3R)Exel6205*. **(A)** Representative mounted CNS images acquired with phase contrast using Zeiss Axioplan 2 (for genotypes *yw*, *spz$^{2}$ca$^{1}$* and *spz$^{2}$ca$^{1}$/ Df(3R)Exel6205*) and Zeiss LSM710 (*spz$^{MA05}$/Df(3R)Exel6205*). ROIs included are those for brain area, VNC area and VNC length. Scale bars, 100μm. **(B)** Markers representing brain and VNC areas of individual larvae. Each blue diamond marker represents a *yw* individual (n=25). Red squares, *spz$^{2}$ca$^{1}$* (n=15). Green triangles, *spz$^{2}$ca$^{1}$/Df(3R)Exel6205* (n=8). Black cross, *spz$^{MA05}$/Df(3R)Exel6205* (n=1). **(C)** Markers representing VNC areas and lengths of individual larvae. Blue diamonds, *yw* (n=25). Red squares, *spz$^{2}$ca$^{1}$* (n=15). Green triangles: *spz$^{2}$ca$^{1}$/Df(3R)Exel6205* (n=9). Black cross, *spz$^{MA05}$/Df(3R)Exel6205* (n=1). **(D)** Boxplots showing ranges and outliers for brain area, VNC area and VNC length. Genotypes plotted for each size variable: *yw*, *spz$^{2}$ca$^{1}$* and *spz$^{2}$ca$^{1}$/Df(3R)Exel6205*. **(E)** Bar charts showing mean brain area, mean VNC area and mean VNC length. Genotypes plotted for each mean size variables: *yw*, *spz$^{2}$ca$^{1}$* and *spz$^{2}$ca$^{1}$/Df(3R)Exel6205*. Brain area statistics: Levene's statistic=4.0, $p<0.05$; Welch ANOVA $F(2,23.7)=145.4$, $p<0.001$. VNC area: Levene's statistic=3.7, $p<0.05$; Welch ANOVA $F(2,24.8)=17.7$, $p<0.001$. VNC length: Levene's statistic=2.7, $p=0.076$; one-way ANOVA $F(2,46)=17.1$, $p<0.001$.

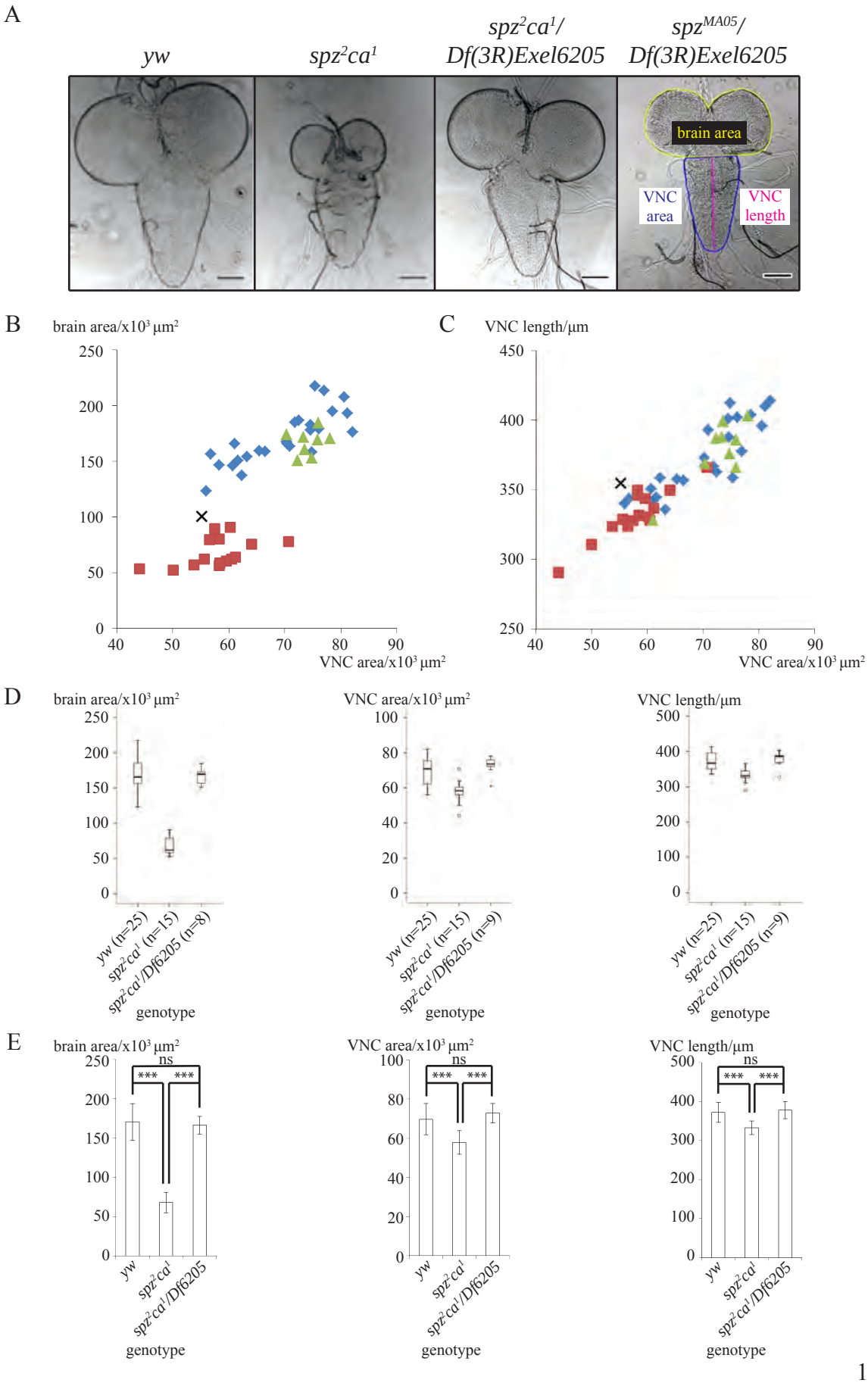
A
yw
spz2ca1
spz2ca1/ Df(3R)Exel6205
spzMA05/ Df(3R)Exel6205
brain area
VNC area
VNC length
B
brain area/x10³ µm²
VNC area/x10³ µm²
C
VNC length/µm
VNC area/x10³ µm²
D
brain area/x10³ µm²
VNC area/x10³ µm²
VNC length/µm
yw (n=25)
spz2ca1 (n=15)
spz2ca1/Df6205 (n=8)
spz2ca1/Df6205 (n=9)
genotype
E
ns
***
yw
spz2ca1
spz2ca1/Df6205
genotype

### 5.2.2 Interaction with *claret*

#### 5.2.2.1 Pecularities with $spz^{+}ca^{+}$ Stocks

15 lines of balanced fly stocks carried a confirmed allele of $ca^{+}$ but either $spz^{+}$ or $spz^{2}$ (Table 5.2). Before throwing out stocks which failed the screen for $spz^{2}ca^{+}$, the author observed two peculiarities. Firstly, the stock in line 29 was fully lethal (SI=0) while every other screened lines had semi-lethal phenotype (SI range=0.21-0.41). Secondly, there were locomotion and life span defects present in fly stocks of genotype $spz^{+}ca^{+}$ on their backs.

#### 5.2.2.2 Genotype $ru^{1}h^{1}th^{1}st^{1}cu^{1}sr^{1}e^{s}ca^{1}$ and CNS Size

Independently of $spz^{2}$, $ru^{1}h^{1}th^{1}st^{1}cu^{1}sr^{1}e^{s}ca^{1}$ was smaller in brain and VNC areas than *yw* (Table 5.3, Figure 5.2). The mean VNC length of $ca^{1}$ was shorter to that of *yw,* but not signficantly (Games-Howell test, p = 0.438). Having addressed that $ru^{1}h^{1}th^{1}st^{1}cu^{1}sr^{1}e^{s}ca^{1}$ reduced the mean brain and VNC areas compared to *yw* by ~23% and ~10%, respectively, and that $spz^{2}ca^{1}$ reduced the mean brain and VNC areas compared to *yw* by ~60% and ~17%, respectively, the hypothesis of both genes interacting with each other and affecting CNS size development became more compelling.

#### 5.2.2.3 Genotype $spz^{2}ca^{+}$ and CNS Size

The mean brain and VNC areas of $spz^{2}ca^{+}$*.33* and $spz^{2}ca^{+}$*.56* were not significantly different

| Fly Line | Genotype $spz^2$ $ca^+$? (Yes/No) | SI of Non-Tubby Larvae Reaching Pupal Stages | Observations on Flies Eclosing from Non-Tubby Pupal Cases |
|---|---|---|---|
| 3 | No | 0.31 | One was found dead mid-eclosion. Some were found dead with wings remaining folded. Unbalanced flies cannot right themselves to stand after falling on their backs. |
| 20 | No | 0.33 | Some were found dead with wings remaining folded. |
| 25 | No | 0.41 | |
| 29 | No | 0.00 | |
| 31 | No | 0.41 | Unbalanced flies cannot right themselves to stand after falling on their backs. |
| 33 | Yes | 0.26 | |
| 44 | No | 0.30 | |
| 45 | No | 0.21 | |
| 48 | No | 0.22 | |
| 51 | No | 0.29 | |
| 52 | No | 0.24 | |
| 56 | Yes | 0.21 | Unbalanced flies cannot right themselves to stand after falling on their backs with the exception of one. That fly could stand after being pushed over by a paintbrush but it could not fly. |
| 72 | No | 0.27 | |
| 74 | No | 0.21 | |
| 78 | No | 0.32 | |

Table 5.2 Fly lines screened for $spz^2ca^+$. During screening, SI was recorded. Locomotion and life span defects were noted for fly lines 3, 20, 31 and 56.

| | Brain Area | | | VNC Area | | | VNC Length | | |
|---|---|---|---|---|---|---|---|---|---|
| Genotype | n | Mean ($x10^5\mu m^2$) | SD ($x10^5\mu m^2$) | n | Mean ($x10^4\mu m^2$) | SD ($x10^4\mu m^2$). | n | Mean (μm) | SD (μm) |
| *yw* | 25 | 1.70 | ±0.23 | 25 | 7.0 | ±0.8 | 25 | 372 | ±25 |
| $spz^2ca^1$ | 15 | 0.68 | ±0.13 | 15 | 5.8 | ±0.6 | 15 | 333 | ±18 |
| $ru^1h^1th^1st^1cu^1sr^1e^sca^1$ | 19 | 1.31 | ±0.15 | 16 | 6.3 | ±0.5 | 16 | 360 | ±22 |
| $spz^2ca^+.33$ | 13 | 0.74 | ±0.10 | 16 | 6.5 | ±1.0 | 16 | 363 | ±38 |
| $spz^2ca^+.56$ | 21 | 0.78 | ±0.14 | 22 | 6.1 | ±0.7 | 22 | 325 | ±23 |

Table 5.3 Brain and VNC size quantification for genotypes *yw*, $spz^2ca^1$, $ru^1h^1th^1st^1cu^1sr^1e^sca^1$, $spz^2ca^+.33$ and $spz^2ca^+.56$.

**Figure 5.2** Brain and VNC size characteristics for genotypes *yw*, *spz²ca¹*, *ru¹h¹Diap¹st¹cu¹sr¹ e^s ca¹*, *spz²ca⁺.33* and *spz²ca⁺.56*. **(A)** Representative mounted CNS images acquired with phase contrast using Zeiss Axioplan 2. Scale bars, 100µm. **(B)** Markers representing brain and VNC areas of individual larvae. Each blue diamond marker represents a *yw* individual (n=25). Red squares, *spz²ca¹* (n=15). Green dashes, *ru¹h¹Diap¹st¹cu¹sr¹e^s ca¹* (n=19). Purple crosses, *spz²ca⁺.33* (n=13). Light blue pluses, *spz²ca⁺.56* (n=21). **(C)** Markers representing VNC areas and lengths of individual larvae. Blue diamonds, *yw* (n=25). Red squares, *spz²ca¹* (n=15). Green dashes, *ru¹h¹Diap¹st¹cu¹sr¹e^s ca¹* (n=19). Purple crosses, *spz²ca⁺.33* (n=13). Light blue pluses, *spz²ca⁺.56* (n=21). **(D)** Boxplots showing ranges and outliers for brain area, VNC area and VNC length. Genotypes plotted for each size variables: *yw*, *spz²ca¹, ru¹h¹Diap¹ st¹cu¹sr¹e^s ca¹*, *spz²ca⁺.33* and *spz²ca⁺.56*. **(E)** Bar charts showing mean brain area, mean VNC area and mean VNC length. Genotypes plotted for each mean size variables: *yw*, *spz²ca¹, ru¹ h¹Diap¹st¹cu¹sr¹e^s ca¹*, *spz²ca⁺.33* and *spz²ca⁺.56*. Brain area statistics: Levene's statistic=4.0, $p<0.05$; Welch ANOVA $F(4,42.4)=125.0$, $p<0.001$. VNC area: Levene's statistic=3.2, $p<0.05$; Welch ANOVA $F(4,42.1)=7.2$, $p<0.001$. VNC length: Levene's statistic=4.4, $p<0.05$; Welch ANOVA $F(4,41.8)=14.7$, $p<0.001$.

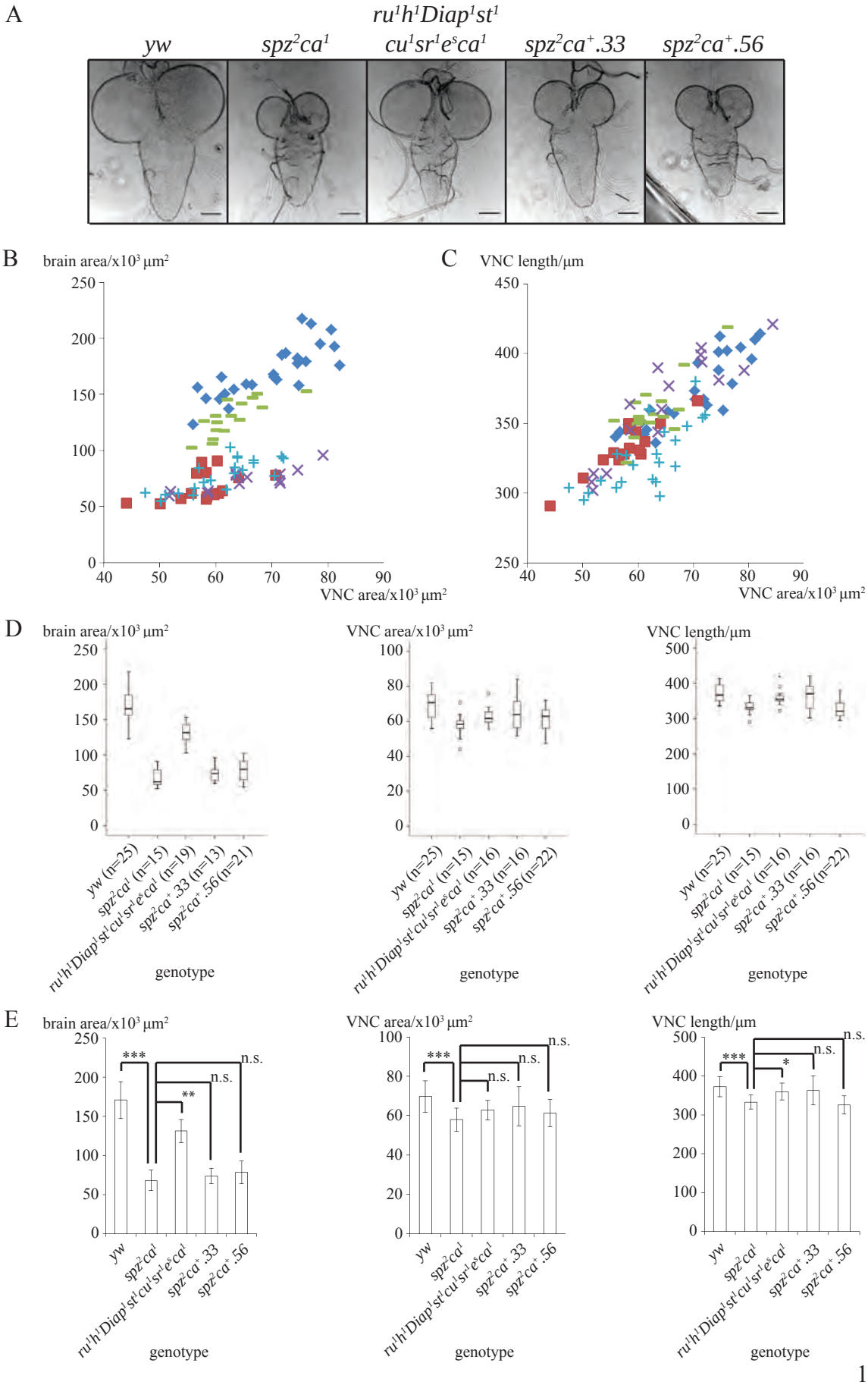
A
ru¹h¹Diap¹st¹
yw
spz²ca¹
cu¹sr¹e^sca¹
spz²ca⁺.33
spz²ca⁺.56
B
brain area/x10³ µm²
VNC area/x10³ µm²
C
VNC length/µm
VNC area/x10³ µm²
D
brain area/x10³ µm²
VNC area/x10³ µm²
VNC length/µm
yw (n=25)
spz²ca¹ (n=15)
ru¹h¹Diap¹st¹cu¹sr¹e^sca¹ (n=19)
spz²ca⁺.33 (n=13)
spz²ca⁺.56 (n=21)
yw (n=25)
spz²ca¹ (n=15)
ru¹h¹Diap¹st¹cu¹sr¹e^sca¹ (n=16)
spz²ca⁺.33 (n=16)
spz²ca⁺.56 (n=22)
yw (n=25)
spz²ca¹ (n=15)
ru¹h¹Diap¹st¹cu¹sr¹e^sca¹ (n=16)
spz²ca⁺.33 (n=16)
spz²ca⁺.56 (n=22)
genotype
E
brain area/x10³ µm²
VNC area/x10³ µm²
VNC length/µm
***
**
*
n.s.
yw
spz²ca¹
ru¹h¹Diap¹st¹cu¹sr¹e^sca¹
spz²ca⁺.33
spz²ca⁺.56
genotype

from each other (Table 5.3, Figure 5.2). However, their mean lengths were significantly different (Table 5.3, Figure 5.2). *Spz$^{2}$ca$^{+}$.33* and *spz$^{2}$ca$^{+}$.56* each were not significantly different to *spz$^{2}$ca$^{1}$* in terms of brain area, VNC area and VNC length (Table 5.3, Figure 5.2).

#### 5.2.2.4 Genotype *spz$^{2}$ca$^{+}$* and SI

Upon recombining *spz$^{2}$ca$^{1}$* with *spz$^{2}$ca$^{+}$*, the viability of the latter animals reaching into pupal stages improved (Figure 5.3; $\chi^2(2)=24.0$, $p<0.001$). The survival index (SI) for *spz$^{2}$ca$^{1}$* larvae reaching pupation is 0.14, and both *spz$^{2}$ca$^{+}$*.33 (SI=0.21) and *spz$^{2}$ca$^{+}$*.56 (SI=0.26) have significantly higher SIs (SI=0.21, $\chi^2(1)=24.2$, Bonferroni post hoc $p<0.001$; SI=0.26, $\chi^2(1)=10.6$, Bonferroni post hoc $p<0.005$), although each SI quoted did not reflect rescue to wild-type numbers.

### 5.2.3 Rescue of SI and CNS Size using *elavGAL4*

*Spz$^{2}$elav-GAL4/TM6B* had an SI of 0.25 (Figure 5.4). Overexpressing *actSpz* increased viability (SI=0.43, $\chi^2(1)=14.1$, $p<0.001$), but not to expected wild-type level ($\chi^2(1) = 52.4$, $p<0.001$). The overexpression of active Toll receptors, *Toll$^{10bB}$*, *Toll6$^{CY}$* and *Toll7$^{CY}$*, also increased viability (SI=0.75, 0.67 and 0.47, respectively). The best of the three receptors in improving viability of *spz$^{2}$* animals is *Toll$^{10bB}$* ($\chi^2(1)=134.5$, $p<0.001$) although not to the extent of wild-type levels ($\chi^2(1)=31.1$, $p<0.001$). Viability improvement from *Toll$^{10bB}$* was comparable to that from *Toll6$^{CY}$* ($\chi^2(1)=2.0$, $p=0.156$) but not from *Toll7$^{CY}$* ($\chi^2(1)=21.1$, $p<0.001$). When *p35* protein was overexpressed, viability of *spz$^{2}$* improved (SI=0.47), similar

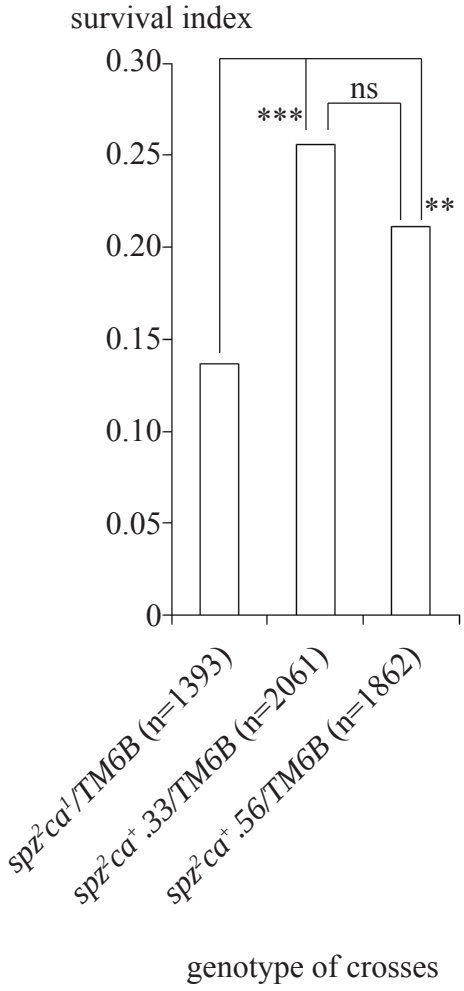


**Figure 5.3** Survival indexes of *spz*$^{2}$ allele when accompanied by wild-type *claret* (*ca*$^{+}$).

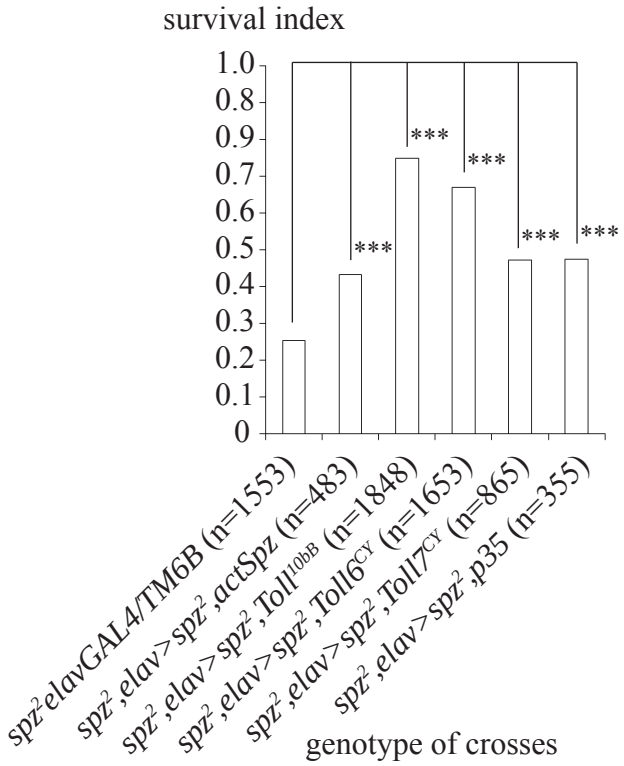


**Figure 5.4** Survival index of *spz*$^{2}$ larvae when neurons overexpressed activated form of Spz (*UAS-actSpz(2)*), activated Toll (*UAS-Toll*$^{10bB}$), activated Toll6 (*UAS-Toll6*$^{CY}$), activated Toll7 (*UAS-Toll7*$^{CY}$) and caspase inhibitor p35 (*UAS-p35(2)*).

to levels as a result of overexpressing *actSpz(2)* ($\chi^2(1)=0.248$, p=0.618) or *Toll7*$^{CY}$ ($\chi^2(1)=0.248$, p=0.974).

Whilst viability of *spz*$^2$ animals could be partially rescued by overexpression of *Toll*$^{10bB}$, *Toll6*$^{CY}$ and *p35*, the brain areas were not (Table 5.4, Figure 5.5). In the case of overexpressing *Toll7*$^{CY}$, the brain size decreased significantly (Table 5.4, Figure 5.5). When there was only a single allele of *spz*$^2$ in genotype *spz*$^2$*elav-GAL4/+*, the mean brain size was smaller than in *yw* (Games Howell post hoc, p<0.005), and was doubled that of *spz*$^2$*ca*$^1$ (Table 5.4, Figure 5.5). However, when comparing VNC, those of *spz*$^2$*elav-GAL4/+* and *spz*$^2$*ca*$^1$ were similar to each other (Table 5.4, Figure 5.5). Mean VNC area of *spz*$^2$*elav-GAL4/+* was smaller than *yw* (Bonferroni post hoc, p<0.005) but lengths of both genotypes were comparable (Bonferroni post hoc, p=0.171). Increasing sampling of *spz*$^2$*elav-GAL4/+* could resolve the issue.

| | Brain Area | | | VNC Area | | | VNC Length | | |
|---|---|---|---|---|---|---|---|---|---|
| Genotype | n | Mean (x$10^5$ μm$^2$) | SD (x$10^5$ μm$^2$) | n | Mean (x$10^4$ μm$^2$) | n | N | Mean (μm) | SD (μm) |
| *yw* | 25 | 1.70 | ±0.23 | 25 | 7.0 | ±0.8 | 25 | 372 | ±25 |
| *spz*$^2$*ca*$^1$ | 15 | 0.68 | ±0.13 | 15 | 5.8 | ±0.6 | 15 | 333 | ±18 |
| *spz*$^2$*elavGAL4/+* | 11 | 1.39 | ±0.16 | 12 | 6.0 | ±0.6 | 12 | 349 | ±25 |
| *spz*$^2$*,elav>spz*$^2$*,Toll*$^{10bB}$ | 6 | 0.72 | ±0.07 | 7 | 7.0 | ±0.7 | 7 | 386 | ±37 |
| *spz*$^2$*,elav>spz*$^2$*,Toll6*$^{CY}$ | 8 | 0.67 | ±0.07 | 8 | 7.0 | ±0.6 | 8 | 381 | ±19 |
| *spz*$^2$*,elav>spz*$^2$*,Toll7*$^{CY}$ | 5 | 0.54 | ±0.04 | 5 | 6.0 | ±0.5 | 5 | 362 | ±17 |
| *spz*$^2$*,elav>spz*$^2$*,p35* | 3 | 0.81 | ±0.13 | 5 | 7.7 | ±0.7 | 5 | 450 | ±29 |

Table 5.4 CNS size rescue of *spz*$^2$ mutant background using various *UAS* lines overexpressed under *elavGAL4* driver.

Even though brain areas were not rescued with pan-neuronal overexpression of *Toll*$^{10bB}$, *Toll6*$^{CY}$ and *p35*, VNC sizes of *spz*$^2$*ca*$^1$ were rescued (Table 5.4, Figure 5.5). Rescues by *Toll*$^{10bB}$ and *Toll6*$^{CY}$ were to the full extent (Table 5.4, Figure 5.5). With *p35*, mean VNC area was higher than *yw* but not statistically significant. However, the mean VNC length was

**Figure 5.5** CNS size rescue of *spz*$^{2}$ mutant background using various UAS lines overexpressed under *elav-GAL4* driver. **(A)** Representative mounted CNS images acquired with phase contrast using Zeiss Axioplan 2. Scale bars, 100μm. **(B)** Markers representing brain and VNC areas of individual larvae. Each blue diamond marker represents a *yw* individual (n=25). Red squares, *spz*$^{2}$ (n=15). Green triangles, *spz*$^{2}$*elav-GAL4/+* (n=11). Purple circles, *spz*$^{2}$*,elav>spz*$^{2}$*,Toll10*$^{bB}$ (n=6). Light blue crosses, *spz*$^{2}$*,elav>spz*$^{2}$*,Toll6*$^{CY}$ (n=8). Black dashes, *spz*$^{2}$*,elav>spz*$^{2}$*,Toll7*$^{CY}$ (n=5). Orange pluses, *spz*$^{2}$*,elav>spz*$^{2}$*,p35* (n=3) **(C)** Markers representing VNC areas and lengths of individual larvae. Blue diamonds, *yw* (n= 5). Red squares, *spz*$^{2}$ (n=15). Green triangles, *spz*$^{2}$*-elav-GAL4/+* (n=12). Purple circles, *spz*$^{2}$*,elav> spz*$^{2}$*,Toll10*$^{bB}$ (n=7). Light blue crosses, *spz*$^{2}$*,elav>spz*$^{2}$*,Toll6*$^{CY}$ (n=8). Black dashes, *spz*$^{2}$*,elav> spz*$^{2}$*,Toll7*$^{CY}$ (n=5). Orange pluses, *spz*$^{2}$*,elav>spz*$^{2}$*,p35* (n=5) **(D)** Boxplots showing ranges and outliers for brain area, VNC area and VNC length. **(E)** Bar charts showing mean brain area, mean VNC area and mean VNC length. Brain area statistics: Levene's statistic=4.4, $p<0.001$; Welch ANOVA $F(6,16.253)=102.0$, $p<0.001$. VNC area: Levene's statistic=1.2, $p = 0.307$; one-way ANOVA $F(6,70)=10.7$, $p<0.001$. VNC length, Levene's statistic=1.4, $p=0.233$; one-way ANOVA $F(6,70)=16.9$, $p<0.001$.

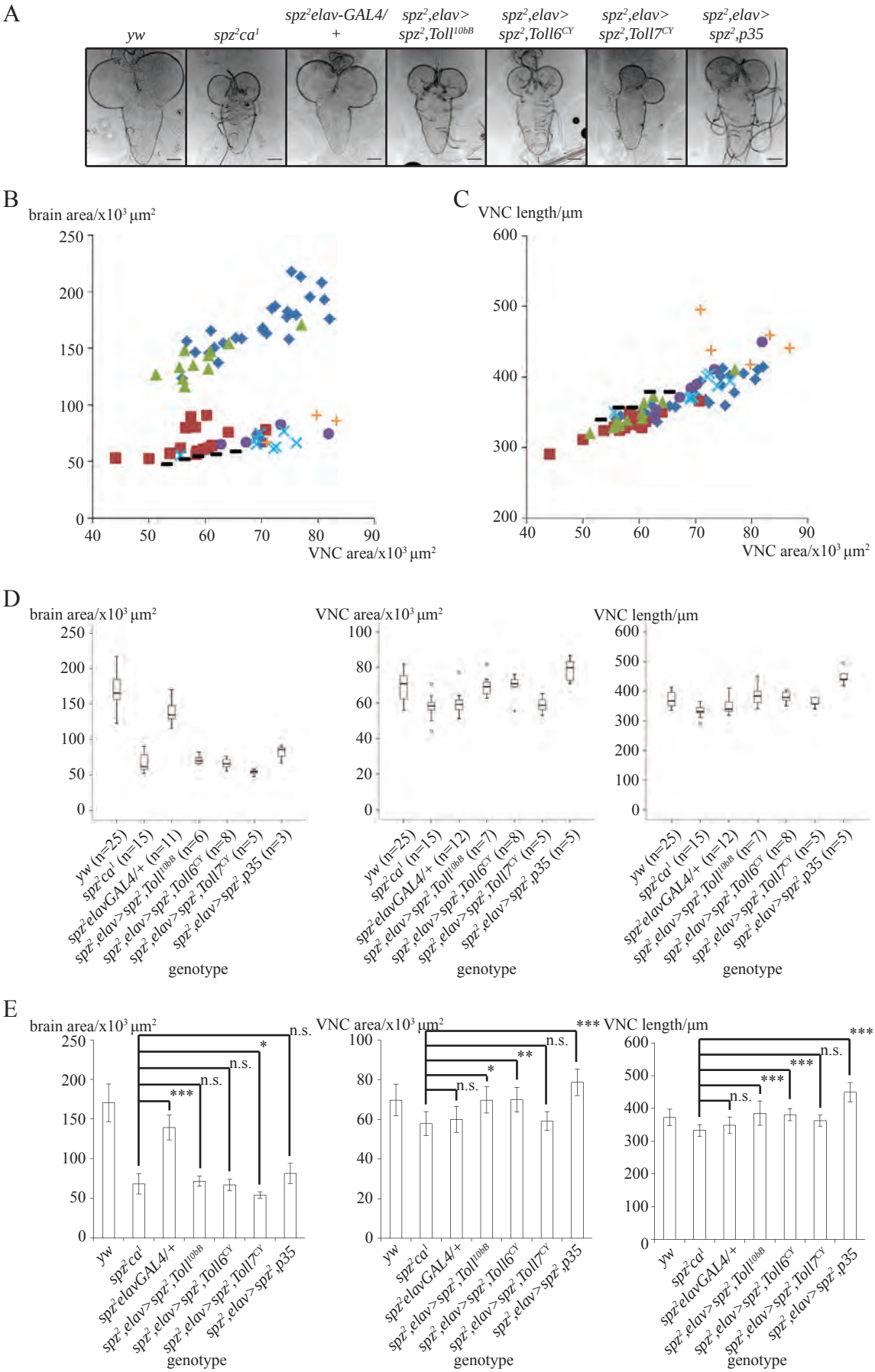
A
yw
spz2ca1
spz2elav-GAL4/ +
spz2,elav> spz2,Toll10bB
spz2,elav> spz2,Toll6CY
spz2,elav> spz2,Toll7CY
spz2,elav> spz2,p35
B
brain area/x10³ µm²
VNC area/x10³ µm²
C
VNC length/µm
VNC area/x10³ µm²
D
brain area/x10³ µm²
VNC area/x10³ µm²
VNC length/µm
yw (n=25)
spz2ca1 (n=15)
spz2elavGAL4/+ (n=11)
spz2,elav>spz2,Toll10bB (n=6)
spz2,elav>spz2,Toll6CY (n=8)
spz2,elav>spz2,Toll7CY (n=5)
spz2,elav>spz2,p35 (n=3)
yw (n=25)
spz2ca1 (n=15)
spz2elavGAL4/+ (n=12)
spz2,elav>spz2,Toll10bB (n=7)
spz2,elav>spz2,Toll6CY (n=8)
spz2,elav>spz2,Toll7CY (n=5)
spz2,elav>spz2,p35 (n=5)
yw (n=25)
spz2ca1 (n=15)
spz2elavGAL4/+ (n=12)
spz2,elav>spz2,Toll10bB (n=7)
spz2,elav>spz2,Toll6CY (n=8)
spz2,elav>spz2,Toll7CY (n=5)
spz2,elav>spz2,p35 (n=5)
genotype
genotype
genotype
E
brain area/x10³ µm²
VNC area/x10³ µm²
*** VNC length/µm
n.s.
*
**
***
yw
spz2ca1
spz2elavGAL4/+
spz2,elav>spz2,Toll10B
spz2,elav>spz2,Toll6CY
spz2,elav>spz2,Toll7CY
spz2,elav>spz2,p35
genotype
genotype
genotype

significantly longer. Undoubtedly, increasing sampling would clear the issue on whether VNC size was rescued by *p35* to *yw* level or beyond. Nonetheless, *p35* rescues $spz^2$ VNC size. The rescue of VNC size to *yw* levels by pan-neuronal overexpression of $Toll^{10b}$ and $Toll6^{CY}$ (Figure 5.5) correlated with the results in which the viability of $spz^2$ animals reaching pupal stages were highest with overexpression of these two receptors (Figure 5.4).

The controls $spz^2$*elav-GAL4/+* and *elav-GAL4/+* were similar to each other in terms of CNS size (Table 5.5; Figure 5.6). When $Toll^{10b}$ was overexpressed under *elavGAL4*, CNS size was similar to control *elavGAL4/+*, indicating no gross whole organ size effect (Table 5.5; Figure 5.6). The mean VNC sizes in $spz^2$,*elav>*$spz^2$,$Toll^{10bB}$ and *elav>*$Toll^{10bB}$ had negligible differences, indicating full rescue without perturbation of VNC organ size (Table 5.5; Figure 5.6).

| | Brain Area | | | VNC Area | | | VNC Length | | |
|---|---|---|---|---|---|---|---|---|---|
| Genotype | n | Mean ($x10^5$ $\mu m^2$) | SD ($x10^5$ $\mu m^2$) | n | Mean ($x10^4$ $\mu m^2$) | SD ($x10^4$ $\mu m^2$) | n | Mean (μm) | SD (μm) |
| *yw* | 25 | 1.70 | ±0.23 | 25 | 7.0 | ±0.8 | 25 | 372 | ±25 |
| $spz^2ca^1$ | 15 | 0.68 | ±0.13 | 15 | 5.8 | ±0.6 | 15 | 333 | ±18 |
| $spz^2$*elav-GAL4/+* | 11 | 1.39 | ±0.16 | 12 | 6.0 | ±0.6 | 12 | 349 | ±25 |
| $spz^2$,*elav>*$spz^2$,$Toll^{10bB}$ | 6 | 0.72 | ±0.07 | 7 | 7.0 | ±0.7 | 7 | 386 | ±37 |
| *elav-GAL4/+* | 11 | 1.25 | ±0.21 | 11 | 6.0 | ±0.7 | 11 | 359 | ±19 |
| *elav>*$Toll^{10bB}$ | 10 | 1.24 | ±0.09 | 15 | 6.7 | ±0.4 | 15 | 375 | ±23 |

Table 5.5 CNS sizes for *elav>*$Toll^{10bB}$ with and without the background $spz^2$.

### 5.2.4 Rescue of SI CNS Size using *repoGAL4*

The stocks $spz^2ca^1$/TM6B and $spz^2$*repo-GAL4/TM6B* were semi- (SI=0.15) and fully lethal (SI=0), respectively. With *repo-GAL4* overexpression of *actSpz(2)*, $Toll^{10bB}$, $Toll6^{CY}$ and

**Figure 5.6** Comparing CNS size for *elav>Toll$^{10bB}$* with and without the background *spz$^{2}$*. **(A)** Representative mounted CNS images acquired with phase contrast using Zeiss Axioplan 2 except for genotype *elav>Toll$^{10bB}$* for which acquisition were from Zeiss LSM710. Scale bars, 100µm. **(B)** Markers representing brain and VNC areas of individual larvae. Each blue diamond marker represents a *yw* individual (n=25). Red squares, *spz$^{2}$* (n=15). Green triangles, *spz$^{2}$elav-GAL4/+* (n=11). Purple circles, *spz$^{2}$,elav>spz$^{2}$,Toll$^{10bB}$* (n=6). Black crosses, *elav-GAL4/+* (n=11). Orange dashes, *elav>Toll$^{10b}$* (n=10). **(C)** Markers representing VNC areas and lengths of individual larvae. Blue diamonds, *yw* (n=25). Red squares, *spz$^{2}$* (n=15). Green triangles, *spz$^{2}$elav-GAL4/+* (n=12). Purple circles, *spz$^{2}$,elav>spz$^{2}$,Toll$^{10bB}$* (n=7). Black crosses, *elav-GAL4/+* (n = 11). Orange dashes, *elav>Toll$^{10b}$* (n=15). **(D)** Boxplots showing ranges and outliers for brain area, VNC area and VNC length. **(E)** Bar charts showing mean brain area (dotted bars), mean VNC area (diagonally-lined bars) and mean VNC length (empty white bars). Brain area statistics: Levene's statistic=3.8, $p<0.001$; Welch ANOVA $F(5,28.5)=105.6$, $p<0.001$. VNC area: Levene's statistic=1.9, $p=0.108$; one-way ANOVA $F(5,79)=9.8$, $p<0.001$. VNC length, Levene's statistic=8.2, $p=0.178$; one-way ANOVA $F(5,79)=17.1$, $p<0.001$.

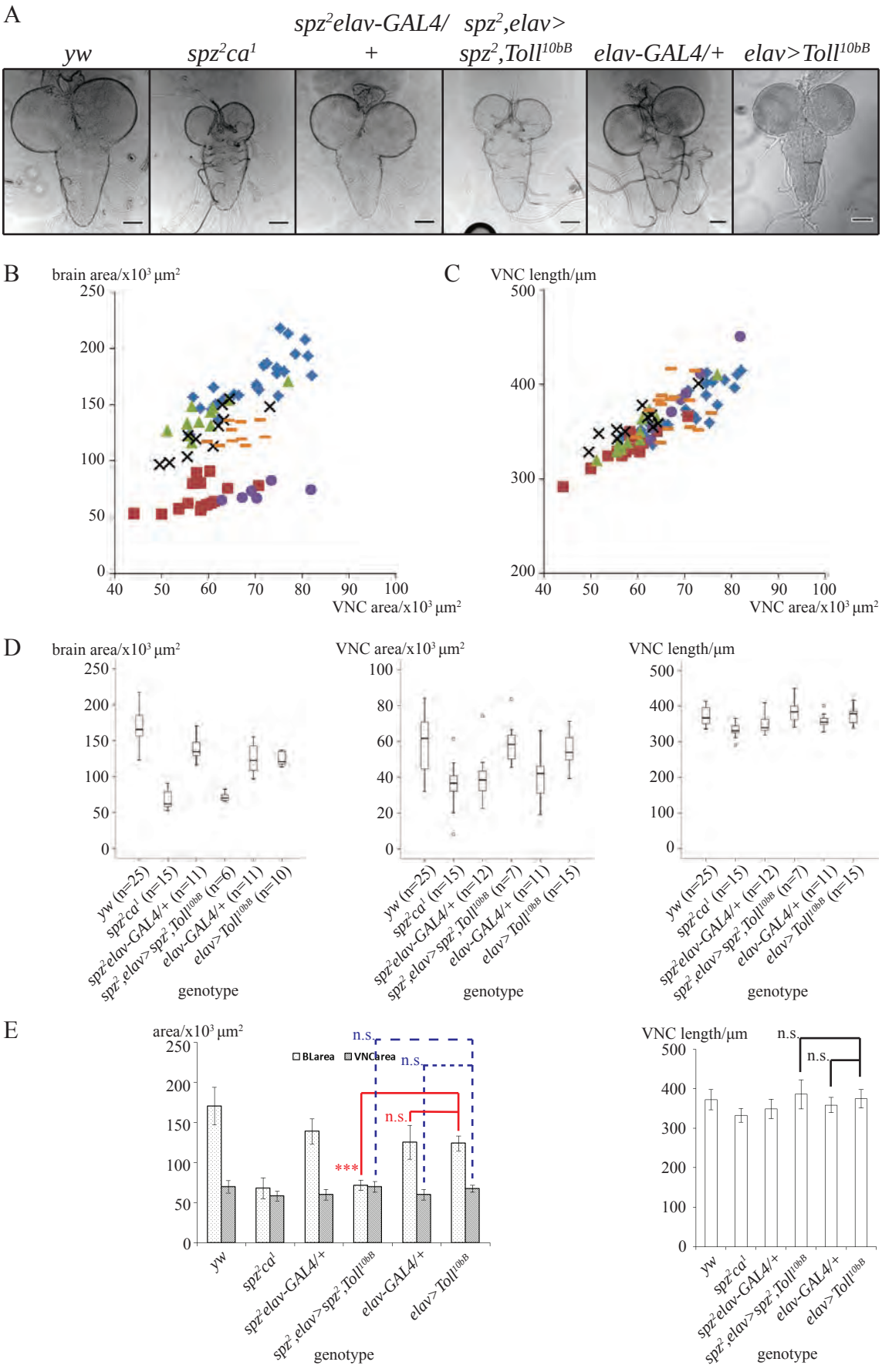
A
yw
spz2ca1
spz2elav-GAL4/ +
spz2,elav> spz2,Toll10bB
elav-GAL4/+
elav>Toll10bB
B
brain area/x10³ µm²
VNC area/x10³ µm²
C
VNC length/µm
VNC area/x10³ µm²
D
brain area/x10³ µm²
VNC area/x10³ µm²
VNC length/µm
yw (n=25)
spz2ca1 (n=15)
spz2elav-GAL4/+ (n=11)
spz2,elav>spz2,Toll10bB (n=6)
elav-GAL4/+ (n=11)
elav>Toll10bB (n=10)
yw (n=25)
spz2ca1 (n=15)
spz2elav-GAL4/+ (n=12)
spz2,elav>spz2,Toll10bB (n=7)
elav-GAL4/+ (n=11)
elav>Toll10bB (n=15)
genotype
E
area/x10³ µm²
BLarea
VNCarea
n.s.
***
VNC length/µm
yw
spz2ca1
spz2elav-GAL4/+
spz2,elav>spz2,Toll10bB
elav-GAL4/+
elav>Toll10bB
genotype

*Toll7*$^{CY}$, viability of *spz*$^{2}$ animals reaching pupal stages across all genotypes improved (Table 5.6, Figure 5.7; $\chi^2(4)=383.7$, $p<0.001$). *Toll6*$^{CY}$ being overexpressed was the best at improving viability (SI=0.74) and this was comparable with glial overexpression of *actSpz(2)* (SI=0.64; $\chi^2(1)=1.3$, $p=0.253$) but not to wild-type levels ($\chi^2(1)=16.5$, $p<0.001$). Overexpressing *Toll*$^{10bB}$ and *Toll7*$^{CY}$ improved viability at similar levels (Table 5.6; $\chi^2(1) = 0.2$, $p = 0.641$). While the overexpression of *Toll6*$^{CY}$ and *Toll7*$^{CY}$ under both *elav-* and *repo-GAL4* provided similar viability to *spz*$^{2}$ mutants, this was not the case for *actSpz(2)* and *Toll*$^{10bB}$. It was better for *spz*$^{2}$ viability with *repo>actSpz(2)* than *elav>actSpz(2)*, and vice versa for *Toll*$^{10bB}$ (Table 5.6).

| UAS Construct Overexpressed | SI of *spz*$^{2}$ | | $\chi^2$ value | P value |
|---|---|---|---|---|
| | Overexpression using *elav-GAL4* | Overexpression using *repo-GAL4* | | |
| *actSpz(2)* | 0.43 | 0.64 | 5.8 | 0.016 |
| *Toll*$^{10bB}$ | 0.75 | 0.46 | 14.0 | 0.000 |
| *Toll6*$^{CY}$ | 0.67 | 0.74 | 1.0 | 0.309 |
| *Toll7*$^{CY}$ | 0.47 | 0.43 | 0.8 | 0.381 |

Table 5.6 Comparing SI rescues of *spz*$^{2}$ using neuronal and glial drivers.

| | Brain Area | | | VNC Area | | | VNC Length | | |
|---|---|---|---|---|---|---|---|---|---|
| Genotype | n | Mean (x$10^5$ μm$^2$) | SD (x$10^5$ μm$^2$) | n | Mean (x$10^4$ μm$^2$) | SD (x$10^4$ μm$^2$) | n | Mean (μm) | SD (μm) |
| *yw* | 25 | 1.70 | ±0.23 | 25 | 7.0 | ±0.8 | 25 | 372 | ±25 |
| *spz*$^{2}$*ca*$^{1}$ | 15 | 0.68 | ±0.13 | 15 | 5.8 | ±0.6 | 15 | 333 | ±18 |
| *spz*$^{2}$*repoGAL4/+* | 11 | 1.63 | ±0.18 | 12 | 6.9 | ±0.6 | 12 | 382 | ±20 |
| *spz*$^{2}$*,repo>spz*$^{2}$*,Toll*$^{10bB}$ | 10 | 0.70 | ±0.09 | 11 | 8.4 | ±0.7 | 11 | 583 | ±49 |
| *spz*$^{2}$*,repo>spz*$^{2}$*,Toll6*$^{CY}$ | 1 | 0.45 | - | 1 | 5.6 | - | 1 | 377 | - |
| *spz*$^{2}$*,repo>spz*$^{2}$*,Toll7*$^{CY}$ | 2 | 0.63 | ±0.04 | 3 | 6.6 | ±0.5 | 3 | 397 | ±19 |

Table 5.7 CNS size rescue of *spz*$^{2}$ mutant background using various *UAS* lines overexpressed under *repo-GAL4* driver.

The *repo-GAL4* overexpression of *Toll*$^{10bB}$, *Toll6*$^{CY}$ and *Toll7*$^{CY}$ was insufficient to rescue brain areas of *spz*$^{2}$ mutant backgrounds (Figure 5.8). When there was only a single dose of *spz*$^{2}$ in genotype *spz*$^{2}$*repo-GAL4/+*, unlike in *spz*$^{2}$*elav-GAL4/+*, mean CNS sizes were alike to

*yw*'s (Table 5.7). With respect to the VNC, due to low sampling numbers of *spz*$^{2}$,*repo>spz*$^{2}$,*Toll6*$^{CY}$ (n=1) and *spz*$^{2}$,*repo>spz*$^{2}$,*Toll7*$^{CY}$ (n=3), whether or not VNC sizes were rescued remained inconclusive. With the overexpression of *Toll*$^{10bB}$, mean VNC area and length were higher than rescued levels (Table 5.7, Figure 5.8).

As with the control *elav-GAL4/+*, the control *yw* differs from the control *repo-GAL4/+* in brain and VNC areas (Table 5.8, Figure 5.9). When compared to the more appropriate control, that is *repo-GAL4/+*, *repo>Toll*$^{10bB}$ did not change brain area (Table 5.8, Figure 5.9). However, an increase in gross size was seen in the VNC (Table 5.8, Figure 5.9). Additionally, while overexpressing *Toll*$^{10bB}$ constitutively in *spz*$^{2}$ resulted in mean VNC area larger than *yw*, this mean was comparable to that in *repo>Toll*$^{10bB}$ (Table 5.8, Figure 5.9). However, the mean VNC length in *spz*$^{2}$,*repo>spz*$^{2}$,*Toll*$^{10bB}$ still surpassed the mean length in *repo>Toll*$^{10bB}$ significantly (Table 5.8, Figure 5.9), suggesting an interaction between *spz*$^{2}$ and *repo>Toll*$^{10bB}$ to deform gross morphology further.

| | Brain Area | | | VNC Area | | | VNC Length | | |
|---|---|---|---|---|---|---|---|---|---|
| Genotype | n | Mean (x$10^5$ μm$^2$) | SD (x$10^5$ μm$^2$) | n | Mean (x$10^4$ μm$^2$) | SD (x$10^4$ μm$^2$) | n | Mean (μm) | SD (μm) |
| *yw* | 25 | 1.70 | ±0.23 | 25 | 7.0 | ±8 | 25 | 372 | ±25 |
| *spz*$^{2}$*ca*$^{1}$ | 15 | 0.68 | ±0.13 | 15 | 5.8 | ±6 | 15 | 333 | ±18 |
| *spz*$^{2}$*repoGAL4/+* | 11 | 1.63 | ±0.18 | 12 | 6.9 | ±6 | 12 | 382 | ±20 |
| *spz*$^{2}$,*repo>spz*$^{2}$,*Toll*$^{10bB}$ | 10 | 0.70 | ±0.09 | 11 | 8.4 | ±7 | 11 | 583 | ±49 |
| *repoGAL4/+* | 12 | 0.45 | ±0.12 | 12 | 5.9 | ±2 | 12 | 364 | ±21 |
| *repo>Toll*$^{10bB}$ | 12 | 0.63 | ±0.11 | 12 | 7.8 | ±5 | 12 | 516 | ±33 |

Table 5.8 CNS sizes for *repo>Toll*$^{10bB}$ with and without the background *spz*$^{2}$.

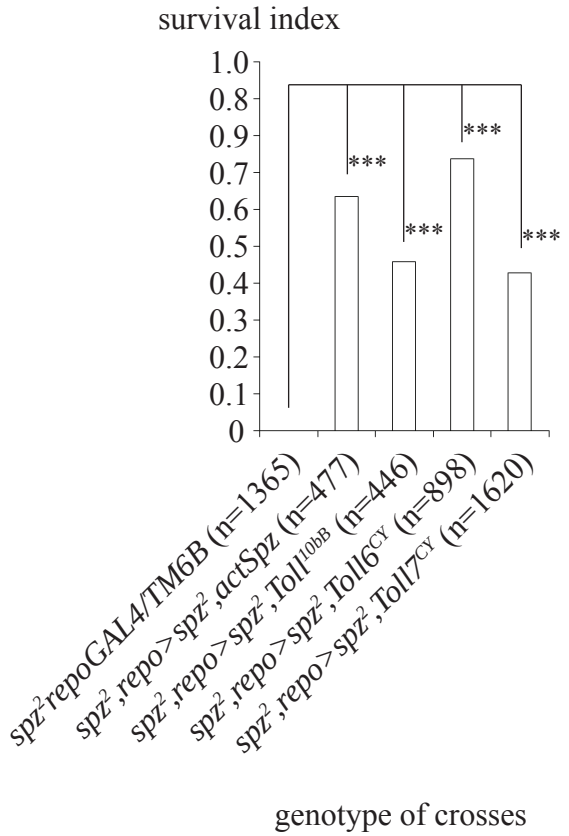


**Figure 5.7** Survival index of *spz*$^{2}$ larvae when their glia overexpressed activated form of Spz (*UAS-actSpz(2)*), activated Toll (*UAS-Toll*$^{10bB}$), activated Toll6 (*UAS-Toll6*$^{CY}$), and activated Toll7 (*UAS-Toll7*$^{CY}$).

**Figure 5.8** CNS size rescue of *spz*$^{2}$ mutant background using various UAS lines overexpressed under *repo-GAL4* driver. **(A)** Representative mounted CNS images acquired with phase contrast using Zeiss Axioplan 2. Scale bars, 100μm. **(B)** Markers representing brain and VNC areas of individual larvae. Each blue diamond marker represents a *yw* individual (n=25). Red squares, *spz*$^{2}$ (n=15). Green triangles, *spz*$^{2}$*repo-GAL4/+* (n=11). Purple circles, *spz*$^{2}$*,repo>spz*$^{2}$*,Toll*$^{10bB}$ (n=10). Light blue crosses, *spz*$^{2}$*,repo>spz*$^{2}$*,Toll6*$^{CY}$ (n=1). Black dashes, *spz*$^{2}$*,repo>spz*$^{2}$*,Toll7*$^{CY}$ (n=2). **(C)** Markers representing VNC areas and lengths of individual larvae. Blue diamonds, *yw* (n=25). Red squares, *spz*$^{2}$ (n=15). Green triangles, *spz*$^{2}$*repo-GAL4/+* (n=12). Purple circles, *spz*$^{2}$*,repo>spz*$^{2}$*,Toll*$^{10bB}$ (n=11). Light blue crosses, s*pz*$^{2}$*,repo>spz*$^{2}$*,Toll6*$^{CY}$ (n=1). Black dashes, *spz*$^{2}$*,repo>spz*$^{2}$*,Toll7*$^{CY}$ (n=3). **(D)** Boxplots showing ranges and outliers for brain area, VNC area and VNC length. **(E)** Bar charts showing mean brain area, mean VNC area and mean VNC length. Brain area statistics: Levene's statistic=3.9, $p<0.05$; Welch ANOVA $F(3,27.8)=173.8$, $p<0.001$. VNC area: Levene's statistic=2.0, $p=0.120$; one-way ANOVA $F(3,59)=29.0$, $p<0.001$. VNC length, Levene's statistic=5.6, $p<0.005$; Welch ANOVA $F(3,26.4)=88.6$, $p<0.001$.

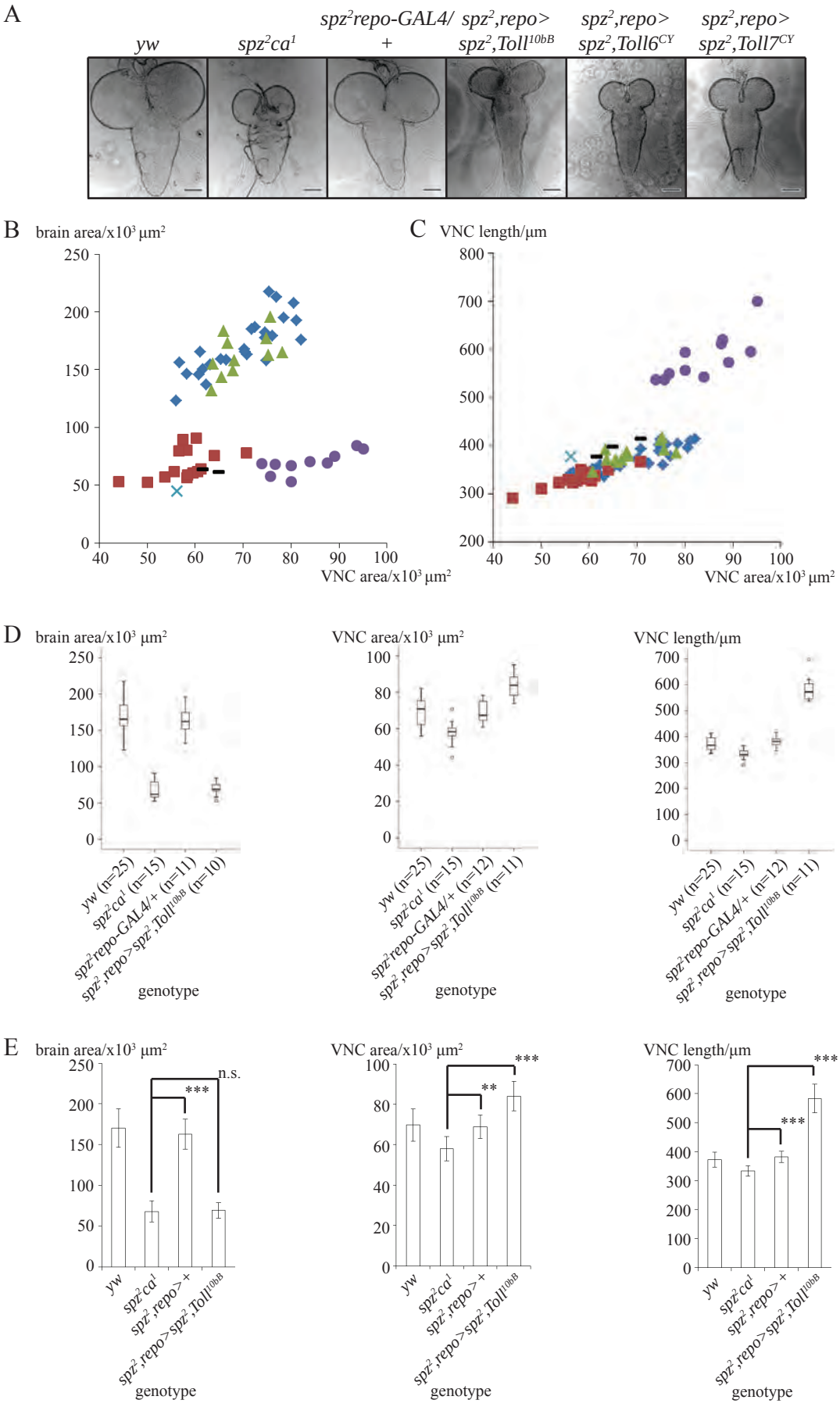
A
yw
spz2ca1
spz2repo-GAL4/ +
spz2,repo> spz2,Toll10bB
spz2,repo> spz2,Toll6CY
spz2,repo> spz2,Toll7CY
B
brain area/x10³ µm²
VNC area/x10³ µm²
C
VNC length/µm
VNC area/x10³ µm²
D
brain area/x10³ µm²
VNC area/x10³ µm²
VNC length/µm
yw (n=25)
spz2ca1 (n=15)
spz2repo-GAL4/+ (n=11)
spz2repo-GAL4/+ (n=12)
spz2,repo>spz2,Toll10B (n=10)
spz2,repo>spz2,Toll10B (n=11)
genotype
E
brain area/x10³ µm²
VNC area/x10³ µm²
VNC length/µm
n.s.
***
**
yw
spz2ca1
spz2,repo>+
spz2,repo>spz2,Toll10B
genotype

**Figure 5.9** Comparing CNS size for *repo>Toll$^{10bB}$* with and without the background *spz$^{2}$*. **(A)** Representative mounted CNS images acquired with phase contrast using Zeiss Axioplan 2 except for genotypes *repo-GAL4/+* and *repo>Toll$^{10bB}$* for which acquisition were from Zeiss LSM710. Scale bars, 100μm. **(B)** Markers representing brain and VNC areas of individual larvae. Each blue diamond marker represents a *yw* individual (n=25). Red squares, *spz$^{2}$* (n=15). Green triangles, *spz$^{2}$repo-GAL4/+* (n=11). Purple circles, *spz$^{2}$,repo>spz$^{2}$,Toll$^{10bB}$* (n=10). Black crosses, *repo-GAL4/+* (n=12). Orange dashes, *repo>Toll$^{10bB}$* (n=12). **(C)** Markers representing VNC areas and lengths of individual larvae. Blue diamonds, *yw* (n=25). Red squares, *spz$^{2}$* (n=15). Green triangles, *spz$^{2}$repo-GAL4/+* (n=12). Purple circles, *spz$^{2}$,repo>spz$^{2}$,Toll$^{10bB}$* (n=11). Black crosses, *repo-GAL4/+* (n= 12). Orange dashes, *repo>Toll$^{10bB}$* (n=12). **(D)** Boxplots showing ranges and outliers for brain area, VNC area and VNC length. **(E)** Bar charts showing mean brain area (dotted bars), mean VNC area (diagonally-lined bars) and mean VNC length (empty white bars). Brain area statistics: Levene's statistic =4.1, $p<0.005$; Welch ANOVA $F(5,33.7)=115.8$, $p<0.001$. VNC area: Levene's statistic=4.2, $p<0.005$; Welch ANOVA $F(5,33.8)=51.0$, $p<0.001$. VNC length, Levene's statistic=3.6, $p=0.005$; one-way ANOVA $F(5,81)=155.3$, $p<0.001$.

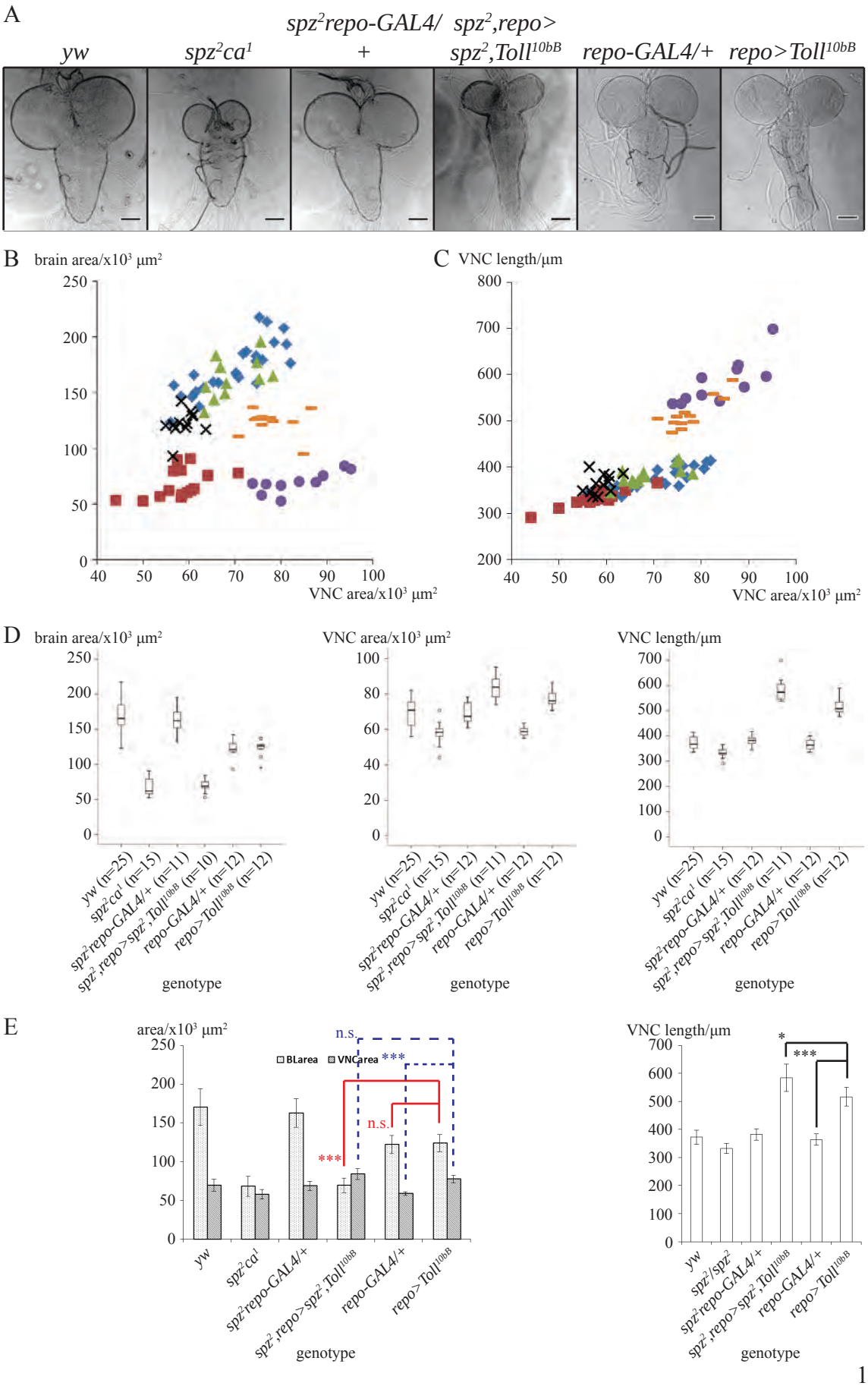
A
yw
spz2ca1
spz2repo-GAL4/ +
spz2,repo> spz2,Toll10bB
repo-GAL4/+
repo>Toll10bB
B
brain area/x10³ µm²
VNC area/x10³ µm²
C
VNC length/µm
VNC area/x10³ µm²
D
brain area/x10³ µm²
VNC area/x10³ µm²
VNC length/µm
yw (n=25)
spz2ca1 (n=15)
spz2repo-GAL4/+ (n=11)
spz2,repo>spz2,Toll10bB (n=10)
repo-GAL4/+ (n=12)
repo>Toll10bB (n=12)
spz2repo-GAL4/+ (n=12)
spz2,repo>spz2,Toll10bB (n=11)
genotype
E
area/x10³ µm²
BLarea
VNCarea
n.s.
***
n.s.
***
VNC length/µm
*
***
spz2/spz2
spz2repo-GAL4/+
spz2,repo>spz2,Toll10bB
repo-GAL4/+
repo>Toll10bB
genotype

### 5.2.5 Overexpressing Different Forms of Spz under *spzGAL4*

Neither Spz-CK nor Spz-FL had an effect on brain and VNC areas through *spzGAL4* (Table 5.9; Figure 5.10). VNC of *spz>Spz-FL* had the same mean length as the control while the mean VNC length amongst *spz>Spz-CK* was higher than those of the control *spz-GAL4/+* and *spz>Spz-FL* (Table 5.9; Figure 5.10).

| | Brain Area | | | VNC Area | | | VNC Length | | |
|---|---|---|---|---|---|---|---|---|---|
| Genotype | n | Mean ($x10^5$ $\mu m^2$) | SD ($x10^5$ $\mu m^2$) | n | Mean ($x10^4$ $\mu m^2$) | SD ($x10^4$ $\mu m^2$) | n | Mean (μm) | SD (μm) |
| *spz-GAL4* | 12 | 1.31 | ±0.19 | 12 | 6.0 | ±0.4 | 12 | 361 | ±18 |
| *spz>actSpz(2)* | 8 | 1.20 | ±0.18 | 9 | 6.2 | ±0.7 | 9 | 389 | ±29 |
| *spz>Spz-FL* | 6 | 1.21 | ±0.16 | 6 | 5.7 | ±0.4 | 6 | 359 | ±9 |

Table 5.9 Overexpressing two different forms of Spätzle using *spz-GAL4*.

### 5.2.6 Interaction with *Notch$^{ICD}$*

| | VNC Length | | |
|---|---|---|---|
| Genotype | n | Mean (μm) | SD (μm) |
| *repo>Notch$^{ICD}$* | 11 | 702 | ±54 |
| *repo>Notch$^{ICD}$,actSpz(2)* | 19 | 622 | ±59 |
| *repo>Notch$^{ICD}$,spz-FL* | 12 | 598 | ±52 |
| *repo>Notch$^{ICD}$,spz-E$^{1}$* | 12 | 645 | ±64 |
| *spz$^{2}$,repo>spz$^{2}$,Notch$^{ICD}$* | 11 | 993 | ±164 |

Table 5.10 Effects on VNC length by overexpressing *repo>Notch$^{ICD}$* with different Spätzle forms or with *spz$^{2}$* mutant background.

Against the background *repo>Notch$^{ICD}$*, the overexpression of *actSpz(2)*, *spz-FL* and *spz$^{2}$-E1* resulted in similar mean VNC lengths among each other (Table 5.10, Figure 5.11). However, the mean length of the VNC in larvae overexpressing *actSpz(2)* and *spz-FL* were significantly shorter than that of the control *repo>Notch$^{ICD}$*. In *spz$^{2}$,repo>spz$^{2}$,Notch$^{ICD}$*, the CNS size was

**Figure 5.10** Effect of active and full-length Spätzle protein through *spz-GAL4* on CNS size. **(A)** Representative mounted CNS images acquired with phase contrast using Zeiss Axioplan 2. Scale bars, 100μm. **(B)** Markers representing brain and VNC areas of individual larvae. Each blue diamond marker represents a control *spz-GAL4/+* individual (n=12). Red squares, *spz>actSpz(2)* (n=8). Green triangles, *spz>Spz-FL* (n=6). **(C)** Markers representing VNC areas and lengths of individual larvae. Blue diamonds, *spz-GAL4/+* (n=12). Red squares, *spz>actSpz(2)* (n=9). Green triangles, *spz>Spz-FL* (n=6). **(D)** Boxplots showing ranges and outliers for brain area, VNC area and VNC length. **(E)** Bar charts showing mean brain area, mean VNC area and mean VNC length. Brain area statistics: Levene's statistic=0.0, p=0.979; one-way ANOVA $F(2,23)=1.2$, $p=0.321$. VNC area: Levene's statistic=0.6, p=0.568; one-way ANOVA $F(2,24)=1.8$, $p=0.195$. VNC length, Levene's statistic=1.8, p=0.183; one-way ANOVA $F(2,24)=5.6$, $p<0.05$.

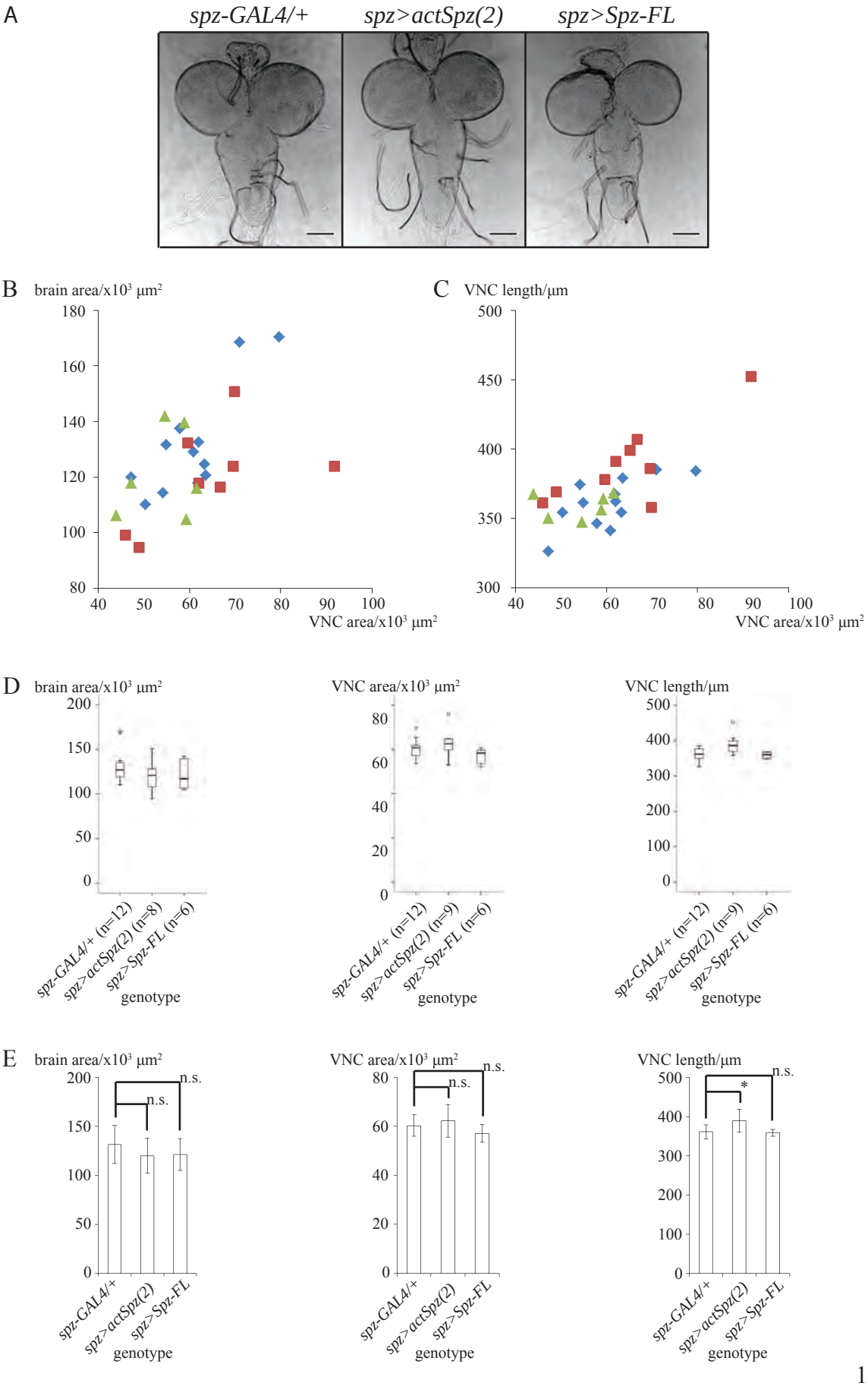
A
spz-GAL4/+
spz>actSpz(2)
spz>Spz-FL
B
brain area/x10³ µm²
VNC area/x10³ µm²
C
VNC length/µm
VNC area/x10³ µm²
D
brain area/x10³ µm²
VNC area/x10³ µm²
VNC length/µm
spz-GAL4/+ (n=12)
spz>actSpz(2) (n=8)
spz>actSpz(2) (n=9)
spz>Spz-FL (n=6)
genotype
E
brain area/x10³ µm²
VNC area/x10³ µm²
VNC length/µm
n.s.
*
spz-GAL4/+
spz>actSpz(2)
spz>Spz-FL
genotype

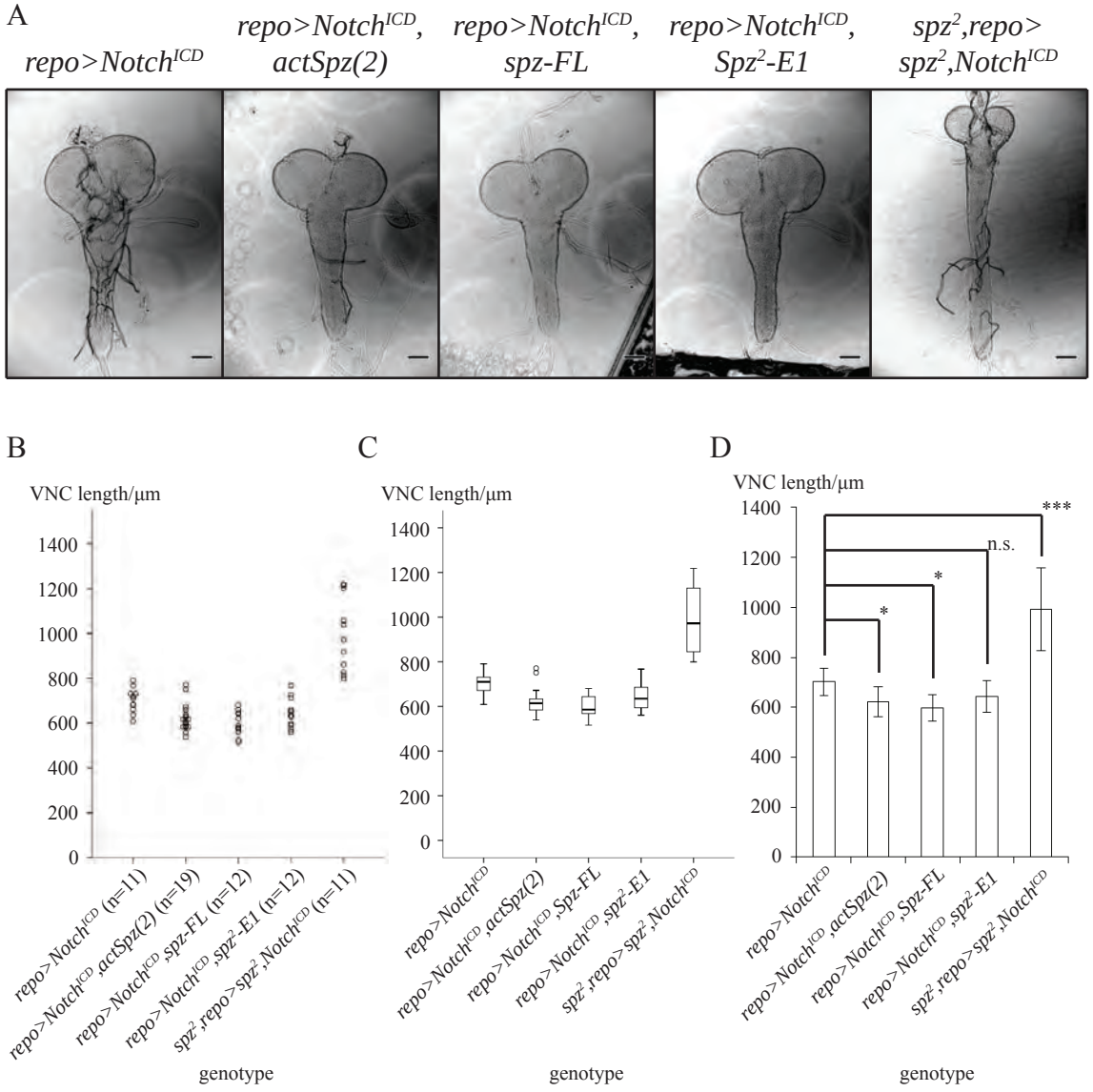


**Figure 5.11** Effect on VNC length by *repo>Notch$^{ICD}$* with Spätzle in different protein forms. **(A)** Representative mounted CNS images acquired with phase contrast using Zeiss Axioplan 2. Scale bars, 100µm. **(B)** Scatter plot with each dot representing an individual larvae's VNC length. **(C)** Boxplots showing ranges and outliers for VNC length in each genotype. **(D)** Bar charts showing mean VNC length in each genotype. VNC length, Levene's statistic=10.6, $p<0.001$; Welch ANOVA $F(4,27.3)=17.3$, $p<0.001$.

not rescued. Brain area looked as small as those of *spz*$^{2}$*ca*$^{2}$ (Figure 5.1). VNC morphology was perturbed to a large extent – an absolute length of approximately 1mm (Figure 5.11). The viability of *spz*$^{2}$,*repo>spz*$^{2}$,*Notch*$^{ICD}$ larvae reaching pupal stages was very poor, with SI lower than that *spz*$^{2}$*ca*$^{1}$(SI=0.04 and 0.15, respectively; $\chi^2(1)=37.5$, $p<0.001$; Figure 5.12).

In 4 different experimental groups, overexpression of activated and full length forms of both DNT1 and DNT2 in the background of *repo>Notch*$^{ICD}$ neither shorten nor lengthen the mean VNC length in control genotype *repo>Notch*$^{ICD}$ (Figure 5.13; one-way ANOVA, p=0.278).

### 5.2.7 Loss of Function Morphology and Cell Numbers

#### 5.2.7.1 Optic Lobe Morphology

The medulla neuropile in the larval optic lobe is normally stained by anti-BP102 (Figure 5.14A; *G9* as control genotype). In homozygous *spz*$^{2}$*ca*$^{1}$ mutants, anti-BP102 staining revealed that the medulla neuropile were almost non-existent (Figure 5.14B). The medulla neuropile structures were retained in *spz*$^{2}$*ca*$^{1}$*/ru*$^{1}$*st*$^{1}$*ea*$^{14}$*spz*$^{3}$*ca*$^{1}$, *ru*$^{1}$*h*$^{1}$*th*$^{1}$*st*$^{1}$*cu*$^{1}$*sr*$^{1}$*e*$^{s}$*ca*$^{1}$, *spz*$^{2}$*ca*$^{1}$*/Df(3R)Exel6205, spz*$^{MA05}$*/Df(3R)Exel6205* and *dnt1*$^{41}$*/dnt1*$^{55}$ mutants (Figure 5.14C-G). Loss of medulla neuropile structure in *spz*$^{2}$*ca*$^{1}$ accounted for the small brain areas of all *spz*$^{2}$ animals (Figure 5.1, Figure 5.2, Figure 5.5, Figure 5.8).

Adult eyes of *spz*$^{2}$*ca*$^{1}$*/ru*$^{1}$*st*$^{1}$*ea*$^{14}$*spz*$^{3}$*ca*$^{1}$, *spz*$^{2}$*ca*$^{1}$*/ru*$^{1}$*Diap*$^{1}$*st*$^{1}$*kni*$^{ri-1}$*rn*$^{roe-1}$*p*$^{p}$*e*$^{1}$*spz*$^{4}$, and *spz*$^{2}$*ca*$^{1}$*/Df(3R)Exel6205* were largely normal in structure in comparison to wild-type eyes of *Oregon-R*. Although *spz*$^{2}$*ca*$^{1}$ lost the medulla neuropile during third instar larvae, the adult

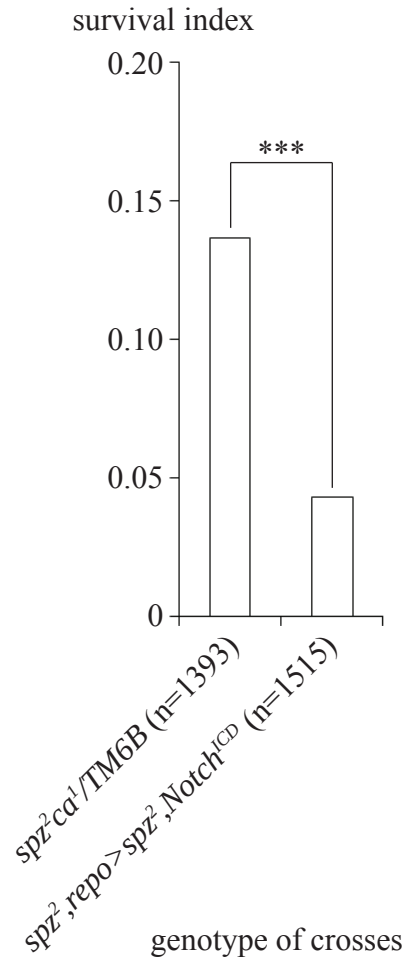


**Figure 5.12** Survival index as a measure of animal viability for genotypes *spz*$^{2}$*ca*$^{1}$*/TM6B* and *spz*$^{2}$*,repo>spz*$^{2}$*,Notch*$^{ICD}$.

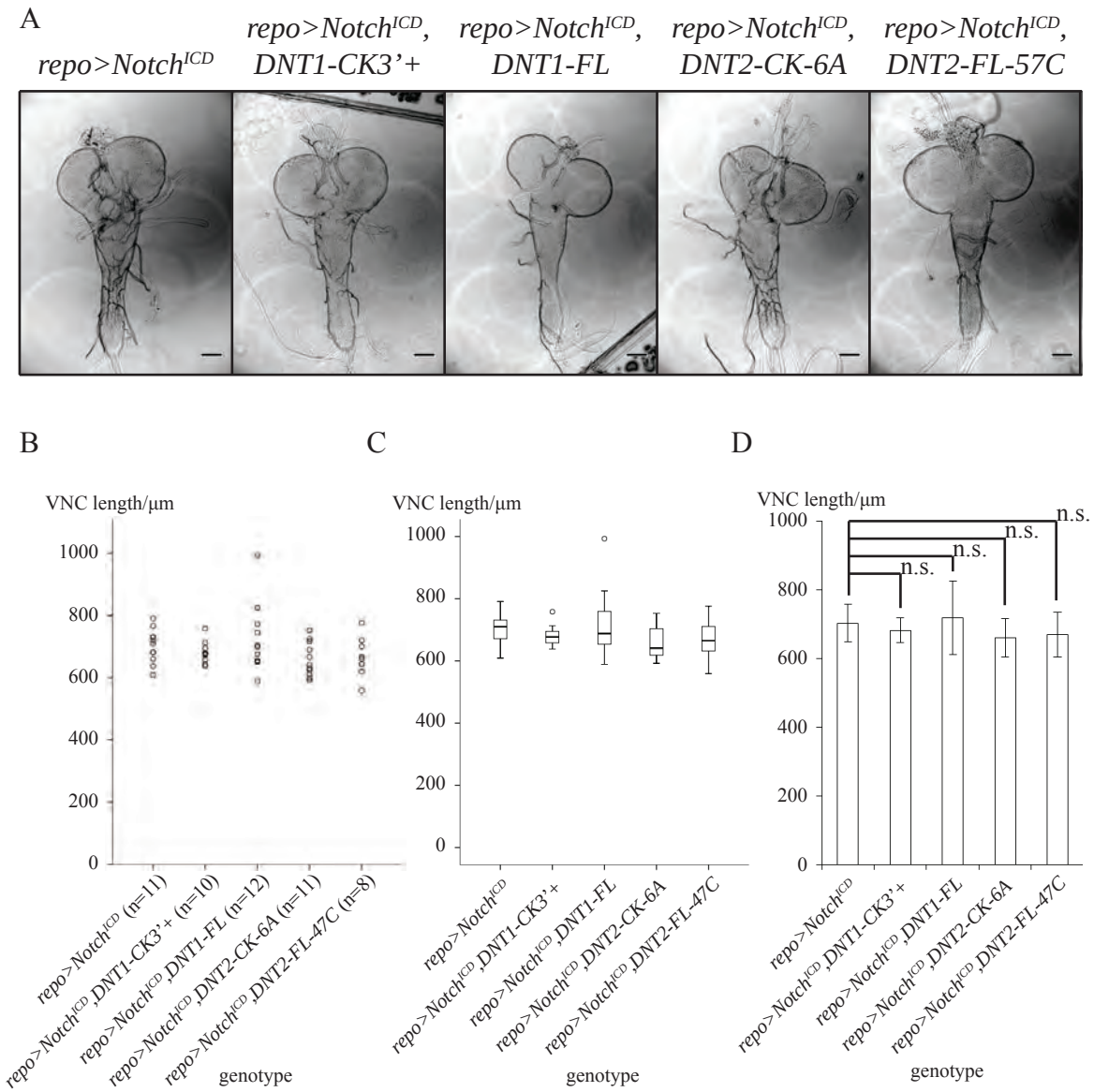


**Figure 5.13** Effect on VNC length by *repo>Notch$^{ICD}$* with DNT1 and DNT2 in different protein forms. **(A)** Representative mounted CNS images acquired with phase contrast using Zeiss Axioplan 2. Scale bars, 100µm. **(B)** Scatter plot with each dot representing an individual larvae's VNC length. **(C)** Boxplots showing ranges and outliers for VNC length in each genotype. **(D)** Bar charts showing mean VNC length in each genotype. VNC length, Levene's statistic=2.2, p=0.088; one-way ANOVA F(4,47)=1.3, p=0.278.

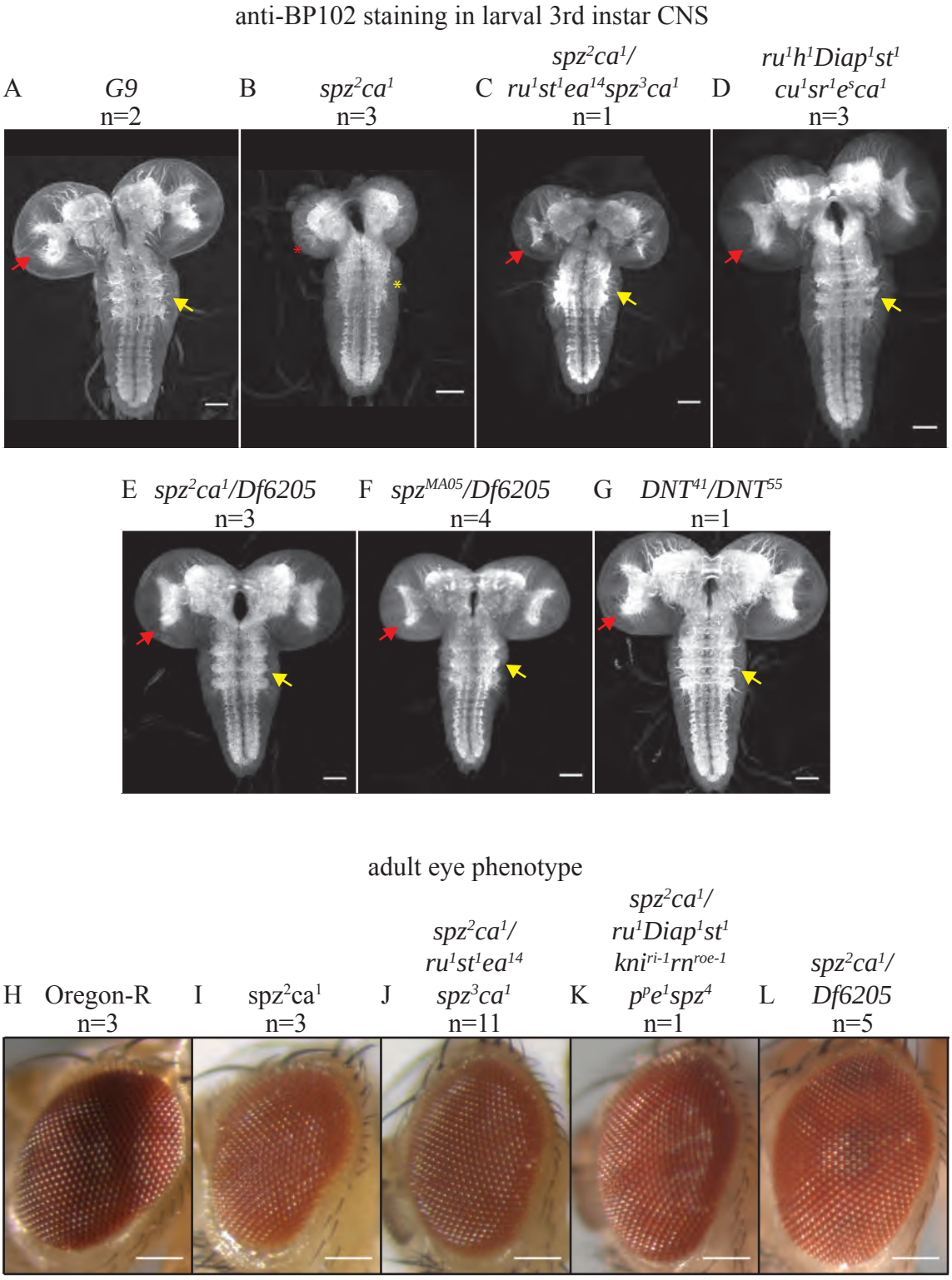


**Figure 5.14** Optic lobe and eye development of *spz* and *dnt1* mutants. **(A to G)** Horizontal views of anti-BP102 staining in larval third instar CNS. **(H to L)** Eyes of adult flies with $w^+$ background. Red arrows and asterisk refer to medulla neuropile. Yellow arrows and asterisk refer to thoracic processes. Scale bars, (A to G) 50 µm; (H to L) 100 µm.

eyes retained normal gross morphology (Figure 5.14).

#### 5.2.7.2 VNC Cortex Organisation

Anti-Elav staining in *yw* and $spz^{2}ca^{1}$ showed no obvious morphological differences between the two genotypes (Figure 5.15). The same applied between *yw* and $spz^{MA05}$/*Df(3R)Exel6205* (Figure 5.16).

Double staining of anti-GS2 and anti-Elav stainings, however, revealed a subtle difference between *yw* and $spz^{2}ca^{1}$ (Figure 5.15), not pertaining to glial cell shape but to cell organisation instead. In the dorsal maximum projections, the neuropile-associated glia labelled by anti-GS2 in $spz^{2}ca^{1}$ appeared to be more compactly packed than in *yw*. The subtle cell disorganisation was reflected in double anti-Ebony and anti-Repo staining, in which the organisation of the ventral interface glia (vIG) looked affected (Figure 5.17). The organisation looked affected but the categorisation of the vIG pairing showed that the differences were not signficant (Table 5.6). The number of Ebony+ cells in the abdomen was not affected in $spz^{2}ca^{1}$ (Figure 5.18).

| Genotype | No. of VNC with ≤ 5 pairings | No. of VNC with > 5 pairings but not all cell are in pairs | No. of VNC with all cells in pairs (either 7/7 or 8/8 pairs in full) |
|---|---|---|---|
| *yw* | 2 | 7 | 1 |
| $spz^{2}ca^{1}$ | 1 | 7 | 5 |

Table 5.11 Pairing of Ebony+ in the ventral half of the abdominal nerve cord.
$\chi^{2}(2)=2.6$, $p=0.265$.

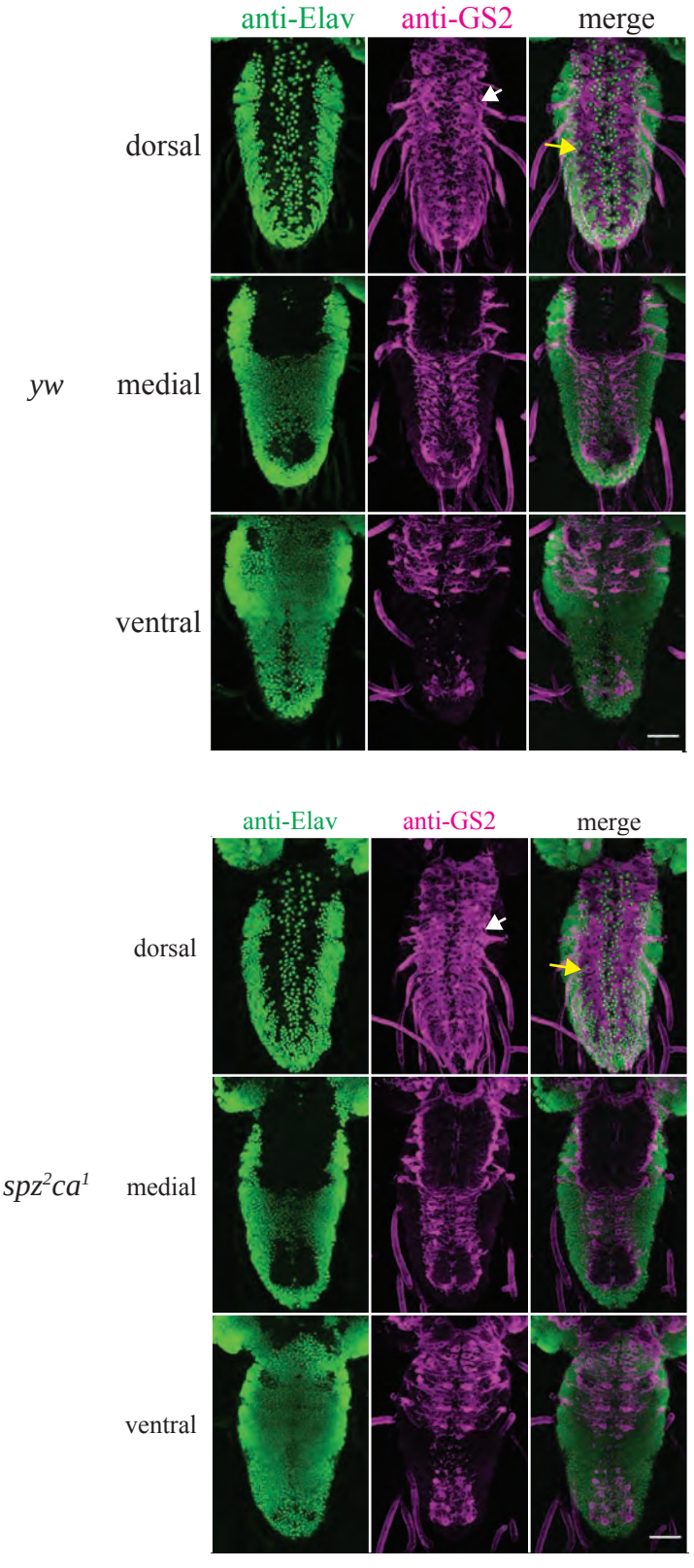


**Figure 5.15** Anti-Elav and anti-GS2 staining in *yw* (n=7) and *spz*$^{2}$*ca*$^{1}$ (n=11). Maximum projections were used throughout. **White arrows:** corresponding thoracic spaces. **Yellow arrows:** corresponding abdominal areas. Scale bars, 50µm.

anti-Elav staining in *yw* VNC (n=12)

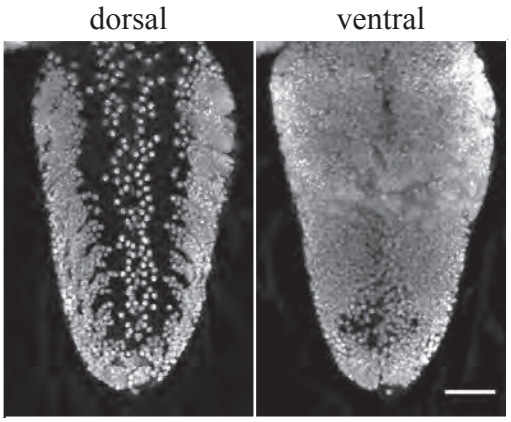


anti-Elav staining in *spz*$^{MA05}$*/Df(3R)Exel6205* VNC (n=4)

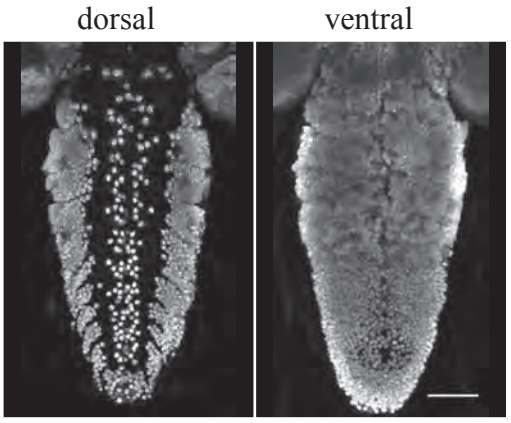


**Figure 5.16** Anti-Elav staining in *yw* (n=12) and *spz*$^{MA05}$*/Df(3R)Exel6205* (n=4). Maximum projections were used throughout. Scale bars, 50µm.

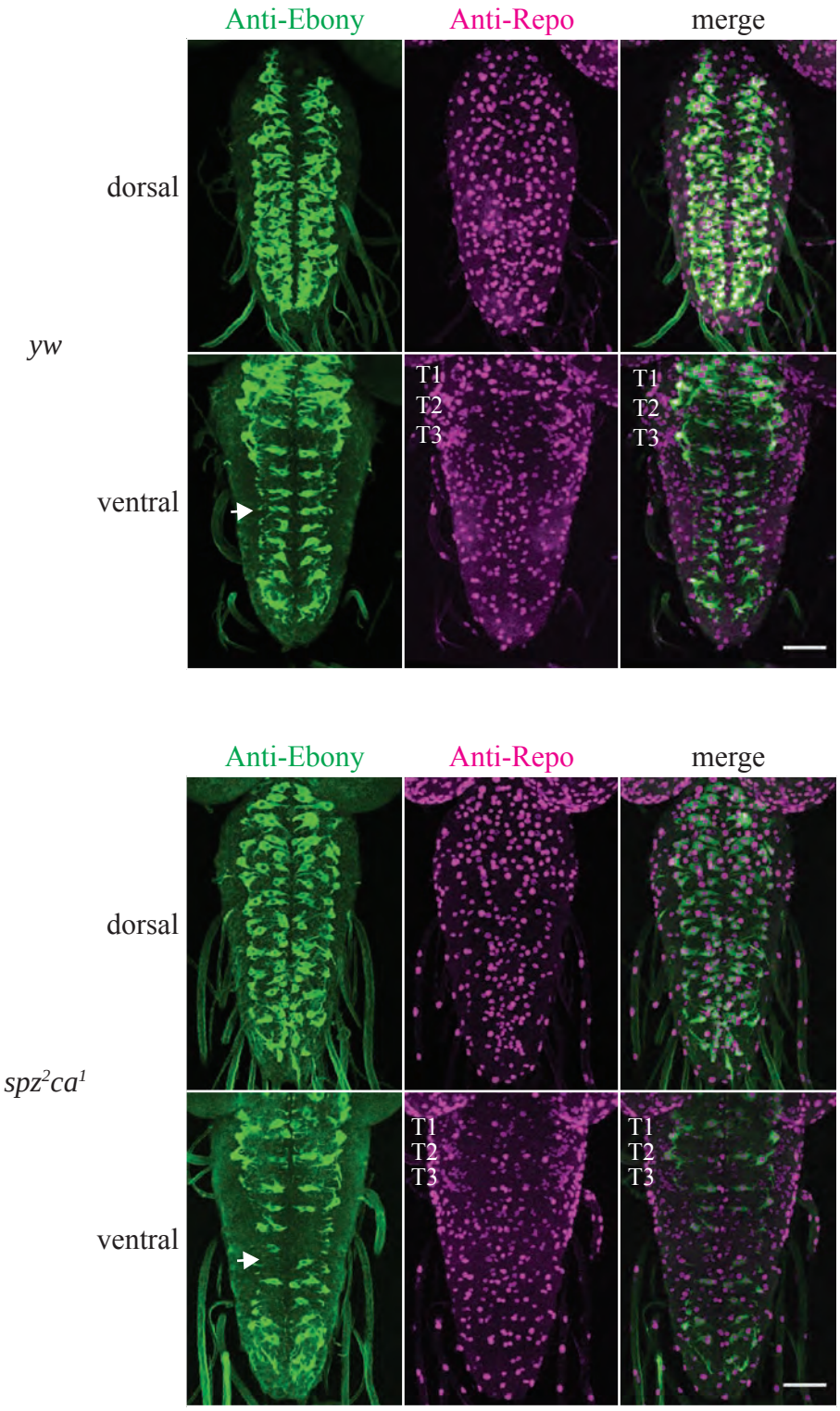


**Figure 5.17** Anti-Ebony and anti-Repo staining in *yw* (n=13) and *spz*$^{2}$*ca*$^{1}$ (n=10). **White arrows:** corresponding abdominal spaces. Scale bars, 50µm.

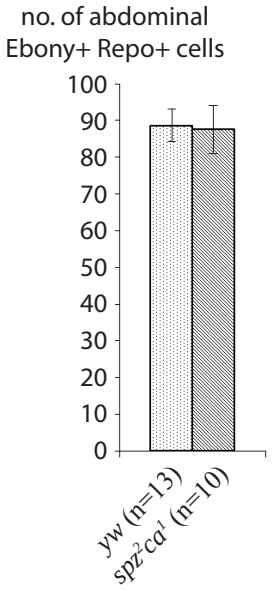


**Figure 5.18** Counting abdominal Ebony+ Repo+ cells in larval third instar VNC. Genotypes: *yw* (dotted bar; n=13) and *spz*$^{2}$*ca*$^{1}$ (diagonally-lined bar; n = 10) from corresponding Figure 5.17.

#### 5.2.7.3 Repo+ Glia Numbers

The mean numbers of thoracic and abdominal Repo+ cells in *spz*$^{2}$*ca*$^{1}$ mutants were not significantly different from those in *yw* (Figure 5.19). The genotypes *spz*$^{2}$*ca*$^{1}$*/Df(3R)Exel6205* and *spz*$^{MA05}$*/ Df(3R)Exel6205* had increased mean Repo+ cells than *yw* (Figure 5.19).

Results in Figure 5.20 show that glial numbers in the VNC of *dnt1*$^{41}$*/Df(3L)Exel6101* and *dnt2*$^{37}$*/Df(3L)Exel6101* were unaffected. Double *Toll7* and *Toll6* mutants had more abdominal Repo+ glia than *yw*, but their thoracic glial numbers were not affected (Figure 5.21).

#### 5.2.7.4 Survival Index of *Toll*$^{r3}$

When *Toll*$^{r3}$*ca*$^{1}$*/TM6B* flies were crossed to *Df(3R)ro80b,st*$^{1}$*e*$^{1}$*/TM6B* flies, the resulting SI of their non-tubby progeny (with normal embryogenesis at 18°C but loss of function larval life at 29°C) was 0.13 (Figure 5.22).

#### 5.2.7.5 pH3+ Mitotic Cells

The number of pH3+ cells in loss of function *spz* mutants were not significantly affected (Figure 5.23). Neither were proliferative levels in *dnt1* and *dnt2* mutants (Figure 5.24). In double *Toll7* and *Toll6* mutants, there was an increase in mitotic events in the thorax (Figure 5.25) while mitosis was unaffected in the abdomen (Figure 5.25).

**Figure 5.19** Counting Repo+ cells in genotypes *yw, spz$^{2}$ca$^{1}$*, *spz$^{2}$ca$^{1}$/Df(3R)Exel6205* and *spz$^{MA05}$/Df(3R)Exel6205*. **(A)** Horizontal views of anti-Repo staining in thoracic VNC. **(B)** Profile of Repo+ in each genotype's thoracic VNC, accounting all values from larvae (scatter plot), value distributions (box plot) and means as average (bar chart). Levene's statistic=0.2, p=0.910; one-way ANOVA $F(3,48)=2.4$, p=0.076. **(C)** Horizontal views of anti-Repo staining in abdominal VNC. **(D)** Profile of Repo+ cells in each genotype's abdominal VNC, accounting all values from larvae (scatter plot), value distributions (box plot) and means as average (bar chart). Levene's statistic=1.6, p=0.204; one-way ANOVA $F(3,72)=6.9$, $p<0.001$. Scale bars, 25μm.

A anti-Repo staining in THORAX

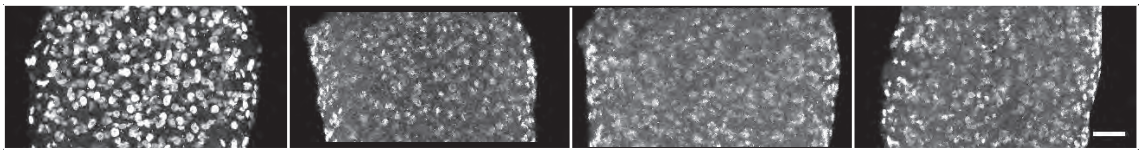

*yw* *spz²ca¹* *spz²ca¹/Df6205* *spz^MA05/Df6205*

B

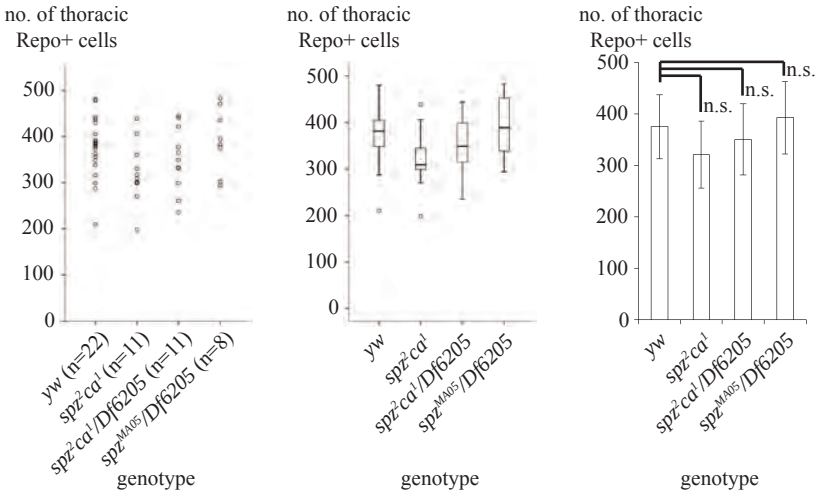


C anti-Repo staining in ABDOMEN

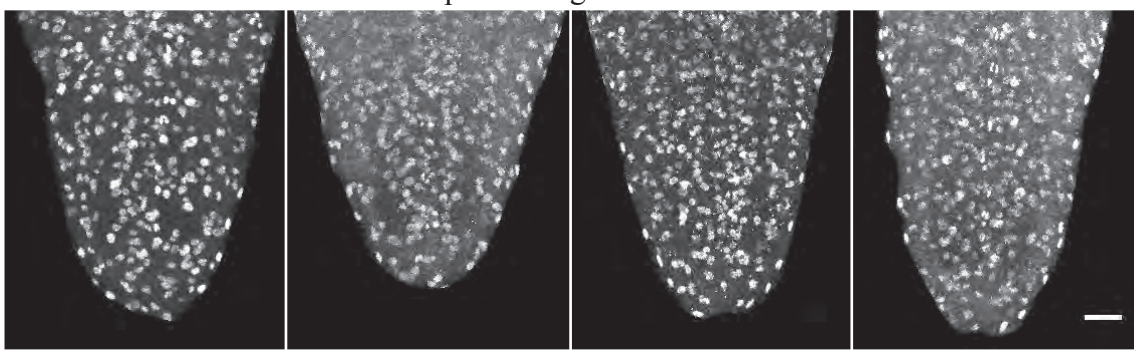

*yw* *spz²ca¹* *spz²ca¹/Df6205* *spz^MA05/Df6205*

D

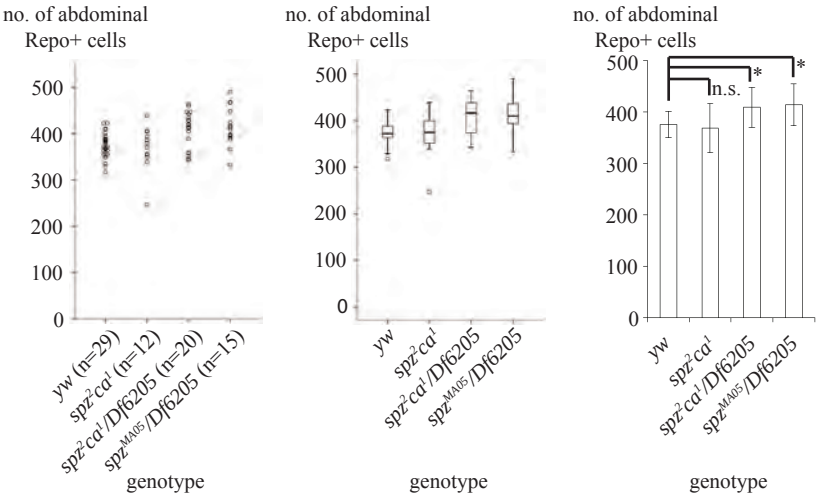

**Figure 5.20** Counting Repo+ cells in genotypes *yw*, *dnt1*$^{41}$*/Df(3L)Exel6101* and *dnt2*$^{37}$*/ Df(3L)Exel6092*. **(A)** Horizontal views of anti-Repo staining in thoracic VNC. **(B)** Profile of Repo+ cells in each genotype's thoracic VNC, accounting all values from larvae (scatter plot), value distributions (box plot) and means as average (bar chart). Levene's statistic=0.3, p=0.726; one-way ANOVA F(2,37)=0.1, p=0.929. **(C)** Horizontal views of anti-Repo staining in abdominal VNC. **(D)** Profile of Repo+ cells in each genotype's abdominal VNC, accounting all values from larvae (scatter plot), value distributions (box plot) and means as average (bar chart). Levene's statistic=0.2, p=0.803; one-way ANOVA F(2,45)=0.4, p=0.685. Scale bars, 25μm.

A

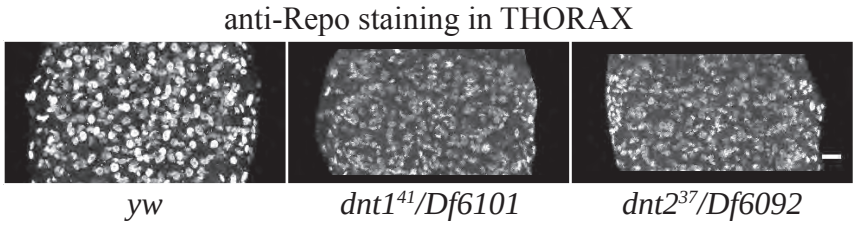
anti-Repo staining in THORAX
yw
dnt1^41/Df6101
dnt2^37/Df6092

B

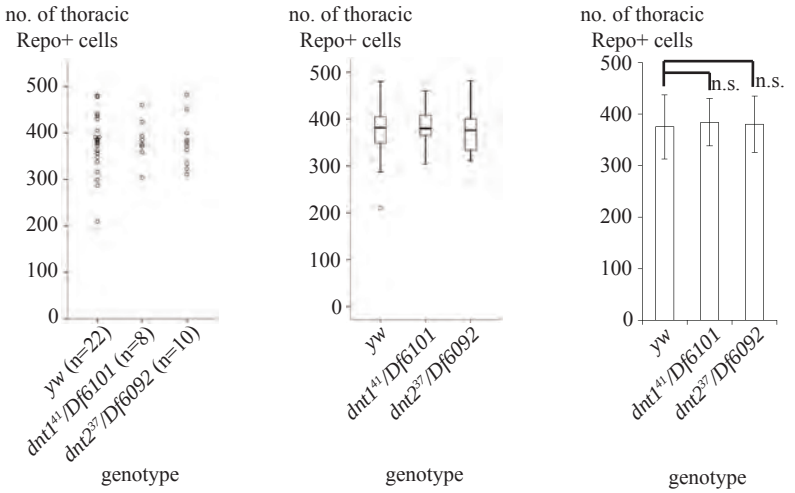
no. of thoracic Repo+ cells
500
400
300
200
100
0
yw (n=22)
dnt1^41/Df6101 (n=8)
dnt2^37/Df6092 (n=10)
genotype
no. of thoracic Repo+ cells
yw
dnt1^41/Df6101
dnt2^37/Df6092
genotype
no. of thoracic Repo+ cells
n.s.
n.s.
yw
dnt1^41/Df6101
dnt2^37/Df6092
genotype

C

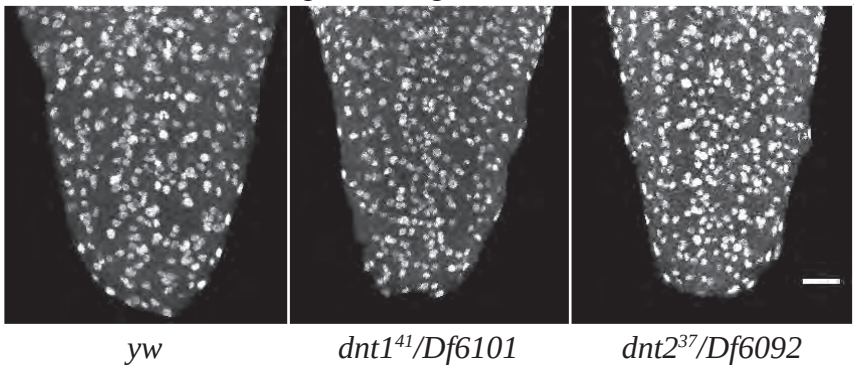
anti-Repo staining in ABDOMEN
yw
dnt1^41/Df6101
dnt2^37/Df6092

D

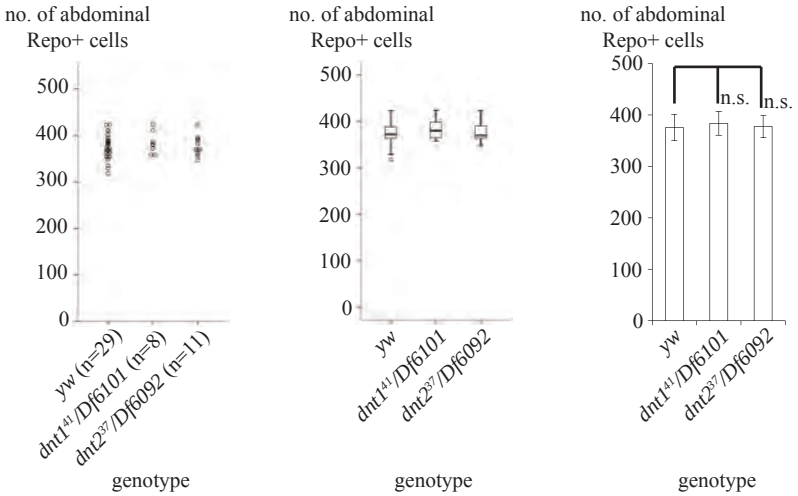
no. of abdominal Repo+ cells
500
400
300
200
100
0
yw (n=29)
dnt1^41/Df6101 (n=8)
dnt2^37/Df6092 (n=11)
genotype
no. of abdominal Repo+ cells
yw
dnt1^41/Df6101
dnt2^37/Df6092
genotype
no. of abdominal Repo+ cells
n.s.
n.s.
yw
dnt1^41/Df6101
dnt2^37/Df6092
genotype

**Figure 5.21** Counting Repo+ cells in genotypes *yw* and $Toll7^{P114}/Toll7^{P8};Toll6^{31}/Toll6^{26}$. **(A)** Horizontal views of anti-Repo staining in thoracic VNC. **(B)** Profile of Repo+ cells in each genotype's thoracic VNC, accounting all values from larvae (scatter plot), value distributions (box plot) and means as average (bar chart). Levene's statistic=0.1, p=0.790; t-test t(26)=-1.3, p = 0.193. **(C)** Horizontal views of anti-Repo staining in abdominal VNC. **(D)** Profile of Repo+ cells in each genotype's abdominal VNC, accounting all values from larvae (scatter plot), value distributions (box plot) and means as average (bar chart). Levene's statistic=0.1, p=0.748; t-test t(37)=-6.3, p<0.001. Scale bars, 25μm.

A

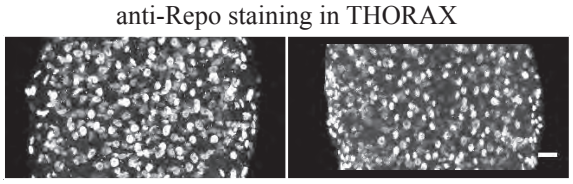
anti-Repo staining in THORAX
yw
Toll7P114/Toll7P8;
Toll631/Toll626

B

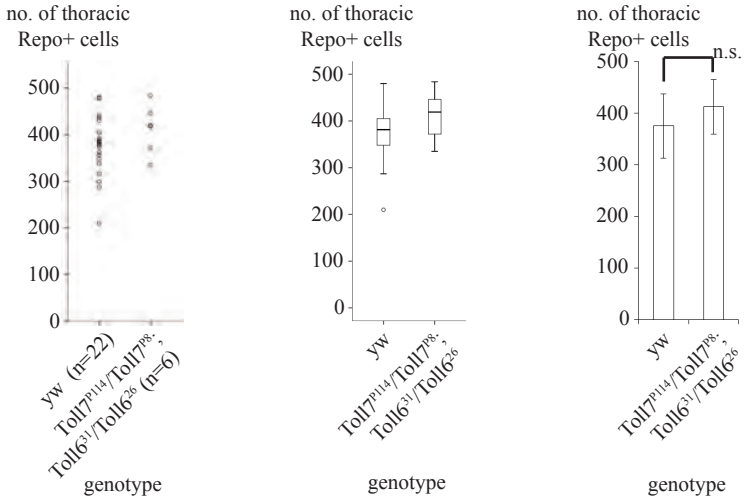
no. of thoracic Repo+ cells
500
400
300
200
100
0
yw (n=22)
Toll7P114/Toll7P8; Toll631/Toll626 (n=6)
genotype
no. of thoracic Repo+ cells
yw
Toll7P114/Toll7P8; Toll631/Toll626
genotype
no. of thoracic Repo+ cells
n.s.
yw
Toll7P114/Toll7P8; Toll631/Toll626
genotype

C

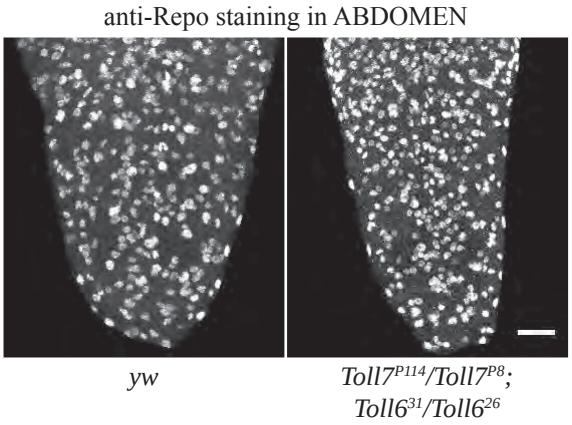
anti-Repo staining in ABDOMEN
yw
Toll7P114/Toll7P8;
Toll631/Toll626

D

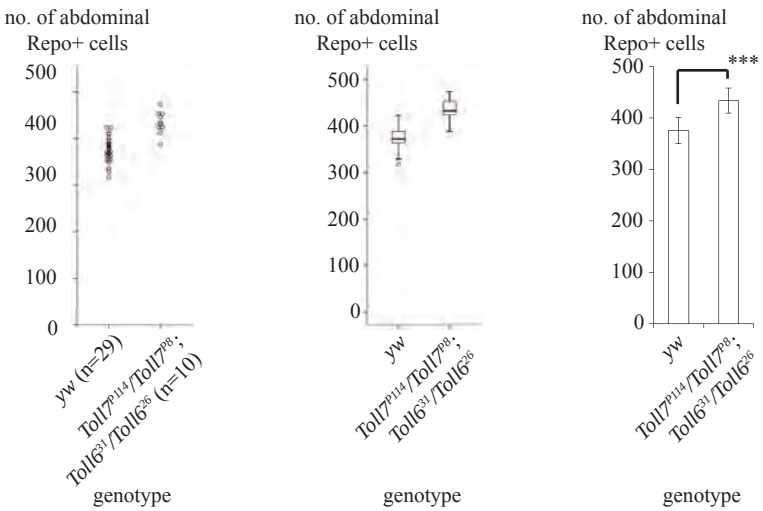
no. of abdominal Repo+ cells
500
400
300
200
100
0
yw (n=29)
Toll7P114/Toll7P8; Toll631/Toll626 (n=10)
genotype
no. of abdominal Repo+ cells
yw
Toll7P114/Toll7P8; Toll631/Toll626
genotype
no. of abdominal Repo+ cells
***
yw
Toll7P114/Toll7P8; Toll631/Toll626
genotype

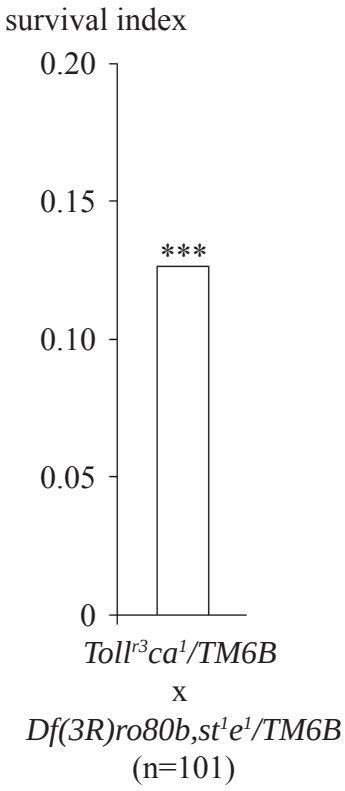


**Figure 5.22** Survival index as a measure of animal viability for *Toll$^{r3}$ca$^{1}$/Df(3R)ro80b,st$^{1}$e$^{1}$*. In this experiment, embryogenesis was at permissive temperature 18°C and larval life stages at restrictive temperature 29°C. The statistical result in the chart above was a result of the comparison between the test genotype and the expected wild-type (SI=1).

**Figure 5.23** Counting pH3+ cells in genotypes *yw*, *spz*$^{2}$*ca*$^{1}$, *spz*$^{2}$*ca*$^{1}$*/Df(3R)Exel6205* and *spz*$^{MA05}$*/Df(3R)Exel6205*. **(A)** Horizontal views of anti-pH3 staining in thoracic VNC. **(B)** Profile of pH3+ cells in each genotype's thoracic VNC, accounting all values from larvae (scatter plot), value distributions (box plot) and means as average (bar chart). Levene's statistic=1.8, p=0.173; one-way ANOVA F(3,28)=1.9, p=0.160. **(C)** Horizontal views of anti-pH3 staining in abdominal VNC. **(D)** Profile of pH3+ cells in each genotype's abdominal VNC, accounting all values from larvae (scatter plot), value distributions (box plot) and means as average (bar chart). Levene's statistic=1.1, p=0.340; one-way ANOVA F(3,47)=1.9, p=0.139. Scale bars, 25µm.

A

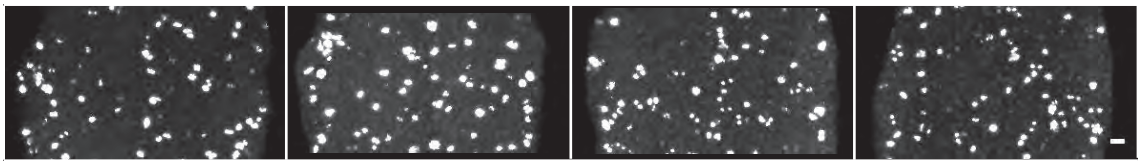
anti-pH3 staining in THORAX
yw
spz2/spz2
spz2/Df6205
spzMA05/Df6205

B

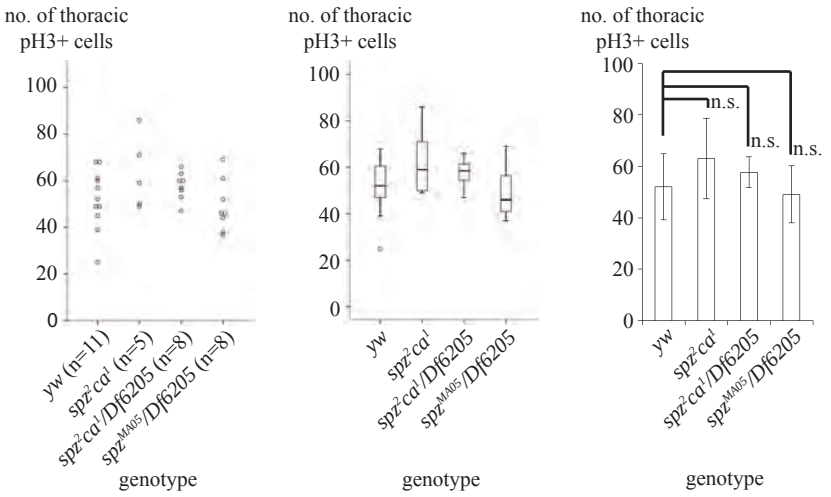
no. of thoracic pH3+ cells
yw (n=11)
spz2ca1 (n=5)
spz2ca1/Df6205 (n=8)
spzMA05/Df6205 (n=8)
genotype
no. of thoracic pH3+ cells
yw
spz2ca1
spz2ca1/Df6205
spzMA05/Df6205
genotype
no. of thoracic pH3+ cells
n.s.
n.s.
n.s.
yw
spz2ca1
spz2ca1/Df6205
spzMA05/Df6205
genotype

C

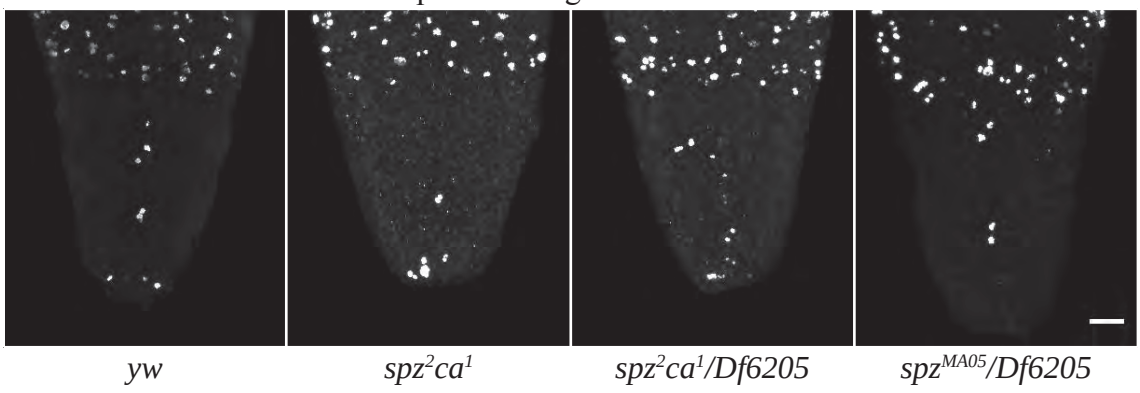
anti-pH3 staining in ABDOMEN
yw
spz2ca1
spz2ca1/Df6205
spzMA05/Df6205

D

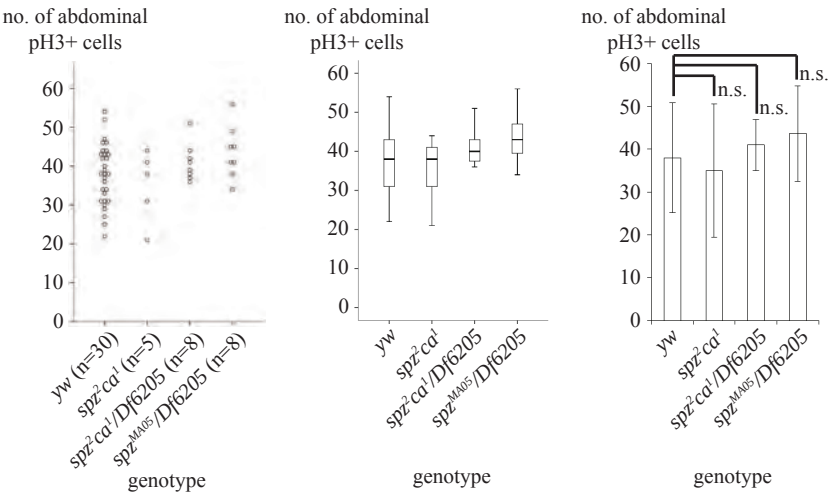
no. of abdominal pH3+ cells
yw (n=30)
spz2ca1 (n=5)
spz2ca1/Df6205 (n=8)
spzMA05/Df6205 (n=8)
genotype
no. of abdominal pH3+ cells
yw
spz2ca1
spz2ca1/Df6205
spzMA05/Df6205
genotype
no. of abdominal pH3+ cells
n.s.
n.s.
n.s.
yw
spz2ca1
spz2ca1/Df6205
spzMA05/Df6205
genotype

**Figure 5.24** Counting pH3+ cells in genotypes *yw*, *dnt1*$^{41}$*/Df(3L)Exel6101* and *dnt2*$^{37}$*/ Df(3L)Exel6092*. **(A)** Horizontal views of anti-pH3 staining in thoracic VNC. **(B)** Profile of pH3+ cells in each genotype's thoracic VNC, accounting all values from larvae (scatter plot), value distributions (box plot) and means as average (bar chart). Levene's statistic=2.6, p=0.105; one-way ANOVA F(2,18)=1.8, p=0.187. **(C)** Horizontal views of anti-pH3 staining in abdominal VNC. **(D)** Profile of pH3+ cells in each genotype's abdominal VNC, accounting all values from larvae (scatter plot), value distributions (box plot) and means as average (bar chart). Levene's statistic=1.6, p=0.206; one-way ANOVA F(2,38)=1.6, p=0.207. Error bars represent standard deviations. Scale bars, 25µm.

A

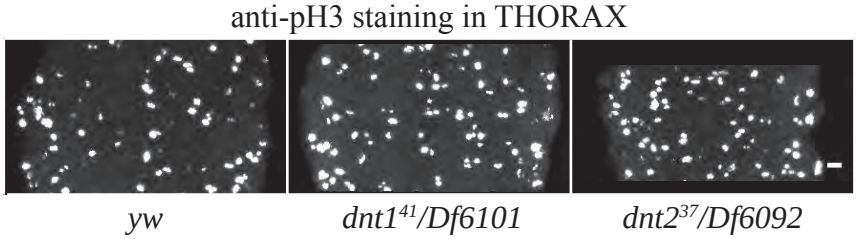
anti-pH3 staining in THORAX
yw
dnt1^41/Df6101
dnt2^37/Df6092

B

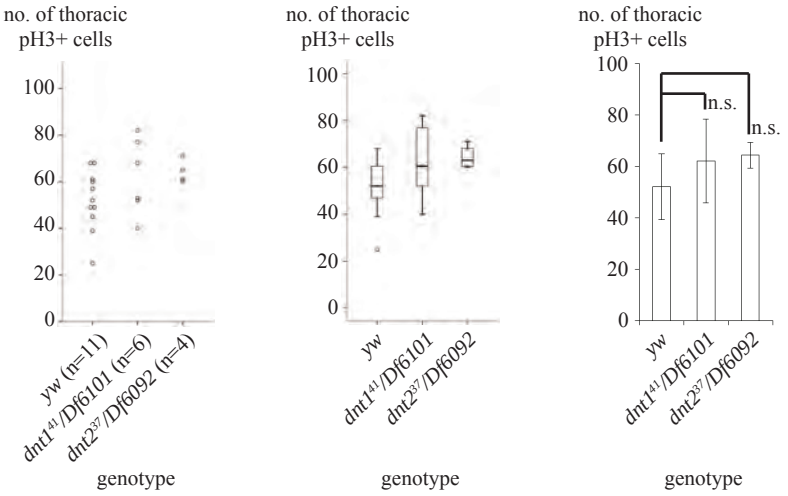
no. of thoracic pH3+ cells
yw (n=11)
dnt1^41/Df6101 (n=6)
dnt2^37/Df6092 (n=4)
genotype
n.s.
n.s.

C

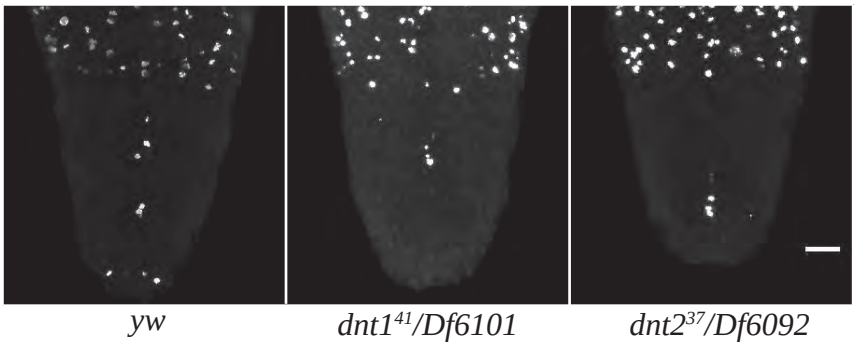
anti-pH3 staining in ABDOMEN
yw
dnt1^41/Df6101
dnt2^37/Df6092

D

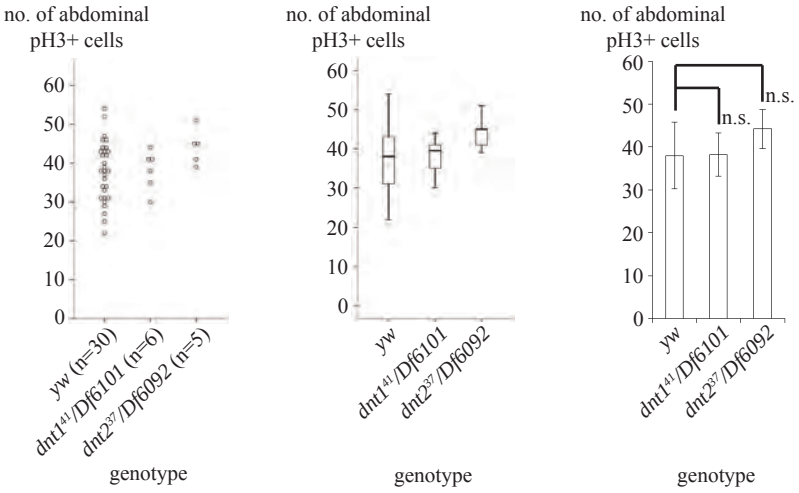
no. of abdominal pH3+ cells
yw (n=30)
dnt1^41/Df6101 (n=6)
dnt2^37/Df6092 (n=5)
genotype
n.s.
n.s.

**Figure 5.25** Counting pH3+ cells in genotypes *yw* and $Toll7^{P114}/Toll7^{P8};Toll6^{31}/Toll6^{26}$. **(A)** Horizontal views of anti-pH3 staining in thoracic VNC. **(B)** Profile of pH3+ cells in each genotype's thoracic VNC, accounting all values from larvae (scatter plot), value distributions (box plot) and means as average (bar chart). Levene's statistic=0.6, p=0.444; t-test t(13)=-2.6, p=0.023. **(C)** Horizontal views of anti-pH3 staining in abdominal VNC. **(D)** Profile of pH3+ cells in each genotype's abdominal VNC, accounting all values from larvae (scatter plot), value distributions (box plot) and means as average (bar chart). Levene's statistic=0.3, p=0.582; t-test t(32)=-1.7, p=0.102. Scale bars, 25μm.

A

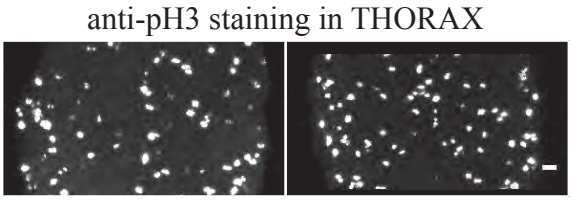
anti-pH3 staining in THORAX
yw
Toll7P114/Toll7P8;
Toll631/Toll626

B

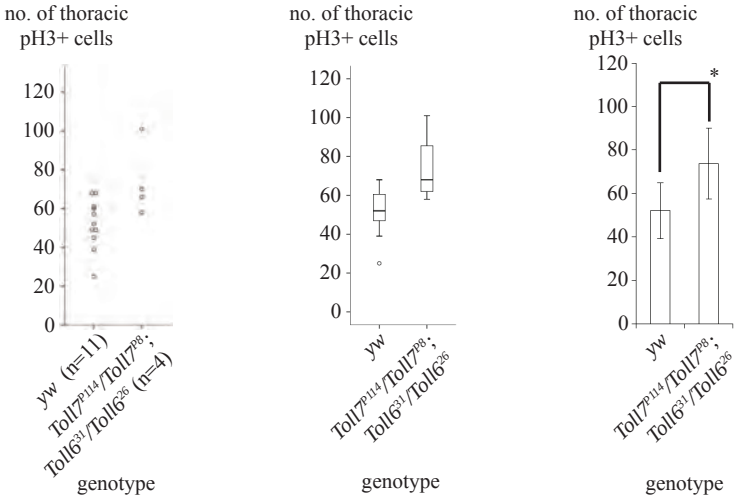
no. of thoracic pH3+ cells
120
100
80
60
40
20
0
yw (n=11)
Toll7P114/Toll7P8;
Toll631/Toll626 (n=4)
genotype
no. of thoracic pH3+ cells
yw
Toll7P114/Toll7P8;
Toll631/Toll626
genotype
no. of thoracic pH3+ cells
*
yw
Toll7P114/Toll7P8;
Toll631/Toll626
genotype

C

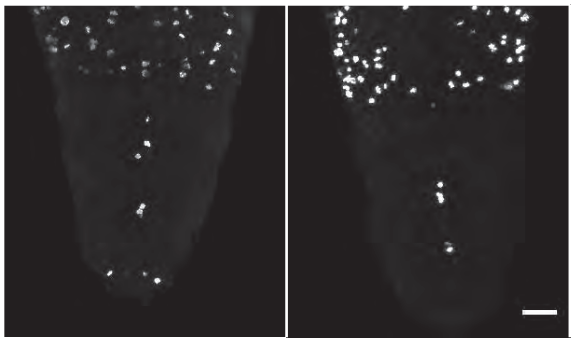
anti-pH3 staining in ABDOMEN
yw
Toll7P114/Toll7P8;
Toll631/Toll626

D

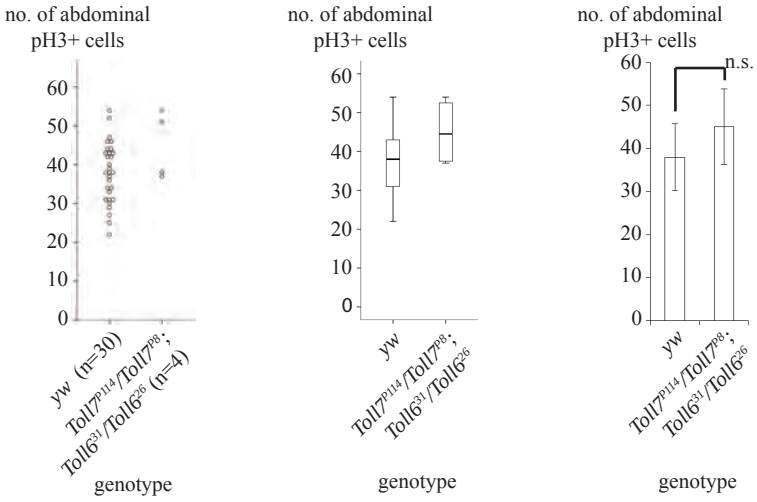
no. of abdominal pH3+ cells
60
50
40
30
20
10
0
yw (n=30)
Toll7P114/Toll7P8;
Toll631/Toll626 (n=4)
genotype
no. of abdominal pH3+ cells
yw
Toll7P114/Toll7P8;
Toll631/Toll626
genotype
no. of abdominal pH3+ cells
n.s.
yw
Toll7P114/Toll7P8;
Toll631/Toll626
genotype

Within the 'non-mitotic' zone of the abdomen (Figure 5.26), the number of pH3+ could go up to 12 and the collective mean across all genotypes was 5 cells (Table 5.12). Across all genotypes, the number of pH3+ cells did not differ significantly from each other.

| Genotype | No. of VNC with pH3+ cells ≤ 5 | No. of VNC with pH3+ cells > 5 | % of VNC with pH3+ cells ≤ 5 | % of VNC with pH3+ cells > 5 |
|---|---|---|---|---|
| *yw* | 18 | 12 | 60.0 | 40.0 |
| $spz^{2}ca^{1}$ | 3 | 2 | 60.0 | 40.0 |
| $spz^{2}/Df6205$ | 1 | 7 | 12.5 | 87.5 |
| $spz^{MA05}/Df6205$ | 2 | 6 | 25.0 | 75.0 |
| $dnt1^{41}/Df6101$ | 4 | 2 | 66.7 | 33.3 |
| $dnt2^{37}/Df6092$ | 3 | 1 | 75.0 | 25.0 |
| $Toll7^{P114}/Toll7^{P8};Toll6^{31}/Toll6^{26}$ | 2 | 2 | 50.0 | 50.0 |

Table 5.12 Proliferative levels in the 'non-mitotic' zone.
$\chi^2(6)=9.6$, p=0.145.

### 5.2.7.6 Dcp1+ Apoptotic Cells

Abdominal apoptotic levels of loss of function *spz* were lowered than in *yw* (Figure 5.27). Among the loss of function groups, only the $spz^{2}ca^{1}$ group had apoptosis at levels significantly below *yw*. When considering only the 'non-apoptotic' zone, the levels of apoptosis were correlated with global levels in the abdominal region (Table 5.13).

| Genotype | N | No. of Abdominal Dcp1+ Cells | | No. of Dcp1+ Cells in 'Non-Apoptotic' Zone | |
|---|---|---|---|---|---|
| | | Mean No. | SD | Mean No. | SD |
| *yw* | 17 | 101 | ±12 | 27 | ±8 |
| $spz^{2}ca^{1}$ | 5 | 69 | ±25 | 12 | ±6 |
| $spz^{2}/Df6205$ | 5 | 94 | ±4 | 21 | ±4 |
| $spz^{MA05}/Df6205$ | 5 | 92 | ±16 | 24 | ±6 |

Table 5.13 Apoptotic levels in *spz* loss of function genotypes.

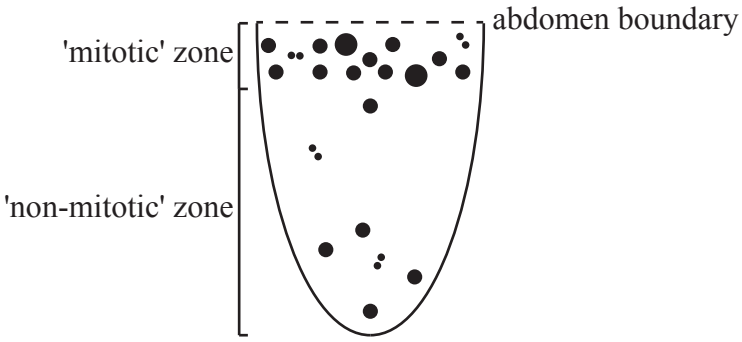


**Figure 5.26** Illustration of the areas within the abdomen which contained either dense pH3+ signal anteriorly (defined as ‘mitotic’ zone) or sparse pH3+ signal (defined as ‘non-mitotic’ zone).

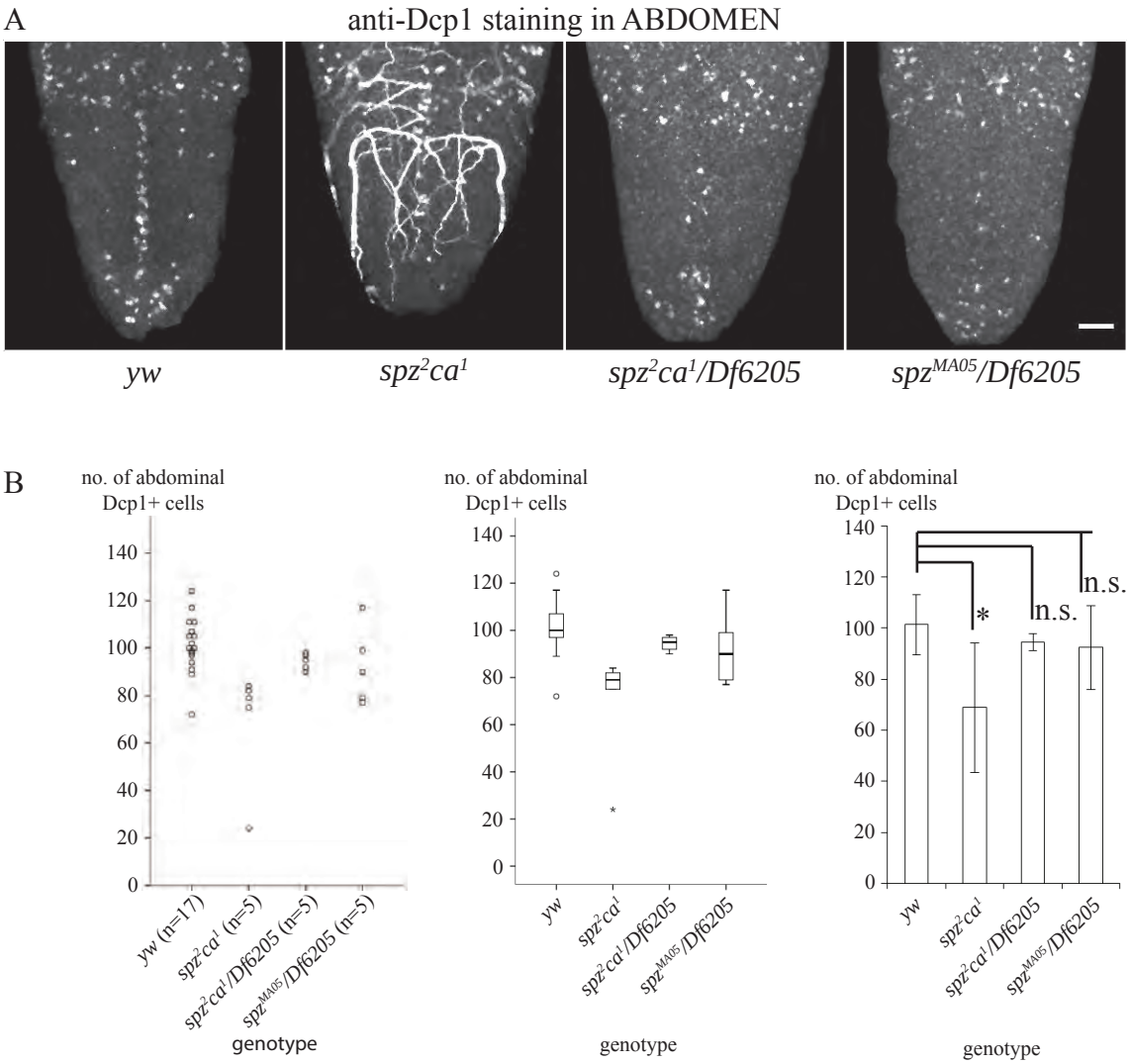


**Figure 5.27** Counting Dcp1+ cells in genotypes *yw*, *spz²ca¹*, *spz²ca¹/Df(3R)Exel6205* and *spz^MA05/Df(3R)Exel6205*. **(A)** Horizontal views of anti-Dcp1 staining in thoracic VNC. **(C)** Profile of Dcp1+ in each genotype's thoracic VNC, accounting all values from larvae (scatter plot), value distributions (box plot) and means as average (bar chart). Levene's statistic=2.7, p=0.066; one-way ANOVA F(3,28)=6.5, p<0.005. Scale bars, 25μm.

### 5.2.7.7 Sholl Analysis of *spz*$^2$ Loss of Function

In the thorax, RP2 neurons of *spz*$^2$ (Figure 5.28B) appeared to occupy smaller volumes than the control (Figure 5.28A) in terms of space occupied by dendrites. RP2 cell bodies looked similar in size (Figure 5.28A, B). The furthest dendrite intersection recorded at 50 µm away from the *spz*$^2$ soma in comparison to 95 µm from the control soma (Figure 5.28C). RP2 of *spz*$^2$ had denser branching than control at 10 microns away from the cell body (Figure 5.28D). At 40 microns distance from the control soma, the highest mean number of intersection was within 10 microns of the edge of the *spz*$^2$ RP2 dendrite branches (Figure 5.28D). Independent of the distance from soma variable, the linear Sholl plots for control and *spz*$^2$ looked similar in terms of fitting peak and trough curves (Figure 5.28D). All together, these results indicate that RP2 neurons of *spz*$^2$ occupied smaller volumes than wild-type in VNC but branching complexity between the two might not be different.

Within the first three abdominal segments, RP2 neurons from control, *spz*$^2$ and *spz*$^2$*/Df(3R)Exel6205* genotypes were sampled and cross-compared (Figure 5.29). The linear Sholl plots for each genotype show somewhat bell-shaped curves (Figure 5.30). Fitted curve for *spz*$^2$ in A1-3 was similar to that in the thorax (Figure 5.29D) for the highest mean number of intersection occurring at 15 microns away from the peripheral. For the control and *spz*$^2$*/Df(3R)Exel6205*, their peaks were approximately half-way of their respective furthest distance from the soma. RP2 neurons of *spz*$^2$ and *spz*$^2$*/Df6205* showed smaller volume occupancy than those of *yw* (Figure 5.30A, B).

**Figure 5.28** Sholl analysis comparing between control and *spz*$^{2}$ thoracic RFP+ RP2 neurons. **(A, B)** Raw images in maximum projection and in horizontal view. **(A', B')** Corresponding segmented images. **(A", B")** Sholl profiles. **(C)** Profile of number of intersection points at distances in 5µm increments from the soma. Each blue diamond marker represents an intersection for the control genotype (n=5). Red squares, *spz*$^{2}$ (n=3). **(D)** Corresponding mean profile with curve fitted to polynomial function. Red arrows emphasises the yellow dots marking the point at which the main axon leaves the soma. Scale bar, 25µm.

Thorax Segments 1-3

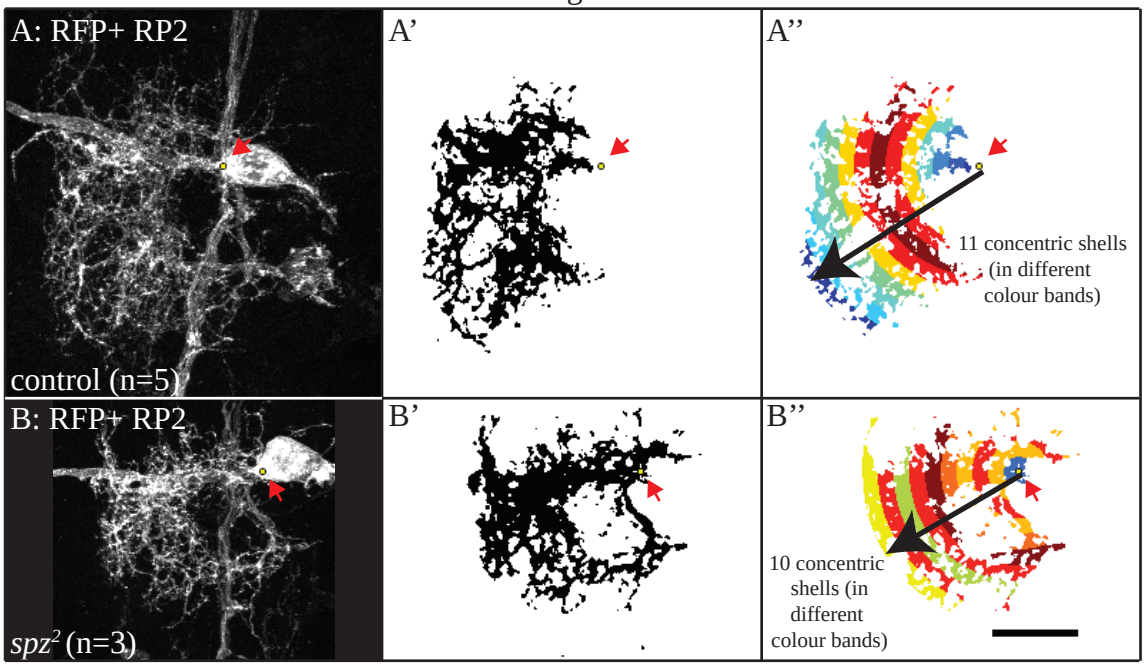


C no. of intersections

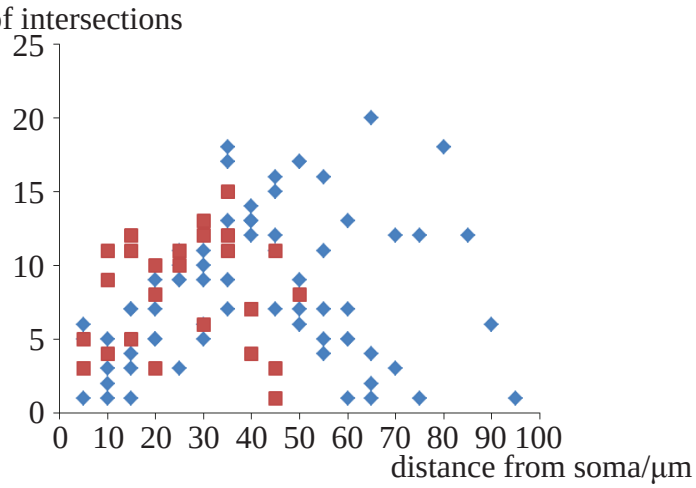


D mean no. of intersections

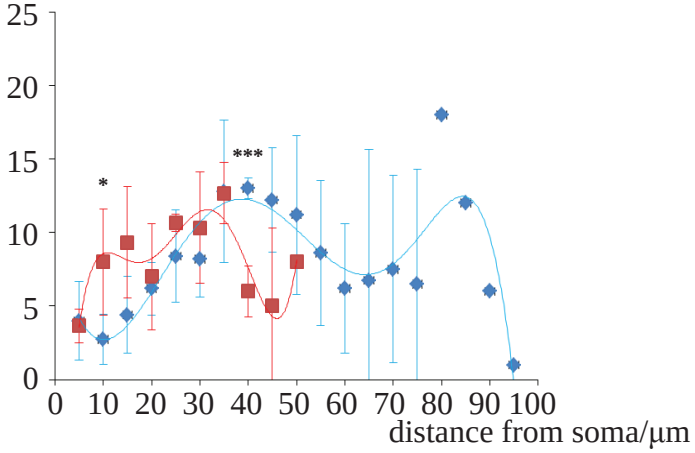

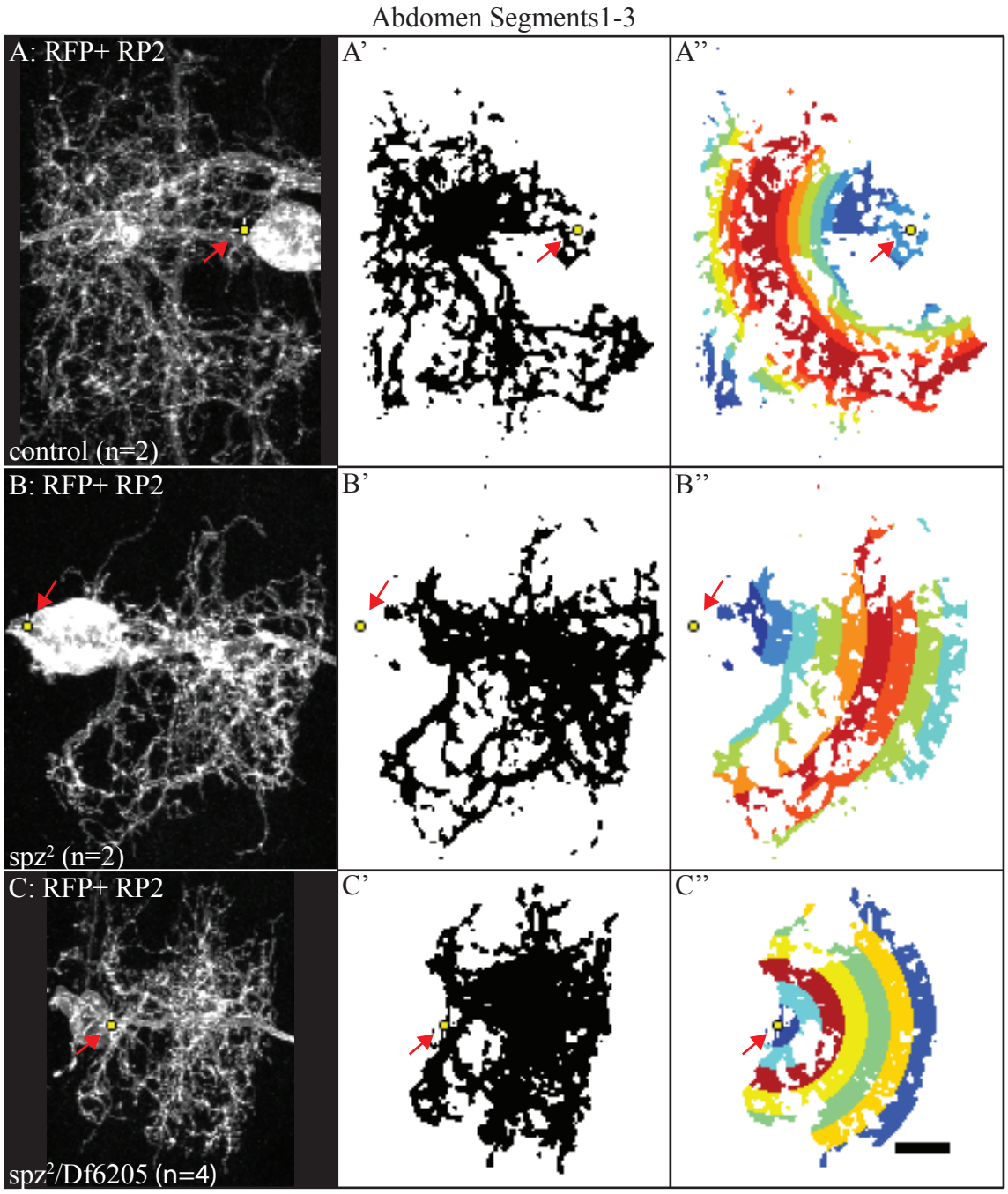


**Figure 5.29** Sholl analysis comparing control, *spz²* and *spz²/Df(3R)Exel6205* abdominal 1-3 RFP+ RP2 neurons. **(A, B, C)** Raw images in maximum projection and in horizontal view. **(A', B', C')** Corresponding segmented images. **(A", B", C")** Sholl profiles.

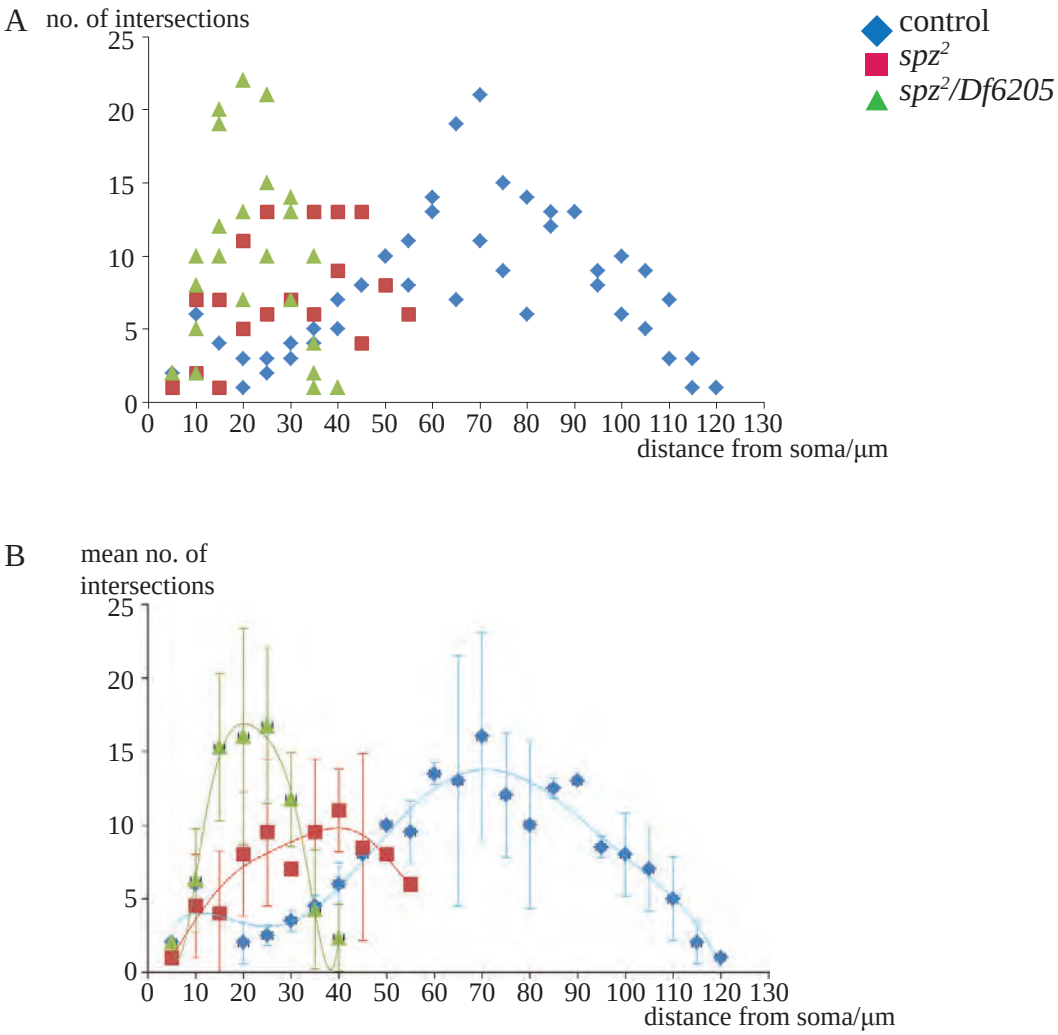


**Figure 5.30** Sholl profile corresponding to Figure 5.29. **(A)** Profile of number of intersection points at distances in 5µm increments from the soma. Each blue diamond marker represents an intersection for the control genotype (n=2). Red squares, *spz*$^{2}$ (n=2). Green triangles, *spz*$^{2}$/*Df(3R)Exel6205* (n=4). **(B)** Corresponding mean profile with curve fitted to polynomial function. Red arrows emphasises the yellow dots marking the point at which the main axon leaves the soma. Scale bar, 10µm.

Volume occupancy of RP2 neurons between control and *spz$^{2}$/Df(3R)Exel6205* overlapped in the abdominal segments 6-7 (Figure 5.31).

## 5.3 Discussion

### 5.3.1 CNS Size Experiments

The brains of *spz$^{2}$ca$^{1}$/Df6205* did not phenocopy those of *spz$^{2}$ca$^{1}$* in size. Given that the allele *spz$^{2}$* arose through chemical mutagenesis, it is conceivable that there are other possible mutated genes, in the form of recessive alleles, elsewhere of *Df(3R)Exel6205*, which interact with *spz$^{2}$* in homozygosis to result in the small brain phenotype. However, the suggestion of *ca$^{1}$* interacting with *spz$^{2}$* to reduce CNS size has been tested to be incorrect because *spz$^{2}$ca$^{1}$*, *spz$^{2}$ca$^{+}$.33* and *spz$^{2}$ca$^{+}$.56* brains were similar to each other. Therefore, the interacting factor of *spz$^{2}$* to affect CNS size remains unknown. This unknown interaction would have disrupted the development of the medulla neuropile in *spz$^{2}$ca$^{1}$* as shown in Figure 5.14.

While the *spz$^{2}$ca$^{1}$* VNC was smaller than *yw*, the Ebony+ neuropile associated glia numbers were unaffected and the Ebony+ glia were more tightly packed into the VNC. Repo+ glial numbers were also not affected in *spz$^{2}$ca$^{1}$*. Therefore, the small VNC size of *spz$^{2}$ca$^{1}$* could not be a result of deficient glia numbers packing in the VNC. While there was no obvious qualitative difference between anti-Elav stainings of *yw* and *spz$^{2}$ca$^{1}$*, whether or not the small VNC could be attributed to neuronal numbers, the current combination of staining with anti-Elav followed by automatic counting with DeadEasy would not be an accurate means to measure neuronal abundance in the VNC cortex.

**Figure 5.31** Sholl analysis comparing between control and *spz²/Df(3R)Exel6205* abdominal 6-7 RFP+ RP2 neurons. **(A, B)** Raw images in maximum projection and in horizontal view. **(A', B')** Corresponding segmented images. **(A", B")** Sholl profiles. **(C)** Profile of number of intersection points at distances in 5 µm increments from the soma. Each blue diamond marker represents an intersection for the control genotype (n=2). Green triangles, *spz²/ Df(3R)Exel6205* (n=3). **(D)** Corresponding mean profile with curve fitted to polynomial function. Red arrows emphasises the yellow dots marking the point at which the main axon leaves the soma. Scale bar, 25µm.

Abdomen Segments 6-7

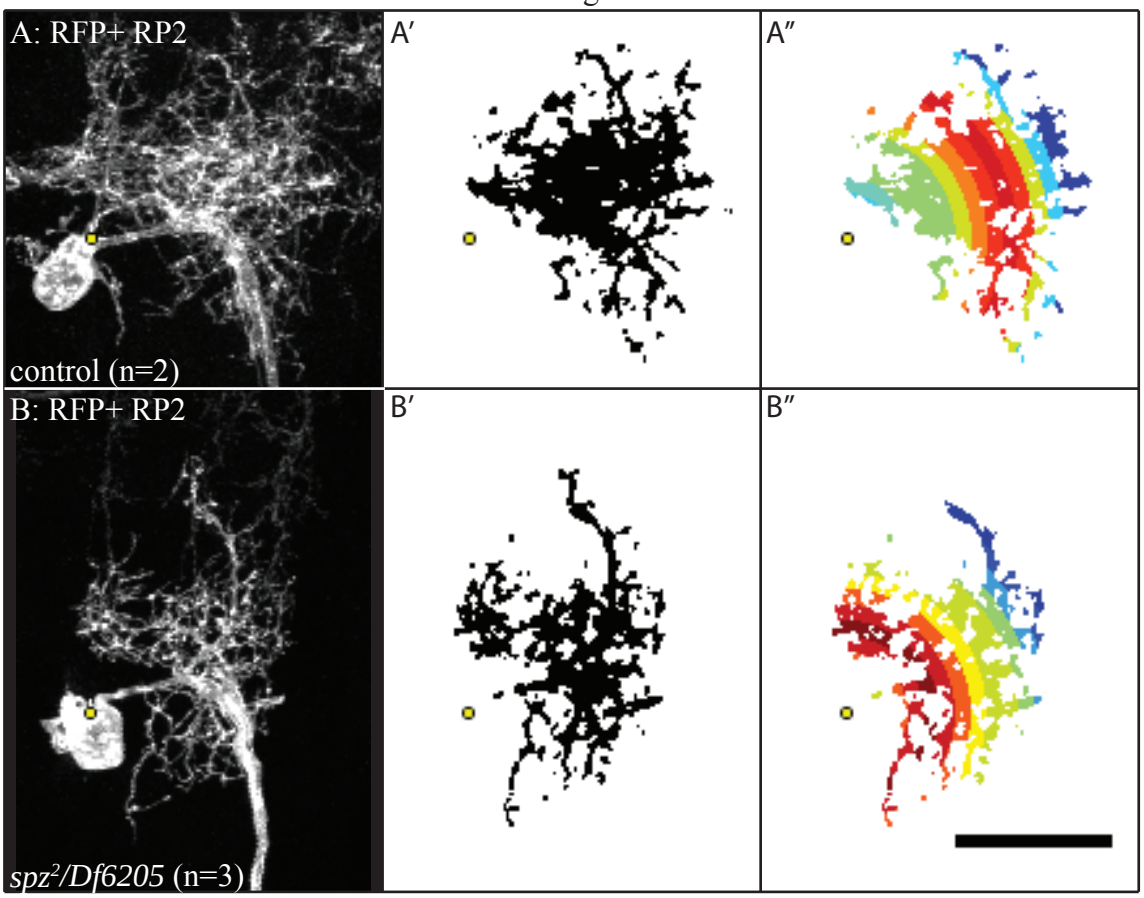


C

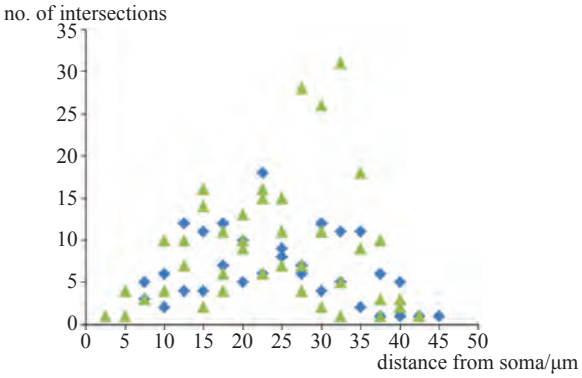



D

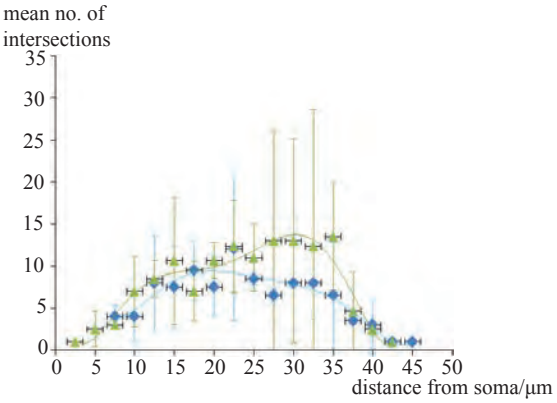

VNC size of $spz^2$ could be rescued with $spz^2$,*elav*> $spz^2$,$Toll^{10b}$ and $spz^2$,*elav*> $spz^2$,$Toll6^{CY}$. VNC size were extended longer than *yw* in $spz^2$,*elav*>$spz^2$,*p35*, $spz^2$,*repo*>$spz^2$,$Toll^{10bB}$ and $spz^2$,*repo*> $spz^2$,$Notch^{ICD}$. Accordingly, there was a positive association between rescued VNC size with higher SI values and extended VNC size with lower SI values. The extended VNC in genotypes $spz^2$,*repo*> $spz^2$,$Toll^{10bB}$ and $spz^2$,*repo*> $spz^2$,$Notch^{ICD}$ could be due to genetic interactions affecting a combination of the extracellular matrix and glia that result in an elongated VNC phenotype. Toll is known to mediate cell-cell interactions to orient cell arrangements (Pare *et al.*, 2014). Notch signalling in glia has been reported to cause neighbouring differentiating enruons to extrude a mesh of filopodia into the extracellular space (Kuzina *et al.*, 2011). Also, glycosyltransferase Fringe has been reported to induce longitudinal glia to activation of Notch signalling (Thomas and van Meyel, 2007).

It was observed that $spz^2$ viability was better in $spz^2$,*repo*>$spz^2$,*actSpz(2)* than $spz^2$,*elav*>$spz^2$,*actSpz(2)*, and vice versa for $Toll^{10bB}$. An explanation was provided in the above paragraph for $Toll^{10bB}$, but more data is required in the form of CNS sizes from genotypes $spz^2$,*repo*>$spz^2$,*actSpz(2)* and $spz^2$,*elav*>$spz^2$,*actSpz(2)* to formulate an explanation.

The overexpression of different forms of Spz protein, CysKnot or full-length form, using *spz-GAL4* could have differential effect in VNC length whereby the CK-form gave a longer VNC than the FL-form. However, this conclusion could be marred by the presence of an outlier to skew the mean. Increasing biological samples would resolve the issue. With the combined used of *UAS-myr-Tomato*, *spz-GAL4* was shown to be active in the surface glia and in the neurons. Thus, *spz-GAL4* and *repo-GAL4* would overlap in promoter activity in the surface glia. When CK- and FL-forms were overexpressed in the background of *repo*>$Notch^{ICD}$, their

effect on VNC length did not differ from each other. Therefore, it is unlikely for the CK-form to give a longer VNC than the FL-form unless there were penetrance issues from overexpressing the CK-form. Overexpression of different forms of DNT1 and DNT2 did not affect VNC length.

### 5.3.2 Mitosis and Apoptosis Experiments

Within the non-mitotic zone across all genotypes, the numbers of pH3+ cells did not differ significantly from each other. It was difficult to draw conclusions from these data given the large variance in control group and the low sampling numbers in test groups.

Up to the point of the wandering larvae, the $spz^{2}ca^{1}$ CNS did not grow to wild-type size. Abdominal apoptotic levels were about half that of wild-type in the VNC while abdominal proliferative levels were unchanged. The average absolute numbers of Dcp+ cells in *yw* wandering stage was not instructed in the small CNS of $spz^{2}ca^{1}$. However, whether or not this is biological meaningful at wandering larval stage would require more data analysis to take into account the ratio of dying cells per unit VNC area or volume for control and test genotypes. The VNC of wandering $spz^{2}$,*elav*>$spz^{2}$,*p35* was larger than the VNC of $spz^{2}ca^{1}$. Given that *p35* is an apoptotic inhibitor, this would suggest that the wandering $spz^{2}ca^{1}$ is small due to earlier events of apoptosis.

In the embryos, there were increase cell death in loss of function *dnt1* and *dnt2* loss of function mutants. Although apoptosis was not investigated here for DNT1 and DNT2, proliferation and glial numbers were. These numbers were maintained. If the aim of the larval

life stage is to grow and to do so with organ size adjusted properly to each other before entering pupal stages, perhaps redundancy is employed to achieve this. When the *dnt1* and *dnt2* receptors were affected, that is, Toll7 and Toll6, the double *Toll7 Toll6* mutants have higher proliferative levels, in particular, in the thorax. The number of glial in the thorax is higher but not significant (possibly due to low sample numbers) while the number is significantly higher in the abdomen, therefore the VNC of double mutants *Toll7 Toll6* had more glia, and this might be due to slight qualitative lengthening of the nerve cord. While smaller CNS may compact basal number of glia, longer CNS would require more surface materials and glial support. Perhaps more proliferative signal were instructed too.

### 5.3.3 Sholl Analysis

Sholl analysis gave surprising results. It is not unexpected to expect small RP2 neurons with smaller coverage of dendrites in tightly packed neuropile of $spz^2$. However, $spz^2$*/Df(3R)Exel6205* had no CNS gross size effect but the coverage of A1-3 RP2 neurons in the abdomen was smaller than $spz^2$ and the control. Therefore, at the single cell resolution level, $spz^2$*/Df(3R)Exel6205* were affected. Increasing sample sizes would strengthen the results of this analysis. Whether or not the dendrites were cell-autonomously or non-cell-automously affected would require MARCM clones or the use of dominant negative Spz receptors in the RP2 cells.

### 5.3.4 Locomotion Defects

The $spz^{2}ca^{1}$ flies have been reported to barely walk (Zhu *et al.*, 2008). During the screen for $spz^{2}ca^{+}$ flies, some $spz^{+}$ lines were observed to have locomotion defects (Table 5.2). Therefore, locomotion defects in $spz^{2}ca^{+}$ might be due to a yet identified gene. Given the lack of rescue of $spz^{2}$ brain area (and thereby, the medulla neuropile structure), the unidentified gene is very likely one related to both optic lobe structures and to locomotion. Mutants such as *lobula plateless* (*lop*), *minibrain* (*mnb*), *optomotor blind* (*omb*), *sine oculis* (*so)* and *small optic lobes* (*sol*), as well as double mutants *mnb* with *so,* and *so* with *sol*, exhibit reduction in optic lobe structures as a result of cell date, and the mutants were correlated with locomotor activity rhythm and behaviour changes (Delaney *et al.*, 1991; Helfrich, 1986).

It is important to bear in mind when making future fly stocks to incorporate *spz* loss of function alleles that the locomotion or lethality phenotype is not the criteria used to determine the presence of *spz* loss of function alleles. Instead, the protocol in Figure 2.9 should be used.

### 5.3.5 Limitations of Chapter 5

Males and females were not considered. In hindsight, such a lack of consideration was a limitation to the experiments which involved measuring CNS size experiments, counting cell death number and profiling A6-7 abdominal neurons. This is because there is plenty of evidence in the CNS for prevalent sexual dimorphism (Cachero *et al.*, 2010; Goto *et al.*, 2011; Kimura, 2011; Kimura *et al.*, 2005; Sanders and Arbeitman, 2008; Taylor, 1989). To improve the experiments in this chapter would require repeating the experiments and increasing the sample size to ensure sufficient CNS were collected from each sex.

# Chapter 6

# 6 Functions of the DNTs and the Tolls in Repair Response to Injury

## 6.1 Introduction

With neuropile axon bundles visualised by *G9* and glia with *repo>DsRed* (genotype: *UAS-DsRed/+;G9/+;repo-GAL4/+*), Kato *et al.* (2011) observed in injured VNC that the wound initially expanded, but after 6 hours of culture, the neuropile wound would shrink, and by 22 hours in culture, the wound could closed in completely. The overexpression of the intracellular domain of Notch in glia (genotype: *UAS-DsRed/+;G9/+;repo-GAL4/UAS-Notch$^{ICD}$-myc*) prevented injury-induced apoptosis and there was no observation of wound expansion (Kato *et al.*, 2011). Only wound reduction was observed, and by 13 hours in culture, the neuropile restored in its gross appearance neatly-arranged axon bundles. The above findings suggested that Notch$^{ICD}$ (or the overproduction of glia upon the overexpression of Notch$^{ICD}$) could lead to the production of a trophic factor that promotes wound closure. Here, this chapter is about investigating if Spz, DNT1 or DNT1 could be the factor to promote gross CNS repair.

### 6.1.1 Technical Aspects of the Injury Model

In the stabbing injury model, dissected larval CNS is pierced through the abdomen from the dorsal side with a fine needle. This is technically very difficult because the model is prone to degradation problems. Degradation is common as a result of dissection and tissue piercing.

Degraded CNS has a rough cauliflower-like surface appearance, which is visible under a dissecting stereomicroscope. Within the tissue of non-stabbed samples, degradation can be recognised by cortex or neuropile vacuoles seen with the background signal of immunostained samples (Kato and Hidalgo, 2013). The vacuoles in the degrading larval CNS are reminiscent of inflammation- and injury-induced cavitation in the brain and spinal cord of Sprague Dawley rats, respectively (Ahmed *et al.*, 2014; Fitch *et al.*, 1999).

To avoid degradation, CNS needs to be extracted gently from the larval body without forceful pulling and tugging of surrounding tissue (Kato and Hidalgo, 2013). The damage of the CNS as a consequence of forceful extraction is naked to the visible eye but damaged CNS will disintegrate in culture (Kato and Hidalgo, 2013). During dissection, it is possible to spill the contents of the larval gut – there would be a sudden appearance of food suspensions in the dissecting medium upon breaking the larval body. At this point, the dissecting medium must be replaced so that the food suspensions are not carried over into sterile culture environment. Microbial growth in culture can cause dissected CNS to disintegrate. When piercing the VNC, the needle goes through the abdomen from the dorsal side until the needle hits the bottom of the dissecting dish. It is easy to blunt the tip of the needle, but a larger than necessary wound will inevitably cause the CNS to disintegrate. The wound made by the needle is naked to the visible eye under a dissecting stereomicroscope, so it is important to maintain a sharp needle tip and to ensure that the needle only pierced through the abdomen once without being forceful (Kato and Hidalgo, 2013).

Regular upkeeping of a sharp needle also contributes to achieving consistency in the stabbing injury model. Another way to reach consistency is to use the posterior half of the VNC as the

reference point for the needle to pierce through. CNS samples with cauliflower-like appearance or with extensive vacuolisations are not considered for analysis. Due to the inherent problems in using the stabbing injury model, before investigating whether or not the DNTs and Tolls could affect CNS repair, it was first necessary to observe wound closure in time-lapse.

### 6.1.2 Technical Aspects of Time-Lapse Imaging

The protein-trap line *G9* drives GFP expression from the locus of the *reticulon* gene, whose protein products are associated with the secretory pathway including the endoplasmic reticulum organelle (Morin *et al.*, 2001; Wakefield and Tear, 2006). Effectively, *G9* 3$^{rd}$ instar larvae have high expression of GFP in their VNC neuropile (Morin *et al.*, 2001; O'Sullivan *et al.*, 2012; Wakefield and Tear, 2006). This effectiveness of *G9*'s fluorescing VNC neuropile was therefore utilised to carry out stabbing injury and time-lapse imaging.

It was difficult to book an imaging session of more than 3 hours during the day for time-lapse recordings due to high demand for the Leica confocal system. Therefore, imaging sessions 10 to 15 hours long were done during the evenings. As the computer hardware operating the Leica is old and limited on processing memory, there is a tendency for the image acquisition software to stop operating and close on itself during the overnight imaging. Whenever this happens, the acquired image is lost without being saved. One way to overcome this problem is to use the newer Zeiss confocal system which has a bigger memory and processing capacity. However, the Zeiss system was found to be less effective in maintaining a stable temperature at 25°C in comparison to the Leica. After a session of 12 hours overnight imaging on the

Zeiss, the heated stage recorded a temperature of 28°C. So, time-lapse imaging was preferentially recorded on the Leica despite the risk of losing data. Given that Kato *et al.* (2011) observed wound closure between 6 to 22 hours after stabbing, and that it was necessary to observe for wound closure in this chapter, the time-lapse recording was set up with overnight recording beginning at 6 hours post-stabbing.

### 6.1.3 Specific Aims

The specific aims of this chapter are:

- To reproduce the wound closure in the stabbing injury model as published in papers by Kato *et al.* (2011) and Kato and Hidalgo (2013).
- To assess the effect of $spz^{MA05}$ on the ability of the nerve cord to close nervous system wound.
- To also assess the effect of *Toll6* and *Toll7* loss of function alleles on nervous system wound closure.
- To examine the effects on wound closure by an activated form of Spz, a CysKnot with 3'tail form of DNT1, and a CysKnot-only form of DNT2.

### 6.1.4 Methods in Brief

3 *G9* VNC were stabbed using a needle and subsequently their wound progression was recorded by Z-stack time-lapse imaging. Throughout each Z-stack of images, at each time point, the largest outline of the neuropile wound was set as the ROI area and measured in square microns in ImageJ. Paired t-test were used to compare mean wound areas from two

time points because of related sampling, as opposed to independent sampling, at hourly time points (Section 9.3.1). Bonferroni post hoc corrections were applied to paired t-test p-values (Section 9.3.1).

Using time-lapse imaging to investigate the effect of various genes on VNC wound would be too laborious and would require generating stocks in a *G9* background. Instead, the VNC of test and control (*yw*) genotypes were stabbed using a needle and cultured for 20 to 24 hours before fixing and staining with anti-GS2 antibody. After confocal imaging, ROI was again defined by the largest outline of the neuropile wound throughout each Z-stack, and measured in $\mu m^2$. The data sampled for each genotype were normally distributed with equal variances, so one-way ANOVA and Dunnett post hoc correction were applied to compare mean wound areas of test genotypes to the mean wound area of *yw* (Section 9.3.2 and 9.3.3).

All mean neuropile wound areas were quoted with standard deviation.

## 6.2 Results

### 6.2.1 Assessment of Wound Progression in *G9* VNC Neuropile

In the first recording of an injured *G9* VNC, imaging took place 6 to 21 hours after applying injury (Table 6.1). There was a wound epicentre observed at 6 hours after stabbing injury in the posterior medial of the neuropile (Figure 6.1A). There were also vacuoles surrounding the wound epicentre at the posterior lateral (Figure 6.1A). The vacuoles were considered to be lesion resulting from stabbing injury and were included into the wound ROI. From 6 to 21

| $n^{th}$ *G9* sample | $1^{st}$ | $2^{nd}$ | $3^{rd}$ | Mean wound area, $W_{mean}$ ($\pm$SD $\mu m^2$) |
|---|---|---|---|---|
| Hours after stabbing (hr) | Wound area, W ($\mu m^2$) | | | |
| 3 | | | 2547 | |
| 4 | | | 3303 | |
| 5 | | | 3683 | |
| 6 | 7387 | 3614 | 4359 | 5120±1988 |
| 7 | 7605 | 3428 | 4327 | 5120±2199 |
| 8 | 7948 | 3578 | 4611 | 5379±2284 |
| 9 | 7837 | 3506 | 4401 | 5248±2286 |
| 10 | 6776 | 3072 | 4683 | 4844±1857 |
| 11 | 7475 | 2838 | 5029 | 5114±2320 |
| 12 | 6292 | 2682 | 4561 | 4512±1806 |
| 13 | 5883 | 2614 | 4644 | 4380±1650 |
| 14 | 5745 | 2487 | 4223 | 4152±1630 |
| 15 | 5907 | 1490 | 3751 | 3716±2209 |
| 16 | 5420 | 1645 | | 3533±2669 |
| 17 | 5468 | 1241 | | 3355±2989 |
| 18 | 5541 | | | |
| 19 | 5366 | | | |
| 20 | 5661 | | | |
| 21 | 5493 | | | |
| | $\Delta W/\Delta T_{6\text{-}21h}$ $=-126.3\mu m^2h^{-1}$ | $\Delta W/\Delta T_{6\text{-}17h}$ $=-215.7\mu m^2h^{-1}$ | $\Delta W/\Delta T_{3\text{-}15h}$ $=+100.3\mu m^2h^{-1}$ | $\Delta W_{mean}/\Delta T_{6\text{-}17h}$ $=-160.5\mu m^2h^{-1}$ |
| | $\delta W/\delta T_{6\text{-}15h}$ $=-164.4\mu m^2h^{-1}$ | $\delta W/\delta T_{6\text{-}15h}$ $=-236.0\mu m^2h^{-1}$ | $\delta W/\delta T_{3\text{-}6h}$ $=+604.0\mu m^2h^{-1}$ | |
| | $\delta W/\delta T_{6\text{-}17h}$ $=-174.5\mu m^2h^{-1}$ | | $\delta W/\delta T_{6\text{-}15h}$ $=-67.6\mu m^2h^{-1}$ | |

Table 6.1 Hourly measurements of neuropile wound areas corresponding to the 3 time-lapse imaging events of stabbed *G9* VNC depicted in Figure 6.1.
$\Delta W/\Delta T$ (to 1 d.p.) is the rate of change in wound area from the initial to final time points. $\delta W/\delta T$ (to 1 d.p.) is the rate of change in wound area over smaller defined time periods.

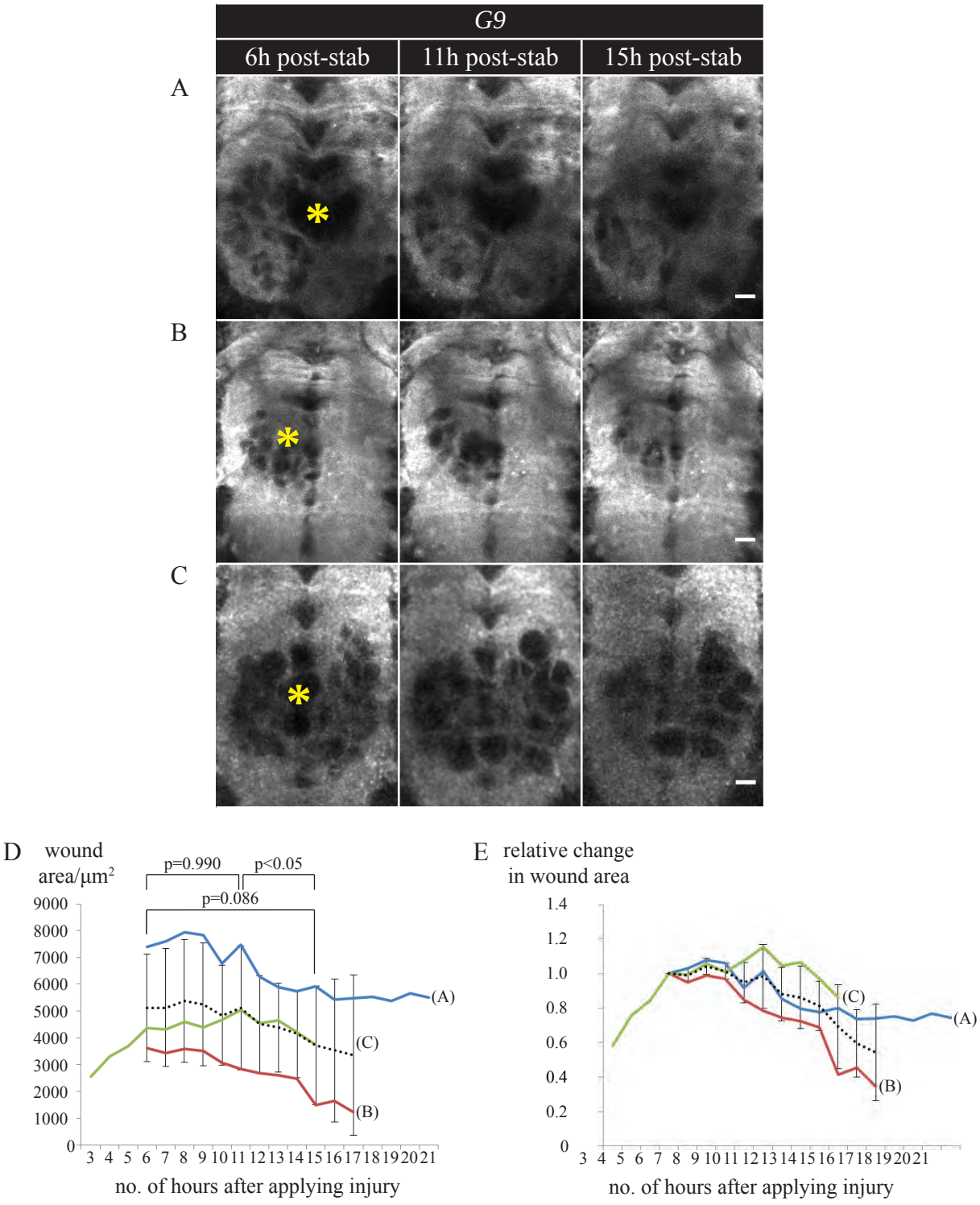


**Figure 6.1** Wound progression among stabbed *G9* larval VNC neuropile (n=3). The yellow asterisk indicates the lesion epicentre in the **(A)** 1st, **(B)** 2nd and **(C)** 3rd *G9* sample. **(D)** Wound area profile of 3 individual *G9* samples from (A) to (C), each represented by solid coloured lines. The mean wound area profile is represented by a dotted black line. Statistics: paired t-test. **(E)** Corresponding profile of relative change in wound area. The reference time is the initial time point common to all the time-lapse recordings, that is, 6 hours after applying injury. Scale bars in (A) to (C) represent 10µm.

hours after injury, the wound area decreased from 7387μm$^2$ to 5493μm$^2$ (Table 6.1, Figure 6.1D), a decrease of approximately a quarter of its initial size (relative change in wound area=0.744, Table 6.2, Figure 6.1E,).

The second injured *G9* VNC was imaged from 6 to 17 hours after stabbing injury (Table 6.1, Figure 6.1B). Wound area was at its largest (3614μm$^2$) and smallest (1241μm$^2$) at the start and end of time-lapse imaging, respectively (Table 6.1, Figure 6.1D). By 17 hours after applying injury, the wound area decreased by approximately two-thirds of its initial size (relative change in wound area=0.343, Table 6.2, Figure 6.1E).

For the third time-lapse recording, stabbed *G9* VNC was imaged beginning at 3 hours after applying stabbing injury (Table 6.1, Figure 6.1C). Between 3 to 6 hours post-injury, the wound area steadily increased ($\delta W/\delta T_{3\text{-}6h}$=+604.0μm$^2$h$^{-1}$, Table 6.1, Figure 6.1D). From 6 hours onwards after injury, the wound area continued to increase, until at 11 hours post-stabbing, the wound area began to decrease, and by 15 hours after stabbing, the wound area decreased by approximately one- tenth of the size at 6 hours post-injury (relative change in wound area=0.861, Table 6.2, Figure 6.1E).

The wound kinetics in each of the three stabbed *G9* VNC were different to each other in terms of when the wound area stopped expanding upon injury (1$^{st}$ *G9*: 8 hours after injury; 2$^{nd}$ *G9*: 11 hours after injury; 3$^{rd}$ *G9*: wound expansion not observed). There was also a difference in the degree of wound area change. For example, from 6 to 15 hours post-injury, the relative changes in wound area for the 1$^{st}$, 2$^{nd}$ and 3$^{rd}$ *G9* sample were 0.800, 0.412 and 0.861, respectively (Table 6.2). The corresponding rates of change in wound area ($\delta W/\delta T_{6\text{-}15h}$)

| *N*th *G9* sample | 2nd | 3rd | 4th | Mean relative change in wound area |
|---|---|---|---|---|
| Hours after stabbing (hr) | Relative change in wound area | | | |
| 3 | | | 0.584 | |
| 4 | | | 0.758 | |
| 5 | | | 0.845 | |
| 6* | 1.000 | 1.000 | 1.000 | 1.000 |
| 7 | 1.030 | 0.949 | 0.993 | 0.990 |
| 8 | 1.076 | 0.990 | 1.058 | 1.041 |
| 9 | 1.061 | 0.970 | 1.010 | 1.014 |
| 10 | 0.917 | 0.850 | 1.074 | 0.947 |
| 11 | 1.012 | 0.785 | 1.154 | 0.984 |
| 12 | 0.852 | 0.742 | 1.046 | 0.880 |
| 13 | 0.796 | 0.723 | 1.065 | 0.862 |
| 14 | 0.778 | 0.688 | 0.969 | 0.812 |
| 15 | 0.800 | 0.412 | 0.861 | 0.691 |
| 16 | 0.734 | 0.455 | | 0.594 |
| 17 | 0.740 | 0.343 | | 0.542 |
| 18 | 0.750 | | | |
| 19 | 0.726 | | | |
| 20 | 0.766 | | | |
| 21 | 0.744 | | | |

Table 6.2 Relative changes in neuropile wound areas for the corresponding 3 time-lapse imaging events of stabbed *G9* VNC depicted in Figure 6.1.
The relative change in wound area is the ratio of wound area at any given time point over the reference wound area at 6 hours (*) after applying injury. The reference wound area is the initial time point which is common to all 3 time-lapse imaging events.

were -164.4μm$^2$h$^{-1}$, -236.0μm$^2$h$^{-1}$ and -67.6μm$^2$h$^{-1}$, respectively (Table 6.1). There could be an association between the smaller wound in the 2$^{nd}$ *G9* sample (Figure 6.1B) with faster wound shrinkage ($\delta W/\delta T_{6\text{-}15h}$ =-236.0μm$^2$h$^{-1}$), and the larger wounds in the 1$^{st}$ and 3$^{rd}$ samples (Figure 6.1A and C) with slower wound closure (1$^{st}$ *G9*: $\delta W/\delta T_{6\text{-}15h}$ =-164.4μm$^2$h$^{-1}$; 3$^{rd}$ *G9*: $\delta W/\delta T_{6\text{-}15h}$=-67.6μm$^2$h$^{-1}$) (Dr A. Hidalgo and Dr K. Kato, personal communication). The differences in wound kinetics in terms of when wound stopped enlarging, and in terms of how fast the rate of shrinkage occurred, reflect the challenges in using the current injury model. Nonetheless, the wound at 6 hours post-injury could shrink to approximately half of its size by 17 hours after stabbing (mean relative change in wound area=0.542, Table 6.2, Figure 6.1E). Wound enlargements were no longer observed among stabbed *G9* samples at 11 hours after injury. So, while the mean wound areas between 6 and 15 hours post-stabbing were not statistically different to each other (paired t-test $t(2)=3.196$, $p=0.086$), the mean wound areas between 6 and 15 hours post-injury were statistically different (paired t-test $t(2)=16.001$, $p<0.01$, Bonferroni post hoc $p<0.05$). The significant reduction in mean wound area indicates that wound closure using the stabbing injury model was reproducible in this project.

### 6.2.2 Effect of Spz on Wound Size

Stabbing *yw* VNC (n=24) resulted in a mean neuropile wound area of 4575±1858μm$^2$ between 20 to 24 hours later (Figure 6.2). In loss of function genotype *spz$^{MA05}$/ Df(3R)Exel6205* (n=6), stabbing resulted in a mean wound of 6674±1935μm$^2$ at 20 hours after injury. The mean wound area as a result of stabbing injury in *spz$^{MA05}$/Df(3R)Exel6205* was statistically larger than the mean in *yw* (one-way ANOVA $F(3)=4.087$, $p<0.05$, Dunnett post-hoc $p=0.031$). Overexpression of an activated form of Spz (genotype: *UAS-actSpz(2)*) under

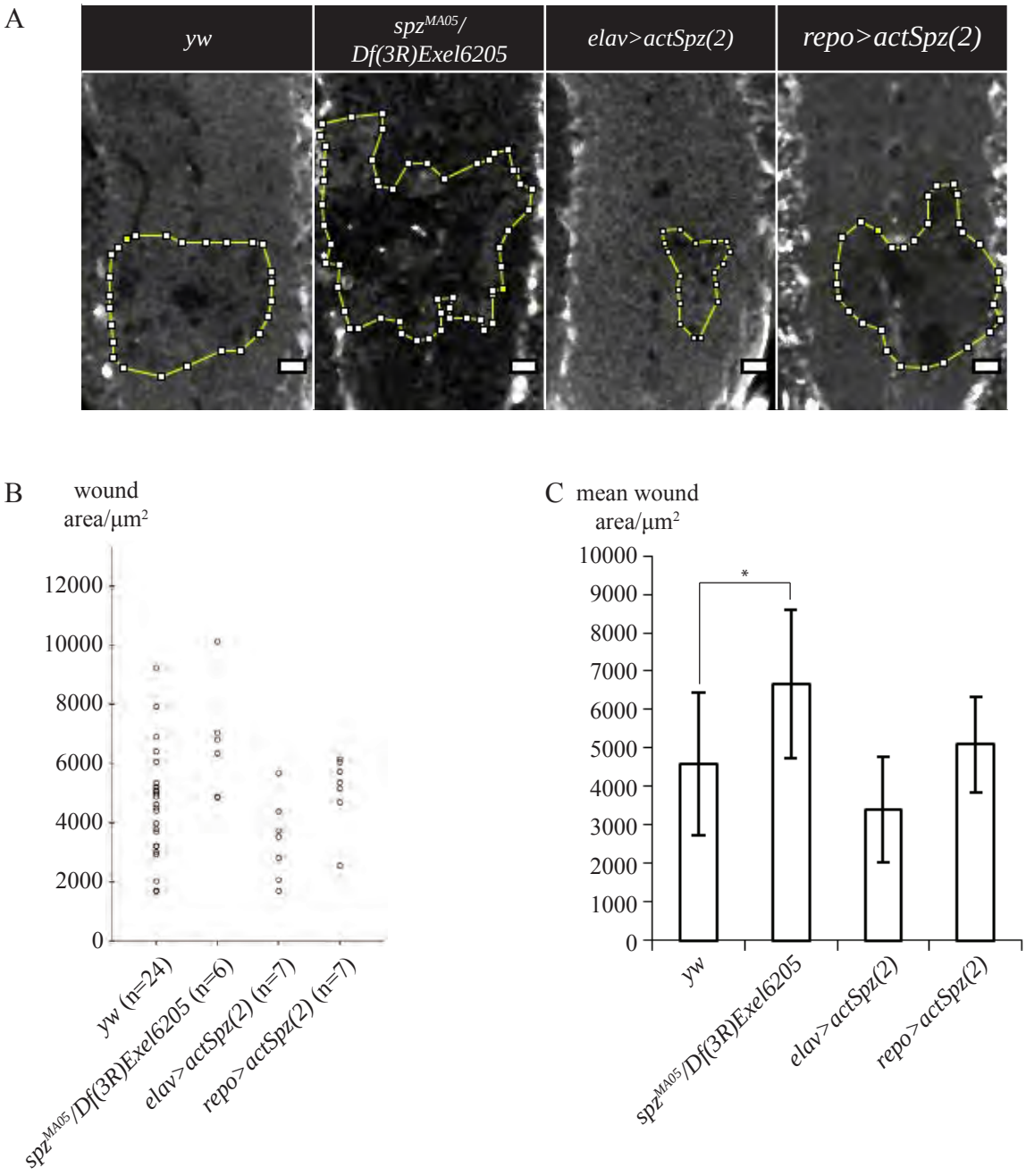


**Figure 6.2** Effect of Spz on neuropile wound. **(A)** Single optical slice examples of wound in genotypes *yw*, *spz*$^{MA05}$*/Df(3R)Exel6205*, *elav>actSpz(2)* and *repo>actSpz(2)*. **(B)** Values of neuropile wound area between 20 to 24 hours after applying stabbing injury. **(C)** Corresponding mean neuropile wound area. Scale bars in **(A)** represent 10µm.

neuronal driver *elavGAL4* (n=7) lowered the mean wound area from control to 3411± 1373μm$^2$ at 24 hours after injury, albeit not significantly (one-way ANOVA F(3)=4.087, p=0.314). When activated Spz was overexpressed under glial driver *repoGAL4* (n=7), the mean neuropile wound area increased to control to 5097±1231μm$^2$ at 21 hours after injury, but not significantly (one-way ANOVA F(3)=4.087, p=0.853).

### 6.2.3 Effect of Toll6, Toll7, DNT1 and DNT2 on Wound Size

The mean neuropile wound area at 20 to 21 hours after injury in *Toll7$^{P114}$/Toll7$^{P8}$;Toll6$^{31}$/ Toll6$^{26}$* double loss of function mutant was 4516±1562μm$^2$ (Figure 6.3). This mean value was virtually not different to control whose mean was 4575±1858μm$^2$ at 20 to 24 hours post injury. When *elav-GAL4* was used to overexpress an activated DNT1 in the form of CysKnot with 3' tail (genotype: *UAS-DNT1-CK3'+*), the mean wound area (4399±1352μm$^2$) at 22 hours post stabbing was also virtually not different to control. The lack of difference in comparing to control mean wound area was also observed when *elav-GAL4* overexpressed activated DNT2 CysKnot (genotype: *UAS-DNT2-CK-6A*) and the resulting mean wound area after 21hours of applying injury was 4666±1869μm$^2$. In contrast, when *repo-GAL4* was crossed to *UAS-DNT1-CK3'+*, the mean neuropile wound area at 22 hours after injury was lowered from control to 3893±149μm$^2$. This was also the case in *repo>DNT2-CK-6A*, in which the mean wound area at 21 hours post-injury was 3172±908μm$^2$. However, the reduction in mean neuropile wound areas were not statistically different in the data set of Figure 6.3 (one-way ANOVA F(5)=0.708, p=0.621).

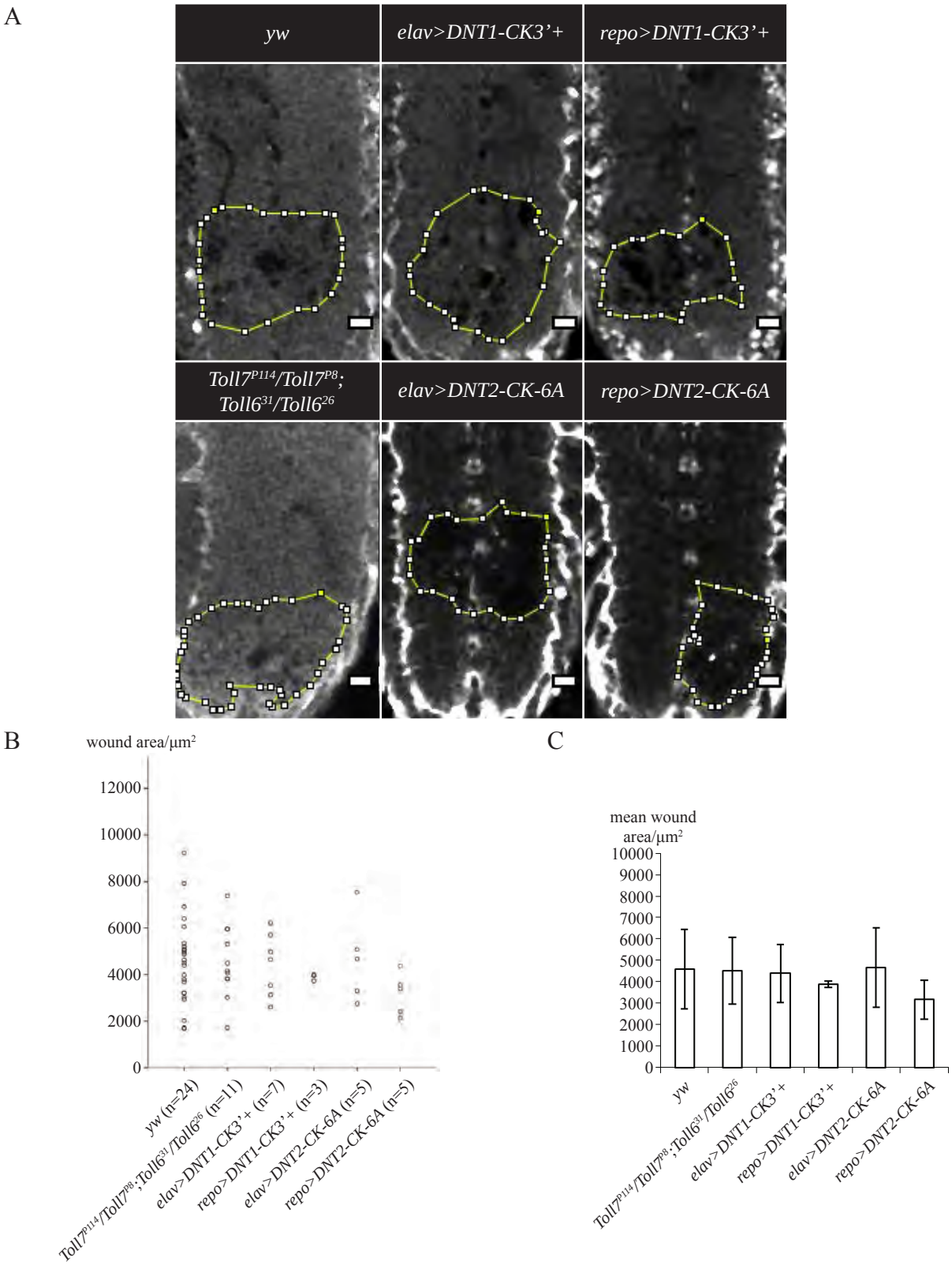


**Figure 6.3** Effect of Toll6, Toll7, DNT1 and DNT2 on neuropile wound. **(A)** Single optical slice examples of wound in genotypes *yw*, *Toll7$^{P114}$/Toll7$^{P8}$;Toll6$^{31}$/Toll6$^{26}$*, *elav>DNT1-CK3'+*, *repo>DNT1-CK3'+*, *elav>DNT2-CK-6A* and *repo>DNT2-CK-6A*. **(B)** Values of neuropile wound area between 20 to 24 hours after applying stabbing injury. **(C)** Corresponding mean neuropile wound area. Scale bars in (A) represent 10µm.

## 6.3 Discussion

### 6.3.1 Importance of Replicating Injury Model

One of the main characteristics of the stabbing injury model described in the papers by Kato *et al.* (2011) and (Kato and Hidalgo, 2013) is a natural wound area shrinkage over time in the VNC. A similar shrinking in wound area over time was demonstrated in this project too, particularly between 11 and 15 hours after applying stabbing injury to *G9* VNC (Figure 6.1D). However, Kato *et al.* (2011) observed that wound closure began at 6 hours after stabbing injury. The 5-hour difference in the start of wound closure reflects the technical difficulties in using the stabbing injury model, which is sensitive to degradation. Also, the exact size of the starting lesion cannot be fully controlled in the stabbing injury model. Nonetheless, technical care, such as gentle dissection and frequent maintenance of a sharp needle tip, were taken to achieve consistency in applying stabbing injury. Due to the challenges in carrying out the stabbing injury model, before investigating the effects of genes on the ability of the CNS to close a wound as a result of piercing the nerve cord, it was important to have demonstrated wound shrinking first in Figure 6.1.

### 6.3.2 Effects on Wound Closure

In this project, almost all cases of test genotypes did not have an effect on the nerve cord to close a stabbing injury wound. The test genotypes which were not significant different from control *yw* are: *$Toll7^{P114}$/$Toll7^{P8}$;$Toll6^{31}$/ $Toll6^{26}$*, *elav>DNT1-CK3'+*, *repo>DNT1-CK3'+*, *elav>DNT2-CK-6A*, *repo>DNT2-CK-6A*, *elav>actSpz(2)*, *repo>actSpz(2)*. The only

genotype which resulted in a statistically significant increase in mean VNC neuropile wound area was $spz^{MA05}/Df(3R)Exel6205$. The loss of *spz* function could have exacerbated wound expansion, or slowed down wound closure, or a combination of both.

# Chapter 7

# 7 Discussion

## 7.1 Summary of Findings

### 7.1.1 Major Findings in Chapter 3

The specific aims of this chapter were:

- To characterise reporter patterns of *dnt1-*, *dnt2-* and *spz-GAL4* in the larval VNC.
- To characterise larval VNC EGFP patterns of *Mi{MIC}* insertions into the *spz* and *Toll6* gene.
- To characterise immunostaining patterns of anti-DNT1, anti-DNT2 and anti-Spz antibodies in the larval VNC.
- To characterise immunostaining patterns on anti-Toll and anti-Toll7 antibodies in the larval VNC.

The author characterised the reporter patterns of *dnt1-*, *dnt2-* and *spz-GAL4* successfully. The *Mi{MIC}*-GFP patterns in the larval VNC were also successfully characterised. While there was extensive work done for the characterisation of anti-DNT1, anti-DNT2 and anti-Spz, these antibodies were not specific. Despite this limitation, anti-DNT1-VRY and anti-DNT2-KRLwere able to detect the epitopes of activated DNT1 and DNT2 in genotypes *elav>DNT1-CK-3'+* and *elav>DNT2-CK-6A*.

Anti-Spz-GLR did not detect activated Spz in genotype *repo>actSpz(2)*. However, anti-Spz-GLR and the EGFP pattern in $spz^{Mi08633}$ matched spatially in the larval VNC. The axon bundles in the mechanosensory domain were revealed with both anti-Spz-GLR and anti-EGFP stainings. In addition, *spz>myr-tdTomato* reporter signal was complementary to the anti-Spz-GLR and EGFP patterns. Given that myr-tdTomato is targeted to the membrane, Spz could be inferred to be a secreted protein that is deposited into synaptic rich areas of the mechanosensensory domain with the third instar larval VNC neuropile.

The patterns of anti-Toll-d300 and anti-Toll7-AAQ were characterised successfully in *G9* and *yw* control genotypes, respectively. Although the aim of characterising anti-Toll-d300 and anti-Toll7-AAQ was achieved, future work would benefit from immunostaining third instar larval VNC in loss of function genotypes for *Toll* and *Toll7*.

### 7.1.2 Major Findings in Chapter 4

The specific aims of this chapter were:

- To generate a loss of function allele of *dnt2* and *spz* by hsFLP-FRT deletion.
- To classify any newly generated *spz* allele.
- To characterise the viability of any newly generated *dnt2* and *spz* allele.

The author did not generate a loss of function allele of *dnt2*. The fly stock carrying the allele $dnt2^{37}$ was a gift of Dr. J. Wentzell, and this allele was shown to be semi-lethal, reducing viability of larvae reaching pupal stages.

Only new alleles of *spz* were established. The new allele $spz^{MA05}$ has been shown to have a loss of function nature through the lack of ventralising signal when patterning the DV axis in offspring of $spz^{MA05}$/*Df(3R)Exel6205* mothers. The larvae of genotype $spz^{MA05}$/*Df(3R)Exel 6205* are semi-lethal.

### 7.1.3 Major Findings in Chapter 5

The specific aims of this chapter are:

- To characterise $spz^2ca^1$ and $spz^2ca^+$ in terms of CNS size.
- To test *Toll6* and *Toll7* as putative receptors of *spz* using SI assays.
- To test *Toll6* and *Toll7* as putative receptors of *spz* using CNS size.
- To characterise the CNS size when *spz* is overexpressed by *spz-GAL4*.
- To test for an interaction between DNTs and Notch using VNC size phenotype.
- To investigate if Spz, DNT1, DNT2, Toll, Toll6 and Toll7 affect Repo+ cell number.
- To investigate if Spz, DNT1, DNT2, Toll, Toll6 and Toll7 affect pH3+ cell number.
- To investigate if Spz, DNT1, DNT2, Toll, Toll6 and Toll7 affect Dcp1+ cell number.
- To characterise the dendrites of $spz^2$ RP2 neurons according to Sholl analysis.

The genotypes $spz^2ca^1$ and $spz^2ca^+$ were characterised in terms of CNS size, and it has been concluded that $ca^1$ is not the contributing factor leading to loss of medulla neuropile. The locomotion defect in genotype $spz^2ca^1$ is very likely not attributed to $spz^2$.

According to SI assays, there is a stronger genetic interaction between *Toll* and *Toll6* with *spz* from overexpression using *elav-GAL4*. More CNS data is required for *Toll6* and *Toll7* from

overexpression using *repo-GAL4*, although SI assays from *spz*$^{2}$,*elav>spz*$^{2}$,*Toll6*$^{CY}$ suggest *Toll6* is a good candidate for Spz as a receptor.

VNC lengths were characterised from overexpression *spz-GAL4* lines. No conclusion can be derived from this experiment due to negative results.

*Repo>Notch*$^{ICD}$ together with either mature Spz (*actSpz*) or full-length Spz (*spz-FL*) significantly reduced the extended VNC length exhibited by *repo>Notch*$^{ICD}$ alone. When *repo>Notch*$^{ICD}$ took place in homozygous *spz*$^{2}$ mutant background, the VNC significantly lengthen when compared to the control background, *repo>Notch*$^{ICD}$ alone. *Repo>Notch*$^{ICD}$ with mature or full-length DNT1 and DNT2 did not have an effect on the extended VNC length exhibited by *repo>Notch*$^{ICD}$ alone. Rather than assessing whether the DNTs interacted with Notch, these VNC length assay instead informed Spz was different from DNT1 and DNT2 in exerting effects on VNC length in the background *repo>Notch*$^{ICD}$.

The following genotypes were assessed for counting glia: *spz*$^{2}$*ca*$^{1}$*/spz*$^{2}$*ca*$^{1}$, *spz*$^{2}$*ca*$^{1}$*/Df(3R)Exel6205*, *spz*$^{MA05}$*/Df(3R)Exel6205*, *dnt1*$^{41}$*/Df(3L)Exel6101*, *dnt2*$^{37}$*/Df(3L)Exel6092* and *Toll7*$^{P114}$*/Toll7*$^{P8}$*;Toll6*$^{31}$*/Toll6*$^{26}$. The mean number of thoracic Repo-positive cells from each genotype did not significantly differ from *yw.* The genotypes with a significantly increased mean number of abdominal Repo-positive cells than *yw* were *spz*$^{2}$*ca*$^{1}$*/Df(3R)Exel6205, spz*$^{MA05}$*/Df(3R)Exel6205* and *Toll7*$^{P114}$*/Toll7*$^{P8}$*;Toll6*$^{31}$*/Toll6*$^{26}$. Due to lack of time, single mutant *Toll6*$^{31}$*/Toll6*$^{26}$ and gain of function studies were not explored.

Again, due to the lack of time, no gain of function studies was done with anti-pH3 stainings. The only genotype with a mean number of thoracic pH3-positive cells to significantly increase from *yw* was $Toll7^{P114}/Toll7^{P8};Toll\text{-}6^{31}/Toll\text{-}6^{26}$. The mean number of abdominal pH3-positive cells from each genotype did not significantly differ from *yw*.

The mean numbers of abdominal Dcp1-positive cells in $spz^{2}ca^{1}/Df(3R)Exel6205$ and $spz^{MA05}/Df(3R)Exel6205$ were not significantly different from *yw*, while there was significantly less Dcp1-positive cells in homozygous $spz^{2}ca^{1}$ mutants. Given time constraints, thoracic regions and gain of function studies were left out.

The RP2 dendrites in thoracic segments 1-3 of homozygous $spz^{2}$ occupied a smaller field than the RP2 dendrites of control genotype. So did the RP2 neurons of both homozygous $spz^{2}$ and heterozygous $spz^{2}/Df6205$ in the abdominal segments 1-3.

The major limitation of this chapter is the general low sampling number throughout experiments coupled with neglecting sexual dimorphism in the larval CNS. A minor limitation is the lack of normalised data between cell counts and VNC area or volume.

### 7.1.4 Major Findings in Chapter 6 and Future Work

The specific aims of this chapter were:

- To reproduce the wound closure in the stabbing injury model as published in papers by Kato *et al.* (2011) and Kato and Hidalgo (2013).

- To assess the effect of $spz^{MA05}$ on the ability of the nerve cord to close nervous system wound.
- To also assess the effect of *Toll6* and *Toll7* loss of function alleles on nervous system wound closure.
- To examine the effects on wound closure by an activated form of Spz, a CysKnot with 3'tail form of DNT1, and a CysKnot-only form of DNT2.

Wound closure in stabbed *G9* samples was reproduced in this project. However, the kinetics of the wound closure in this project was slower in comparison to the kinetic measured by Kato *et al.* (2011). This reflects the technical difficulty for the author to master application of the stabing injury model. Therefore, all assessments of genetic effects on the ability of the nerve cord to close a wound must be treated with pessimism, in particular when concluding an association between loss of *spz* and lack of wound closure. For this association to strengthen, the sample size of stabbed $spz^{MA05}$*/Df(3R)Exel6205* VNC must increase to at least match the sampled size of control genotype. With respect to meeting the aims of this chapter and contributing to scientific knowledge, the author acknowledged that the results of this chapter require replication.

The author avoided describing a closure in wound area as wound repair because only gross neuropile structures were observed through the use of *G9* and anti-GS2 antibodies. There were no attempts in this work to label single axons to observe any fine structural changes upon stabbing injury. Due to the lack of definition for structural 'repair' in this project, the author found it challenging to apply the results of this chapter to mammalian studies of CNS development and regeneration. In addition, there was no time to experiment on how lack of

*spz* contributed to increasing wound area. While losing *spz* function was found weakly associated to a negative effect on wound closure, overexpressing Spz either under neuronal or glial driver had no impact on the rate of wound closure. In order to explain this, future work would have to include overexpressing activated Spz in the background of $spz^{MA05}$*/Df(3R)Exel 6205*. If the overexpression of functional Spz should lower the wound area in $spz^{MA05}$*/Df(3R) Exel6205*, it would indicate that Spz is one of the factors required in repair but that an excess amount of Spz is unnecessary and insufficient to further close in wound area, thus explaining the neutral effect on wound closure when neurons overexpressed activated Spz.

## 7.2 Conclusions on the DNTs and Tolls in the Larval VNC

During the course of this thesis, and together with the author's data, the Hidalgo lab published that Toll-6 and Toll-7 are neurotrophic receptors (McIlroy *et al.*, 2013). DNT1 is found to bind Toll7, while DNT2 binds both Toll-6 and Toll-7 (McIlroy *et al.*, 2013). There are no good antibodies for labelling Toll-6, but there is an available Mi{MIC}-GFP for Toll-6. Toll-6 is expressed in many cell bodies, dorsally and ventrally. The Mi{MIC}-GFP pattern do not match to the *in situs* pattern clearly (McIlroy, 2012; McIlroy *et al.*, 2013). However, the combine use of Toll-6 Mi{MIC}-GFP and *D42(Toll-6)-GAL4* motoneuron reporter show that Toll-6 is expressed in the the aCC motoneurons, but not the RP2s. Motoneurons underlie larval locomotion behaviour and *Toll-6* mutants exhibit locomotion defects (McIlroy *et al.*, 2013). Anti-Toll7-AAQ reveals Toll-7 in the neuropile of the VNC, central brain and optic lobes. The staining pattern matches the *in situ* pattern of *Toll-7* transcripts, especially in the neuropile of the central brain and optic lobes (McIlroy, 2012; McIlroy *et al.*, 2013). Toll-6 in aCC motoneurons and Toll-7 in the neuropile are in VNC areas relevant to DNT2 in the

dorsal neuropile. DNT1 in the neuropile also is in the relevant VNC region to Toll-7. Given that the Toll protein family is collectively known for innate immunity functions (Leulier and Lemaitre, 2008; Ooi *et al.*, 2002; Tauszig *et al.*, 2000), the discovery of Toll-6 and Toll-7 as neurotrophic factors provides an insight into understanding how receptors in the same protein family can signal and function in different systems. This is relevant for studies of vertebrate Toll-like receptors in neurobiology and of neurotrophic factors in immunity (Barak *et al.*, 2014; Hepburn *et al.*, 2014; Larsen *et al.*, 2007; Okun *et al.*, 2011).

Spz is restricted to the mechanosensory domain while DNT2 are distributed along DM and DL neurons. Neurites of sensory projections project into the ventral region while neurites of motoneurons project into the dorsal region (Landgraf *et al.*, 2003). There are few, if any, direct monosynaptic connections between sensory and motoneurons (Landgraf *et al.*, 2003). This suggests Spz and DNT2 are very likely expressed by different neurons in the VNC. Because specific neuronal classes project to different medio-lateral domains and to different dorso-ventral layers of the neuropile (Zlatic *et al.*, 2009), Spz and DNT2 can be thought to serve different modalities. This situation is reflected in embryonic motoneuron targeting and at the larval NMJ whereby DNT function with neuron-type specificity (Sutcliffe *et al.*, 2013; Zhu *et al.*, 2008). *Spz* mutation affects embryonic SNa motor axons and larval muscle 4 NMJ; *dnt1* mutation affects embryonic ISNb/d motor axons; and double *dnt1 dnt2* mutations affect muscle 6-7 NMJ (Sutcliffe *et al.*, 2013; Zhu *et al.*, 2008). Therefore, DNT in the larval VNC lends more semblances to vertebrate NTs in displaying function which depends on neuronal modalities (Zhu *et al.*, 2008).

Toll is the receptor for Spz, and commercial anti-Toll-d300 reveals Toll signal in the larval CNS too. However, the larval atterns of Spz and Toll distribution do not match. In stage 15 embryos, *spz* transcripts are expressed in the midline while Toll is detected the in CNS axons and in some midline cells (Zhu *et al.*, 2008). Spz's larval distribution is along the entire mechanosensory domain of the VNC while Toll is restricted to simple neuronal processes in the thorax. In the optic lobe, Spz is missing while Toll is in the neuroepithelia, inner proliferative centre (IPC) and OPC. This suggests Toll's expression in the VNC is temporally regulated from embryonic to larval stages. The neuronal processes in the thorax revealed by anti-Toll-d300 are indicative of immature neuronal cells in arrest, acting as functional stockpile for future use in the adult (Li *et al.*, 2014). This may even suggests that Toll's expression is spatially regulated to prevent signalling with Spz and any resulting inappropriate neuronal function such as misspecification of normal VNC length.

Biochemical studies are required to follow up from SI assays and CNS size experiments to confirm that Toll6 and Spz bind to each other. Spz has already been proposed to bind Toll2, Toll3, Toll8 and Toll9 through the investigating apoptosis (Meyer *et al.*, 2014b).

## 8 References


ABRESCIA, C., SJOSTRAND, D., KJAER, S. & IBANEZ, C. F. 2005. Drosophila RET contains an active tyrosine kinase and elicits neurotrophic activities in mammalian cells. *FEBS Lett,* 579**,** 3789-96.

AHMED, Z., BANSAL, D., TIZZARD, K., SUREY, S., ESMAEILI, M., GONZALEZ, A. M., BERRY, M. & LOGAN, A. 2014. Decorin blocks scarring and cystic cavitation in acute and induces scar dissolution in chronic spinal cord wounds. *Neurobiol Dis,* 64**,** 163-76.

AHMED, Z., JACQUES, S. J., BERRY, M. & LOGAN, A. 2009. Epidermal growth factor receptor inhibitors promote CNS axon growth through off-target effects on glia. *Neurobiol Dis,* 36**,** 142-50.

AHUJA, A. & SINGH, R. S. 2008. Variation and evolution of male sex combs in Drosophila: nature of selection response and theories of genetic variation for sexual traits. *Genetics,* 179**,** 503-9.

AIRAKSINEN, M. S. & SAARMA, M. 2002. The GDNF family: signalling, biological functions and therapeutic value. *Nat Rev Neurosci,* 3**,** 383-94.

ALIVISATOS, A. P., CHUN, M., CHURCH, G. M., GREENSPAN, R. J., ROUKES, M. L. & YUSTE, R. 2012. The Brain Activity Map Project and the Challenge of Functional Connectomics. *Neuron,* 74**,** 970-974.

ALLEN, S. J. & DAWBARN, D. 2006. Clinical relevance of the neurotrophins and their receptors. *Clin Sci (Lond),* 110**,** 175-91.

ANASTASIA, A., DEINHARDT, K., CHAO, M. V., WILL, N. E., IRMADY, K., LEE, F. S., HEMPSTEAD, B. L. & BRACKEN, C. 2013. Val66Met polymorphism of BDNF alters prodomain structure to induce neuronal growth cone retraction. *Nat Commun,* 4**,** 2490.

ANDERSON, K. V. & NUSSLEIN-VOLHARD, C. 1984. Information for the dorsal--ventral pattern of the Drosophila embryo is stored as maternal mRNA. *Nature,* 311**,** 223-7.

ANGERER, L. M., YAGUCHI, S., ANGERER, R. C. & BURKE, R. D. 2011. The evolution of nervous system patterning: insights from sea urchin development. *Development,* 138**,** 3613-23.

ARENDT, D., DENES, A. S., JÉKELY, G. & TESSMAR-RAIBLE, K. 2008. The evolution of nervous system centralization. *Philos Trans R Soc Lond B Biol Sci,* 363**,** 1523-8.

ARNOT, C. J., GAY, N. J. & GANGLOFF, M. 2010. Molecular mechanism that induces activation of Spätzle, the ligand for the Drosophila Toll receptor. *J Biol Chem,* 285**,** 19502-9.

ARON, L., KLEIN, P., PHAM, T. T., KRAMER, E. R., WURST, W. & KLEIN, R. 2010. Pro-survival role for Parkinson's associated gene DJ-1 revealed in trophically impaired dopaminergic neurons. *PLoS Biol,* 8**,** e1000349.

ASHBURNER, M., GOLIC, K. G. & HAWLEY, R. S. 2005. *Drosophila: A Laboratory Handbook*, Cold Spring Harbor Laboratory Press.

AWASAKI, T., LAI, S. L., ITO, K. & LEE, T. 2008. Organization and postembryonic development of glial cells in the adult central brain of Drosophila. *J Neurosci,* 28**,** 13742-53.

BALLARD, S. L., MILLER, D. L. & GANETZKY, B. 2014. Retrograde neurotrophin signaling through Tollo regulates synaptic growth in Drosophila. *The Journal of Cell Biology,* 204**,** 1157-1172.
BALOH, R. H., ENOMOTO, H., JOHNSON, E. M., JR. & MILBRANDT, J. 2000. The GDNF family ligands and receptors - implications for neural development. *Curr Opin Neurobiol,* 10**,** 103-10.
BARAK, B., FELDMAN, N. & OKUN, E. 2014. Toll-like receptors as developmental tools that regulate neurogenesis during development: an update. *Front Neurosci,* 8**,** 272.
BARTKOWSKA, K., TURLEJSKI, K. & DJAVADIAN, R. L. 2010. Neurotrophins and their receptors in early development of the mammalian nervous system. *Acta Neurobiol Exp (Wars),* 70**,** 454-67.
BATH, K. G., JING, D. Q., DINCHEVA, I., NEEB, C. C., PATTWELL, S. S., CHAO, M. V., LEE, F. S. & NINAN, I. 2012. BDNF Val66Met impairs fluoxetine-induced enhancement of adult hippocampus plasticity. *Neuropsychopharmacology,* 37**,** 1297-304.
BATH, K. G., MANDAIRON, N., JING, D., RAJAGOPAL, R., KAPOOR, R., CHEN, Z. Y., KHAN, T., PROENCA, C. C., KRAEMER, R., CLELAND, T. A., HEMPSTEAD, B. L., CHAO, M. V. & LEE, F. S. 2008. Variant brain-derived neurotrophic factor (Val66Met) alters adult olfactory bulb neurogenesis and spontaneous olfactory discrimination. *J Neurosci,* 28**,** 2383-93.
BELLEN, H. J., TONG, C. & TSUDA, H. 2010. 100 years of Drosophila research and its impact on vertebrate neuroscience: a history lesson for the future. *Nat Rev Neurosci,* 11**,** 514-22.
BERGMANN, A., TUGENTMAN, M., SHILO, B. Z. & STELLER, H. 2002. Regulation of cell number by MAPK-dependent control of apoptosis: a mechanism for trophic survival signaling. *Dev Cell,* 2**,** 159-70.
BERGNER, A., OGANESSYAN, V., MUTA, T., IWANAGA, S., TYPKE, D., HUBER, R. & BODE, W. 1996. Crystal structure of a coagulogen, the clotting protein from horseshoe crab: a structural homologue of nerve growth factor. *EMBO J,* 15**,** 6789-97.
BIER, E. 2005. Drosophila, the golden bug, emerges as a tool for human genetics. *Nat Rev Genet,* 6**,** 9-23.
BLUM, R. & KONNERTH, A. 2005. Neurotrophin-mediated rapid signaling in the central nervous system: mechanisms and functions. *Physiology (Bethesda),* 20**,** 70-8.
BOYD, J. G. & GORDON, T. 2003. Neurotrophic factors and their receptors in axonal regeneration and functional recovery after peripheral nerve injury. *Mol Neurobiol,* 27**,** 277-324.
BRAND, A. H. & PERRIMON, N. 1993. Targeted gene expression as a means of altering cell fates and generating dominant phenotypes. *Development,* 118**,** 401-15.
BRIDGES, C. 1936. D.I.S. work sheet no. 1: external structure of Drosophila. *Drosophila Information Service,* 6**,** 76.
BUCHON, N., POIDEVIN, M., KWON, H.-M., GUILLOU, A., SOTTAS, V., LEE, B.-L. & LEMAITRE, B. 2009. A single modular serine protease integrates signals from pattern-recognition receptors upstream of the Drosophila Toll pathway. *Proc Natl Acad Sci U S A,* 106**,** 12442-7.
CACHERO, S., OSTROVSKY, A. D., YU, J. Y., DICKSON, B. J. & JEFFERIS, G. S. 2010. Sexual dimorphism in the fly brain. *Curr Biol,* 20**,** 1589-601.
CAMPBELL, G., GÖRING, H., LIN, T., SPANA, E., ANDERSSON, S., DOE, C. Q. & TOMLINSON, A. 1994. RK2, a glial-specific homeodomain protein required for

embryonic nerve cord condensation and viability in Drosophila. *Development (Cambridge, England),* 120**,** 2957-2966.
CARLSON, B. M. 2007. *Principles of Regenerative Biology*.
CARROLL, S. B., WINSLOW, G. M., TWOMBLY, V. J. & SCOTT, M. P. 1987. Genes that control dorsoventral polarity affect gene expression along the anteroposterior axis of the Drosophila embryo. *Development,* 99**,** 327-32.
CARVALHO, L., JACINTO, A. & MATOVA, N. 2014. The Toll/NF-κB signaling pathway is required for epidermal wound repair in Drosophila. *Proceedings of the National Academy of Sciences*.
CHASAN, R., JIN, Y. & ANDERSON, K. V. 1992. Activation of the easter zymogen is regulated by five other genes to define dorsal-ventral polarity in the Drosophila embryo. *Development,* 115**,** 607-16.
CHELI, V. T., DANIELS, R. W., GODOY, R., HOYLE, D. J., KANDACHAR, V., STARCEVIC, M., MARTINEZ-AGOSTO, J. A., POOLE, S., DIANTONIO, A., LLOYD, V. K., CHANG, H. C., KRANTZ, D. E. & DELL'ANGELICA, E. C. 2010. Genetic modifiers of abnormal organelle biogenesis in a Drosophila model of BLOC-1 deficiency. *Human Molecular Genetics,* 19**,** 861-878.
CHEN, Z. Y., IERACI, A., TENG, H., DALL, H., MENG, C. X., HERRERA, D. G., NYKJAER, A., HEMPSTEAD, B. L. & LEE, F. S. 2005. Sortilin controls intracellular sorting of brain-derived neurotrophic factor to the regulated secretory pathway. *J Neurosci,* 25**,** 6156-66.
CHEN, Z. Y., JING, D., BATH, K. G., IERACI, A., KHAN, T., SIAO, C. J., HERRERA, D. G., TOTH, M., YANG, C., MCEWEN, B. S., HEMPSTEAD, B. L. & LEE, F. S. 2006. Genetic variant BDNF (Val66Met) polymorphism alters anxiety-related behavior. *Science,* 314**,** 140-3.
CHEN, Z. Y., PATEL, P. D., SANT, G., MENG, C. X., TENG, K. K., HEMPSTEAD, B. L. & LEE, F. S. 2004. Variant brain-derived neurotrophic factor (BDNF) (Met66) alters the intracellular trafficking and activity-dependent secretion of wild-type BDNF in neurosecretory cells and cortical neurons. *J Neurosci,* 24**,** 4401-11.
CHO, Y. S., STEVENS, L. M., SIEVERMAN, K. J., NGUYEN, J. & STEIN, D. 2012. A ventrally localized protease in the Drosophila egg controls embryo dorsoventral polarity. *Curr Biol,* 22**,** 1013-8.
COHEN, S. & LEVI-MONTALCINI, R. 1956. A NERVE GROWTH-STIMULATING FACTOR ISOLATED FROM SNAKE VENOM. *Proc Natl Acad Sci U S A,* 42**,** 571-4.
COHEN, S., LEVI-MONTALCINI, R. & HAMBURGER, V. 1954. A NERVE GROWTH-STIMULATING FACTOR ISOLATED FROM SARCOM AS 37 AND 180. *Proc Natl Acad Sci U S A,* 40**,** 1014-8.
COULOM, H. & BIRMAN, S. 2004. Chronic exposure to rotenone models sporadic Parkinson's disease in Drosophila melanogaster. *J Neurosci,* 24**,** 10993-8.
DAVIES, A. M. 1996. The neurotrophic hypothesis: where does it stand? *Philos Trans R Soc Lond B Biol Sci,* 351**,** 389-94.
DEISTER, C. & SCHMIDT, C. E. 2006. Optimizing neurotrophic factor combinations for neurite outgrowth. *J Neural Eng,* 3**,** 172-9.
DELANEY, S. J., HAYWARD, D. C., BARLEBEN, F., FISCHBACH, K. F. & MIKLOS, G. L. 1991. Molecular cloning and analysis of small optic lobes, a structural brain gene of Drosophila melanogaster. *Proceedings of the National Academy of Sciences of the United States of America,* 88**,** 7214-7218.

DELOTTO, Y. & DELOTTO, R. 1998. Proteolytic processing of the Drosophila Spätzle protein by easter generates a dimeric NGF-like molecule with ventralising activity. *Mech Dev,* 72**,** 141-8.

DEVESA, I. & FERRER-MONTIEL, A. 2014. Neurotrophins, endocannabinoids and thermo-transient receptor potential: a threesome in pain signalling. *Eur J Neurosci,* 39**,** 353-62.

DOHERTY, J., LOGAN, M. A., TASDEMIR, O. E. & FREEMAN, M. R. 2009. Ensheathing Glia Function as Phagocytes in the Adult Drosophila Brain. *The Journal of neuroscience : the official journal of the Society for Neuroscience,* 29**,** 4768-4781.

DOS SANTOS, G., SCHROEDER, A. J., GOODMAN, J. L., STRELETS, V. B., CROSBY, M. A., THURMOND, J., EMMERT, D. B., GELBART, W. M. & CONSORTIUM, F. 2015. FlyBase: introduction of the Drosophila melanogaster Release 6 reference genome assembly and large-scale migration of genome annotations. *Nucleic Acids Res,* 43**,** D690-7.

DOUGLAS, M. R., MORRISON, K. C., JACQUES, S. J., LEADBEATER, W. E., GONZALEZ, A. M., BERRY, M., LOGAN, A. & AHMED, Z. 2009. Off-target effects of epidermal growth factor receptor antagonists mediate retinal ganglion cell disinhibited axon growth. *Brain,* 132**,** 3102-21.

EGAN, M. F., KOJIMA, M., CALLICOTT, J. H., GOLDBERG, T. E., KOLACHANA, B. S., BERTOLINO, A., ZAITSEV, E., GOLD, B., GOLDMAN, D., DEAN, M., LU, B. & WEINBERGER, D. R. 2003. The BDNF val66met polymorphism affects activity-dependent secretion of BDNF and human memory and hippocampal function. *Cell,* 112**,** 257-69.

ENGLUND, C., UV, A. E., CANTERA, R., MATHIES, L. D., KRASNOW, M. A. & SAMAKOVLIS, C. 1999. adrift, a novel bnl-induced Drosophila gene, required for tracheal pathfinding into the CNS. *Development,* 126**,** 1505-14.

FERRARO, G. B., ALABED, Y. Z. & FOURNIER, A. E. 2004. Molecular targets to promote central nervous system regeneration. *Curr Neurovasc Res,* 1**,** 61-75.

FERREIRA, F. R. M., NOGUEIRA, M. I. & DEFELIPE, J. 2014a. The influence of James and Darwin on Cajal and his research into the neuron theory and evolution of the nervous system. *Front Neuroanat,* 8**,** 1.

FERREIRA, T. A., BLACKMAN, A. V., OYRER, J., JAYABAL, S., CHUNG, A. J., WATT, A. J., SJOSTROM, P. J. & VAN MEYEL, D. J. 2014b. Neuronal morphometry directly from bitmap images. *Nat Methods,* 11**,** 982-4.

FITCH, M. T., DOLLER, C., COMBS, C. K., LANDRETH, G. E. & SILVER, J. 1999. Cellular and molecular mechanisms of glial scarring and progressive cavitation: in vivo and in vitro analysis of inflammation-induced secondary injury after CNS trauma. *J Neurosci,* 19**,** 8182-98.

FITCH, M. T. & SILVER, J. 2008. CNS injury, glial scars, and inflammation: Inhibitory extracellular matrices and regeneration failure. *Exp Neurol,* 209**,** 294-301.

FLICI, H., CATTENOZ, P. B., KOMONYI, O., LANEVE, P., ERKOSAR, B., KARATAS, O. F., REICHERT, H., BERZSENYI, S. & GIANGRANDE, A. 2014. Interlocked loops trigger lineage specification and stable fates in the Drosophila nervous system. *Nat Commun,* 5.

FLORENTIN, A. & ARAMA, E. 2012. Caspase levels and execution efficiencies determine the apoptotic potential of the cell. *J Cell Biol,* 196**,** 513-27.

FORERO, M. G., KATO, K. & HIDALGO, A. 2012. Automatic cell counting in vivo in the larval nervous system of Drosophila. *J Microsc,* 246**,** 202-12.

GANGLOFF, M., MURALI, A., XIONG, J., ARNOT, C. J., WEBER, A. N., SANDERCOCK, A. M., ROBINSON, C. V., SARISKY, R., HOLZENBURG, A., KAO, C. & GAY, N. J. 2008. Structural insight into the mechanism of activation of the Toll receptor by the dimeric ligand Spätzle. *J Biol Chem,* 283**,** 14629-35.

GODOY-HERRERA, R., BURNET, B., CONNOLLY, K. & GOGARTY, J. 1984. The development of locomotor activity in Drosophila melanogaster larvae. *Heredity,* 52**,** 63-75.

GOLIC, K. G. & GOLIC, M. M. 1996. Engineering the Drosophila genome: chromosome rearrangements by design. *Genetics,* 144**,** 1693-711.

GOMES, F. C., SPOHR, T. C., MARTINEZ, R. & MOURA NETO, V. 2001. Cross-talk between neurons and glia: highlights on soluble factors. *Braz J Med Biol Res,* 34**,** 611-20.

GOTO, J., MIKAWA, Y., KOGANEZAWA, M., ITO, H. & YAMAMOTO, D. 2011. Sexually dimorphic shaping of interneuron dendrites involves the hunchback transcription factor. *J Neurosci,* 31**,** 5454-9.

GOTZ, R., KOSTER, R., WINKLER, C., RAULF, F., LOTTSPEICH, F., SCHARTL, M. & THOENEN, H. 1994. Neurotrophin-6 is a new member of the nerve growth factor family. *Nature,* 372**,** 266-9.

GURTHRIE, S. 2007. Neurotrophic Factors: Are They Axon Guidance Molecules? *In:* BAGNARD, D. (ed.) *Axon Growth and Guidance.*

HAHN, M. & BISHOP, J. 2001. Expression pattern of Drosophila ret suggests a common ancestral origin between the metamorphosis precursors in insect endoderm and the vertebrate enteric neurons. *Proc Natl Acad Sci U S A,* 98**,** 1053-8.

HALFON, M. S., HASHIMOTO, C. & KESHISHIAN, H. 1995. The Drosophila toll gene functions zygotically and is necessary for proper motoneuron and muscle development. *Dev Biol,* 169**,** 151-67.

HALFON, M. S. & KESHISHIAN, H. 1998. The Toll pathway is required in the epidermis for muscle development in the Drosophila embryo. *Dev Biol,* 199**,** 164-74.

HAMBURGER, V. 1939. Motor and Sensory Hyperplasia following Limb-Bud Transplantation in Chick Embryos. *Physiological Zoology,* 12**,** 268-284.

HAMBURGER, V. & LEVI-MONTALCINI, R. 1949. Proliferation, differentiation and degeneration in the spinal ganglia of the chick embryo under normal and experimental conditions. *Journal of Experimental Zoology,* 111**,** 457-501.

HAREL, N. Y. & STRITTMATTER, S. M. 2006. Can regenerating axons recapitulate developmental guidance during recovery from spinal cord injury? *Nat Rev Neurosci,* 7**,** 603-16.

HARIRI, A. R., GOLDBERG, T. E., MATTAY, V. S., KOLACHANA, B. S., CALLICOTT, J. H., EGAN, M. F. & WEINBERGER, D. R. 2003. Brain-derived neurotrophic factor val66met polymorphism affects human memory-related hippocampal activity and predicts memory performance. *J Neurosci,* 23**,** 6690-4.

HARRINGTON, A. W., LEINER, B., BLECHSCHMITT, C., AREVALO, J. C., LEE, R., MORL, K., MEYER, M., HEMPSTEAD, B. L., YOON, S. O. & GIEHL, K. M. 2004. Secreted proNGF is a pathophysiological death-inducing ligand after adult CNS injury. *Proc Natl Acad Sci U S A,* 101**,** 6226-30.

HARRIS, D. A., KIM, K., NAKAHARA, K., VÁSQUEZ-DOORMAN, C. & CARTHEW, R. W. 2011. Cargo sorting to lysosome-related organelles regulates siRNA-mediated gene silencing. *Journal of Cell Biology,* 194**,** 77-87.

HARTENSTEIN, V. 1993. *Atlas of Drosophila Development* Cold Spring Harbor Laboratory Press.
HECHT, P. M. & ANDERSON, K. V. 1992. Extracellular proteases and embryonic pattern formation. *Trends Cell Biol,* 2**,** 197-202.
HELFRICH, C. 1986. Role of the optic lobes in the regulation of the locomotor activity rhythm of Drosophila melanogaster: behavioral analysis of neural mutants. *Journal of Neurogenetics,* 3**,** 321-343.
HEPBURN, L., PRAJSNAR, T. K., KLAPHOLZ, C., MORENO, P., LOYNES, C. A., OGRYZKO, N. V., BROWN, K., SCHIEBLER, M., HEGYI, K., ANTROBUS, R., HAMMOND, K. L., CONNOLLY, J., OCHOA, B., BRYANT, C., OTTO, M., SUREWAARD, B., SENEVIRATNE, S. L., GROGONO, D. M., CACHAT, J., NY, T., KASER, A., TOROK, M. E., PEACOCK, S. J., HOLDEN, M., BLUNDELL, T., WANG, L., LIGOXYGAKIS, P., MINICHIELLO, L., WOODS, C. G., FOSTER, S. J., RENSHAW, S. A. & FLOTO, R. A. 2014. Innate immunity. A Spaetzle-like role for nerve growth factor beta in vertebrate immunity to Staphylococcus aureus. *Science,* 346**,** 641-6.
HIDALGO, A. & FFRENCH-CONSTANT, C. 2003. The control of cell number during central nervous system development in flies and mice. *Mechanisms of Development,* 120**,** 1311-1325.
HIDALGO, A. & GRIFFITHS, R. 2004. Coupling glial numbers and axonal patterns. *Cell Cycle,* 3**,** 1118-20.
HIDALGO, A., KATO, K., SUTCLIFFE, B., MCILROY, G., BISHOP, S. & ALAHMED, S. 2011. Trophic neuron-glia interactions and cell number adjustments in the fruit fly. *Glia,* 59**,** 1296-303.
HIDALGO, A., KINRADE, E. F. & GEORGIOU, M. 2001. The Drosophila neuregulin vein maintains glial survival during axon guidance in the CNS. *Dev Cell,* 1**,** 679-90.
HOFFMANN, A., FUNKNER, A., NEUMANN, P., JUHNKE, S., WALTHER, M., SCHIERHORN, A., WEININGER, U., BALBACH, J., REUTER, G. & STUBBS, M. T. 2008. Biophysical characterization of refolded Drosophila Spätzle, a cystine knot protein, reveals distinct properties of three isoforms. *J Biol Chem,* 283**,** 32598-609.
HOLTZMAN, S. & KAUFMAN, T. 2013. *RE: Large-scale imaging of Drosophila melanogaster mutations.*
HORNER, P. J. & GAGE, F. H. 2000. Regenerating the damaged central nervous system. *Nature,* 407**,** 963-70.
HU, X., YAGI, Y., TANJI, T., ZHOU, S. & IP, Y. T. 2004. Multimerization and interaction of Toll and Spätzle in Drosophila. *Proc Natl Acad Sci U S A,* 101**,** 9369-74.
HUANG, E. J. & REICHARDT, L. F. 2001. Neurotrophins: roles in neuronal development and function. *Annu Rev Neurosci,* 24**,** 677-736.
INAKI, M., SHINZA-KAMEDA, M., ISMAT, A., FRASCH, M. & NOSE, A. 2010. Drosophila Tey represses transcription of the repulsive cue Toll and generates neuromuscular target specificity. *Development,* 137**,** 2139-46.
INAMORI, K., ARIKI, S. & KAWABATA, S. 2004. A Toll-like receptor in horseshoe crabs. *Immunol Rev,* 198**,** 106-15.
IP, Y. T., REACH, M., ENGSTROM, Y., KADALAYIL, L., CAI, H., GONZALEZ-CRESPO, S., TATEI, K. & LEVINE, M. 1993. Dif, a dorsal-related gene that mediates an immune response in Drosophila. *Cell,* 75**,** 753-63.
IRVING, P., UBEDA, J.-M., DOUCET, D., TROXLER, L., LAGUEUX, M., ZACHARY, D., HOFFMANN, J. A., HETRU, C. & MEISTER, M. 2005. New insights into

Drosophila larval haemocyte functions through genome-wide analysis. *Cell Microbiol,* 7**,** 335-50.
ITO, K., URBAN, J. & TECHNAU, G. M. 1995. Distribution, classification, and development of Drosophila glial cells in the late embryonic and early larval ventral nerve cord *Roux's Arch Dev Biol* 204**,** 284-307.
IWANAGA, S. 1993. The limulus clotting reaction. *Curr Opin Immunol,* 5**,** 74-82.
JACQUES, S. J., AHMED, Z., FORBES, A., DOUGLAS, M. R., VIGENSWARA, V., BERRY, M. & LOGAN, A. 2012. AAV8(gfp) preferentially targets large diameter dorsal root ganglion neurones after both intra-dorsal root ganglion and intrathecal injection. *Mol Cell Neurosci,* 49**,** 464-74.
JANG, I.-H., CHOSA, N., KIM, S.-H., NAM, H.-J., LEMAITRE, B., OCHIAI, M., KAMBRIS, Z., BRUN, S., HASHIMOTO, C., ASHIDA, M., BREY, P. T. & LEE, W.-J. 2006. A Spätzle-processing enzyme required for toll signaling activation in Drosophila innate immunity. *Dev Cell,* 10**,** 45-55.
JANG, I. H., NAM, H. J. & LEE, W. J. 2008. CLIP-domain serine proteases in Drosophila innate immunity. *BMB Rep,* 41**,** 102-7.
JANSEN, P., GIEHL, K., NYENGAARD, J. R., TENG, K., LIOUBINSKI, O., SJOEGAARD, S. S., BREIDERHOFF, T., GOTTHARDT, M., LIN, F., EILERS, A., PETERSEN, C. M., LEWIN, G. R., HEMPSTEAD, B. L., WILLNOW, T. E. & NYKJAER, A. 2007. Roles for the pro-neurotrophin receptor sortilin in neuronal development, aging and brain injury. *Nat Neurosci,* 10**,** 1449-57.
JEIBMANN, A. & PAULUS, W. 2009. Drosophila melanogaster as a model organism of brain diseases. *Int J Mol Sci,* 10**,** 407-40.
JONES, B. W., FETTER, R. D., TEAR, G. & GOODMAN, C. S. 1995. glial cells missing: a genetic switch that controls glial versus neuronal fate. *Cell,* 82**,** 1013-23.
KALLIJARVI, J., STRATOULIAS, V., VIRTANEN, K., HIETAKANGAS, V., HEINO, T. I. & SAARMA, M. 2012. Characterization of Drosophila GDNF receptor-like and evidence for its evolutionarily conserved interaction with neural cell adhesion molecule (NCAM)/FasII. *PLoS One,* 7**,** e51997.
KAMBRIS, Z., BRUN, S., JANG, I.-H., NAM, H.-J., ROMEO, Y., TAKAHASHI, K., LEE, W.-J., UEDA, R. & LEMAITRE, B. 2006. Drosophila immunity: a large-scale in vivo RNAi screen identifies five serine proteases required for Toll activation. *Curr Biol,* 16**,** 808-13.
KATO, K., AWASAKI, T. & ITO, K. 2009. Neuronal programmed cell death induces glial cell division in the adult Drosophila brain. *Development,* 136**,** 51-9.
KATO, K., FORERO, M. G., FENTON, J. C. & HIDALGO, A. 2011. The glial regenerative response to central nervous system injury is enabled by pros-notch and pros-NFkappaB feedback. *PLoS Biol,* 9**,** e1001133.
KATO, K. & HIDALGO, A. 2013. An Injury Paradigm to Investigate Central Nervous System Repair in Drosophila. *Journal of Visualized Experiments***,** e50306.
KEITH, F. J. & GAY, N. J. 1990. The Drosophila membrane receptor Toll can function to promote cellular adhesion. *The EMBO Journal,* 9**,** 4299-4306.
KIMURA, K.-I. 2011. Role of cell death in the formation of sexual dimorphism in the Drosophila central nervous system. *Development, Growth & Differentiation,* 53**,** 236-244.
KIMURA, K.-I., OTE, M., TAZAWA, T. & YAMAMOTO, D. 2005. Fruitless specifies sexually dimorphic neural circuitry in the Drosophila brain. *Nature,* 438**,** 229-233.

KINRADE, E. F., BRATES, T., TEAR, G. & HIDALGO, A. 2001. Roundabout signalling, cell contact and trophic support confine longitudinal glia and axons in the Drosophila CNS. *Development,* 128**,** 207-16.
KOPP, A., DUNCAN, I., GODT, D. & CARROLL, S. B. 2000. Genetic control and evolution of sexually dimorphic characters in Drosophila. *Nature,* 408**,** 553-9.
KUZINA, I., SONG JK FAU - GINIGER, E. & GINIGER, E. 2011. How Notch establishes longitudinal axon connections between successive segments of the Drosophila CNS.
LAI, S.-L. & DOE, C. Q. 2014. *Transient nuclear Prospero induces neural progenitor quiescence*.
LANDGRAF, M., SANCHEZ-SORIANO, N., TECHNAU, G. M., URBAN, J. & PROKOP, A. 2003. Charting the Drosophila neuropile: a strategy for the standardised characterisation of genetically amenable neurites. *Dev Biol,* 260**,** 207-25.
LARSEN, P. H., HOLM, T. H. & OWENS, T. 2007. Toll-like receptors in brain development and homeostasis. *Sci STKE,* 2007**,** pe47.
LE GALL, M., DE MATTEI, C. & GINIGER, E. 2008. Molecular separation of two signaling pathways for the receptor, Notch. *Developmental biology,* 313**,** 556-567.
LEARTE, A., FORERO, M. & HIDALGO, A. 2008. Gliatrophic and gliatropic roles of PVF/PVR signaling during axon guidance. *Glia,* 56**,** 164 - 176.
LEHMANN, R., JIMÉNEZ, F., DIETRICH, U. & CAMPOS-ORTEGA, J. 1983. On the phenotype and development of mutants of early neurogenesis inDrosophila melanogaster. *Wilhelm Roux's archives of developmental biology,* 192**,** 62-74.
LEMAITRE, B., NICOLAS, E., MICHAUT, L., REICHHART, J. M. & HOFFMANN, J. A. 1996. The dorsoventral regulatory gene cassette spätzle/Toll/cactus controls the potent antifungal response in Drosophila adults. *Cell,* 86**,** 973-83.
LEULIER, F. & LEMAITRE, B. 2008. Toll-like receptors--taking an evolutionary approach. *Nat Rev Genet,* 9**,** 165-78.
LEVI-MONTALCINI, R. & COHEN, S. 1960. Effects of the extract of the mouse submaxillary salivary glands on the sympathetic system of mammals. *Ann N Y Acad Sci,* 85**,** 324-41.
LEWIN, G. R. & BARDE, Y. A. 1996. Physiology of the neurotrophins. *Annu Rev Neurosci,* 19**,** 289-317.
LI, H. H., KROLL, J. R., LENNOX, S. M., OGUNDEYI, O., JETER, J., DEPASQUALE, G. & TRUMAN, J. W. 2014. A GAL4 driver resource for developmental and behavioral studies on the larval CNS of Drosophila. *Cell Rep,* 8**,** 897-908.
LIN, Y.-R., REDDY, B. V. V. G. & IRVINE, K. D. 2008. Requirement for a core 1 galactosyltransferase in the Drosophila nervous system. *Developmental dynamics : an official publication of the American Association of Anatomists,* 237**,** 3703-3714.
LINDHOLM, P. & SAARMA, M. 2010. Novel CDNF/MANF family of neurotrophic factors. *Dev Neurobiol,* 70**,** 360-71.
LINDSLEY, D. L. & ZIMM, G. G. 1992. *The Genome of Drosophila Melanogaster*, Academic Press.
LIU, K., TEDESCHI, A., PARK, K. K. & HE, Z. 2011. Neuronal intrinsic mechanisms of axon regeneration. *Annu Rev Neurosci,* 34**,** 131-52.
LU, B., PANG, P. T. & WOO, N. H. 2005. The yin and yang of neurotrophin action. *Nat Rev Neurosci,* 6**,** 603-14.
MA, J., PLESKEN, H., TREISMAN, J. E., EDELMAN-NOVEMSKY, I. & REN, M. 2004. Lightoid and Claret: a rab GTPase and its putative guanine nucleotide exchange factor

in biogenesis of Drosophila eye pigment granules. *Proceedings of the National Academy of Sciences of the United States of America,* 101**,** 11652-11657.
MANNING, G., PLOWMAN, G. D., HUNTER, T. & SUDARSANAM, S. 2002. Evolution of protein kinase signaling from yeast to man. *Trends in Biochemical Sciences,* 27**,** 514-520.
MARCHETTI, L., LUIN, S., BONSIGNORE, F., DE NADAI, T., BELTRAM, F. & CATTANEO, A. 2015. Ligand-induced dynamics of neurotrophin receptors investigated by single-molecule imaging approaches. *Int J Mol Sci,* 16**,** 1949-79.
MARDER, E. & PRINZ, A. A. 2003. Current Compensation in Neuronal Homeostasis. *Neuron,* 37**,** 2-4.
MARTINOWICH, K., MANJI, H. & LU, B. 2007. New insights into BDNF function in depression and anxiety. *Nat Neurosci,* 10**,** 1089-93.
MAURANGE, C. & GOULD, A. P. 2005. Brainy but not too brainy: starting and stopping neuroblast divisions in Drosophila.
MAURANGE, C. & LANET, E. 2014. Building a brain under nutritional restriction: insights on sparing and plasticity from Drosophila studies. *Frontiers in Physiology,* 5.
MCDONALD, N. Q. & HENDRICKSON, W. A. 1993. A structural superfamily of growth factors containing a cystine knot motif. *Cell,* 73**,** 421-424.
MCILROY, G. 2012. *Toll-7 and Toll-6: central nervous system functions as Drosophila neurotrophin receptors.* Ph.D., University of Birmingham.
MCILROY, G., FOLDI, I., AURIKKO, J., WENTZELL, J. S., LIM, M. A., FENTON, J. C., GAY, N. J. & HIDALGO, A. 2013. Toll-6 and Toll-7 function as neurotrophin receptors in the Drosophila melanogaster CNS. *Nat Neurosci,* 16**,** 1248-56.
MEYER, S., SCHMIDT, I. & KLÄMBT, C. 2014a. Glia ECM interactions are required to shape the Drosophila nervous system. *Mech Dev,* 133**,** 105-16.
MEYER, S. N., AMOYEL, M., BERGANTIÑOS, C., DE LA COVA, C., SCHERTEL, C., BASLER, K. & JOHNSTON, L. A. 2014b. An ancient defense system eliminates unfit cells from developing tissues during cell competition. *Science,* 346**,** 1258236.
MICHEL, T., REICHHART, J. M., HOFFMANN, J. A. & ROYET, J. 2001. Drosophila Toll is activated by Gram-positive bacteria through a circulating peptidoglycan recognition protein. *Nature,* 414**,** 756-9.
MING, G. L. & SONG, H. 2011. Adult neurogenesis in the mammalian brain: significant answers and significant questions. *Neuron,* 70**,** 687-702.
MISRA, S., HECHT, P., MAEDA, R. & ANDERSON, K. V. 1998. Positive and negative regulation of Easter, a member of the serine protease family that controls dorsal-ventral patterning in the Drosophila embryo. *Development,* 125**,** 1261-7.
MIZUGUCHI, K., PARKER, J. S., BLUNDELL, T. L. & GAY, N. J. 1998. Getting knotted: a model for the structure and activation of Spätzle. *Trends Biochem Sci,* 23**,** 239-42.
MORIN, X., DANEMAN, R., ZAVORTINK, M. & CHIA, W. 2001. A protein trap strategy to detect GFP-tagged proteins expressed from their endogenous loci in Drosophila. *Proc Natl Acad Sci U S A,* 98**,** 15050-5.
MORISATO, D. & ANDERSON, K. V. 1994. The spatzle gene encodes a component of the extracellular signaling pathway establishing the dorsal-ventral pattern of the Drosophila embryo. *Cell,* 76**,** 677-88.
MORISATO, D. & ANDERSON, K. V. 1995. Signaling pathways that establish the dorsal-ventral pattern of the Drosophila embryo. *Annu Rev Genet,* 29**,** 371-99.
MOWLA, S. J., PAREEK, S., FARHADI, H. F., PETRECCA, K., FAWCETT, J. P., SEIDAH, N. G., MORRIS, S. J., SOSSIN, W. S. & MURPHY, R. A. 1999.

Differential sorting of nerve growth factor and brain-derived neurotrophic factor in hippocampal neurons. *J Neurosci,* 19**,** 2069-80.
MULINARI, S., HACKER, U. & CASTILLEJO-LOPEZ, C. 2006. Expression and regulation of Spatzle-processing enzyme in Drosophila. *FEBS Letters,* 580**,** 5406-5410.
NAGAPPAN, G., ZAITSEV, E., SENATOROV, V. V., JR., YANG, J., HEMPSTEAD, B. L. & LU, B. 2009. Control of extracellular cleavage of ProBDNF by high frequency neuronal activity. *Proc Natl Acad Sci U S A,* 106**,** 1267-72.
NEWQUIST, G., DRENNAN, J. M., LAMANUZZI, M., WALKER, K., CLEMENS, J. C. & KIDD, T. 2013. Blocking apoptotic signaling rescues axon guidance in Netrin mutants. *Cell Rep,* 3**,** 595-606.
NG, C. S. & KOPP, A. 2008. Sex combs are important for male mating success in Drosophila melanogaster. *Behav Genet,* 38**,** 195-201.
NI, J. Q., ZHOU, R., CZECH, B., LIU, L. P., HOLDERBAUM, L., YANG-ZHOU, D., SHIM, H. S., TAO, R., HANDLER, D., KARPOWICZ, P., BINARI, R., BOOKER, M., BRENNECKE, J., PERKINS, L. A., HANNON, G. J. & PERRIMON, N. 2011. A genome-scale shRNA resource for transgenic RNAi in Drosophila. *Nat Methods,* 8**,** 405-7.
NICOLAS, E., REICHHART, J. M., HOFFMANN, J. A. & LEMAITRE, B. 1998. In vivo regulation of the IkappaB homologue cactus during the immune response of Drosophila. *J Biol Chem,* 273**,** 10463-9.
NILSSON, A. S., FAINZILBER, M., FALCK, P. & IBANEZ, C. F. 1998. Neurotrophin-7: a novel member of the neurotrophin family from the zebrafish. *FEBS Lett,* 424**,** 285-90.
NYKJAER, A., WILLNOW, T. E. & PETERSEN, C. M. 2005. p75NTR--live or let die. *Curr Opin Neurobiol,* 15**,** 49-57.
O'SULLIVAN, N. C., JAHN, T. R., REID, E. & O'KANE, C. J. 2012. Reticulon-like-1, the Drosophila orthologue of the hereditary spastic paraplegia gene reticulon 2, is required for organization of endoplasmic reticulum and of distal motor axons. *Hum Mol Genet,* 21**,** 3356-65.
OKUN, E., GRIFFIOEN, K. J. & MATTSON, M. P. 2011. Toll-like receptor signaling in neural plasticity and disease. *Trends Neurosci,* 34**,** 269-81.
OLOFSSON, B. & PAGE, D. T. 2005. Condensation of the central nervous system in embryonic Drosophila is inhibited by blocking hemocyte migration or neural activity. *Developmental biology,* 279**,** 233-243.
OLSEN, S. R. & WILSON, R. I. 2008. Cracking neural circuits in a tiny brain: new approaches for understanding the neural circuitry of Drosophila. *Trends Neurosci,* 31**,** 512-20.
OOI, J. Y., YAGI, Y., HU, X. & IP, Y. T. 2002. The Drosophila Toll-9 activates a constitutive antimicrobial defense. *EMBO Rep,* 3**,** 82-7.
OU, Y., CHWALLA, B., LANDGRAF, M. & VAN MEYEL, D. J. 2008. Identification of genes influencing dendrite morphogenesis in developing peripheral sensory and central motor neurons. *Neural Dev,* 3**,** 16.
PALGI, M., GRECO, D., LINDSTRÖM, R., AUVINEN, P. & HEINO, T. I. 2012. Gene expression analysis of Drosophilaa Manf mutants reveals perturbations in membrane traffic and major metabolic changes. *BMC Genomics,* 13**,** 134.
PALGI, M., LINDSTRÖM, R., PERÄNEN, J., PIEPPONEN, T. P., SAARMA, M. & HEINO, T. I. 2009. Evidence that DmMANF is an invertebrate neurotrophic factor supporting dopaminergic neurons. *Proc Natl Acad Sci U S A,* 106**,** 2429-34.

PANDEY, R., BLANCO, J. & UDOLPH, G. 2011. The Glucuronyltransferase *GlcAT-P* Is Required for Stretch Growth of Peripheral Nerves in *Drosophila*. *PLoS ONE,* 6**,** e28106.

PANG, P. T., TENG, H. K., ZAITSEV, E., WOO, N. T., SAKATA, K., ZHEN, S., TENG, K. K., YUNG, W. H., HEMPSTEAD, B. L. & LU, B. 2004. Cleavage of proBDNF by tPA/plasmin is essential for long-term hippocampal plasticity. *Science,* 306**,** 487-91.

PARE, A. C., VICHAS, A., FINCHER, C. T., MIRMAN, Z., FARRELL, D. L., MAINIERI, A. & ZALLEN, J. A. 2014. A positional Toll receptor code directs convergent extension in Drosophila. *Nature,* 515**,** 523-527.

PARKER, J. S., MIZUGUCHI, K. & GAY, N. J. 2001. A family of proteins related to Spätzle, the toll receptor ligand, are encoded in the Drosophila genome. *Proteins,* 45**,** 71-80.

PARKS, A. L., COOK, K. R., BELVIN, M., DOMPE, N. A., FAWCETT, R., HUPPERT, K., TAN, L. R., WINTER, C. G., BOGART, K. P., DEAL, J. E., DEAL-HERR, M. E., GRANT, D., MARCINKO, M., MIYAZAKI, W. Y., ROBERTSON, S., SHAW, K. J., TABIOS, M., VYSOTSKAIA, V., ZHAO, L., ANDRADE, R. S., EDGAR, K. A., HOWIE, E., KILLPACK, K., MILASH, B., NORTON, A., THAO, D., WHITTAKER, K., WINNER, M. A., FRIEDMAN, L., MARGOLIS, J., SINGER, M. A., KOPCZYNSKI, C., CURTIS, D., KAUFMAN, T. C., PLOWMAN, G. D., DUYK, G. & FRANCIS-LANG, H. L. 2004. Systematic generation of high-resolution deletion coverage of the Drosophila melanogaster genome. *Nat Genet,* 36**,** 288-92.

PARTHIER, C., STELTER, M., URSEL, C., FANDRICH, U., LILIE, H., BREITHAUPT, C. & STUBBS, M. T. 2014. Structure of the Toll-Spatzle complex, a molecular hub in Drosophila development and innate immunity. *Proc Natl Acad Sci U S A,* 111**,** 6281-6.

PEREANU, W., SPINDLER, S., CRUZ, L. & HARTENSTEIN, V. 2007. Tracheal development in the Drosophila brain is constrained by glial cells. *Dev Biol,* 302**,** 169-80.

PFEIFFER, B. D., NGO, T. T., HIBBARD, K. L., MURPHY, C., JENETT, A., TRUMAN, J. W. & RUBIN, G. M. 2010. Refinement of tools for targeted gene expression in Drosophila. *Genetics,* 186**,** 735-55.

POO, M. M. 2001. Neurotrophins as synaptic modulators. *Nat Rev Neurosci,* 2**,** 24-32.

RATTENHOLL, A., RUOPPOLO, M., FLAGIELLO, A., MONTI, M., VINCI, F., MARINO, G., LILIE, H., SCHWARZ, E. & RUDOLPH, R. 2001. Pro-sequence assisted folding and disulfide bond formation of human nerve growth factor. *J Mol Biol,* 305**,** 523-33.

REICHARDT, L. F. 2006. Neurotrophin-regulated signalling pathways. *Philos Trans R Soc Lond B Biol Sci,* 361**,** 1545-64.

ROOTE, J. & PROKOP, A. 2013. How to design a genetic mating scheme: a basic training package for Drosophila genetics. *G3 (Bethesda),* 3**,** 353-8.

ROSCH, H., SCHWEIGREITER, R., BONHOEFFER, T., BARDE, Y. A. & KORTE, M. 2005. The neurotrophin receptor p75NTR modulates long-term depression and regulates the expression of AMPA receptor subunits in the hippocampus. *Proc Natl Acad Sci U S A,* 102**,** 7362-7.

ROSE, D., ZHU, X., KOSE, H., HOANG, B., CHO, J. & CHIBA, A. 1997. Toll, a muscle cell surface molecule, locally inhibits synaptic initiation of the RP3 motoneuron growth cone in Drosophila. *Development,* 124**,** 1561-71.

SAINI, N. & REICHERT, H. 2012. Neural Stem Cells in Drosophila: Molecular Genetic Mechanisms Underlying Normal Neural Proliferation and Abnormal Brain Tumor Formation. *Stem Cells International,* 2012**,** 10.

SANCHEZ-SORIANO, N., BOTTENBERG, W., FIALA, A., HAESSLER, U., KERASSOVITI, A., KNUST, E., LOHR, R. & PROKOP, A. 2005. Are dendrites in Drosophila homologous to vertebrate dendrites? *Dev Biol,* 288**,** 126-38.

SANDERS, L. E. & ARBEITMAN, M. N. 2008. Doublesex establishes sexual dimorphism in the Drosophila central nervous system in an isoform-dependent manner by directing cell number. *Developmental biology,* 320**,** 378-390.

SCHNEIDER, D. S., JIN, Y., MORISATO, D. & ANDERSON, K. V. 1994. A processed form of the Spatzle protein defines dorsal-ventral polarity in the Drosophila embryo. *Development,* 120**,** 1243-50.

SHOREY, M. L. 1909. The effect of the destruction of peripheral areas on the differentiation of the neuroblasts. *Journal of Experimental Zoology,* 7**,** 25-63.

SILVA, F. J. & MENSUA, J. L. 1985. Synergistic effects between eye-color genes of Drosophila melanogaster. *Drosophila Information Service,* 61**,** 156.

SOUTHALL, TONY D., DAVIDSON, CATHERINE M., MILLER, C., CARR, A. & BRAND, ANDREA H. 2014. Dedifferentiation of Neurons Precedes Tumor Formation in lola Mutants. *Developmental Cell,* 28**,** 685-696.

SOUTHALL, T. D., EGGER, B., GOLD, K. S. & BRAND, A. H. 2008. Regulation of self-renewal and differentiation in the Drosophila nervous system. *Cold Spring Harb Symp Quant Biol,* 73**,** 523-8.

STEIN, D. & NUSSLEIN-VOLHARD, C. 1992. Multiple extracellular activities in Drosophila egg perivitelline fluid are required for establishment of embryonic dorsal-ventral polarity. *Cell,* 68**,** 429-40.

STELTER, M., FANDRICH, U., FRANZKE, K., SCHIERHORN, A., BREITHAUPT, C., PARTHIER, C. & STUBBS, M. T. 2013. High level expression of the Drosophila Toll receptor ectodomain and crystallization of its complex with the morphogen Spätzle. *Biol Chem,* 394**,** 1091-6.

STERN, D. L. & SUCENA, E. 2000. Preparation of Larval and Adult Cuticles for Light Microscopy. *In:* SULLIVAN, W., ASHBURNER, M. & HAWLEY, R. S. (eds.) *Drosophila Protocols.* Cold Spring Harbor, New York: Cold Spring Harbor Laboratory Press.

SUGAYA, R., ISHIMARU, S., HOSOYA, T., SAIGO, K. & EMORI, Y. 1994. A Drosophila homolog of human proto-oncogene ret transiently expressed in embryonic neuronal precursor cells including neuroblasts and CNS cells. *Mech Dev,* 45**,** 139-45.

SUTCLIFFE, B. 2011. *Functional analysis of Drosophila neurotrophins: from neuronal survival to behaviour.* Ph.D. , University of Birmingham.

SUTCLIFFE, B., FORERO, M. G., ZHU, B., ROBINSON, I. M. & HIDALGO, A. 2013. Neuron-type specific functions of DNT1, DNT2 and Spz at the Drosophila neuromuscular junction. *PLoS One,* 8**,** e75902.

SUTER, U., HEYMACH, J. V., JR. & SHOOTER, E. M. 1991. Two conserved domains in the NGF propeptide are necessary and sufficient for the biosynthesis of correctly processed and biologically active NGF. *Embo j,* 10**,** 2395-400.

TAKAHASHI, M. 2001. The GDNF/RET signaling pathway and human diseases. *Cytokine Growth Factor Rev,* 12**,** 361-73.

TAUSZIG, S., JOUANGUY, E., HOFFMANN, J. A. & IMLER, J. L. 2000. Toll-related receptors and the control of antimicrobial peptide expression in Drosophila. *Proc Natl Acad Sci U S A,* 97**,** 10520-5.

TAYLOR, B. J. 1989. Sexually dimorphic neurons of the terminalia of Drosophila melanogaster: II. Sex-specific axonal arborizations in the central nervous system. *J Neurogenet,* 5**,** 193-213.

TEARLE, R. G. & NUSSLEIN-VOLHARD, C. 1987. Tubingen mutants and stock list. *Drosophila Information Service,* 66**,** 209-269.

THIBAULT, S. T., SINGER, M. A., MIYAZAKI, W. Y., MILASH, B., DOMPE, N. A., SINGH, C. M., BUCHHOLZ, R., DEMSKY, M., FAWCETT, R., FRANCIS-LANG, H. L., RYNER, L., CHEUNG, L. M., CHONG, A., ERICKSON, C., FISHER, W. W., GREER, K., HARTOUNI, S. R., HOWIE, E., JAKKULA, L., JOO, D., KILLPACK, K., LAUFER, A., MAZZOTTA, J., SMITH, R. D., STEVENS, L. M., STUBER, C., TAN, L. R., VENTURA, R., WOO, A., ZAKRAJSEK, I., ZHAO, L., CHEN, F., SWIMMER, C., KOPCZYNSKI, C., DUYK, G., WINBERG, M. L. & MARGOLIS, J. 2004. A complementary transposon tool kit for Drosophila melanogaster using P and piggyBac. *Nat Genet,* 36**,** 283-7.

THOMAS, G. B. & VAN MEYEL, D. J. 2007. The glycosyltransferase Fringe promotes Delta-Notch signaling between neurons and glia, and is required for subtype-specific glial gene expression.

TRIPODI, M., EVERS, J. F., MAUSS, A., BATE, M. & LANDGRAF, M. 2008. Structural homeostasis: compensatory adjustments of dendritic arbor geometry in response to variations of synaptic input. *PLoS Biol,* 6**,** e260.

UV, A., CANTERA, R. & SAMAKOVLIS, C. 2003. Drosophila tracheal morphogenesis: intricate cellular solutions to basic plumbing problems. *Trends Cell Biol,* 13**,** 301-9.

VENKEN, K. J., SIMPSON, J. H. & BELLEN, H. J. 2011a. Genetic manipulation of genes and cells in the nervous system of the fruit fly. *Neuron,* 72**,** 202-30.

VENKEN, K. J. T., SCHULZE, K. L., HAELTERMAN, N. A., PAN, H., HE, Y., EVANS-HOLM, M., CARLSON, J. W., LEVIS, R. W., SPRADLING, A. C., HOSKINS, R. A. & BELLEN, H. J. 2011b. MiMIC: a highly versatile transposon insertion resource for engineering Drosophila melanogaster genes. *Nature Methods,* 8**,** 737-743.

WAKEFIELD, S. & TEAR, G. 2006. The Drosophila reticulon, Rtnl-1, has multiple differentially expressed isoforms that are associated with a sub-compartment of the endoplasmic reticulum. *Cell Mol Life Sci,* 63**,** 2027-38.

WANG, C., LIU, Z. & HUANG, X. 2012. Rab32 Is Important for Autophagy and Lipid Storage in *Drosophila*. *PLoS ONE,* 7**,** e32086.

WEBER, A. N. R., GANGLOFF, M., MONCRIEFFE, M. C., HYVERT, Y., IMLER, J.-L. & GAY, N. J. 2007. Role of the Spatzle Pro-domain in the generation of an active toll receptor ligand. *J Biol Chem,* 282**,** 13522-31.

WEBER, A. N. R., MONCRIEFFE, M. C., GANGLOFF, M., IMLER, J.-L. & GAY, N. J. 2005. Ligand-receptor and receptor-receptor interactions act in concert to activate signaling in the Drosophila toll pathway. *J Biol Chem,* 280**,** 22793-9.

WEBER, A. N. R., TAUSZIG-DELAMASURE, S., HOFFMANN, J. A., LELIÈVRE, E., GASCAN, H., RAY, K. P., MORSE, M. A., IMLER, J.-L. & GAY, N. J. 2003. Binding of the Drosophila cytokine Spätzle to Toll is direct and establishes signaling. *Nat Immunol,* 4**,** 794-800.

WEIGMANN, K., KLAPPER, R., STRASSER, T., RICKERT, C., TECHNAU, G., JÄCKLE, H., JANNING, W. & KLÄMBT, C. 2003. FlyMove--a new way to look at development of Drosophila. *Trends Genet,* 19**,** 310-1.

WHITWORTH, A. J., WES, P. D. & PALLANCK, L. J. 2006. Drosophila models pioneer a new approach to drug discovery for Parkinson's disease. *Drug Discov Today,* 11**,** 119-26.

WOO, N. H., TENG, H. K., SIAO, C. J., CHIARUTTINI, C., PANG, P. T., MILNER, T. A., HEMPSTEAD, B. L. & LU, B. 2005. Activation of p75NTR by proBDNF facilitates hippocampal long-term depression. *Nat Neurosci,* 8**,** 1069-77.

YAMAMOTO, A. H., KOMMA, D. J., SHAFFER, C. D., PIRROTTA, V. & ENDOW, S. A. 1989. The claret locus in Drosophila encodes products required for eye color and for meiotic chromosome segregation. *The EMBO Journal,* 8**,** 3543-3552.

ZHU, B., PENNACK, J. A., MCQUILTON, P., FORERO, M. G., MIZUGUCHI, K., SUTCLIFFE, B., GU, C. J., FENTON, J. C. & HIDALGO, A. 2008. Drosophila neurotrophins reveal a common mechanism for nervous system formation. *PLoS Biol,* 6**,** e284.

ZLATIC, M., LI, F., STRIGINI, M., GRUEBER, W. & BATE, M. 2009. Positional Cues in the Drosophila Nerve Cord: Semaphorins Pattern the Dorso-Ventral Axis. *PLoS Biol,* 7**,** e1000135.

# 9 Appendix I

STATISTICAL REPORTS

## 9.1 Statistical Tests in Chapter 4

### 9.1.1 Figure 4.8 Survival Index

| Genotype | Sample Type & n | Comparison | Test | Normality Tests | Homogeneity of Variance | Descriptive Statistics | Test Value & df | p-Value | Multiple Comparisons & Correction |
|---|---|---|---|---|---|---|---|---|---|
| | No. of pupae | All together | $\chi^2$ | n/a | n/a | categorical data | $\chi^2$=707.723, df=13 | p<0.001 | Bonferroni: $p \times 14$ |
| *spz²ca¹/TM6B* | 1393 | To expected wild-type | | | | | $\chi^2$=455.088, df=1 | p<0.001 | |
| *spz²ca¹/TM6B* x *ru¹st¹ea¹⁴spz³ca¹/TM6B* | 876 | To expected wild-type<br>To *spz²ca¹/TM6B* | | | | | $\chi^2$=0.622, df=1<br>$\chi^2$=299.251 | 0.430<br>p<0.001 | <br>p<0.001 |
| *spz²ca¹/TM6B* x *ru¹Diap¹st¹kni^ri-1rn^roe-1p^pe¹spz⁴/TM6B* | 250 | To expected wild-type<br>To *spz²ca¹/TM6B* | | | | | $\chi^2$=5.618, df=1<br>$\chi^2$=239.743 | p<0.05<br>p<0.001 | <br>p<0.001 |
| *spz²ca¹/TM6B* x *spz^MA05/TM6B* | 685 | To expected wild-type<br>To *spz²ca¹/TM6B* | | | | | $\chi^2$=0.292, df=1<br>$\chi^2$=271.935, df=1 | 0.589<br>p<0.001 | <br>p<0.001 |
| *spz²ca¹/TM6B* x *Df(3R)Exel6205/TM6B* | 662 | To expected wild-type<br>To *spz²ca¹/TM6B* | | | | | $\chi^2$=1.208, df=1<br>$\chi^2$=284.065, df=1 | 0.272<br>p<0.001 | <br>p<0.001 |
| *spz^MA05/TM6B* | 382 | To expected wild-type | | | | | n/a | | |
| *spz^MA05/TM6B* x *spz²ca¹/TM6B* | 473 | To expected wild-type<br>To *spz^MA05/TM6B*<br>To *spz²ca¹/TM6B* x *spz^MA05/TM6B* | | | | | $\chi^2$=1.526, df=1<br>$\chi^2$=141.012, df=1<br>$\chi^2$=1.692, df=1 | 0.217<br>p<0.001<br>0.193 | <br>p<0.001<br>2.707 |
| *spz^MA05/TM6B* x *ru¹st¹ea¹⁴spz³ca¹/TM6B* | 222 | To expected wild-type<br>To *spz^MA05/TM6B* | | | | | $\chi^2$=2.453, df=1<br>$\chi^2$=170.215, df=1 | 0.117<br>p<0.001 | <br>p<0.001 |
| *spz^MA05/TM6B* x *ru¹Diap¹st¹kni^ri-1rn^roe-1p^pe¹spz⁴/TM6B* | 375 | To expected wild-type<br>To *spz^MA05/TM6B* | | | | | $\chi^2$=0.192, df=1<br>$\chi^2$=146.709, df=1 | 0.661<br>p<0.001 | <br>p<0.001 |
| *spz^MA05/TM6B* x *spz^MA10/TM6B* | 321 | To expected wild-type<br>To *spz^MA05/TM6B* | | | | | $\chi^2$=0.505, df=1<br>$\chi^2$=140.359, df=1 | 0.477<br>p<0.001 | <br>p<0.001 |
| *spz^MA05/TM6B* x *spz^MA12/TM6B* | 329 | To expected wild-type | | | | | n/a | | |
| *spz^MA05/TM6B* x *Df(3R)Exel6205/TM6B* | 719 | To expected wild-type<br>To *spz^MA05/TM6B* | | | | | $\chi^2$=12.487, df=1<br>$\chi^2$=125.901, df=1 | p<0.001<br>p<0.001 | <br>p<0.001 |
| *Df(3R)Exel6205/TM6B* x *spz^MA10/TM6B* | 280 | To expected wild-type<br>To *spz^MA05/TM6B*<br>To *spz^MA05/TM6B* x *Df(3R)Exel6205/TM6B* | | | | | $\chi^2$=17.857, df=1<br>$\chi^2$=125.901, df=1<br>$\chi^2$=3.435, df=1 | p<0.001<br>p<0.001<br>0.064 | <br>p<0.001<br>0.894 |
| *Df(3R)Exel6205/TM6B* x *spz^MA12/TM6B* | 238 | To expected wild-type<br>To *spz^MA05/TM6B*<br>To *spz^MA05/TM6B* x *Df(3R)Exel6205/TM6B* | | | | | $\chi^2$=16.269, df=1<br>$\chi^2$=87.292, df=1<br>$\chi^2$=3.508, df=1 | p<0.001<br>p<0.001<br>0.061 | <br>p<0.001<br>0.855 |

### 9.1.2 Figure 4.9 Survival Index

| Genotype | Sample Type & n | Comparison | Test | Normality Tests | Homogeneity of Variance | Descriptive Statistics | Test Value & df | p-Value | Multiple Comparisons & Correction |
|---|---|---|---|---|---|---|---|---|---|
| | No. of pupae | SI | $\chi^2$ | n/a | n/a | categorical data | | | n/a |
| *dnt2*$^{37}$*/TM6B* | 473 | To expected wild-type | | | | | $\chi^2$=69.819, df=1 | p<0.001 | |
| *dnt2*$^{37}$*/TM6B* x *Df(3L)Exel6092/TM6B* | 1254 | To expected wild-type<br>To *dnt2*$^{37}$*/TM6B* | | | | | $\chi^2$=47.458, df=1<br>$\chi^2$=16.150, df=1 | p<0.001<br>p<0.001 | |

## 9.2 Statistical Tests in Chapter 5

### 9.2.1 Figure 5.1 CNS Size Characteristics

| Genotype | Brain Area | | | VNC Area | | | VNC Length | | |
|---|---|---|---|---|---|---|---|---|---|
| | n | Mean (x10$^5$µm$^2$) | SD (x10$^5$µm$^2$) | n | Mean (x10$^4$µm$^2$) | SD (x10$^4$µm$^2$) | n | Mean (µm) | SD (µm) |
| *yw* | 25 | 1.70 | ±0.23 | 25 | 7.0 | ±0.8 | 25 | 372 | ±25 |
| *spz*$^2$*ca*$^1$ | 15 | 0.68 | ±0.13 | 15 | 5.8 | ±0.6 | 15 | 333 | ±18 |
| *spz*$^2$*ca*$^1$*/Df(3R)Exel6205* | 8 | 1.67 | ±0.11 | 9 | 7.3 | ±0.5 | 9 | 378 | ±22 |
| *spz*$^{MA05}$*/Df(3R)Exel6205* | 1 | 1.01 | - | 1 | 5.5 | - | 1 | 355 | - |

Table 9.1 Brain and VNC mean size quantification for genotypes *yw*, *spz*$^2$*ca*$^1$, *spz*$^2$*ca*$^1$*/Df(3R)Exel6205* and *spz*$^{MA05}$*/Df(3R)Exel6205*.

| Genotype | Sample Type & n | Comparison | Test | Normality Tests | Homogeneity of Variance | Descriptive Statistics | Test Value & df | p-Value | Multiple Comparisons & Correction |
|---|---|---|---|---|---|---|---|---|---|
| | No. of brain | Brain area | Welch ANOVA | kurtosis (k); skewness (s); Kolmogorov-Smirnov (KS); Shapiro-Wilk (SW) | Levene's Test | Mean±SD ($x10^5 \mu m^2$) | F=145.425, df=2,23.696 | p<0.001 | Games-Howell |
| | | All together | | | 4.030, p<0.05 | | | | |
| *yw* | 25 | | | k=-0.214; s=0.250; p(KS)=0.200; p(SW)=0.894 (all normal) | | 1.70±0.23 | | | |
| *spz²ca¹* | 15 | To *yw* | | k=-1.135; s=0.559; p(KS)<0.05; p(SW)=0.067 (treat as normal) | | 0.68±0.13 | | | p<0.001 |
| *spz²ca¹/Df(3R)Exel6205* | 8 | To *yw* | | k=-0.583, s=-0.079; p(KS)=0.200; p(SW)=0.683 (all normal) | | 1.67±0.11 | | | p=0.805 |
| | | To *spz²ca¹* | | | | | | | p<0.001 |
| | No. of VNC | VNC area | Welch ANOVA | kurtosis (k); skewness (s); Kolmogorov-Smirnov (KS); Shapiro-Wilk (SW) | Levene's Test | Mean±SD ($x10^4 \mu m^2$) | F=17.692, df=2,24.797 | p<0.001 | Games-Howell |
| | | All together | | | 3.748, p<0.05 | | | | |
| *yw* | 25 | | | k=-1.167, s=-0.204, p(KS)=0.200, p(SW)=0.209 (all normal) | | 7.0±0.8 | | | |
| *spz²ca¹* | 15 | To *yw* | | k=2.055, s=-0.320, p(KS)=0.200, p(SW=0.398 (treat as normal) | | 5.8±0.6 | | | p<0.001 |
| *spz²ca¹/Df(3R)Exel6205* | 9 | To *yw* | | k=4.367, s=-1.888, p(KS)=0.156, p(SW)<0.05 (treat as normal) | | 7.3±0.5 | | | p=0.387 |
| | | To *spz²ca¹* | | | | | | | p<0.001 |
| | No. of VNC | VNC length | one-way ANOVA | kurtosis (k); skewness (s); Kolmogorov-Smirnov (KS); Shapiro-Wilk (SW) | Levene's Test | Mean±SD (μm) | F=17.069, df=2,46 | p<0.001 | Bonferroni |
| | | All together | | | 2.733, p=0.076 | | | | |
| *yw* | 25 | | | k=-1.344, s=0.301, p(KS)=0.200, p(SW)=0.051 (all normal) | | 372±25 | | | |
| *spz²ca¹* | 15 | To *yw* | | k=1.357, s=-0.488, p(KS)=0.200, p(SW)=0.614 (all normal) | | 333±18 | | | p<0.001 |
| *spz²ca¹/Df(3R)Exel6205* | 9 | To *yw* | | k=2.658, s=-1.421, p(KS)=0.200, p(SW)=0.161 (treat as normal) | | 378±22 | | | p=1.000 |
| | | To *spz²ca¹* | | | | | | | p<0.001 |

## 9.2.2 Figure 5.2 CNS Size Characteristics

| Genotype | Sample Type & n | Comparison | Test | Normality Tests | Homogeneity of Variance | Descriptive Statistics | Test Value & df | p-Value | Multiple Comparisons & Correction |
|---|---|---|---|---|---|---|---|---|---|
| | No. of brain | Brain area | Welch ANOVA | Kolmogorov-Smirnov (KS); Shapiro-Wilk (SW) | Levene's Test | Mean±SD ($x10^5 \mu m^2$) | F=124.983, df=4,42.419 | p<0.001 | Bonferroni |
| | | All together | | | 3.966, p<0.05 | | | | |
| *yw* | 25 | | | p(KS)=0.200; p(SW)=0.894 (all normal) | | 1.70±0.23 | | | |
| *spz²ca¹* | 15 | To *yw* | | p(KS)<0.05; p(SW)=0.067 (treat as normal) | | 0.68±0.13 | | | p<0.001 |
| *ru¹h¹Diap¹st¹cu¹sr¹e^sca¹* | 19 | To *spz²ca¹* | | p(KS)=0.200; p(SW)=0.608 (all normal) | | 1.31±0.15 | | | p<0.001 |
| *spz²ca⁺.33* | 13 | To *spz²ca¹* | | p(KS)=0.200; p(SW)=0.558 (all normal) | | 0.74±0.10 | | | p=0.714 |
| *spz²ca⁺.56* | 21 | To *spz²ca¹* | | p(KS)=0.200; p(SW)=0.540 (all normal) | | 0.78±0.14 | | | p=0.190 |
| | No. of VNC | VNC area | Welch ANOVA | Kolmogorov-Smirnov (KS); Shapiro-Wilk (SW) | Levene's Test | Mean±SD ($x10^4 \mu m^2$) | F=7.212, df=4,42.065 | p<0.001 | Games-Howell |
| | | All together | | | 3.232, p<0.05 | | | | |
| *yw* | 25 | | | p(KS)=0.200; p(SW)=0.209 (all normal) | | 7.0±0.8 | | | |
| *spz²ca¹* | 15 | To *yw* | | p(KS)=0.200; p(SW)=0.398 (all normal) | | 5.8±0.6 | | | p<0.001 |
| *ru¹h¹Diap¹st¹cu¹sr¹e^sca¹* | 16 | To *spz²ca¹* | | p(KS)=0.200; p(SW)=0.140 (all normal) | | 6.3±0.5 | | | p=0.130 |
| *spz²ca⁺.33* | 16 | To *spz²ca¹* | | p(KS)=0.200; p(SW)=0.428 (all normal) | | 6.5±1.0 | | | p=0.174 |
| *spz²ca⁺.56* | 22 | To *spz²ca¹* | | p(KS)=0.200; p(SW)=0.595 (all normal) | | 6.1±0.7 | | | p=0.534 |
| | No. of VNC | VNC length | Welch ANOVA | Kolmogorov-Smirnov (KS); Shapiro-Wilk (SW) | Levene's Test | Mean±SD (µm) | F=14.653, df=4,41.781 | p<0.001 | Games-Howell |
| | | All together | | | 4.359, p<0.05 | | | | |
| *yw* | 25 | | | p(KS)=0.200; p(SW)=0.051 (all normal) | | 372±25 | | | |
| *spz²ca¹* | 15 | To *yw* | | p(KS)=0.200; p(SW)=0.614 (all normal) | | 333±18 | | | p<0.001 |
| *ru¹h¹Diap¹st¹cu¹sr¹e^sca¹* | 16 | To *spz²ca¹* | | p(KS)=0.200; p(SW)=0.030 (treat as normal) | | 360±22 | | | p<0.005 |
| *spz²ca⁺.33* | 16 | To *spz²ca¹* | | p(KS)=0.200; p(SW)=0.248 (all normal) | | 363±38 | | | p=0.063 |
| *spz²ca⁺.56* | 22 | To *spz²ca¹* | | p(KS)=0.200; p(SW)=0.142 (all normal) | | 325±23 | | | p=0.518 |

### 9.2.3 Figure 5.3 Survival Index

| Genotype | Sample Type & n | Comparison | Test | Normality Tests | Homogeneity of Variance | Descriptive Statistics | Test Value & df | p-Value | Multiple Comparisons & Correction |
|---|---|---|---|---|---|---|---|---|---|
| | No. of pupae | All together | $\chi^2$ | n/a | n/a | categorical data | $\chi^2$=24.062, df=2 | p<0.001 | Bonferroni: $p \times 3$ |
| *spz²ca¹/TM6B* | 1393 | To expected wild-type | | | | | $\chi^2$=455.088, df=1 | p<0.001 | |
| *spz²ca⁺.33/TM6B* | 2061 | To expected wild-type<br>To *spz²ca¹/TM6B* | | | | | $\chi^2$=448.055, df=1<br>$\chi^2$=24.168, df=1 | p<0.001<br>p<0.001 | <br>p<0.001 |
| *spz²ca⁺.56/TM6B* | 1862 | To expected wild-type<br>To *spz²ca¹/TM6B*<br>To *spz²ca⁺.33/TM6B* | | | | | $\chi^2$=473.573, df=1<br>$\chi^2$=10.638, df=1<br>$\chi^2$=3.350, df=1 | p<0.001<br>p<0.005<br>0.067 | <br>p<0.005<br>0.201 |

### 9.2.4 Figure 5.4 Survival Index

| Genotype | Sample Type & n | Comparison | Test | Normality Tests | Homogeneity of Variance | Descriptive Statistics | Test Value & df | p-Value | Multiple Comparisons & Correction |
|---|---|---|---|---|---|---|---|---|---|
| | No. of pupae | All together | $\chi^2$ | n/a | n/a | categorical data | $\chi^2$=154.672, df=5 | p<0.001 | Bonferroni: $p \times 6$ |
| *spz²,elav-GAL4/TM6B* | 1553 | To expected wild-type | | | | | $\chi^2$=340.240, df=1 | p<0.001 | |
| *spz²,elav>spz²,actSpz(2)* | 483 | To expected wild-type<br>To *spz²,elav-GAL4/TM6B* | | | | | $\chi^2$=52.407, df=1<br>$\chi^2$=14.086, df=1 | p<0.001<br>p<0.001 (p=0.000175) | <br>p<0.01 (p= 0.00105) |
| *spz²,elav>spz²,Toll10$^{bB}$* | 1848 | To expected wild-type<br>To *spz²,elav-GAL4/TM6B* | | | | | $\chi^2$=31.093, df=1<br>$\chi^2$=134.502, df=1 | p<0.001<br>p<0.001 | <br>p<0.001 |
| *spz²,elav>spz²,Toll6$^{CY}$* | 1653 | To expected wild-type<br>To *spz²,elav-GAL4/TM6B*<br>To *spz²,elav>spz²,Toll10$^{bB}$* | | | | | $\chi^2$=50.352, df=1<br>$\chi^2$=102.100, df=1<br>$\chi^2$=2.013, df=1 | p<0.001<br>p<0.001<br>0.156 | <br>p<0.001<br>0.936 |
| *spz²,elav>spz²,Toll7$^{CY}$* | 865 | To expected wild-type<br>To *spz²,elav-GAL4/TM6B*<br>To *spz²,elav>spz²,Toll10$^{bB}$*<br>To *spz²,elav>spz²,Toll6$^{CY}$* | | | | | $\chi^2$=79.133, df=1<br>$\chi^2$=28.019, df=1<br>$\chi^2$=21.053, df=1<br>$\chi^2$=11.649, df=1 | p<0.001<br>p<0.001<br>p<0.001 (p=0.000004)<br>p<0.001 (p=0.000642) | <br>p<0.001<br>p<0.001 (p=0.000024)<br>p<0.05 (p=0.003852) |
| *spz²,elav>spz²,p35* | 355 | To expected wild-type<br>To *spz²,elav-GAL4/TM6B*<br>To *spz²,elav>spz²,actSpz(2)*<br>To *spz²,elav>spz²,Toll7$^{CY}$* | | | | | $\chi^2$=32.114, df=1<br>$\chi^2$=16.170, df=1<br>$\chi^2$=0.248, df=1<br>$\chi^2$= 0.001, df=1 | p<0.001<br>p<0.001 (p=0.000058)<br>0.618<br>0.974 | <br>p<0.001 (p=0.000348)<br>3.708<br>5.844 |

## 9.2.5 Figure 5.5 Rescue of CNS Size

| Genotype | Sample Type & n | Comparison | Test | Normality Tests | Homogeneity of Variance | Descriptive Statistics | Test Value & df | p-Value | Multiple Comparisons & Correction |
|---|---|---|---|---|---|---|---|---|---|
| | No. of brain | Brain area | Welch ANOVA | kurtosis (k); skewness (s); Kolmogorov-Smirnov (KS); Shapiro-Wilk (SW) | Levene's Test | Mean±SD ($x10^5 \mu m^2$) | F=102.025, df=6,16.253 | p<0.001 | Games-Howell |
| | | All together | | | 4.376, p<0.001 | | | | |
| *yw* | 25 | | | k=-0.214; s=0.250; p(KS)=0.200; p(SW)=0.894 (all normal) | | 1.70±0.23 | | | |
| *spz²ca¹* | 15 | | | k=-1.135; s=0.559; p(KS)<0.05; p(SW)=0.067 (treat as normal) | | 0.68±0.13 | | | |
| *spz²elavGAL4/+* | 11 | To *spz²ca¹* | | k=0.154; s=0.548; p(KS)=0.200; p(SW)=0.902 (all normal) | | 1.39±0.16 | | | p<0.001 |
| *spz²,elav>spz²,Toll^10bB* | 6 | To *spz²ca¹* | | k=0.219; s=0.933; p(KS)=0.200; p(SW)=0.350 (all normal) | | 0.72±0.07 | | | p=0.977 |
| *spz²,elav>spz²,Toll6^CY* | 8 | To *spz²ca¹* | | k=-0.569; s=0.028; p(KS)=0.200; p(SW)=0.915 (all normal) | | 0.67±0.07 | | | p=1.000 |
| *spz²,elav>spz²,Toll7^CY* | 5 | To *spz²ca¹* | | k=0.221; s=-0.640; p(KS)=0.200; p(SW)=0.923 (all normal) | | 0.54±0.04 | | | p<0.05 |
| *spz²,elav>spz²,p35* | 3 | To *spz²ca¹* | | k=n/a; s=-1.470; p(KS)=n/a; p(SW)=0.355 (treat as normal) | | 0.81±0.13 | | | p=0.679 |
| | No. of VNC | VNC area | one-way ANOVA | kurtosis (k); skewness (s); Kolmogorov-Smirnov (KS); Shapiro-Wilk (SW) | Levene's Test | Mean±SD ($x10^4 \mu m^2$) | F=10.652, df=6,70 | p<0.001 | Bonferroni |
| | | All together | | | 1.218, p=0.307 | | | | |
| *yw* | 25 | | | k=-1.167, s=-0.204, p(KS)=0.200, p(SW)=0.209 (all normal) | | 7.0±0.8 | | | |
| *spz²ca¹* | 15 | | | k=2.055, s=-0.320, p(KS)=0.200, p(SW=0.398 (treat as normal) | | 5.8±0.6 | | | |
| *spz²elavGAL4/+* | 12 | To *spz²ca¹* | | k=4.394; s=1.170; p(KS)=0.200; p(SW)<0.05 (treat as normal) | | 6.0±0.6 | | | p=1.000 |
| *spz²,elav>spz²,Toll^10bB* | 7 | To *spz²ca¹* | | k=1.178; s=1.004; p(KS)=0.200; p(SW)=0.443 (all normal) | | 7.0±0.7 | | | p<0.05 |
| *spz²,elav>spz²,Toll6^CY* | 8 | To *spz²ca¹* | | k=4.664; s=-1.941; p(KS)<0.05; p(SW)<0.05 (treat as normal) | | 7.0±0.6 | | | p<0.05 |
| *spz²,elav>spz²,Toll7^CY* | 5 | To *spz²ca¹* | | k=0.855; s=0.152; p(KS)=0.200; p(SW)=0.985 (all normal) | | 6.0±0.5 | | | p=1.000 |
| *spz²,elav>spz²,p35* | 5 | To *spz²ca¹* | | k=-2.312; s=-0.092; p(KS)=0.200; p(SW)=0.606 (all normal) | | 7.7±0.7 | | | p<0.001 |

Please turn over

| Genotype | Sample Type & n | Comparison | Test | Normality Tests | Homogeneity of Variance | Descriptive Statistics | Test Value & df | p-Value | Multiple Comparisons & Correction |
|---|---|---|---|---|---|---|---|---|---|
| | No. of VNC | VNC length | one-way ANOVA | kurtosis; skewness; Kolmogorov-Smirnov; Shapiro-Wilk | Levene's Test | Mean±SD (µm) | F=16.873, df=6,70 | p<0.001 | Bonferroni |
| | | All together | | | 1.384, p=0.233 | | | | |
| *yw* | 25 | | | k=-1.344, s=0.301, p(KS)=0.200, p(SW)=0.051 (all normal) | | 372±25 | | | |
| *spz$^{2}$ca$^{1}$* | 15 | | | k=1.357, s=-0.488, p(KS)=0.200, p(SW)=0.614 (all normal) | | 333±18 | | | |
| *spz$^{2}$elavGAL4/+* | 12 | To *spz$^{2}$ca$^{1}$* | | k=2.223; s=1.387; p(KS)=0.162; p(SW)=0.098 (all normal) | | 349±25 | | | p=1.000 |
| *spz$^{2}$,elav>spz$^{2}$,Toll$^{10bB}$* | 7 | To *spz$^{2}$ca$^{1}$* | | k=0.436; s=0.729; p(KS)=0.200; p(SW)=0.838 (all normal) | | 386±37 | | | p<0.001 |
| *spz$^{2}$,elav>spz$^{2}$,Toll6$^{CY}$* | 8 | To *spz$^{2}$ca$^{1}$* | | k=-0.938; s=-0.276; p(KS)=0.200; p(SW)=0.581 (all normal) | | 381±19 | | | p<0.001 |
| *spz$^{2}$,elav>spz$^{2}$,Toll7$^{CY}$* | 5 | To *spz$^{2}$ca$^{1}$* | | k=-1.435; s=-0.216; p(KS)=0.200; p(SW)=0.299 (all normal) | | 362±17 | | | p=0.455 |
| *spz$^{2}$,elav>spz$^{2}$,p35* | 5 | To *spz$^{2}$ca$^{1}$* | | k=1.077; s=0.913; p(KS)=0.200; p(SW)=0.679 (all normal) | | 450±29 | | | p<0.001 |

## 9.2.6 Figure 5.6 CNS Size Characteristics

| Genotype | Sample Type & n | Comparison | Test | Normality Tests | Homogeneity of Variance | Descriptive Statistics | Test Value & df | p-Value | Multiple Comparisons & Correction |
|---|---|---|---|---|---|---|---|---|---|
| | No. of brain | Brain area | Welch ANOVA | kurtosis (k); skewness (s); Kolmogorov-Smirnov (KS); Shapiro-Wilk (SW) | Levene's Test | Mean±SD ($x10^5 \mu m^2$) | F=105.547, df=5,28.450 | p<0.001 | Games-Howell |
| | | All together | | | 3.728, p<0.001 | | | | |
| *yw* | 25 | | | k=-0.214; s=0.250; p(KS)=0.200; p(SW)=0.894 (all normal) | | 1.70±0.23 | | | |
| *spz²ca¹* | 15 | | | k=-1.135; s=0.559; p(KS)<0.05; p(SW)=0.067 (treat as normal) | | 0.68±0.13 | | | |
| *spz²elavGAL4/+* | 11 | | | k=0.154; s=0.548; p(KS)=0.200; p(SW)=0.902 (all normal) | | 1.39±0.16 | | | |
| *spz²,elav>spz²,Toll$^{10bB}$* | 6 | To *elav>Toll$^{10bB}$* | | k=0.219; s=0.933; p(KS)=0.200; p(SW)=0.350 (all normal) | | 0.72±0.07 | | | p<0.001 |
| *elavGAL4/+* | 11 | To *elav>Toll$^{10bB}$* | | k=-1.396; s=0.057; p(KS)=0.200; p(SW)=0.482 (all normal) | | 1.25±0.21 | | | p=1.000 |
| *elav>Toll$^{10bB}$* | 10 | | | k=-1.613; s=-0.456; p(KS)=0.200; p(SW)=0.093 (all normal) | | 1.24±0.09 | | | |
| | No. of VNC | VNC area | one-way ANOVA | kurtosis (k); skewness (s); Kolmogorov-Smirnov (KS); Shapiro-Wilk (SW) | Levene's Test | Mean±SD ($x10^4 \mu m^2$) | F=9.846, df=5,79 | p<0.001 | Bonferroni |
| | | All together | | | 1.878, p=0.108 | | | | |
| *yw* | 25 | | | k=-1.167, s=-0.204, p(KS)=0.200, p(SW)=0.209 (all normal) | | 7.0±0.8 | | | |
| *spz²ca¹* | 15 | | | k=2.055, s=-0.320, p(KS)=0.200, p(SW=0.398 (treat as normal) | | 5.8±0.6 | | | |
| *spz²elavGAL4/+* | 12 | | | k=4.394; s=1.170; p(KS)=0.200; p(SW)<0.05 (treat as normal) | | 6.0±0.6 | | | |
| *spz²,elav>spz²,Toll$^{10bB}$* | 7 | To *elav>Toll$^{10bB}$* | | k=1.178; s=1.004; p(KS)=0.200; p(SW)=0.443 (all normal) | | 7.0±0.7 | | | p=1.000 |
| *elavGAL4/+* | 11 | To *elav>Toll$^{10bB}$* | | k=0.401; s=0.369; p(KS)=0.200; p(SW)=0.779 (treat as normal) | | 6.0±0.7 | | | p=0.060 |
| *elav>Toll$^{10bB}$* | 15 | | | k=0.368; s=0.207; p(KS)=0.200; p(SW)=0.861 (all normal) | | 6.7±0.4 | | | |
| Please turn over | | | | | | | | | |

| Genotype | Sample Type & n | Comparison | Test | Normality Tests | Homogeneity of Variance | Descriptive Statistics | Test Value & df | p-Value | Multiple Comparisons & Correction |
|---|---|---|---|---|---|---|---|---|---|
| | No. of VNC | VNC length | one-way ANOVA | kurtosis; skewness; Kolmogorov-Smirnov; Shapiro-Wilk | Levene's Test | Mean±SD (µm) | F=8.240, df=5,79 | p<0.001 | Bonferroni |
| | | All together | | | 1.570, p=0.178 | | | | |
| *yw* | 25 | | | k=-1.344, s=0.301, p(KS)=0.200, p(SW)=0.051 (all normal) | | 372±25 | | | |
| *spz²ca¹* | 15 | | | k=1.357, s=-0.488, p(KS)=0.200, p(SW)=0.614 (all normal) | | 333±18 | | | |
| *spz²elavGAL4/+* | 12 | | | k=2.223; s=1.387; p(KS)=0.162; p(SW)=0.098 (all normal) | | 349±25 | | | |
| *spz²,elav>spz²,Toll$^{10bB}$* | 7 | To *elav>Toll$^{10bB}$* | | k=0.436; s=0.729; p(KS)=0.200; p(SW)=0.838 (all normal) | | 386±37 | | | p=1.000 |
| *elavGAL4/+* | 11 | To *elav>Toll$^{10bB}$* | | k=1.551; s=0.838; p(KS)=0.200; p(SW)=0.671 (all normal) | | 359±19 | | | p=1.000 |
| *elav>Toll$^{10bB}$* | 15 | | | k=-0.417; s=0.258; p(KS)=0.200; p(SW)=0.390 (all normal) | | 375±23 | | | |

## 9.2.7 Figure 5.7 Survival Index

| Genotype | Sample Type & n | Comparison | Test | Normality Tests | Homogeneity of Variance | Descriptive Statistics | Test Value & df | p-Value | Multiple Comparisons & Correction |
|---|---|---|---|---|---|---|---|---|---|
| | No. of pupae | All together | $\chi^2$ | n/a | n/a | categorical data | $\chi^2$=383.717, df=4 | p<0.001 | Bonferroni: $p \times 5$ |
| *spz²,repo-GAL4/TM6B* | 1365 | To expected wild-type | | | | | n/a | | |
| *spz²,repo>spz²,actSpz(2)* | 477 | To *spz²,repo-GAL4/TM6B* | | | | | $\chi^2$=351.002, df=1 | p<0.001 | p<0.001 |
| *spz²,repo>spz²,Toll$^{10bB}$* | 446 | To *spz²,repo-GAL4/TM6B*<br>To *spz²,repo>spz²,actSpz* | | | | | $\chi^2$=266.226, df=1<br>$\chi^2$=4.137, df=1 | p<0.001<br>p<0.05 (p=0.0420) | p<0.001<br>0.21 |
| *spz²,repo>spz²,Toll6$^{CY}$* | 898 | To expected wild-type<br>To *spz²,repo-GAL4/TM6B*<br>To *spz²,repo>spz²,actSpz*<br>To *spz²,repo>spz²,Toll$^{10bB}$* | | | | | $\chi^2$=16.472, df=1<br>$\chi^2$=411.898, df=1<br>$\chi^2$=1.307, df=1<br>$\chi^2$=11.302, df=1 | p<0.001 (p=0.000049)<br>p<0.001<br>0.253<br>p<0.001 (p=0.000774) | <br>p<0.001<br>1.265<br>p<0.05 (p=0.00387) |
| *spz²,repo>spz²,Toll7$^{CY}$* | 1620 | To *spz²,repo-GAL4/TM6B*<br>To *spz²,repo>spz²,Toll$^{10bB}$* | | | | | $\chi^2$=266.517, df=1<br>$\chi^2$=0.218, df=1 | p<0.001<br>0.641 | p<0.001<br>3.205 |

### 9.2.8 Table 5.6 Comparison of Survival Index between Neuronal and Glial Overexpression of Activated Spz, Toll, Toll6 and Toll7

| Genotype | Sample Type & n | Comparison | Test | Normality Tests | Homogeneity of Variance | Descriptive Statistics | Test Value & df | p-Value | Multiple Comparisons & Correction |
|---|---|---|---|---|---|---|---|---|---|
| | No. of pupae | SI | $\chi^2$ | n/a | n/a | categorical data | | | Bonferroni: $p \times 8$ |
| *spz²,elav>spz²,actSpz(2)* | 483 | | | | | | | | |
| *spz²,repo>spz²,actSpz(2)* | 477 | To *spz²,elav>spz²,actSpz(2)* | | | | | $\chi^2$=5.761, df=1 | p<0.05 (p=0.0164) | 0.1312 |
| *spz²,elav>spz²,Toll10$^{bB}$* | 1848 | | | | | | | | |
| *spz²,repo>spz²,Toll$^{10bB}$* | 446 | To *spz²,elav>spz²,Toll10$^{bB}$* | | | | | $\chi^2$=14.000, df=1 | p<0.001 (p=0.000183) | p<0.01 (p=0.001464) |
| *spz²,elav>spz²,Toll6$^{CY}$* | 1653 | | | | | | | | |
| *spz²,repo>spz²,Toll6$^{CY}$* | 898 | To *spz²,repo>spz²,Toll6$^{CY}$* | | | | | $\chi^2$=1.034, df=1 | 0.309 | 2.472 |
| *spz²,elav>spz²,Toll7$^{CY}$* | 865 | | | | | | | | |
| *spz²,repo>spz²,Toll7$^{CY}$* | 1620 | To *spz²,repo>spz²,Toll7$^{CY}$* | | | | | $\chi^2$=0.766, df=1 | 0.381 | 3.048 |

### 9.2.9 Figure 5.8 Rescue of CNS Size

| Genotype | Brain Area | | | VNC Area | | | VNC Length | | |
|---|---|---|---|---|---|---|---|---|---|
| | n | Mean (x10$^5$µm$^2$) | SD (x10$^5$µm$^2$) | n | Mean (x10$^4$µm$^2$) | SD (x10$^4$µm$^2$) | n | Mean (µm) | SD (µm) |
| *yw* | 25 | 1.70 | ±0.23 | 25 | 7.0 | ±0.8 | 25 | 372 | ±25 |
| *spz²ca¹* | 15 | 0.68 | ±0.13 | 15 | 5.8 | ±0.6 | 15 | 333 | ±18 |
| *spz²repoGAL4/+* | 11 | 1.63 | ±0.18 | 12 | 6.9 | ±0.6 | 12 | 382 | ±20 |
| *spz²,repo>spz²,Toll$^{10bB}$* | 10 | 0.70 | ±0.09 | 11 | 8.4 | ±0.7 | 11 | 583 | ±49 |
| *spz²,repo>spz²,Toll6$^{CY}$* | 1 | 0.45 | - | 1 | 5.6 | - | 1 | 377 | - |
| *spz²,repo>spz²,Toll7$^{CY}$* | 2 | 0.63 | ±0.04 | 3 | 6.6 | ±0.5 | 3 | 397 | ±19 |

Table 9.2 CNS size rescue of *spz²/spz²* background using various *UAS* lines overexpressed under *repoGAL4* driver.

| Genotype | Sample Type & n | Comparison | Test | Normality Tests | Homogeneity of Variance | Descriptive Statistics | Test Value & df | p-Value | Multiple Comparisons & Correction |
|---|---|---|---|---|---|---|---|---|---|
| | No. of brain | Brain area | Welch ANOVA | kurtosis (k); skewness (s); Kolmogorov-Smirnov (KS); Shapiro-Wilk (SW) | Levene's Test | Mean±SD ($x10^5 \mu m^2$) | F=173.862, df=3,27.754 | p<0.001 | Games-Howell |
| | | All together | | | 3.882, p<0.05 | | | | |
| *yw* | 25 | | | k=-0.214; s=0.250; p(KS)=0.200; p(SW)=0.894 (all normal) | | 1.70±0.23 | | | |
| *spz²ca¹* | 15 | | | k=-1.135; s=0.559; p(KS)<0.05; p(SW)=0.067 (treat as normal) | | 0.68±0.13 | | | |
| *spz²repoGAL4/+* | 11 | To *spz²ca¹* | | k=-0.257; s=0.124; p(KS)=0.200; p(SW)=1.000 (all normal) | | 1.63±0.18 | | | p<0.001 |
| *spz²,repo>spz²,Toll^10bB* | 10 | To *spz²ca¹* | | k=0.018; s=-0.184; p(KS)=0.200; p(SW)=0.688 (all normal) | | 0.70±0.09 | | | p=0.988 |
| | No. of VNC | VNC area | one-way ANOVA | kurtosis (k); skewness (s); Kolmogorov-Smirnov (KS); Shapiro-Wilk (SW) | Levene's Test | Mean±SD ($x10^4 \mu m^2$) | F=29.028, df=3,59 | p<0.001 | Bonferroni |
| | | All together | | | 2.024, p=0.120 | | | | |
| *yw* | 25 | | | k=-1.167, s=-0.204, p(KS)=0.200, p(SW)=0.209 (all normal) | | 7.0±0.8 | | | |
| *spz²ca¹* | 15 | | | k=2.055, s=-0.320, p(KS)=0.200, p(SW=0.398 (treat as normal) | | 5.8±0.6 | | | |
| *spz²repoGAL4/+* | 12 | To *spz²ca¹* | | k=-1.215; s=0.427; p(KS)=0.139; p(SW)=0.231 (all normal) | | 6.9±0.6 | | | p<0.005 |
| *spz²,repo>spz²,Toll^10bB* | 11 | To *spz²ca¹* | | k=-1.267; s=0.151; p(KS)=0.200; p(SW)=0.571 (all normal) | | 8.4±0.7 | | | p<0.001 |
| | No. of VNC | VNC length | Welch ANOVA | kurtosis (k); skewness (s); Kolmogorov-Smirnov (KS); Shapiro-Wilk (SW) | Levene's Test | Mean±SD (μm) | F=88.598, df=3,26.424 | p<0.001 | Bonferroni |
| | | All together | | | 5.559, p<0.005 | | | | |
| *yw* | 25 | | | k=-1.344, s=0.301, p(KS)=0.200, p(SW)=0.051 (all normal) | | 372±25 | | | |
| *spz²ca¹* | 15 | | | k=1.357, s=-0.488, p(KS)=0.200, p(SW)=0.614 (all normal) | | 333±18 | | | |
| *spz²repoGAL4/+* | 12 | To *spz²ca¹* | | k=0.301; s=0.140; p(KS)=0.200; p(SW)=0.832 (all normal) | | 382±20 | | | p<0.001 |
| *spz²,repo>spz²,Toll^10bB* | 11 | To *spz²ca¹* | | k=2.132; s=1.363; p(KS)=0.200; p(SW)=0.065 (all normal) | | 583±49 | | | p<0.001 |

## 9.2.10 Figure 5.9 CNS Size Characteristics

| Genotype | Sample Type & n | Comparison | Test | Normality Tests | Homogeneity of Variance | Descriptive Statistics | Test Value & df | p-Value | Multiple Comparisons & Correction |
|---|---|---|---|---|---|---|---|---|---|
| | No. of brain | Brain area | Welch ANOVA | kurtosis (k); skewness (s); Kolmogorov-Smirnov (KS); Shapiro-Wilk (SW) | Levene's Test | Mean±SD ($x10^5 \mu m^2$) | F=115.809, df=5,33.6 | p<0.001 | Games-Howell |
| | | All together | | | 4.143, p<0.005 | | | | |
| *yw* | 25 | | | k=-0.214; s=0.250; p(KS)=0.200; p(SW)=0.894 (all normal) | | 1.70±0.23 | | | |
| *spz²ca¹* | 15 | | | k=-1.135; s=0.559; p(KS)<0.05; p(SW)=0.067 (treat as normal) | | 0.68±0.13 | | | |
| *spz²repoGAL4/+* | 11 | | | k=-0.257; s=0.124; p(KS)=0.200; p(SW)=1.000 (all normal) | | 1.63±0.18 | | | |
| *spz²,repo>spz²,Toll$^{10bB}$* | 10 | To *repo>Toll$^{10bB}$* | | k=0.018; s=-0.184; p(KS)=0.200; p(SW)=0.688 (all normal) | | 0.70±0.09 | | | p<0.001 |
| *repoGAL4/+* | 12 | To *repo>Toll$^{10bB}$* | | k=3.263; s=-1.007; p(KS)=0.050; p(SW)=0.113 (all normal) | | 1.22±0.12 | | | p=0.999 |
| *repo>Toll$^{10bB}$* | 12 | | | k=3.292; s=-1.568; p(KS)=0.031; p(SW)=0.024 (treat as normal) | | 1.23±0.11 | | | |
| | No. of VNC | VNC area | Welch ANOVA | kurtosis (k); skewness (s); Kolmogorov-Smirnov (KS); Shapiro-Wilk (SW) | Levene's Test | Mean±SD ($x10^4 \mu m^2$) | F=51.033, df=5,33.793 | p<0.001 | Bonferroni |
| | | All together | | | 4.219, p<0.005 | | | | |
| *yw* | 25 | | | k=-1.167, s=-0.204, p(KS)=0.200, p(SW)=0.209 (all normal) | | 7.0±0.8 | | | |
| *spz²ca¹* | 15 | | | k=2.055, s=-0.320, p(KS)=0.200, p(SW=0.398 (treat as normal) | | 5.8±0.6 | | | |
| *spz²repoGAL4/+* | 12 | | | k=-1.215; s=0.427; p(KS)=0.139; p(SW)=0.231 (all normal) | | 6.9±0.6 | | | |
| *spz²,repo>spz²,Toll$^{10bB}$* | 11 | To *repo>Toll$^{10bB}$* | | k=-1.267; s=0.151; p(KS)=0.200; p(SW)=0.571 (all normal) | | 8.4±0.7 | | | p=0.186 |
| *repoGAL4/+* | 12 | To *repo>Toll$^{10bB}$* | | k=-0.019; s=0.352; p(KS)=0.200; p(SW)=0.954 (treat as normal) | | 5.9±0.2 | | | p<0.001 |
| *repo>Toll$^{10bB}$* | 12 | | | k=-0.111; s=-0.779; p(KS)=0.200; p(SW)=0.266 (all normal) | | 7.8±0.5 | | | |

Please turn over

| Genotype | Sample Type & n | Comparison | Test | Normality Tests | Homogeneity of Variance | Descriptive Statistics | Test Value & df | p-Value | Multiple Comparisons & Correction |
|---|---|---|---|---|---|---|---|---|---|
| | No. of VNC | VNC length | one-way ANOVA | kurtosis (k); skewness (s); Kolmogorov-Smirnov (KS); Shapiro-Wilk (SW) | Levene's Test | Mean±SD (µm) | F=155.344, df=5,81 | p<0.001 | Bonferroni |
| | | All together | | | 3.619, p=0.00526 | | | | |
| *yw* | 25 | | | k=-1.344, s=0.301, p(KS)=0.200, p(SW)=0.051 (all normal) | | 372±25 | | | |
| *spz$^{2}$ca$^{1}$* | 15 | | | k=1.357, s=-0.488, p(KS)=0.200, p(SW)=0.614 (all normal) | | 333±18 | | | |
| *spz$^{2}$repoGAL4/+* | 12 | | | k=0.301; s=0.140; p(KS)=0.200; p(SW)=0.832 (all normal) | | 382±20 | | | |
| *spz$^{2}$,repo>spz$^{2}$,Toll$^{10bB}$* | 11 | To *repo>Toll$^{10bB}$* | | k=2.132; s=1.363; p(KS)=0.200; p(SW)=0.065 (all normal) | | 583±49 | | | p<0.001 |
| *repoGAL4/+* | 12 | To *repo>Toll$^{10bB}$* | | k=-1.097; s=0.248; p(KS)=0.200; p(SW)=0.556 (all normal) | | 364±21 | | | p<0.001 |
| *repo>Toll$^{10bB}$* | 12 | | | k=0.711; s=1.134; p(KS)=0.970; p(SW)=0.118 (all normal) | | 516±33 | | | |

## 9.2.11 Figure 5.10 CNS Size Characteristics

| Genotype | Sample Type & n | Comparison | Test | Normality Tests | Homogeneity of Variance | Descriptive Statistics | Test Value & df | p-Value | Multiple Comparisons & Correction |
|---|---|---|---|---|---|---|---|---|---|
| | No. of brain | Brain area | one-way ANOVA | kurtosis (k); skewness (s); Kolmogorov-Smirnov (KS); Shapiro-Wilk (SW) | Levene's Test | Mean±SD ($x10^5 \mu m^2$) | F=1.194, df=2,23 | p=0.321 | Bonferroni |
| | | All together | | | 0.021, p=0.979 | | | | |
| *spzGAL4/+* | 12 | | | k=0.988; s=1.336; p(KS)=0.095; p(SW)<0.05 (treat as normal) | | 1.31±0.19 | | | |
| *spz>actSpz(2)* | 8 | To *spzGAL4/+* | | k=0.281; s=0.229; p(KS)=0.200; p(SW)=0.769 (all normal) | | 1.20±0.18 | | | p=0.539 |
| *spz>spz-FL* | 6 | To *spzGAL4/+* | | k=-1.830, s=0.547; p(KS)=0.200; p(SW)=0.187 (all normal) | | 1.21±0.16 | | | p=0.792 |
| | No. of VNC | VNC area | one-way ANOVA | kurtosis (k); skewness (s); Kolmogorov-Smirnov (KS); Shapiro-Wilk (SW) | Levene's Test | Mean±SD ($x10^4 \mu m^2$) | F=1.750, df=2,24 | p=0.195 | Bonferroni |
| | | All together | | | 0.580, p=0.568 | | | | |
| *spzGAL4/+* | 12 | | | k=0.905, s=0.667, p(KS)=0.190, p(SW)=0.685 (all normal) | | 6.0±0.4 | | | |
| *spz>actSpz(2)* | 9 | To *spzGAL4/+* | | k=1.701, s=0.732, p(KS)=0.181, p(SW=0.399 (all normal) | | 6.2±0.7 | | | p=1.000 |
| *spz>spz-FL* | 6 | To *spzGAL4/+* | | k=-1.541, s=-0.679, p(KS)=0.200, p(SW)=0.308 (all normal) | | 5.7±0.4 | | | p=0.692 |
| | No. of VNC | VNC length | one-way ANOVA | kurtosis (k); skewness (s); Kolmogorov-Smirnov (KS); Shapiro-Wilk (SW) | Levene's Test | Mean±SD (μm) | F=5.599, df=2,24 | p<0.05 | Bonferroni |
| | | All together | | | 1.826, p=0.183 | | | | |
| *spzGAL4/+* | 12 | | | k=-0.365, s=-0.401, p(KS)=0.200, p(SW)=0.829 (all normal) | | 361±18 | | | |
| *spz>actSpz(2)* | 9 | To *spzGAL4/+* | | k=2.199, s=1.306, p(KS)=0.200, p(SW)=0.244 (all normal) | | 389±29 | | | p<0.05 |
| *spz>spz-FL* | 6 | To *spzGAL4/+* | | k=-0.296, s=2.223, p(KS)=0.200, p(SW)=0.335 (all normal) | | 359±9 | | | p=1.000 |

## 9.2.12 Figure 5.11 CNS Size Characteristics

| Genotype | Sample Type & n | Comparison | Test | Normality Tests | Homogeneity of Variance | Descriptive Statistics | Test Value & df | p-Value | Multiple Comparisons & Correction |
|---|---|---|---|---|---|---|---|---|---|
| | No. of VNC | VNC length | Welch ANOVA | kurtosis (k); skewness (s); Kolmogorov-Smirnov (KS); Shapiro-Wilk (SW) | Levene's Test | Mean±SD (µm) | F=17.261, df=4,27.254 | p<0.001 | Games-Howell |
| | | All together | | | 10.615, p<0.001 | | | | |
| *repo>Notch$^{ICD}$* | 11 | | | k=-0.427, s=-0.098, p(KS)=0.200, p(SW)=0.983 (all normal) | | 702±54 | | | |
| *repo>Notch$^{ICD}$,actSpz(2)* | 19 | To *repo>Notch$^{ICD}$* | | k=1.978, s=1.386, p(KS)=0.076, p(SW)<0.05 (treat as normal) | | 622±59 | | | p<0.05 |
| *repo>Notch$^{ICD}$,spz-FL* | 12 | To *repo>Notch$^{ICD}$* | | k=-0.961; s=-0.017; p(KS)=0.200; p(SW)=0.730 (all normal) | | 598±52 | | | p<0.05 |
| *repo>Notch$^{ICD}$,spz$^{2}$-FL* | 12 | To *repo>Notch$^{ICD}$* | | k=-0.366; s=0.608; p(KS)=0.200; p(SW)=0.556 (all normal) | | 645±64 | | | p=0.175 |
| *spz$^{2}$,repo>spz$^{2}$,Notch$^{ICD}$* | 11 | To *repo>Notch$^{ICD}$* | | k=-1.548; s=0.316; p(KS)=0.200; p(SW)=0.117 (all normal) | | 993±164 | | | p<0.001 |

## 9.2.13 Figure 5.12 Survival Index

| Genotype | Sample Type & n | Comparison | Test | Normality Tests | Homogeneity of Variance | Descriptive Statistics | Test Value & df | p-Value | Multiple Comparisons & Correction |
|---|---|---|---|---|---|---|---|---|---|
| | No. of pupae | SI | $\chi^2$ | n/a | n/a | categorical data | | | n/a |
| *spz$^{2}$ca$^{1}$/TM6B* | 1393 | | | | | | | | |
| *spz$^{2}$,repo>spz$^{2}$,Notch$^{ICD}$* | 1515 | To *spz$^{2}$ca$^{1}$/TM6B* | | | | | $\chi^2$=33.288, df=1 | p<0.001 | |

## 9.2.14 Figure 5.13 CNS Size Characteristics

| Genotype | Sample Type & n | Comparison | Test | Normality Tests | Homogeneity of Variance | Descriptive Statistics | Test Value & df | p-Value | Multiple Comparisons & Correction |
|---|---|---|---|---|---|---|---|---|---|
| | No. of VNC | VNC length | one-way ANOVA | kurtosis (k); skewness (s); Kolmogorov-Smirnov (KS); Shapiro-Wilk (SW) | Levene's Test | Mean±SD (µm) | F=1.316, df=4,47 | p=0.278 | Games-Howell |
| | | All together | | | 2.160, p<0.05 | | | | |
| *repo>Notch$^{ICD}$* | 11 | | | k=-0.427, s=-0.098, p(KS)=0.200, p(SW)=0.983 (all normal) | | 702±54 | | | |
| *repo>Notch$^{ICD}$,DNT1-CK3'+* | 10 | To *repo>Notch$^{ICD}$* | | k=1.684, s=1.081, p(KS)=0.200, p(SW)=0.314 (treat as normal) | | 681±35 | | | p=1.000 |
| *repo>Notch$^{ICD}$,DNT1-FL* | 12 | To *repo>Notch$^{ICD}$* | | k=3.342; s=1.664; p(KS)=0.117; p(SW)<0.05 (treat as normal) | | 718±107 | | | p=1.000 |
| *repo>Notch$^{ICD}$,DNT2-CK-6A* | 11 | To *repo>Notch$^{ICD}$* | | k=-1.167; s=0.463; p(KS)=0.200; p(SW)=0.418 (all normal) | | 659±55 | | | p=1.000 |
| *repo>Notch$^{ICD}$,DNT2-FL-47C* | 8 | To *repo>Notch$^{ICD}$* | | k=0.450; s=-0.035; p(KS)=0.200; p(SW)=0.998 (all normal) | | 669±66 | | | p=1.000 |

## 9.2.15 Figure 5.17 Characterising Ebony+ Repo+ Cells in the Ventral VNC

| Genotype | Sample Type & n | Comparison | Test | Normality Tests | Homogeneity of Variance | Descriptive Statistics | Test Value & df | p-Value | Multiple Comparisons & Correction |
|---|---|---|---|---|---|---|---|---|---|
| | No. of VNC | $< \frac{1}{2}$ in pairs, $> \frac{1}{2}$ in pairsor full pairs | $\chi^2$ | n/a | n/a | categorical data | | | n/a |
| *yw* | 13 | | | | | | | | |
| *spz$^2$ca$^1$* | 10 | To *yw* | | | | | $\chi^2$=2.654, df=2 | p=0.265 | |

## 9.2.16 Figure 5.18 Counting Ebony+ Repo+ Cells

| Genotype | Sample Type & n | Comparison | Test | Normality Tests | Homogeneity of Variance | Descriptive Statistics | Test Value & df | p-Value | Multiple Comparisons & Correction |
|---|---|---|---|---|---|---|---|---|---|
| | No. of VNC | Ebony+ Repo+ cell number | t-test | Kolmogorov-Smirnov (KS); Shapiro-Wilk (SW) | Levene's Test 0.054, p=0.819 | Mean±SD | t=0.418, df=21 | p=0.680 | n/a |
| *yw* | 13 | | | p(KS)=0.200; p(SW)=0.485 (all normal) | | 88.62±5.45 | | | |
| *spz*$^{2}$*ca*$^{1}$ | 10 | To *yw* | | p(KS)=0.200; p(SW)=0.989 (all normal) | | 87.60±6.19 | | | |

## 9.2.17 Figure 5.19 Counting Thoracic Repo+ Cells Using DeadEasy

| Genotype | Sample Type & n | Comparison | Test | Normality Tests | Homogeneity of Variance | Descriptive Statistics | Test Value & df | p-Value | Multiple Comparisons & Correction |
|---|---|---|---|---|---|---|---|---|---|
| | No. of VNC | Repo+ cell number: All together | one-way ANOVA | kurtosis (k); skewness (s); Kolmogorov-Smirnov (KS); Shapiro-Wilk (SW) | Levene's Test 0.179, p=0.910 | Mean±SD | F=2.436, df=3,48 | p=0.076 | Dunnett |
| *yw* | 25 | | | k=1.279; s=-0.644; p(KS)=0.200; p(SW)=0.377 (all normal) | | 375±62 | | | |
| *spz*$^{2}$*ca*$^{1}$ | 11 | To *yw* | | k=0.889; s=0.138; p(KS)=0.200; p(SW)=0.597 (all normal) | | 321±65 | | | p=0.837 |
| *spz*$^{2}$*ca*$^{1}$*/Df(3R)Exel6205* | 11 | To *yw* | | k=-0.769; s=-0.186; p(KS)=0.200; p(SW)=0.729 (all normal) | | 350±69 | | | p=0.055 |
| *spz*$^{MA05}$*/Df(3R)Exel6205* | 8 | To *yw* | | k=-1.080; s=-0.214; p(KS)=0.200; p(SW)=0.507 (all normal) | | 392±70 | | | p=0.353 |

## 9.2.18 Figure 5.19 Counting Abdominal Repo+ Cells Using DeadEasy

| Genotype | Sample Type & n | Comparison | Test | Normality Tests | Homogeneity of Variance | Descriptive Statistics | Test Value & df | p-Value | Multiple Comparisons & Correction |
|---|---|---|---|---|---|---|---|---|---|
| | No. of VNC | Repo+ cell number | one-way ANOVA | kurtosis (k); skewness (s); Kolmogorov-Smirnov (KS); Shapiro-Wilk (SW) | Levene's Test | Mean±SD | F=6.893, df=3,72 | p<0.001 | Dunnett |
| | | All together | | | 1.570, p=0.204 | | | | |
| *yw* | 29 | | | k=0.047; s=-0.126; p(KS)=0.200; p(SW)=0.836 (all normal) | | 375±26 | | | |
| *spz$^{2}$ca$^{1}$* | 12 | To *yw* | | k=3.494; s=-1.378; p(KS)=0.200; p(SW)=0.126 (treat as normal) | | 369±48 | | | p=0.934 |
| *spz$^{2}$ca$^{1}$/Df(3R)Exel6205* | 20 | To *yw* | | k=-0.935; s=-0.519; p(KS)=0.130; p(SW)=0.069 (all normal) | | 409±39 | | | p<0.05 |
| *spz$^{MA05}$/Df(3R)Exel6205* | 15 | To *yw* | | k=0.091; s=0.130; p(KS)=0.200; p(SW)=0.755 (all normal) | | 414±41 | | | p<0.05 |

## 9.2.19 Figure 5.20 Counting Thoracic Repo+ Cells Using DeadEasy

| Genotype | Sample Type & n | Comparison | Test | Normality Tests | Homogeneity of Variance | Descriptive Statistics | Test Value & df | p-Value | Multiple Comparisons & Correction |
|---|---|---|---|---|---|---|---|---|---|
| | No. of VNC | Repo+ cell number | one-way ANOVA | kurtosis (k); skewness (s); Kolmogorov-Smirnov (KS); Shapiro-Wilk (SW) | Levene's Test | Mean±SD | F=0.074, df=2,37 | p=0.929 | Dunnett |
| | | All together | | | 0.323, p=0.726 | | | | |
| *yw* | 22 | | | k=1.279; s=-0.644; p(KS)=0.200; p(SW)=0.377 (all normal) | | 375±62 | | | |
| *dnt1$^{41}$/Df(3L)Exel6101* | 8 | To *yw* | | k=1.083; s=-0.042; p(KS)=0.200; p(SW)=0.874 (all normal) | | 384±46 | | | p=0.916 |
| *dnt2$^{37}$/Df(3L)Exel6092* | 10 | To *yw* | | k=0.036; s=0.706; p(KS)=0.200; p(SW)=0.538 (all normal) | | 380±54 | | | p=0.968 |

## 9.2.20 Figure 5.20 Counting Abdominal Repo+ Cells Using DeadEasy

| Genotype | Sample Type & n | Comparison | Test | Normality Tests | Homogeneity of Variance | Descriptive Statistics | Test Value & df | p-Value | Multiple Comparisons & Correction |
|---|---|---|---|---|---|---|---|---|---|
| | No. of VNC | Repo+ cell number | one-way ANOVA | kurtosis (k); skewness (s); Kolmogorov-Smirnov (KS); Shapiro-Wilk (SW) | Levene's Test | Mean±SD | F=0.382, df=2,45 | p=0.685 | Dunnett |
| | | All together | | | 0.221, p=0.803 | | | | |
| *yw* | 29 | | | k=0.047; s=-0.126; p(KS)=0.200; p(SW)=0.836 (all normal) | | 375±26 | | | |
| *dnt1*$^{41}$*/Df(3L)Exel6101* | 8 | To *yw* | | k=-0.281; s=0.750; p(KS)=0.200; p(SW)=0.350 (all normal) | | 384±23 | | | p=0.617 |
| *dnt2*$^{37}$*/Df(3L)Exel6092* | 11 | To *yw* | | k=0.783; s=0.755; p(KS)=0.200; p(SW)=0.671 (all normal) | | 378±21 | | | p=0.950 |

## 9.2.21 Figure 5.21 Counting Thoracic Repo+ Cells Using DeadEasy

| Genotype | Sample Type & n | Comparison | Test | Normality Tests | Homogeneity of Variance | Descriptive Statistics | Test Value & df | p-Value | Multiple Comparisons & Correction |
|---|---|---|---|---|---|---|---|---|---|
| | No. of VNC | Repo+ cell number | t-test | kurtosis (k); skewness (s); Kolmogorov-Smirnov (KS); Shapiro-Wilk (SW) | Levene's Test | Mean±SD | t=-1.336, df=26 | p=0.193 | n/a |
| | | | | | 0.073, p=0.790 | | | | |
| *yw* | 22 | | | k=1.279; s=-0.644; p(KS)=0.200; p(SW)=0.377 (all normal) | | 375±62 | | | |
| *Toll7*$^{P114}$*/Toll7*$^{P8}$*;Toll6*$^{31}$*/Toll7*$^{26}$ | 6 | To *yw* | | k=-0.315; s=-0.260; p(KS)=0.200; p(SW)=0.930 (all normal) | | 413±53 | | | |

## 9.2.22 Figure 5.21 Counting Abdominal Repo+ Cells Using DeadEasy

| Genotype | Sample Type & n | Comparison | Test | Normality Tests | Homogeneity of Variance | Descriptive Statistics | Test Value & df | p-Value | Multiple Comparisons & Correction |
|---|---|---|---|---|---|---|---|---|---|
| | No. of VNC | Repo+ cell number | t-test | kurtosis (k); skewness (s); Kolmogorov-Smirnov (KS); Shapiro-Wilk (SW) | Levene's Test<br>0.104, p=0.748 | Mean±SD | t=-6.334, df=37 | p<0.001 | n/a |
| *yw* | 29 | | | k=0.047; s=-0.126; p(KS)=0.200; p(SW)=0.836 (all normal) | | 375±26 | | | |
| *Toll7$^{P114}$/Toll7$^{P8}$;Toll6$^{31}$/Toll7$^{26}$* | 10 | To *yw* | | k=0.465; s=-0.284; p(KS)=0.200; p(SW)=0.960 (all normal) | | 434±24 | | | |

## 9.2.23 Figure 5.22 Survival Index

| Genotype | Sample Type & n | Comparison | Test | Normality Tests | Homogeneity of Variance | Descriptive Statistics | Test Value & df | p-Value | Multiple Comparisons & Correction |
|---|---|---|---|---|---|---|---|---|---|
| | No. of pupae | SI | $\chi^2$ | n/a | n/a | categorical data | | | n/a |
| *Toll$^{r3}$ca$^{1}$/TM6B* x *Df(3R)ro80b,st$^{1}$e$^{1}$/TM6B* | 101 | To expected wild-type | | | | | $\chi^2$=34.104, df=1 | p<0.001 | |

## 9.2.24 Figure 5.23 Counting Thoracic pH3+ Cells Using DeadEasy

| Genotype | Sample Type & n | Comparison | Test | Normality Tests | Homogeneity of Variance | Descriptive Statistics | Test Value & df | p-Value | Multiple Comparisons & Correction |
|---|---|---|---|---|---|---|---|---|---|
| | No. of VNC | pH3+ cell number | one-way ANOVA | kurtosis (k); skewness (s); Kolmogorov-Smirnov (KS); Shapiro-Wilk (SW) | Levene's Test | Mean±SD | F=1.854, df=3,28 | p=0.160 | Dunnett |
| | | All together | | | 1.783, p=0.173 | | | | |
| *yw* | 11 | | | k=0.630; s=-0.762; p(KS)=0.200; p(SW)=0.578 (all normal) | | 52±13 | | | |
| *spz$^{2}$ca$^{1}$* | 5 | To *yw* | | k=-0.597; s=0.842; p(KS)=0.200; p(SW)=0.428 (all normal) | | 63±16 | | | p=0.225 |
| *spz$^{2}$ca$^{1}$/Df(3R)Exel6205* | 8 | To *yw* | | k=0.398; s=-0.567; p(KS)=0.200; p(SW)=0.729 (all normal) | | 58±6 | | | p=0.616 |
| *spz$^{MA05}$/Df(3R)Exel6205* | 8 | To *yw* | | k=-0.053; s=0.865; p(KS)=0.200; p(SW)=0.377 (all normal) | | 49±11 | | | p=0.912 |

## 9.2.25 Figure 5.23 Counting Abdominal pH3+ Cells Using DeadEasy

| Genotype | Sample Type & n | Comparison | Test | Normality Tests | Homogeneity of Variance | Descriptive Statistics | Test Value & df | p-Value | Multiple Comparisons & Correction |
|---|---|---|---|---|---|---|---|---|---|
| | No. of VNC | pH3+ cell number | one-way ANOVA | kurtosis (k); skewness (s); Kolmogorov-Smirnov (KS); Shapiro-Wilk (SW) | Levene's Test | Mean±SD | F=1.920, df=3,47 | p=0.139 | Dunnett |
| | | All together | | | 1.148, p=0.340 | | | | |
| *yw* | 30 | | | k=-0.392; s=-0.035; p(KS)=0.200; p(SW)=0.950 (all normal) | | 38±8 | | | |
| *spz$^{2}$ca$^{1}$* | 5 | To *yw* | | k=0.160; s=-0.985; p(KS)=0.200; p(SW)=0.576 (all normal) | | 35±9 | | | p=0.785 |
| *spz$^{2}$ca$^{1}$/Df(3R)Exel6205* | 8 | To *yw* | | k=2.008; s=1.350; p(KS)=0.200; p(SW)=0.251 (all normal) | | 41±5 | | | p=0.656 |
| *spz$^{MA05}$/Df(3R)Exel6205* | 8 | To *yw* | | k=0.541; s=0.575; p(KS)=0.200; p(SW)=0.820 (all normal) | | 44±7 | | | p=0.166 |

## 9.2.26 Figure 5.24 Counting Thoracic pH3+ Cells Using DeadEasy

| Genotype | Sample Type & n | Comparison | Test | Normality Tests | Homogeneity of Variance | Descriptive Statistics | Test Value & df | p-Value | Multiple Comparisons & Correction |
|---|---|---|---|---|---|---|---|---|---|
| | No. of VNC | pH3+ cell number | one-way ANOVA | kurtosis (k); skewness (s); Kolmogorov-Smirnov (KS); Shapiro-Wilk (SW) | Levene's Test | Mean±SD | F=1.843, df=2,18 | p=0.929 | Dunnett |
| | | All together | | | 2.565, p=0.105 | | | | |
| *yw* | 11 | | | k=0.630; s=-0.762; p(KS)=0.200; p(SW)=0.578 (all normal) | | 52±13 | | | |
| *dnt1*$^{41}$*/Df(3L)Exel6101* | 6 | To *yw* | | k=-1.644; s=-0.055; p(KS)=0.200; p(SW)=0.677 (all normal) | | 62±16 | | | p=0.267 |
| *dnt2*$^{37}$*/Df(3L)Exel6092* | 4 | To *yw* | | k=-0.002; s=1.055; p(KS)=n/a; p(SW)=0.457 (all normal) | | 64±5 | | | p=0.227 |

## 9.2.27 Figure 5.24 Counting Abdominal pH3+ Cells Using DeadEasy

| Genotype | Sample Type & n | Comparison | Test | Normality Tests | Homogeneity of Variance | Descriptive Statistics | Test Value & df | p-Value | Multiple Comparisons & Correction |
|---|---|---|---|---|---|---|---|---|---|
| | No. of VNC | pH3+ cell number | one-way ANOVA | kurtosis (k); skewness (s); Kolmogorov-Smirnov (KS); Shapiro-Wilk (SW) | Levene's Test | Mean±SD | F=1.641, df=2,38 | p=0.207 | Dunnett |
| | | All together | | | 1.646, p=0.206 | | | | |
| *yw* | 30 | | | k=-0.392; s=-0.035; p(KS)=0.200; p(SW)=0.950 (all normal) | | 38±8 | | | |
| *dnt1*$^{41}$*/Df(3L)Exel6101* | 6 | To *yw* | | k=0.098; s=-0.781; p(KS)=0.200; p(SW)=0.703 (all normal) | | 38±5 | | | p=0.998 |
| *dnt2*$^{37}$*/Df(3L)Exel6092* | 5 | To *yw* | | k=0.274; s=0.606; p(KS)=0.200; p(SW)=0.685 (all normal) | | 44±5 | | | p=0.151 |

## 9.2.28 Figure 5.25 Counting Thoracic pH3+ Cells Using DeadEasy

| Genotype | Sample Type & n | Comparison | Test | Normality Tests | Homogeneity of Variance | Descriptive Statistics | Test Value & df | p-Value | Multiple Comparisons & Correction |
|---|---|---|---|---|---|---|---|---|---|
| | No. of VNC | pH3+ cell number | t-test | kurtosis (k); skewness (s); Kolmogorov-Smirnov (KS); Shapiro-Wilk (SW) | Levene's Test<br>0.623, p=0.444 | Mean±SD | t=-2.568, df=13 | p<0.05 | n/a |
| *yw* | 11 | | | k=0.630; s=-0.762; p(KS)=0.200; p(SW)=0.578 (all normal) | | 52±13 | | | |
| *Toll7$^{P114}$/Toll7$^{P8}$;Toll6$^{31}$/Toll7$^{26}$* | 4 | To *yw* | | k=2.820; s=1.576; p(KS)=n/a; p(SW)=0.252 (treat as normal) | | 74±19 | | | |

## 9.2.29 Figure 5.25 Counting Abdominal pH3+ Cells Using DeadEasy

| Genotype | Sample Type & n | Comparison | Test | Normality Tests | Homogeneity of Variance | Descriptive Statistics | Test Value & df | p-Value | Multiple Comparisons & Correction |
|---|---|---|---|---|---|---|---|---|---|
| | No. of VNC | pH3+ cell number | t-test | kurtosis (k); skewness (s); Kolmogorov-Smirnov (KS); Shapiro-Wilk (SW) | Levene's Test<br>0.309, p=0.582 | Mean±SD | t=-1.682, df=32 | p=0.102 | n/a |
| *yw* | 30 | | | k=-0.392; s=-0.035; p(KS)=0.200; p(SW)=0.950 (all normal) | | 38±8 | | | |
| *Toll7$^{P114}$/Toll7$^{P8}$;Toll6$^{31}$/Toll7$^{26}$* | 4 | To *yw* | | k=-5.360; s=0.089; p(KS)=n/a; p(SW)=0.177 (treat as normal) | | 45±9 | | | |

## 9.2.30 Figure 5.26 Characterising Proliferative Levels in the 'Non-Mitotic' Zone

| Genotype | Sample Type & n | Comparison | Test | Normality Tests | Homogeneity of Variance | Descriptive Statistics | Test Value & df | p-Value | Multiple Comparisons & Correction |
|---|---|---|---|---|---|---|---|---|---|
| | No. of VNC | ≤5 or >5 proliferating cells | $\chi^2$ | n/a | n/a | categorical data | $\chi^2$=9.554, df=6 | p=0.145 | not necessary to test |
| | | All together | | | | | | | |
| *yw* | 30 | | | | | | | | |
| *spz²ca¹* | 5 | | | | | | | | |
| *spz²ca¹/Df(3R)Exel6205* | 8 | | | | | | | | |
| *spz$^{MA05}$/Df(3R)Exel6205* | 8 | | | | | | | | |
| *dnt1$^{41}$/Df(3L)Exel6101* | 6 | | | | | | | | |
| *dnt2$^{37}$/Df(3L)Exel6092* | 5 | | | | | | | | |
| *Toll7$^{P114}$/Toll7$^{P8}$;Toll6$^{31}$/Toll7$^{26}$* | 4 | | | | | | | | |

## 9.2.31 Figure 5.27 Counting Abdominal cDcp1+ Cells Using DeadEasy

| Genotype | Sample Type & n | Comparison | Test | Normality Tests | Homogeneity of Variance | Descriptive Statistics | Test Value & df | p-Value | Multiple Comparisons & Correction |
|---|---|---|---|---|---|---|---|---|---|
| | No. of VNC | cDcp1+ cell number | one-way ANOVA | kurtosis (k); skewness (s); Kolmogorov-Smirnov (KS); Shapiro-Wilk (SW) | Levene's Test | Mean±SD | F=6.484, df=3,28 | p<0.005 | Dunnett |
| | | All together | | | 2.675, p=0.066 | | | | |
| *yw* | 17 | | | k=1.6514; s=-0.474; p(KS)=0.200; p(SW)=0.730 (all normal) | | 101±12 | | | |
| *spz²ca¹* | 5 | To *yw* | | k=4.638; s=-2.137; p(KS)<0.05; p(SW)<0.05 (treat as normal) | | 69±25 | | | p<0.001 |
| *spz²ca¹/Df(3R)Exel6205* | 5 | To *yw* | | k=-1.913; s=-0.379; p(KS)=0.200; p(SW)=0.677 (all normal) | | 94±3 | | | p=0.717 |
| *spz$^{MA05}$/Df(3R)Exel6205* | 5 | To *yw* | | k=-0.041; s=0.865; p(KS)=0.200; p(SW)=0.538 (all normal) | | 92±16 | | | p=0.537 |

## 9.2.32 Figure 5.28 Sholl Analysis of Thoracic RP2 Neurons

| Genotype | Sample Type & n | Comparison | Test | Normality Tests | Homogeneity of Variance | Descriptive Statistics | Test Value & df | p-Value | Multiple Comparisons & Correction |
|---|---|---|---|---|---|---|---|---|---|
| | No. of neurons | no. of intersection at 5µm distance | t-test | Kolmogorov-Smirnov (KS); Shapiro-Wilk (SW) | Levene's Test 3.226, p=0.147 | Mean±SD | t=0.200, df=4 | p=0.851 | n/a |
| control | 3 | | | p(KS)=n/a; p(SW)=0.363 (treat as normal) | | 4.0±2.6 | | | |
| *spz*$^2$ | 3 | To control | | p(KS)=n/a; p(SW)<0.001(treat as not normal) | | 3.7±1.2 | | | |
| | No. of neurons | no. of intersection at 10µm distance | t-test | Kolmogorov-Smirnov (KS); Shapiro-Wilk (SW) | Levene's Test 2.400, p=0.182 | Mean±SD | t=-2.607, df=5 | p<0.05 | n/a |
| control | 4 | | | p(KS)=n/a; p(SW)=0.850 (treat as normal) | | 2.8±1.7 | | | |
| *spz*$^2$ | 3 | To control | | p(KS)=n/a; p(SW)=0.537 (treat as normal) | | 8.0±3.6 | | | |
| | No. of neurons | no. of intersection at 15µm distance | t-test | Kolmogorov-Smirnov (KS); Shapiro-Wilk (SW) | Levene's Test 0.800, p=0.405 | Mean±SD | t=-2.214, df=6 | p=0.069 | n/a |
| control | 5 | | | p(KS)=0.200; p(SW)=0.421 (all normal) | | 4.4±2.6 | | | |
| *spz*$^2$ | 3 | To control | | p(KS)=n/a; p(SW)=0.253 (treat as normal) | | 9.3±3.8 | | | |
| | No. of neurons | no. of intersection at 20µm distance | t-test | Kolmogorov-Smirnov (KS); Shapiro-Wilk (SW) | Levene's Test 2.385, p=0.173 | Mean±SD | t=-0.431, df=6 | p=0.682 | n/a |
| control | 5 | | | p(KS)<0.05; p(SW)<0.05 (not normal) | | 6.2±1.8 | | | |
| *spz*$^2$ | 3 | To control | | p(KS)=n/a; p(SW)=0.537 (treat as normal) | | 7.0±3.6 | | | |
| | No. of neurons | no. of intersection at 25µm distance | t-test | Kolmogorov-Smirnov (KS); Shapiro-Wilk (SW) | Levene's Test 2.076, p=0.200 | Mean±SD | t=-1.204, df=6 | p=0.274 | n/a |
| control | 5 | | | p(KS)<0.05; p(SW)=0.065 (treat as normal) | | 8.4±3.1 | | | |
| *spz*$^2$ | 3 | To control | | p(KS)=n/a; p(SW)<0.001 (treat as not normal) | | 10.7±0.6 | | | |
| | No. of neurons | no. of intersection at 30µm distance | t-test | Kolmogorov-Smirnov (KS); Shapiro-Wilk (SW) | Levene's Test 0.842, p=0.394 | Mean±SD | t=-0.961, df=6 | p=0.374 | n/a |
| control | 5 | | | p(KS)=0.200; p(SW)=0.501 (all normal) | | 8.2±2.6 | | | |
| *spz*$^2$ | 3 | To control | | p(KS)=n/a; p(SW)=0.253 (treat as normal) | | 10.3±3.8 | | | |
| | No. of neurons | no. of intersection at 35µm distance | t-test | Kolmogorov-Smirnov (KS); Shapiro-Wilk (SW) | Levene's Test 2.867, p=0.141 | Mean±SD | t=0.044, df=6 | p=0.966 | n/a |
| control | 5 | | | p(KS)=0.200; p(SW)=0.253 (all normal) | | 12.8±4.8 | | | |
| *spz*$^2$ | 3 | To control | | p(KS)=n/a; p(SW)=0.463 (treat as normal) | | 12.7±2.1 | | | |

Please turn over

| Genotype | Sample Type & n | Comparison | Test | Normality Tests | Homogeneity of Variance | Descriptive Statistics | Test Value & df | p-Value | Multiple Comparisons & Correction |
|---|---|---|---|---|---|---|---|---|---|
| | No. of neurons | no. of intersection at 40µm distance | t-test | Kolmogorov-Smirnov (KS); Shapiro-Wilk (SW) | Levene's Test 5.250, p=0.062 | Mean±SD | t=8.301, df=6 | p<0.001 | n/a |
| control | 5 | | | p(KS)=0.161; p(SW)=0.325 (all normal) | | 13.0±0.7 | | | |
| *spz*$^2$ | 3 | To control | | p(KS)=n/a; p(SW)<0.001 (treat as not normal) | | 6.0±1.7 | | | |
| | No. of neurons | no. of intersection at 45µm distance | t-test | Kolmogorov-Smirnov (KS); Shapiro-Wilk (SW) | Levene's Test 0.869, p=0.387 | Mean±SD | t=2.337, df=6 | p=0.058 | n/a |
| control | 5 | | | p(KS)=0.200; p(SW)=0.738 (all normal) | | 12.2±3.6 | | | |
| *spz*$^2$ | 3 | To control | | p(KS)=n/a; p(SW)=0.097 (treat as normal) | | 5.0±5.3 | | | |
| | No. of neurons | no. of intersection at 50µm distance | n/a | Kolmogorov-Smirnov (KS); Shapiro-Wilk (SW) | n/a | Mean±SD | | | n/a |
| control | 5 | | | p(KS)=0.200; p(SW)=0.097 (all normal) | | 11.2±5.4 | | | |
| *spz*$^2$ | 1 | To control | | p(KS)=n/a; p(SW)=n/a | | 8 | | | |
| | No. of neurons | no. of intersection at 55µm distance | n/a | not necessary to test | n/a | Mean±SD | | | n/a |
| control | 5 | | | | | 8.6±4.9 | | | |
| | No. of neurons | no. of intersection at 60µm distance | n/a | not necessary to test | n/a | Mean±SD | | | n/a |
| control | 5 | | | | | 6.2±4.4 | | | |
| | No. of neurons | no. of intersection at 65µm distance | n/a | not necessary to test | n/a | Mean±SD | | | n/a |
| control | 4 | | | | | 6.8±8.9 | | | |
| | No. of neurons | no. of intersection at 70µm distance | n/a | not necessary to test | n/a | Mean±SD | | | n/a |
| control | 2 | | | | | 7.5±6.4 | | | |
| | No. of neurons | no. of intersection at 75µm distance | n/a | not necessary to test | n/a | Mean±SD | | | n/a |
| control | 2 | | | | | 6.5±7.8 | | | |
| | No. of neurons | no. of intersection at 80µm distance | n/a | not necessary to test | n/a | Mean±SD | | | n/a |
| control | 1 | | | | | 18 | | | |
| | No. of neurons | no. of intersection at 85µm distance | n/a | not necessary to test | n/a | Mean±SD | | | n/a |
| control | 1 | | | | | 12 | | | |
| | No. of neurons | no. of intersection at 90µm distance | n/a | not necessary to test | n/a | Mean±SD | | | n/a |
| control | 1 | | | | | 6 | | | |
| | No. of neurons | no. of intersection at 95µm distance | n/a | not necessary to test | n/a | Mean±SD | | | n/a |
| control | 1 | | | | | 1 | | | |

## 9.2.33 Figure 5.29 and Figure 5.30 Sholl Analysis of Abdominal A1-A3 RP2 Neurons

| Genotype | Sample Type & n | Comparison | Test | Normality Tests | Homogeneity of Variance | Descriptive Statistics | Test Value & df | p-Value | Multiple Comparisons & Correction |
|---|---|---|---|---|---|---|---|---|---|
| | No. of neurons | no. of intersection at 5µm distance<br>All together | Kruskal-Wallis test | Kolmogorov-Smirnov (KS); Shapiro-Wilk (SW) | n/a | Mean±SD | $\chi^2$=4.000, df=2 | p=0.135 | not necessary to test |
| control | 1 | | | p(KS)=n/a; p(SW)=n/a | | 2 | | | |
| *spz*$^2$ | 2 | | | p(KS)=n/a; p(SW)=n/a | | 1.0±0.0 | | | |
| *spz*$^2$*/Df(3R)Exel6205* | 2 | | | p(KS)=n/a; p(SW)=n/a | | 2.0±0.0 | | | |
| | No. of neurons | no. of intersection at 10µm distance<br>All together | Kruskal-Wallis test | Kolmogorov-Smirnov (KS); Shapiro-Wilk (SW) | n/a | Mean±SD | $\chi^2$=0.368, df=2 | p=0.832 | not necessary to test |
| control | 1 | | | p(KS)=n/a; p(SW)=n/a | | 6 | | | |
| *spz*$^2$ | 2 | | | p(KS)=n/a; p(SW)=n/a | | 4.5±3.5 | | | |
| *spz*$^2$*/Df(3R)Exel6205* | 4 | | | p(KS)=n/a; p(SW)=0.894 (treat as normal) | | 6.3±3.5 | | | |
| | No. of neurons | no. of intersection at 15µm distance<br>All together | Kruskal-Wallis test | Kolmogorov-Smirnov (KS); Shapiro-Wilk (SW) | n/a | Mean±SD | $\chi^2$=4.500, df=2 | p=0.105 | not necessary to test |
| control | 1 | | | p(KS)=n/a; p(SW)=n/a | | 4 | | | |
| *spz*$^2$ | 2 | | | p(KS)=n/a; p(SW)=n/a | | 4.0±4.2 | | | |
| *spz*$^2$*/Df(3R)Exel6205* | 4 | | | p(KS)=n/a; p(SW)=0.275 (treat as normal) | | 15.3±5.0 | | | |
| | No. of neurons | no. of intersection at 20µm distance<br>All together | Kruskal-Wallis test | Kolmogorov-Smirnov (KS); Shapiro-Wilk (SW) | n/a | Mean±SD | $\chi^2$=5.187, df=2 | p=0.075 | not necessary to test |
| control | 2 | | | p(KS)=n/a; p(SW)=n/a | | 2.0±1.4 | | | |
| *spz*$^2$ | 2 | | | p(KS)=n/a; p(SW)=n/a | | 8.0±4.2 | | | |
| *spz*$^2$*/Df(3R)Exel6205* | 4 | | | p(KS)=n/a; p(SW)=0.262 (treat as normal) | | 16.0±7.3 | | | |
| | No. of neurons | no. of intersection at 25µm distance<br>All together | Kruskal-Wallis test | Kolmogorov-Smirnov (KS); Shapiro-Wilk (SW) | n/a | Mean±SD | $\chi^2$=5.187, df=2 | p=0.075 | not necessary to test |
| control | 2 | | | p(KS)=n/a; p(SW)=n/a | | 2.5±0.7 | | | |
| *spz*$^2$ | 2 | | | p(KS)=n/a; p(SW)=n/a | | 9.5±4.9 | | | |
| *spz*$^2$*/Df(3R)Exel6205* | 4 | | | p(KS)=n/a; p(SW)=0.275 (treat as normal) | | 16.8±5.3 | | | |

Please turn over

| Genotype | Sample Type & n | Comparison | Test | Normality Tests | Homogeneity of Variance | Descriptive Statistics | Test Value & df | p-Value | Multiple Comparisons & Correction |
|---|---|---|---|---|---|---|---|---|---|
| | No. of neurons | no. of intersection at 30µm distance<br>All together | Kruskal-Wallis test | Kolmogorov-Smirnov (KS); Shapiro-Wilk (SW) | n/a | Mean±SD | $\chi^2$=5.449, df=2 | p=0.066 | not necessary to test |
| control | 2 | | | p(KS)=n/a; p(SW)=n/a | | 3.5±0.7 | | | |
| *spz²* | 2 | | | p(KS)=n/a; p(SW)=n/a | | 7.0±0.0 | | | |
| *spz²/Df(3R)Exel6205* | 4 | | | p(KS)=n/a; p(SW)=0.041 (treat as normal) | | 11.8±3.2 | | | |
| | No. of neurons | no. of intersection at 35µm distance<br>All together | Kruskal-Wallis test | Kolmogorov-Smirnov (KS); Shapiro-Wilk (SW) | n/a | Mean±SD | $\chi^2$=2.983, df=2 | p=0.225 | not necessary to test |
| control | 2 | | | p(KS)=n/a; p(SW)=n/a | | 4.5±0.7 | | | |
| *spz²* | 2 | | | p(KS)=n/a; p(SW)=n/a | | 9.5±4.9 | | | |
| *spz²/Df(3R)Exel6205* | 4 | | | p(KS)=n/a; p(SW)=0.304 (treat as normal) | | 4.3±4.0 | | | |
| | No. of neurons | no. of intersection at 40µm distance<br>All together | Kruskal-Wallis test | Kolmogorov-Smirnov (KS); Shapiro-Wilk (SW) | n/a | Mean±SD | $\chi^2$=5.046, df=2 | p=0.080 | not necessary to test |
| control | 2 | | | p(KS)=n/a; p(SW)=n/a | | 6.0±1.4 | | | |
| *spz²* | 2 | | | p(KS)=n/a; p(SW)=n/a | | 11.0±2.8 | | | |
| *spz²/Df(3R)Exel6205* | 3 | | | p(KS)=n/a; p(SW)<0.001 (treat as not normal) | | 2.3±2.3 | | | |
| | No. of neurons | no. of intersection at 45µm distance | Kruskal-Wallis test | Kolmogorov-Smirnov (KS); Shapiro-Wilk (SW) | n/a | Mean±SD | $\chi^2$=0.000, df=2 | p=1.000 | not necessary to test |
| control | 2 | | | p(KS)=n/a; p(SW)=n/a | | 8.0±0.0 | | | |
| *spz²* | 2 | | | p(KS)=n/a; p(SW)=n/a | | 8.5±6.4 | | | |
| | No. of neurons | no. of intersection at 50µm distance | n/a | not necessary to test | n/a | Mean±SD | | | n/a |
| control | 2 | | | p(KS)=n/a; p(SW)=n/a | | 10.0±0.0 | | | |
| *spz²* | 1 | | | p(KS)=n/a; p(SW)=n/a | | 8 | | | |
| | No. of neurons | no. of intersection at 55µm distance | n/a | not necessary to test | n/a | Mean±SD | | | n/a |
| control | 2 | | | p(KS)=n/a; p(SW)=n/a | | 9.5±2.1 | | | |
| *spz²* | 1 | | | p(KS)=n/a; p(SW)=n/a | | 6 | | | |
| | No. of neurons | no. of intersection at 60µm distance | n/a | not necessary to test | n/a | Mean±SD | | | n/a |
| control | 2 | | | | | 13.5±0.7 | | | |
| | No. of neurons | no. of intersection at 65µm distance | n/a | not necessary to test | n/a | Mean±SD | | | n/a |
| control | 2 | | | | | 13.0±8.5 | | | |
| | No. of neurons | no. of intersection at 70µm distance | n/a | not necessary to test | n/a | Mean±SD | | | n/a |
| control | 2 | | | | | 16.0±7.1 | | | |

Please turn over

| Genotype | Sample Type & n | Comparison | Test | Normality Tests | Homogeneity of Variance | Descriptive Statistics | Test Value & df | p-Value | Multiple Comparisons & Correction |
|---|---|---|---|---|---|---|---|---|---|
| | No. of neurons | no. of intersection at 75µm distance | n/a | not necessary to test | n/a | Mean±SD | | | n/a |
| control | 2 | | | | | 12.0±4.2 | | | |
| | No. of neurons | no. of intersection at 80µm distance | n/a | not necessary to test | n/a | Mean±SD | | | n/a |
| control | 2 | | | | | 10.0±5.7 | | | |
| | No. of neurons | no. of intersection at 85µm distance | n/a | not necessary to test | n/a | Mean±SD | | | n/a |
| control | 2 | | | | | 12.5±0.7 | | | |
| | No. of neurons | no. of intersection at 90µm distance | n/a | not necessary to test | n/a | Mean±SD | | | n/a |
| control | 2 | | | | | 13.0±0.0 | | | |
| | No. of neurons | no. of intersection at 95µm distance | n/a | not necessary to test | n/a | Mean±SD | | | n/a |
| control | 2 | | | | | 8.5±0.7 | | | |
| | No. of neurons | no. of intersection at 100µm distance | n/a | not necessary to test | n/a | Mean±SD | | | n/a |
| control | 2 | | | | | 8.0±2.8 | | | |
| | No. of neurons | no. of intersection at 105µm distance | n/a | not necessary to test | n/a | Mean±SD | | | n/a |
| control | 2 | | | | | 7.0±2.8 | | | |
| | No. of neurons | no. of intersection at 110µm distance | n/a | not necessary to test | n/a | Mean±SD | | | n/a |
| control | 2 | | | | | 5.0±2.8 | | | |
| | No. of neurons | no. of intersection at 115µm distance | n/a | not necessary to test | n/a | Mean±SD | | | n/a |
| control | 2 | | | | | 2.0±1.4 | | | |
| | No. of neurons | no. of intersection at 120µm distance | n/a | not necessary to test | n/a | Mean±SD | | | n/a |
| control | 2 | | | | | 1.0±0.0 | | | |

## 9.2.34 Figure 5.31 Sholl Analysis of Abdominal A6-A7 RP2 Neurons

| Genotype | Sample Type & n | Comparison | Test | Normality Tests | Homogeneity of Variance | Descriptive Statistics | Test Value & df | p-Value | Multiple Comparisons & Correction |
|---|---|---|---|---|---|---|---|---|---|
| | No. of neurons | no. of intersection at 2.5µm distance | | not necessary to test | n/a | Mean±SD | | p=0.135 | not necessary to test |
| control | 0 | | | | | | | | |
| *spz²/Df(3R)Exel6205* | 1 | | | | | 1 | | | |
| | No. of neurons | no. of intersection at 5.0µm distance | | not necessary to test | n/a | Mean±SD | | p=0.832 | not necessary to test |
| control | 0 | | | | | | | | |
| *spz²/Df(3R)Exel6205* | 2 | | | | | 2.5±2.1 | | | |
| | No. of neurons | no. of intersection at 7.5µm distance | | not necessary to test | n/a | Mean±SD | | | not necessary to test |
| control | 2 | | | | | 4.0±1.4 | | | |
| *spz²/Df(3R)Exel6205* | 1 | | | | | 3 | | | |
| | No. of neurons | no. of intersection at 10.0µm distance | t-test | Kolmogorov-Smirnov (KS); Shapiro-Wilk (SW) | Levene's Test: n/a, equal variances not assumed | Mean±SD | t=-0.832, df=1.742 | p=0.504 | not necessary to test |
| control | 2 | | | p(KS)=n/a; p(SW)=n/a | | 4.0±2.8 | | | |
| *spz²/Df(3R)Exel6205* | 2 | | | p(KS)=n/a; p(SW)=n/a | | 7.0±4.2 | | | |
| | No. of neurons | no. of intersection at 12.5µm distance | t-test | Kolmogorov-Smirnov (KS); Shapiro-Wilk (SW) | Levene's Test: n/a, equal variances not assumed | Mean±SD | t=-0.117, df=1.276 | p=0.923 | not necessary to test |
| control | 2 | | | p(KS)=n/a; p(SW)=n/a | | 8.0±5.7 | | | |
| *spz²/Df(3R)Exel6205* | 2 | | | p(KS)=n/a; p(SW)=n/a | | 8.5±2.1 | | | |
| | No. of neurons | no. of intersection at 15.0µm distance | t-test | Kolmogorov-Smirnov (KS); Shapiro-Wilk (SW) | Levene's Test: 1.286, p=0.339 | Mean±SD | t=-0.509, df=3 | p=0.646 | not necessary to test |
| control | 2 | | | p(KS)=n/a; p(SW)=n/a | | 7.5±4.9 | | | |
| *spz²/Df(3R)Exel6205* | 3 | | | p(KS)=n/a; p(SW)=0.253 (treat as normal) | | 10.7±7.6 | | | |
| | No. of neurons | no. of intersection at 17.5µm distance | t-test | Kolmogorov-Smirnov (KS); Shapiro-Wilk (SW) | Levene's Test: 0.021, p=0.893 | Mean±SD | t=0.764, df=3 | p=0.500 | not necessary to test |
| control | 2 | | | p(KS)=n/a; p(SW)=n/a | | 9.5±3.5 | | | |
| *spz²/Df(3R)Exel6205* | 3 | | | p(KS)=n/a; p(SW)=0.537 (treat as normal) | | 7.0±3.6 | | | |

Please turn over

| Genotype | Sample Type & n | Comparison | Test | Normality Tests | Homogeneity of Variance | Descriptive Statistics | Test Value & df | p-Value | Multiple Comparisons & Correction |
|---|---|---|---|---|---|---|---|---|---|
| | No. of neurons | no. of intersection at 20.0µm distance | t-test | Kolmogorov-Smirnov (KS); Shapiro-Wilk (SW) | Levene's Test 2.282, p=0.228 | Mean±SD | t=-1.142, df=3 | p=0.283 | not necessary to test |
| control | 2 | | | p(KS)=n/a; p(SW)=n/a | | 7.5±3.5 | | | |
| *spz²/Df(3R)Exel6205* | 3 | | | p(KS)=n/a; p(SW)=0.463 (treat as normal) | | 10.7±2.1 | | | |
| | No. of neurons | no. of intersection at 22.5µm distance | t-test | Kolmogorov-Smirnov (KS); Shapiro-Wilk (SW) | Levene's Test 1.584, p=0.297 | Mean±SD | t=-0.055, df=3 | p=0.960 | not necessary to test |
| control | 2 | | | p(KS)=n/a; p(SW)=n/a | | 12.0±8.5 | | | |
| *spz²/Df(3R)Exel6205* | 3 | | | p(KS)=n/a; p(SW)=0.174 (treat as normal) | | 12.3±5.5 | | | |
| | No. of neurons | no. of intersection at 25.0µm distance | t-test | Kolmogorov-Smirnov (KS); Shapiro-Wilk (SW) | Levene's Test 1.584, p=0.297 | Mean±SD | t=-0.832, df=3 | p=0.466 | not necessary to test |
| control | 2 | | | p(KS)=n/a; p(SW)=n/a | | 8.5±0.7 | | | |
| *spz²/Df(3R)Exel6205* | 3 | | | p(KS)=n/a; p(SW)=1.000 (treat as normal) | | 11.0±4.0 | | | |
| | No. of neurons | no. of intersection at 27.5µm distance | t-test | Kolmogorov-Smirnov (KS); Shapiro-Wilk (SW) | Levene's Test 7.736, p=0.069 | Mean±SD | t=-0.666, df=3 | p=0.553 | not necessary to test |
| control | 2 | | | p(KS)=n/a; p(SW)=n/a | | 6.5±0.7 | | | |
| *spz²/Df(3R)Exel6205* | 3 | | | p(KS)=n/a; p(SW)=0.220 (treat as normal) | | 13.0±13.1 | | | |
| | No. of neurons | no. of intersection at 30.0µm distance | t-test | Kolmogorov-Smirnov (KS); Shapiro-Wilk (SW) | Levene's Test 1.142, p=0.364 | Mean±SD | t=-0.525, df=3 | p=0.636 | not necessary to test |
| control | 2 | | | p(KS)=n/a; p(SW)=n/a | | 8.0±5.7 | | | |
| *spz²/Df(3R)Exel6205* | 3 | | | p(KS)=n/a; p(SW)=0.726 (treat as normal) | | 13.0±12.1 | | | |
| | No. of neurons | no. of intersection at 32.5µm distance | t-test | Kolmogorov-Smirnov (KS); Shapiro-Wilk (SW) | Levene's Test 4.860, p=0.115 | Mean±SD | t=-0.351, df=3 | p=0.749 | not necessary to test |
| control | 2 | | | p(KS)=n/a; p(SW)=n/a | | 8.0±4.2 | | | |
| *spz²/Df(3R)Exel6205* | 3 | | | p(KS)=n/a; p(SW)=0.235 (treat as normal) | | 12.3±16.3 | | | |
| | No. of neurons | no. of intersection at 35.0µm distance | t-test | Kolmogorov-Smirnov (KS); Shapiro-Wilk (SW) | Levene's Test n/a, equal variances not assumed | Mean±SD | t=-1.100, df=2.000 | p=0.386 | not necessary to test |
| control | 2 | | | p(KS)=n/a; p(SW)=n/a | | 6.5±6.4 | | | |
| *spz²/Df(3R)Exel6205* | 2 | | | p(KS)=n/a; p(SW)=n/a | | 13.5±6.4 | | | |

Please turn over

| Genotype | Sample Type & n | Comparison | Test | Normality Tests | Homogeneity of Variance | Descriptive Statistics | Test Value & df | p-Value | Multiple Comparisons & Correction |
|---|---|---|---|---|---|---|---|---|---|
| | No. of neurons | no. of intersection at 37.5µm distance | t-test | Kolmogorov-Smirnov (KS); Shapiro-Wilk (SW) | Levene's Test<br>0.595, p=0.497 | Mean±SD | t=-0.293, df=3 | p=0.789 | not necessary to test |
| control | 2 | | | p(KS)=n/a; p(SW)=n/a | | 3.5±3.5 | | | |
| *spz$^2$/Df(3R)Exel6205* | 3 | | | p(KS)=n/a; p(SW)=0.407 (treat as normal) | | 4.7±4.7 | | | |
| | No. of neurons | no. of intersection at 40.0µm distance | t-test | Kolmogorov-Smirnov (KS); Shapiro-Wilk (SW) | Levene's Test<br>n/a, equal variances not assumed | Mean±SD | t=0.243, df=1.125 | p=0.845 | not necessary to test |
| control | 2 | | | p(KS)=n/a; p(SW)=n/a | | 3.0±2.8 | | | |
| *spz$^2$/Df(3R)Exel6205* | 2 | | | p(KS)=n/a; p(SW)=n/a | | 2.5±0.7 | | | |
| | No. of neurons | no. of intersection at 42.5µm distance | n/a | not necessary to test | n/a | Mean±SD | | | n/a |
| control | 1 | | | | | 1 | | | |
| *spz$^2$/Df(3R)Exel6205* | 2 | | | | | 1.0±0.0 | | | |
| | No. of neurons | no. of intersection at 45.0µm distance | n/a | not necessary to test | n/a | Mean±SD | | | n/a |
| control | 1 | | | | | 1 | | | |

## 9.3 Statistical Tests in Chapter 6

### 9.3.1 Figure 6.1 Time-Lapse Analysis

| Genotype | Sample Type & n | Comparison | Test | Normality Tests | Homogeneity of Variance | Descriptive Statistics | Test Value & df | p-Value | Multiple Comparisons & Correction |
|---|---|---|---|---|---|---|---|---|---|
| | No. of VNC | Wound area | paired t-test | Kolmogorov-Smirnov (KS); Shapiro-Wilk (SW) | n/a | Mean±SD ($\mu m^2$) | | | Bonferroni: $p \times 10$ |
| *G9* at 6 hours after injury | 3 | To *G9* at 8 hours after injury | | p(KS)=n/a; p(SW)=0.358 (treat as normal) | | 5120±1998 | t=-1.503, df=2 | p=0.272 | |
| | | To *G9* at 11 hours after injury | | | | | t=0.014, df=2 | p=0.990 | |
| | | To *G9* at 15 hours after injury | | | | | t=3.196, df=2 | p=0.086 | |
| *G9* at 7 hours after injury | 3 | | | p(KS)=n/a; p(SW)=0.393 (treat as normal) | | 5120±2199 | | | |
| *G9* at 8 hours after injury | 3 | To *G9* at 11 hours after injury | | p(KS)=n/a; p(SW)=0.436 (treat as normal) | | 5379±2284 | t=0.757, df=2 | p=0.528 | |
| | | To *G9* at 15 hours after injury | | | | | t=4.140, df=2 | p=0.054 | |
| *G9* at 9 hours after injury | 3 | | | p(KS)=n/a; p(SW)=0.376 (treat as normal) | | 5248±2286 | | | |
| *G9* at 10 hours after injury | 3 | | | p(KS)=n/a; p(SW)=0.857 (treat as normal) | | 4844±1857 | | | |
| *G9* at 11 hours after injury | 3 | To *G9* at 15 hours after injury | | p(KS)=n/a; p(SW)=0.939 (treat as normal) | | 5114±2320 | t=16.001, df=2 | p<0.01 (p=0.003883) | p<0.05 (0.03883) |
| *G9* at 12 hours after injury | 3 | | | p(KS)=n/a; p(SW)=0.955 (treat as normal) | | 4512±1806 | | | |
| *G9* at 13 hours after injury | 3 | | | p(KS)=n/a; p(SW)=0.735 (treat as normal) | | 4380±1650 | | | |
| *G9* at 14 hours after injury | 3 | | | p(KS)=n/a; p(SW)=0.928 (treat as normal) | | 4152±1630 | | | |
| *G9* at 15 hours after injury | 3 | | | p(KS)=n/a; p(SW)=0.974 (treat as normal) | | 3716±2209 | | | |

### 9.3.2 Figure 6.2 Wound Area

| Genotype | Sample Type & n | Comparison | Test | Normality Tests | Homogeneity of Variance | Descriptive Statistics | Test Value & df | p-Value | Multiple Comparisons & Correction |
|---|---|---|---|---|---|---|---|---|---|
| | No. of VNC | Wound area | one-way ANOVA | Kolmogorov-Smirnov (KS); Shapiro-Wilk (SW) | Levene's Test | Mean±SD ($\mu m^2$) | F=4.087, df=3 | p<0.05 | Dunnett |
| | | All together | | | 0.547, p=0.653 | | | | |
| *yw* | 24 | | | k=0.565; s=0.610; p(KS)=0.200; p(SW)=0.488 (all normal) | | 4575±1858 | | | |
| *spz$^{MA05}$/Df(3R)Exel6205* | 6 | To *yw* | | k=1.897; s=1.209; p(KS)=0.200; p(SW)=0.229 (all normal) | | 6674±1935 | | | p=0.031 |
| *elav>actSpz(2)* | 7 | To *yw* | | k=-0.214; s=0.446; p(KS)=0.200; p(SW)=0.904 (all normal) | | 3411±1373 | | | p=0.314 |
| *repo>actSpz(2)* | 7 | To *yw* | | k=3.514; s=-1.775; p(KS)=0.200; p(SW)=0.063 (treat as normal) | | 5097±1231 | | | p=0.853 |

### 9.3.3 Figure 6.3 Wound Area

| Genotype | Sample Type & n | Comparison | Test | Normality Tests | Homogeneity of Variance | Descriptive Statistics | Test Value & df | p-Value | Multiple Comparisons & Correction |
|---|---|---|---|---|---|---|---|---|---|
| | No. of VNC | Wound area | one-way ANOVA | Kolmogorov-Smirnov (KS); Shapiro-Wilk (SW) | Levene's Test | Mean±SD ($\mu m^2$) | F=0.708, df=5 | p=0.621 | not necessary to test |
| | | All together | | | 1.130, p=0.357 | | | | |
| *yw* | 24 | | | k=0.565; s=0.610; p(KS)=0.200; p(SW)=0.488 (all normal) | | 4575±1858 | | | |
| *$Toll7^{P114}/Toll7^{P8};Toll6^{31}/Toll7^{26}$* | 11 | | | k=0.244; s=0.121; p(KS)=0.200; p(SW)=0.925 (all normal) | | 4516±1562 | | | |
| *elav>DNT1-CK3'+* | 7 | | | k=-1.577; s=-0.017; p(KS)=0.200; p(SW)=0.753 (all normal) | | 4399±1352 | | | |
| *repo> DNT1-CK3'+* | 3 | | | k=n/a; s=-1.593; p(KS)=n/a; p(SW)=0.257 (treat as normal) | | 3893±149 | | | |
| *elav>DNT2-CK-6A* | 5 | | | k=0.706; s=0.897; p(KS)=0.200; p(SW)=0.629 (all normal) | | 4666±1868 | | | |
| *repo> DNT2-CK-6A* | 5 | | | k=-1.414; s=0.110; p(KS)=0.200; p(SW)=0.700 (all normal) | | 3172±908 | | | |

# 10 Appendix II

PUBLICATION